Kapitel 5: Dampfprozess

1. Beschreibung des Dampfprozesses
2. Vorwärmer
3. Zwischenüberhitzung
4. MAN-Dampfturbinen-Typen
5. Turbine Blading Materials Boost (1996)
6. Stand aktueller Projekte und Entwicklungstendenzen in der Kraftwerkstechnik (2005)
7. Interne Zusatzfeuerung (2003)
8. Übersicht über Siemens-Dampfturbinen
9. Kosten Dampfturbine
10. Organic Rankine Cycles (Manente, 2017)
11. Enhancement of the Electrical Efficiency of Commercial Fuel Cell Units by Means of an Organic Rankine Cycle: A Case Study (2013)

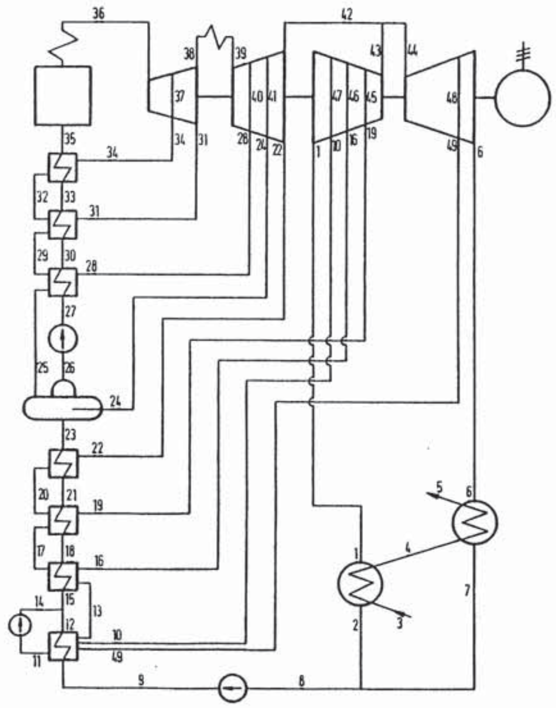

Dampfkreis mit Elektroantrieb der Speisepumpe

Abb. 2.4.9

Die Verbesserung in thermodynamischer Hinsicht, die durch die Vorwärmung erreicht werden kann zeigt die Abb. 2.4.6. Die Verbesserung des Exergieverlustes bei der Wärmezufuhr vom Rauchgas an den Dampf ist durch die folgende Gleichung gegeben :

mit Vorwärmer: $$\eta_{th\ max} = \frac{\int_V^{FD} (1 - \frac{T_u}{T})\, dq}{q_{V\ FD}}$$

ohne Vorwärmer: $$\eta_{th\ max} = \frac{\int_S^{FD} (1 - \frac{T_u}{T})\, dq}{q_{S\ FD}}$$

$$\eta_{th\ max} = \frac{\int_V^{FD} (1 - \frac{T_u}{T})\, dq + \int_{KZÜ}^{ZÜ} (1 - \frac{T_u}{T})\, dq}{q_{V-FD} + q_{KZÜ-ZÜ}}$$

Am günstigsten wäre es daher, den Beginn der Zwischenüberhitzung auf die gleiche Temperatur zu legen, wie der Mittelwert der gesamten Wärmezufuhr im 1. Bereich ergibt. Daraus folgt eine Optimalvorschrift für den Zwischenüberhitzerdruck, die Traupel angegeben hat.

$$p_{ZÜ} = p(T_{opt})$$

$$T_{opt} = \overline{T}_{V-FD} = \frac{(h_{FD} - h_V) + (h_{ZÜ} - h_{KZÜ}) \frac{\dot{m}_{ZÜ}}{\dot{m}_{FD}}}{(s_{FD} - s_V) + (s_{ZÜ} - s_{KZÜ}) \frac{\dot{m}_{ZÜ}}{\dot{m}_{FD}}}$$

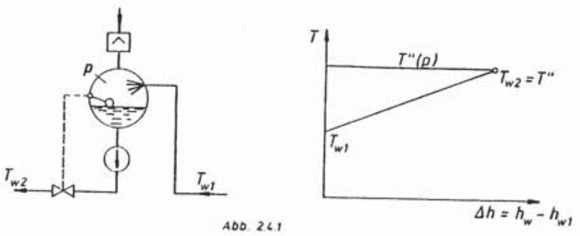

Abb. 2.4.1

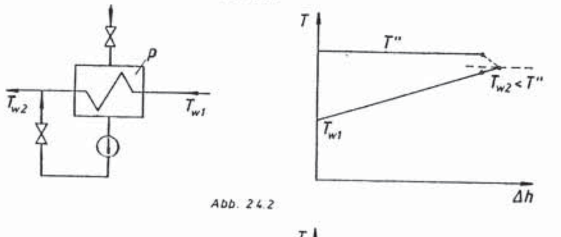

Abb. 2.4.2

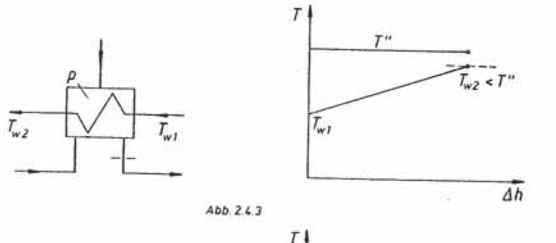

Abb. 2.4.3

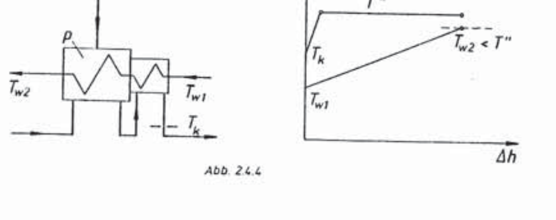

Abb. 2.4.4

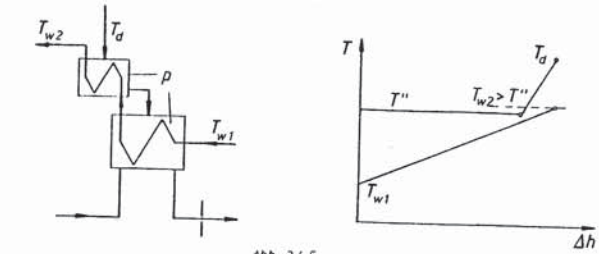

Abb. 2.4.5

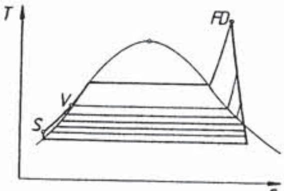

Abb. 2.4.6

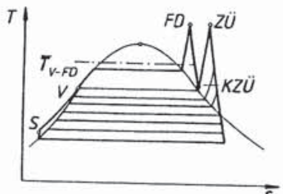

Abb. 2.4.7

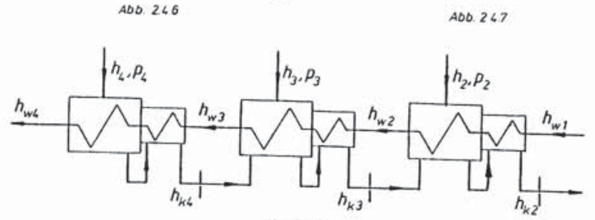

Abb. 2.4.8

Steam Turbine Types:

Condensing Turbines

The MAN TURBO condensing steam turbine features a horizontally split main casing of cast steel; the exhaust casing is a fabricated construction which in turn is welded to the upper and lower part of the main casing.

One advantage of this design is that sealing problems, that may occur with cross partition joints, are completely eliminated, hence power losses are kept to a minimum.

The turbine fixed point is located at the exhaust casing support. The rotor fixed point relative to the turbine casing is the trust bearing housing at the live steam end.

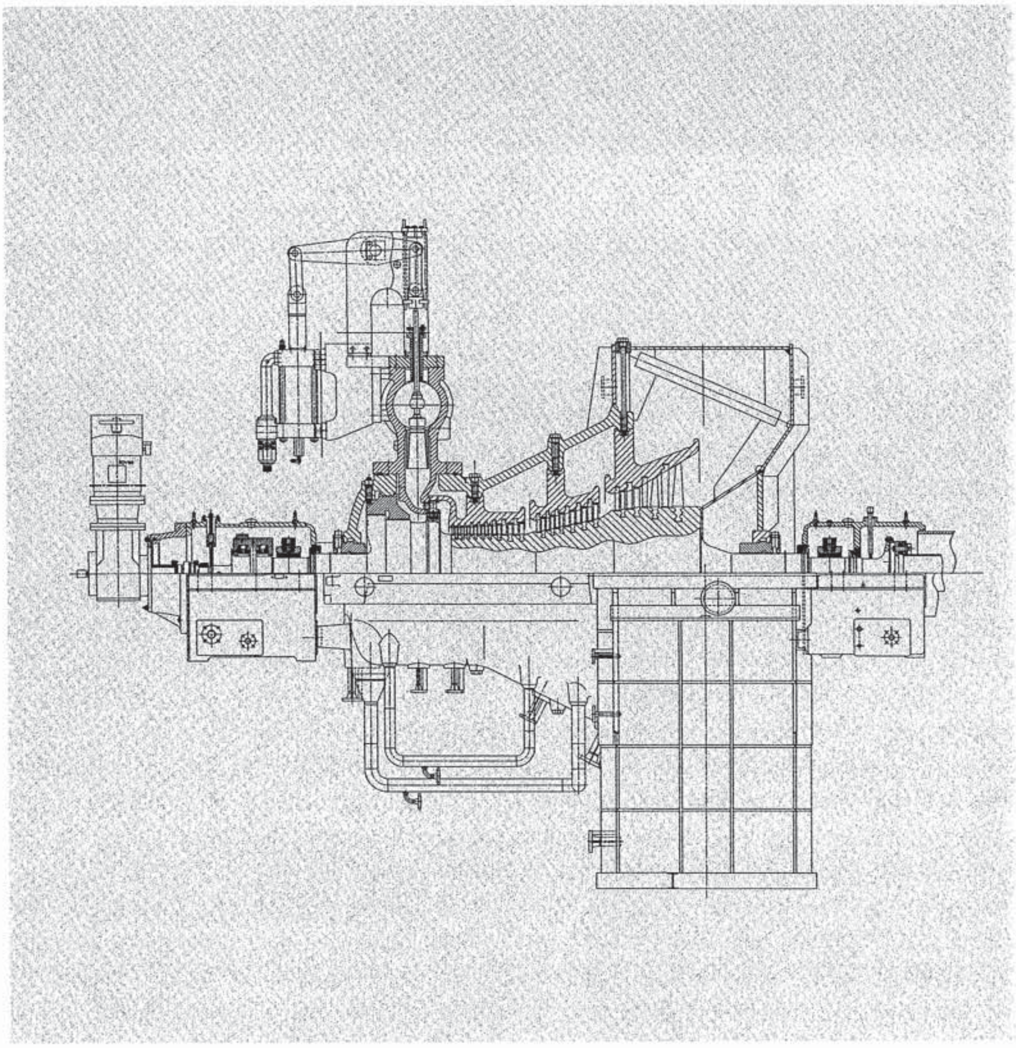

8 Sectional drawing of condensing steam turbine

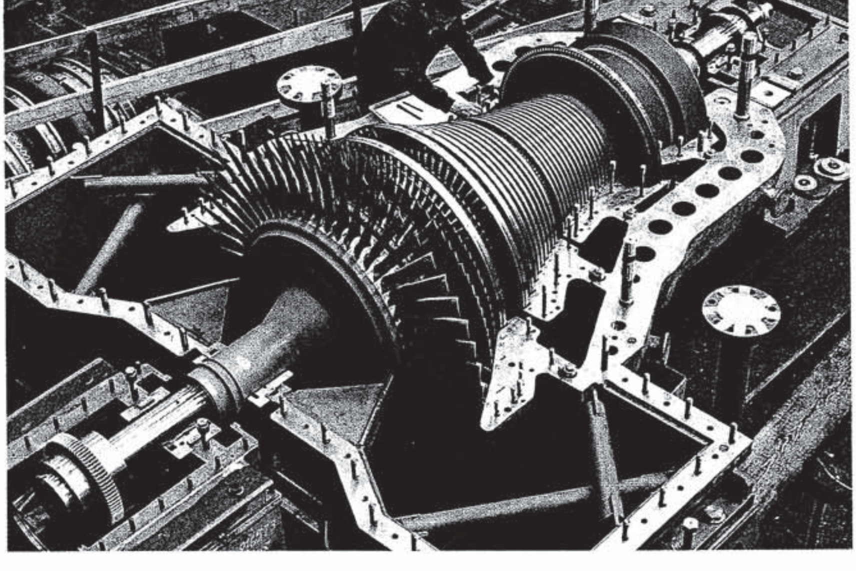

9 Condensing steam turbine driver for an axial compressor

Backpressure Turbines

The turbine features a single horizontally split cast casing incorporating the control stage as well as the transition and exhaust casing modules.

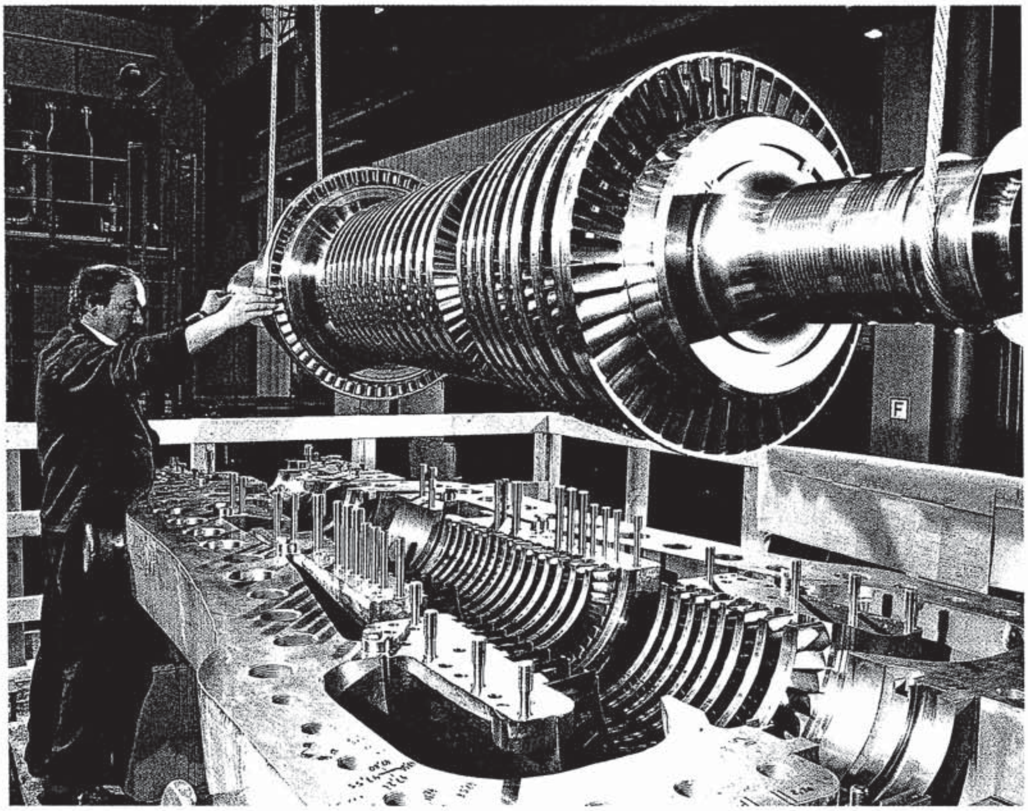

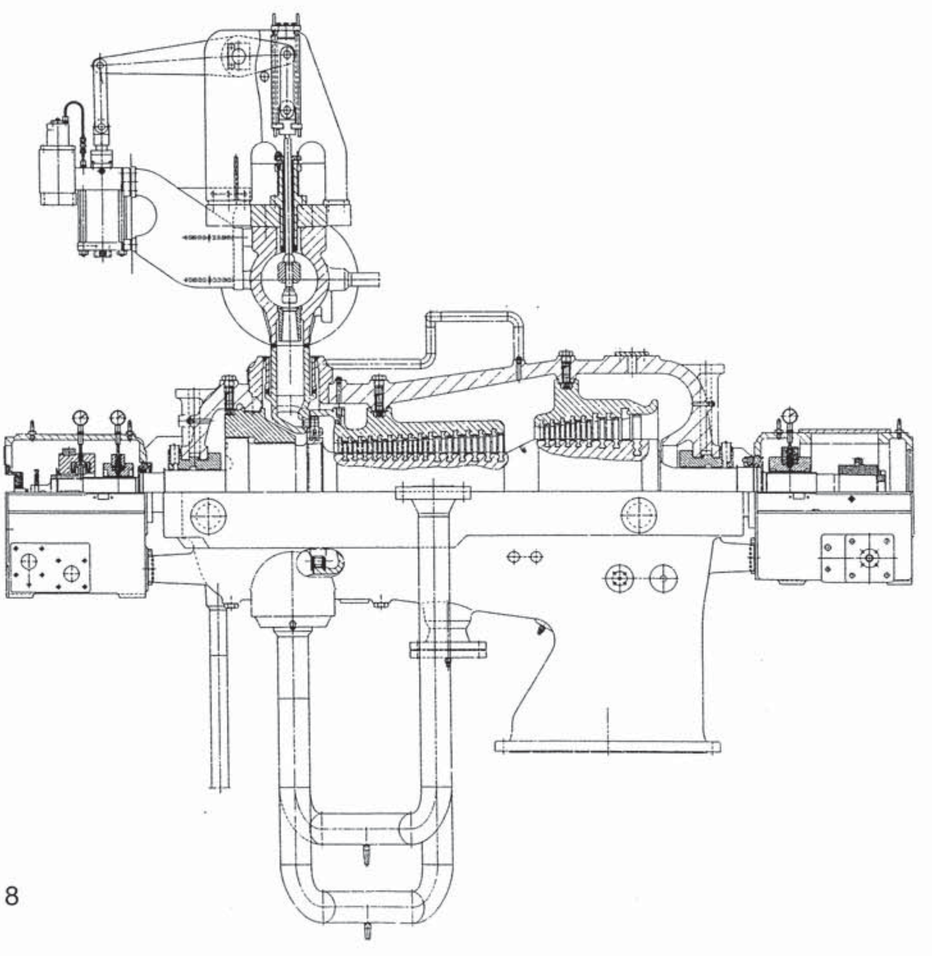

10 12 MW backpressure turbine

11 Sectional drawing of a backpressure turbine

Extraction Turbines

Extraction steam turbines are designed to operate and control the client's steam networks using defined steam parameters.

Depending on the mode of operation, quantity of steam and pressure, three different methods of extraction control are possible:

- extraction control stage
- overflow throttle valve
- variable guide vanes.

The valves of an extraction control stage are located in the upper part of the casing. The extraction nozzles can be arranged downwards or towards the side. The minimum cooling steam flow rate for the low-pressure blading is also ensured at the maximum extraction rate.

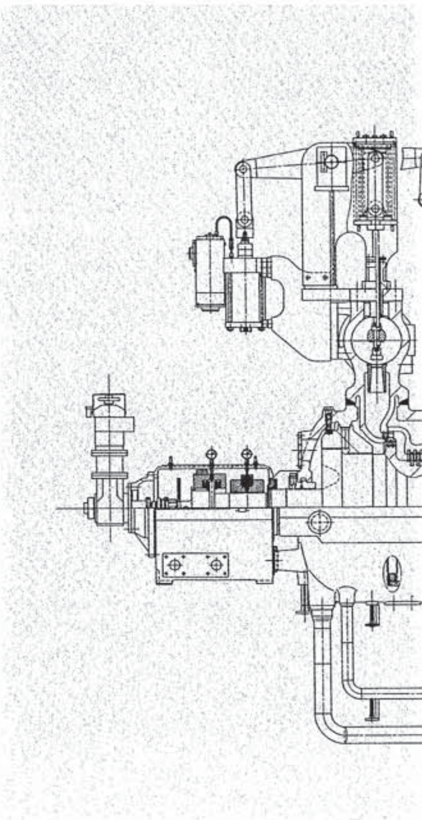

13 Sectional drawing of a double extraction condensing steam turbine, the first is a controlled extraction with control stage, the second extraction uses an overflow throttle valve.

12 Variable guide vanes in open position

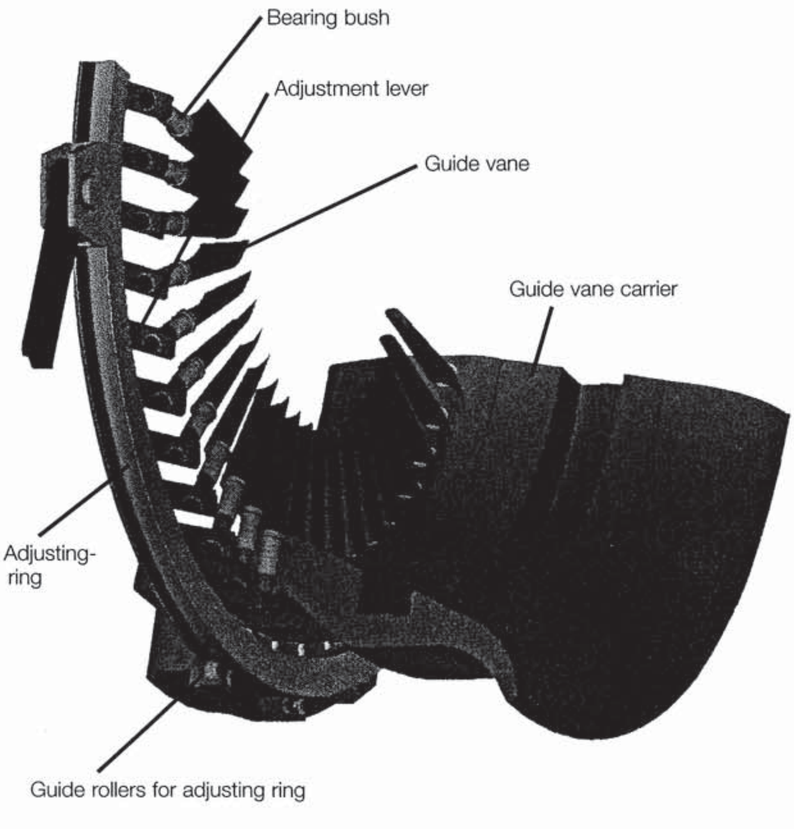

14 25 MW double-extraction condensing steam turbine

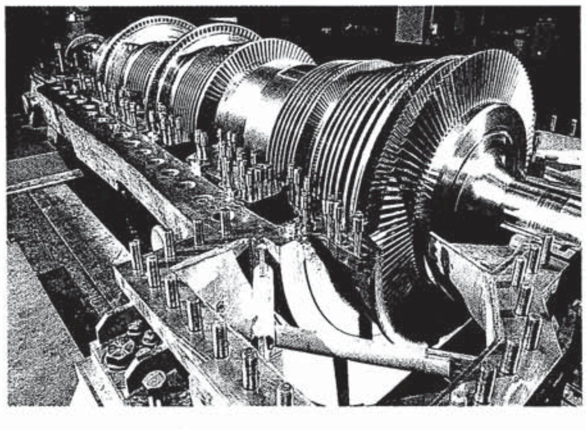

Turbine blading materials boost

Efficiencies are being gained from new materials allowing higher temperatures and pressures to be used. As the result of a new steel, GEC Alsthom has super-efficient plant going into service in Denmark.

Large power plant with advanced steam conditions were first ordered more than 40 years ago. Early operating experience was disappointing, particularly with the boilers, due mainly to the application of austenitic materials to those pressure parts in contact with the highest-temperature steam.

Advanced steam conditions, which can be defined at the turbine as main pressures of 240 bar and above with main and reheat temperatures of 565°C and above, have since been avoided by utilities. They have preferred relatively larger unit sizes with more modest steam conditions.

The incentive for adopting advanced steam conditions was the efficiency improvements to be had. Today, for each one per cent relative efficiency improvement on a coal fired 680 MW machine produces there is an estimated lifetime fuel saving of about $ US 10 million. This is now strongly reinforced by environmental considerations. The same efficiency improvement produces an estimated lifetime reduction in $C0_2$ emission of about 0.8 million tonnes.

For designers, substantial efficiency improvements to the steam cycle can only come from a return to advanced steam conditions. Relative efficiency improvements of 6 per cent are attainable with the single reheat cycle by raising steam pressure to 300 bar and temperature to 600°C rather that the conventional values of 180 bar and 540°C most commonly specified.

Turbines

GEC Alsthom's single reheat steam turbines are of the impulse type with disc and diaphragm construction. Typical of these machines designed for conventional single reheat steam conditions of 180 bar/540°C/540°C is the standard 680 MW unit. All the major components of this machine are in low alloy steel but, by a limited number of material substitutions, it is also suitable for service at main and reheat steam temperatures of 565°C.

The thermodynamic efficiency of the conventional single reheat cycle can be improved by any means which increases the average temperature at which heat is added to the cycle.

Thus as main steam pressure is increased it becomes possible to heat feedwater to higher temperatures by tapping steam from within the turbine, significantly improving cycle efficiency. Optimisation of final feedwater temperatures should include the boiler as it can affect boiler efficiency.

However, the most direct way of increasing the average temperature of heat addition to the cycle is by increasing both main and reheat steam temperatures. This improves relative efficiency by a rate of about 1.0 per cent per 20°C rise over a wide range of temperature and pressure, for both single and double reheat. This improvement is virtually independent of the turbine design.

Increasing main steam pressure also produces large efficiency improvements for low subcritical pressures where there is a large heat input at low evaporation temperatures. However, as pressures increase and corresponding volumetric flows reduce, the HP and IP expansion losses and leakage losses increase, because blade heights shorten to accommodate the reduced volumetric flow and blade widths increase to accommodate the higher steam loading. The lower blade aspect ratios result in an increased proportion of blade end boundary layer losses. Some increased loss is inevitable, although great strides have been made in reducing it by improved blading designs developed using a combination of computational fluid dynamic methods and experimental testing. The magnitude of expansion and leakage losses therefore is dependent on the quality of design and manufacture of the turbine. Increasing main steam pressure also increases the level of steam wetness in the LP cylinder, causing a small

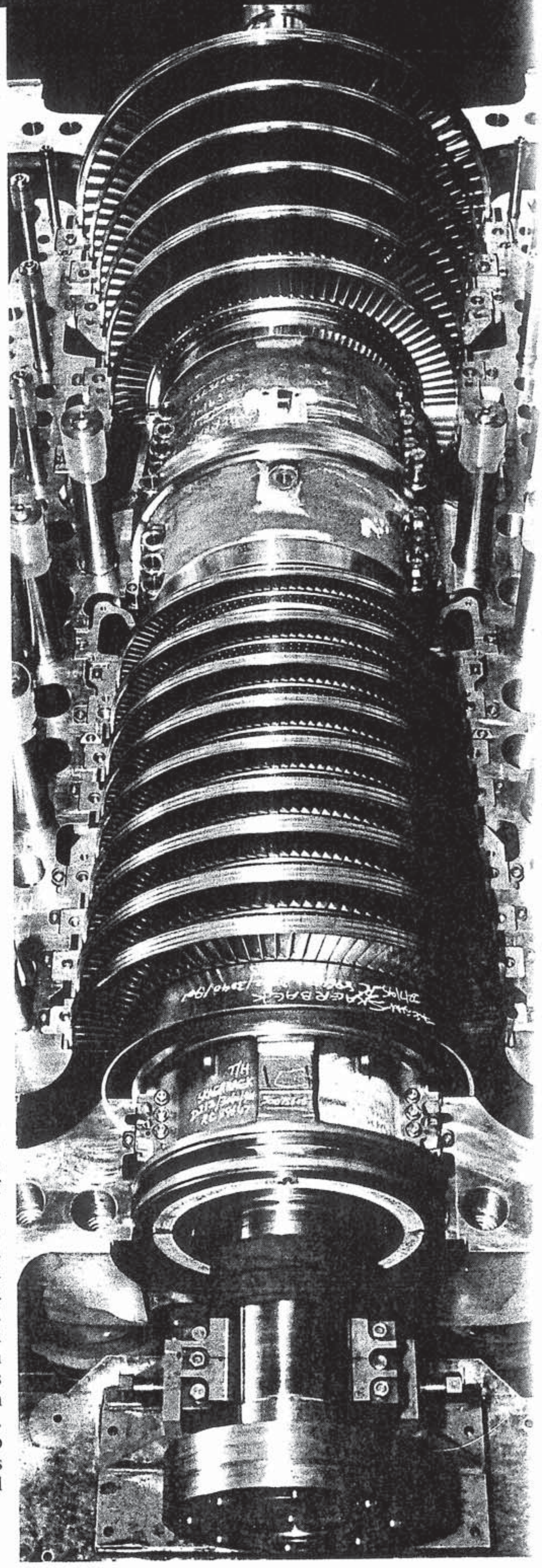

***Right:** Tubine rotor manufactured for the district heating plant at Skaerbaek.*

loss in LP expansion efficiency. The combined effect of all of these factors is that there is a level of steam supply pressure beyond which a further pressure increase produces no further efficiency improvement, and this level will be lower for smaller machines which are more sensitive to blade end leakage losses than large machines.

Double reheating further improves relative efficiency by about two per cent by directly increasing the average temperature of heat addition and by reducing LP steam wetness, even though there is some increase in expansion and leakage losses due to the reduction in steam flow relative to single reheat cycles. Also for double reheat, the level of steam supply pressure for the peak efficiency is higher than for single reheat.

Output and capability

Whenever possible, each GEC Alsthom turbine frame comprises single flow HP and IP expansions. For conventional steam conditions, for 200 MW and 400 MW frames these expansions take place in combined HP/IP cylinders, whereas separate HP and IP cylinders are used for the 680 MW frame, SR.18.68.30. The larger output frames offer improved efficiencies and a lower capital cost per MW than smaller ones and as such are most relevant to larger utilities while the lower output frames offer better operational flexibility.

The limitation to increases in steam inlet temperature is the high temperature strength of the turbine and boiler materials. For both forged and cast major turbine components, low alloy lCrMoV steel has been extensively used for temperatures up to 565°C, beyond which there is a rapid reduction in the creep strength after long term service.

However, a high alloy 9-12Cr ferritic steel has now been fully developed and proven in service for both forged and cast major turbine components with creep strengths suitable for long term service at temperatures up to 600°C. Variants of the 9-12Cr steels after short term testing show potential for long term service at temperatures of 625°C and possibly 650°C. The 9-12Cr steels also have a high temperature proof strength superior to the 1 CrMoV steels.

Under transient operating conditions, high strain fatigue strength limits the allowable surface cyclic strain range. Compared with lCrMoV, the 9-12Cr steels have much higher thermal fatigue strength (consistent with the better combination of creep and proof strength), a thermal expansion coefficient about 15 per cent less, and a thermal diffusivity which is about 25 per cent less. The allowable rapid temperature change of the rotor surface on a hot start is mainly controlled by the thermal expansion coefficient and thermal fatigue strength and is therefore much higher for the 9-12Cr material. For cold starts, the allowable rate of surface temperature rise is also strongly dependent on the diffusivity, resulting in comparable cold start rates at higher temperatures for the 9-12Cr material.

To retain bolted horizontal casing joints under conditions of high pressure and high temperature requires bolting material with much better high temperature creep relaxation properties than the high chrome material normally used for lower steam conditions. The nickel based Nimonic 80A material is ideal for this purpose and has substantial successful service experience in GEC Alsthom turbines.

Steel blading

Turbine blades manufactured by British Steel from a new stainless steel will be used in one of the world's most efficient steam turbine power stations. The new steel will be used for the rotating and stationary diaphragm blades for turbines manufactured by the GEC Alsthom for the power plants at Skaerbaek and Nordjylland in Denmark.

Designers of the two 412 MW steam turbines with district heating capability are claiming they will be the most efficient in the world when they enter service in 1997 and 1998. The blades are designed to operate at 3,000 rpm for 200,000-250,000 hours (the equivalent of 24 hours a day for around 25 years). Advanced ferritic stainless steels allows steam temperatures to be increased to 580C - 620C.

The material has been used in the US for nuclear piping applications and GEC Alsthom is one of the first manufacturers to use it for steam turbines.

The new Danish power stations will achieve an efficiency of 49 per cent, around 10 per cent efficiency improvement relative to existing plant with conventional steam conditions. Further increases in efficiency are being explored in a Europe-wide programme involving partners including British Steel Engineering and GEC Alsthom, known as the COST 501 program. This has a target of 52 per cent efficiency - to be achieved by operating at temperatures of up to 700 C, using new materials.

Denmark

Two 412 MW double reheat machines were ordered from GEC Alsthom in May 1993 for service in Skaerbaek and Nordjylland power stations, Denmark. With advanced steam conditions (285bar/580°C/ 580°C/580°C) and low condenser pressure (23 mbar due to seawater cooling temperature of 10°C), these machines will be the most efficient in the world operating on the steam cycle with an efficiency improvement of about 10 per cent relative to the standard single reheat machine with a condenser pressure of 50 mbar. The turbines are also capable of a large district heating load.

Layout and operating modes

This advanced turbine has 5 cylinders

- *one single flow VHP cylinder*
- *one combined HP/IP cylinder (associated with the district heating)*
- *two double flow LP cylinders (each with 1050mm long last stage blades)*

There are two journal bearings per rotor and the separate thrust bearing is located in the second pedestal.

There are three pairs of steam chests, each pair controlling one of the three steam flows from the boiler. Each chest is spring-mounted on the foundation and connected to the turbine by flexible loop pipes.

In full condensing mode, with a nominal output of 412 MW, the valves in the LP crossover pipes are open wide and the steam from each flow of the unsymmetrical double flow IP cylinder exhausts vertically upwards from the ends of the cylinder and is fully expanded in separate double flow LP cylinders .

In full district heading mode, the LP crossover valves are shut and the steam from each flow of the unsymmetrical double flow IP cylinder, apart from a small quantity for LP cylinder ventilation, exhausts vertically downwards from the ends of the cylinder. This steam passes to two separate district heaters, providing a nominal heating load of 450 MJ/s while a nominal power output of 320 MW is produced by the steam as it expands through the first three cylinders. For intermediate district heating loads the valves in the LP crossover pipes can modulate in an intermediate position to control the steam pressures to the district heating.

Steam chests and loop pipes

All the steam chests and loop pipes are of 9-12 per cent Cr steel.

The VHP steam chests use a self sealing autoclave joint for the chest covers, avoiding any heavy bolting. The valve spindles are guided close to the valve heads which are themselves shaped to minimise buffeting while they are controlling the high energy steam flow. A similar design is used for the HP steam chests.

VHP Cylinder

The single flow expansion is in a separate cylinder which permits a small rotor hub diameter of only 600mm with low centrifugal stress and low thermal inertia. With a length between bearing centres of only 4550mm, there is a high critical speed with good shaft vibration characteristics. The rotor discs are narrow relative to their pitch and have large fillet radii between them and the rotor hub, minimising rotor surface stress concentrations.

This low diameter design allows the longest blades for maximum expansion efficiency and the smallest diameters of interstage glands for minimum steam leakage. Due to the low axial thrust on the

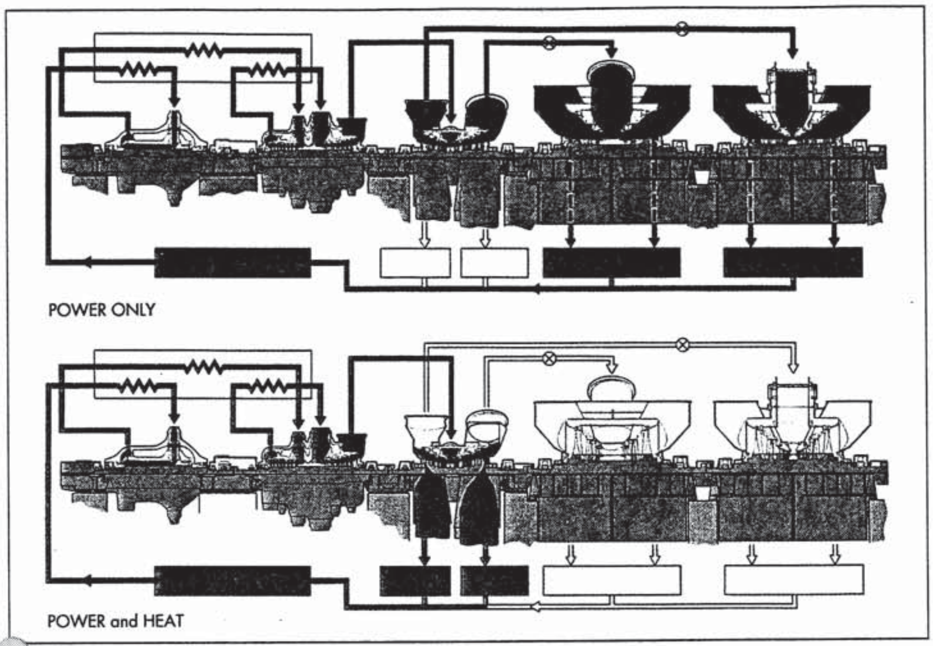

Operating modes of the Skaerbaek power and district heating plant

rotor produced by impulse blading, the balance piston diameter is only 640mm with correspondingly low thermal inertia and low steam leakage characteristics.

If conventional welded construction was used for the early diaphragms, the nozzles of the early diaphragms with large pressure drops would require to be very wide for diaphragm strength, with correspondingly reduced efficiency because of their poor aspect ratio.

Early diaphragms

The early diaphragms are therefore of bridge type construction, where the structural strength is provided by a few wide radial members and narrow efficient nozzle blading is slotted between the rings, all of 9CrMo material. Later diaphragms are of standard spacerband welded construction using 12CrMo material.

The low rotor diameter also minimises the diameters of the triple casing construction, limiting the pressure loading on the casings and permitting them to be of minimum thickness. The inner casing is of 9-12Cr material 120mm thick and the outer casing of 2.25CrMo material 120mm thick.

Nimonic 80A bolting is used close to the inlet section of the inner casing, together with austenitic bolt collars to compensate for the low expansion coefficient of the 9 12Cr casing relative to the Nimonic bolts. The turbine is designed for full arc admission, with the two semi-circular nozzle boxes interconnected by sealed rings at the horizontal joints.

HP/IP Cylinder

The HP and IP blade paths are both single flow, mounted in opposition to balance the small opposite axial thrusts in a single, compact combined HP/IP cylinder. The nominal steam supply pressures to each expansion are 74 bar and 19 bar respectively. The volumetric flows are therefore much higher than for the VHP cylinder and, with lower blade widths permissible because of lower steam loading, good blade aspect ratios allow high expansion efficiencies.

Also because of the lower steam pressures, a lower shah critical speed is allowable and permits a hub diameter of only 640mm with a centre gland diameter of 680mm with a distance between shah bearing centres of 5550mm. The same advantages as for the VHP cylinder therefore apply with respect to low rotor thermal inertia and low interstage steam leakage.

There are higher centrifugal stresses because of the longer runner blades on larger root diameters and therefore a small amount of cooling steam is introduced through the main gland to cool the centre gland region and the first stage discs of both flows of the rotor which is 9-12Cr material. Both HP and IP inlets are protected by 9 12Cr complete heat shields, reducing the maximum temperatures of the inner casing of 9-12Cr material, 100mm thick. Steam taken from before the last stage of the HP flow is used to condition the interspace between the casings before being returned to HP exhaust. The outer casing is of lCrMoV steel, 80mm thick, well suited to sustain the relatively high HP exhaust pressure and temperature. All diaphragms are of welded spacerband construction using 9CrMo material for the early stages and 12CrMo materials for the remainder.

Feedback

The design of the standard GEC Alsthom 680 MW single reheat turbine for conventional steam conditions (180 bar/540°C/540°C), used as a reference in this article, has benefited from such extensive development and feedback of operational experience that there is little scope for improvement. Major improvements in efficiency can come only from advancing steam conditions.

In view of the vast operating experience available, it is particularly important that this same classic design is applicable, with few changes, for steam conditions of 240 bar/565°C/565°C. Basically the same design and the same low alloy steels are used for this more advanced single reheat turbine, except that high chrome ferritic steels are preferred for components in contact with the inlet steam and for the IP rotor.

An efficiency improvement of about three per cent results from using the higher steam conditions relative to the conventional steam conditions. At the same time, the essential qualities of reliability, flexibility, maintainability and life expectancy are the same.

Further, the same classic design is still applicable for steam conditions of 300 bar/600°C/600°C, but with more extensive use of high chrome ferritic materials and conditioning steam. The high temperature strength and other favourable physical properties of the high chrome ferritic steels enable basically the same construction to be used for the currently most advanced single reheat turbine.

An efficiency improvement of about 6 per cent relative to conventional conditions is achieved, whilst again preserving the essential qualities of the machine.

The highest efficiencies currently obtainable are with double reheat, and turbine designs similar to that for Skaerbaek are available for steam conditions up to 300 bar/600°C/600°C/600°C which give an efficiency improvement of about 8 per cent relative to conventional. conditions. Again the classic design principles apply, with corresponding assurances of machine characteristics. The reheat turbine generator, which has always been the main supplier of reliable electrical power, is now being ordered for routine operation at the much higher efficiency levels possible with advanced steam conditions.

At these conditions, it retains the unique capability of expanding the steam produced by firing a wide variety of fuels to efficiently produce large amounts of electrical power and, if required, heat for either district heating or industrial processes. As the versatile capabilities of this mature technology are reconfirmed by further operational experience at advanced steam conditions, there will be many more applications worldwide for advanced steam turbines. ❑

The information in this article has been taken from a technical paper "Steam Turbines for Advanced Steam Conditions" by Dr A N Paterson, G. Simonin and J G Neft of GEC ALSTHOM. For more information contact: GEC ALSTHOM, Power Generation, Large Steam Turbine Group, Newbold Road, Rugby, CV21 2NH UK.
Fax: (UK+) 01788 531981

RWE Power

31. MPA-Seminar in Verbindung mit der Fachtagung
"Werkstoff- & Bauteilverhalten in der Energie- & Anlagentechnik"
Stuttgart, 13. + 14. Oktober 2005

Stand aktueller Projekte und Entwicklungstendenzen in der Kraftwerkstechnik

Dr. Johannes Ewers, Neue Technologien, RWE Power AG
johannes.ewers@rwe.com

Die kraftwerkstechnische Entwicklung steht im Zeichen der CO_2-Minderung

Die adäquate Strategie

Horizont 1 / Horizont 2 / Horizont 3	Umsetzung der Strategie
Ersatz von Altanlagen durch modernste neue Kraftwerkstechnik	■ Umfangreiche Investitionen in Neubauten
Deutliche Effizienzsteigerung für die nächsten Kraftwerksgenerationen	■ Zielgerichtete Entwicklungsprojekte inkl. Komponententests und Prototyperprobung
Prüfung der Zukunftsvision einer CO_2-freien fossilgefeuerten Kraftwerkstechnik	■ Breit aufgestellte Verbundprojekte zur Untersuchung u. Entwickl. der techn. Optionen

Die Stromwirtschaft engagiert sich in allen 3 strategischen Horizonten, um fortlaufend und nachhaltig deutliche CO_2-Minderungen zu verwirklichen.

Kraftwerksprojekte in Deutschland

(Stand: September 2005)

- Steinkohle (staubgefeuertes Dampfkraftwerk)
  - RWE: Hamm 2 x 750 MW
  - E.ON: Datteln 1.100 MW
  - steag/EVN: Duisburg 750 MW
  - Vattenfall: Hamburg 2 x 820 MW
  - } 4.990 MW
- Braunkohle (staubgefeuertes Dampfkraftwerk)
  - RWE: Neurath 2 x 1100 MW
  - Vattenfall: Boxberg 670 MW
  - } 2.870 MW
- Erdgas (Vorschaltgasturbine an Braunkohleblock)
  - RWE: Weisweiler 2 x 270 MW } 540 MW
- Erdgas (GuD)
  - RWE: Lingen 800 MW
  - E.ON: Irsching 800 MW
  - Concord/EnBW: Lubmin 1200 MW
  - Statkraft: Hürth 800 MW
  - Statkraft/Mark-E: Herdecke 400 MW
  - Trianel: Hamm 800 MW
  - } 4.800 MW

} 13.200 MW

Das Volumen der derzeit in Planung befindlichen fossil gefeuerten Kraftwerke beträgt etwa 10 % der gesamten in Deutschland installierten Kraftwerksleistung bzw. 17 % der fossil gefeuerten Kraftwerksleistung. Weitere Projekte sind angekündigt.

Heutiger Stand der Technik

für Braunkohle und Steinkohle

BoA 1, 1.012 MW, Kraftwerk Niederaußem

Status	Dauerbetrieb seit 2003
Dampfparameter	275 bar / 580°C / 600°C
Netto-Wirkungsgrad	> 43 %

BoA 2/3, 2 x 1.100MW, Kraftwerk Neurath

Status	in Bau, 2010 am Netz
Dampfparameter	272 bar / 600°C / 605°C
Netto-Wirkungsgrad	> 43 %

Referenzkraftwerk NRW

Status	Studie, neue Projekte in Planung
Dampfparameter	292 bar / 600°C / 620°C
Netto-Wirkungsgrad	45,9 %

- Dieser Stand der Technik bietet weltweit großes Potential zur Klimavorsorge.
- Die Erfahrungen zeigen aber auch, dass der Einsatz modernster Technik und deren Weiterentwicklung ein besonders sorgfältiges und kritisches Vorgehen verlangt, um Einsatzreife zu sichern.

Zügige effiziente Klimavorsorge durch State of the Art-Kraftwerke weltweit

RWE

Europäische Spitzentechnik des superkritischen Dampfkraftwerks weltweit einsetzbar:

BoA, Deutschland
η > 43 %

Wai Gao Qiao, China
η = 42,4 %

Der Neubaubedarf weltweit bietet die große Chance massiver CO_2-Minderung durch Einsatz modernste State of the Art-Technik.

Sukzessiver Ersatz aller Kohlekraftwerke ▶ **- 2 Mrd. t CO_2/a (- 35 %)**

Erfahrungen mit dem Stand der Technik

BoA 1: Ausfälle durch Werkstoffprobleme

RWE

Abplatzen von inneren Magnetitschichten im ÜH5 / ZÜ3 (April 2004)
=> Ablagerungen → Verstopfungen → Überhitzung → Rohrreißer
- Verfügbarkeitseinbuße: 24 % im Jahr des Schadensfalls
- Minderstromerzeugung: 1,7 TWh

Austausch ZÜ 3 durch DMV 310N (Juni 2004)
- Verfügbarkeitseinbuße: 26 % im Jahr des Austauschs
- Minderstromerzeugung: 1,8 TWh

Werkstoff X3CrNiMoN17-13 wurde erstmalig bei den hohen Temperaturen von 580/600°C eingesetzt und zeigte dieses unerwartete Verhalten.
=> Ausreichend lange Tests unter Betriebsbedingungen erforderlich!
=> Untersuchungen in Werkstoff-Testrigs sind wichtig und notwendig!
=> Geeignete konstruktive Lösungen einbeziehen.

Erfahrungen mit dem Stand der Technik

Aktualisierte Erkenntnisse aus der Werkstoffentwicklung

RWE

100.000 h Zeitstandfestigkeiten für E911 und P92

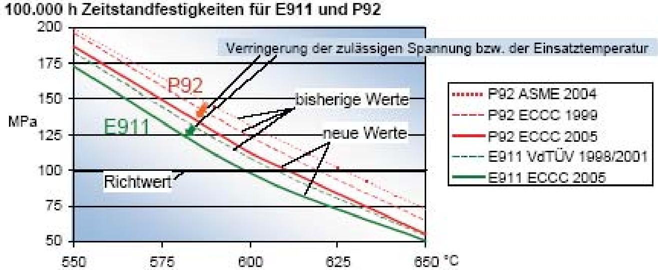

- Aktuelle Auswertungen zeigen deutlich verringerte Zeitstandfestigkeiten, als bisher extrapoliert wurde. Dies lehrt:
- **Werkstoffkennwerte benötigen die Absicherung durch ausreichend lange Erprobung.**

Empfehlungen für Neubauten und Weiterentwicklungen

RWE

Für den Bau modernster State of the Art-Technik:

- Erfahrungen systematisch aufarbeiten, kommunizieren und einfließen lassen.
- Risikominimierung, u. a. ausreichend erprobte Werkstoffe/Komponenten einsetzen.

Für die technische Weiterentwicklung:

- Systematische Werkstoffentwicklung und –qualifizierung.
- Sicherung von Fertigungs- und Montagefähigkeiten für neue Werkstoffe.
  - Anbieterkreis für Großkomponenten drastisch reduziert.
  - Den Herausforderungen bei Schmiedeteilen sind nur noch wenige gewachsen.
  - Fertigungs- und Montage Know-How/ -Kapazitäten immer geringer.
- Vielzahl parallel laufender Entwicklungsprogramme und –initiativen stärker aufeinander abstimmen/zusammenführen.

Dieses Engagement sichert nicht nur den Einsatz modernster Kraftwerkstechnik als wichtigen Beitrag der Klimavorsorge, sondern auch die Wettbewerbsfähigkeit der europäischen Industrie.

Horizont 2: Entwicklungslinien zur weiteren Steigerung der Effizienz

Wirkungsgradsteigerung	Beispiele
Werkstoffentwicklung zur Steigerung der Prozessparameter Druck und Temperatur	Absicherung hochwarmfester Stähle, Nickelbasis-Werkstoffe für 700°C-Kraftwerk
Entwicklung von neuen (Teil-)Prozessen	Braunkohlevortrocknung Steigerung des Turbinenwirkungsgrads,
Optimierung von Komponenten	Senkung d. Eigenbedarfs (REA, Pumpen, ...)

aber auch Steigerung der Verfügbarkeit

Beherrschung wechselnder und/oder schwieriger Kohlen	Optimierung der Heizflächenreinigung

Technologische Meilensteine zur Wirkungsgradsteigerung

2015

BoA-Plus: BoA mit Braunkohlevortrocknung
η: + 4 %-Punkte

Die von RWE entwickelte WTA-Technologie erlaubt die Rückgewinnung der Trocknungsenergie durch Rekondensation des verdampften Wassers.

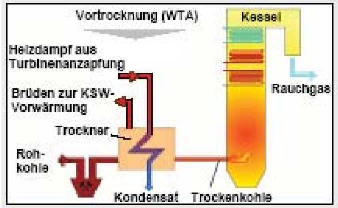

2020

700°C-Kraftwerk
η: + 4 %-Punkte

Die Anhebung der Dampfparameter von 280 bar/600°C auf 350 bar/700°C erfordert eine neue Werkstoffgeneration insbesondere für:

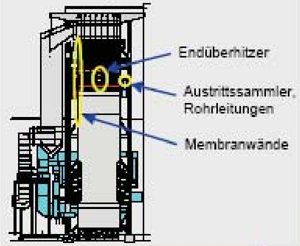

Der Wirkungsgrad von kohlegefeuerten Kraftwerken wird ab 2020 die Schwelle von 50 % überschreiten.

Die Entwicklung von BoA-Plus zur kommerziellen Reife

Entwicklungsziel:
- + 4 %-Pkte Wirkungsgrad-Steigerung
- Gleiche Stromerzeugungskosten

Erreichter Stand:
- Erfolgreicher Abschluss der Entwicklung der WTA-Feinkorntrocknung in Frechen im Okt. 2004, 15 t/h TBK-Leistung

(Im Bild: Einbau des Trockners in Frechen)

Projekt WTA-Prototyp an BoA 1 von RWE Power gestartet:
- Bau u. Betrieb 1:1-Trocknungsmoduls (110 t/h TBK, entspr. 300 MW_{el}, 50 Mio. €)
- Großtechn. Absicherung der TBK-Feuerung (Mitverbrennung in BoA 1)
- Genehmigung liegt vor, Bauentscheidung ist gefallen, Vergaben laufen

Ziel: Vortrocknung für Neubauplanungen ab 2009 kommerziell verfügbar haben.

Werkstoffentwicklung zur Steigerung der Dampfparameter

Wichtige Vorhaben zur Entwicklung des 700°C-Kraftwerks

- **COMTES700 + Turbinenregelventil**
  Herstellung und Erprobung aller wichtigen Dampferzeugerkomponenten und des Turbinenregelventils im Kraftwerk Scholven, Block F.
  Seit 15. Juli 2005 in Betrieb.
  EU-gefördertes Projekt der Industrie.

- **Testrigs in Esbjerg u. Weisweiler, KOMET650 in Westfalen**
  Teststrecken für Überhitzerrohre in Stein- u. Braunkohleblöcken.
  Testrig-Einbau in 2004 erfolgt,
  Eigenfinanzierung der Industrie.

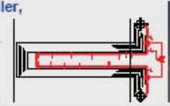

Das 700 °C stellt eine technologische Herausforderung dar insbesondere bezüglich der Erreichung der Wirtschaftlichkeit.

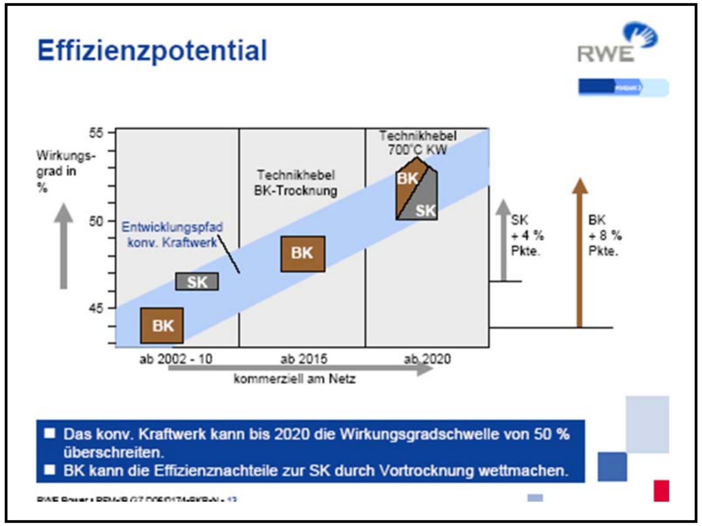
Effizienzpotential
RWE
Wirkungs-
grad in
%
55
50
45
Entwicklungspfad
konv. Kraftwerk
Technikhebel
BK-Trocknung
Technikhebel
700°C KW
BK
SK
BK
SK
BK
SK
+ 4 %
Pkte.
BK
+ 8 %
Pkte.
ab 2002 - 10
ab 2015
ab 2020
kommerziell am Netz
Das konv. Kraftwerk kann bis 2020 die Wirkungsgradschwelle von 50 % überschreiten.
BK kann die Effizienznachteile zur SK durch Vortrocknung wettmachen.

Zur Unterstützung der in Kyoto vereinbarten Emissionsreduktionen klimarelevanter Treibhausgase wurde von der EU die Einführung eines Handels mit Emissionsrechten ab dem Jahr 2005 beschlossen. CO_2-Emissionen bekommen damit einen wirtschaftlichen Wert. Es ist deshalb davon auszugehen, dass künftig in zunehmendem Maße in Technologien zur Vermeidung von CO_2-Emissionen investiert wird. Die interne Zusatzfeuerung mit Erdgas oder Wasserstoff in Dampfkraftwerken ist eine dieser Technologien, mit der sich die spezifischen CO_2-Emissionen bei gleichzeitiger Erhöhung von Wirkungsgrad und Leistung reduzieren lassen.

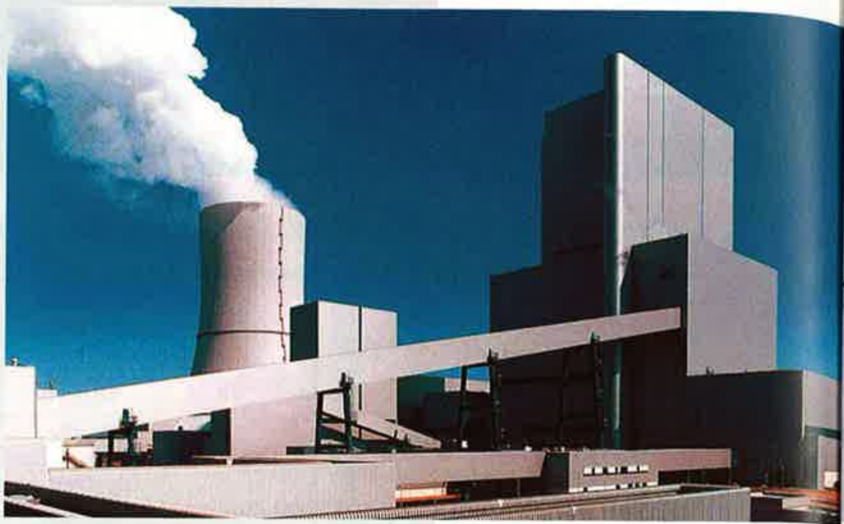

Interne Zusatzfeuerung

Maßnahme zur Reduzierung der CO_2-Emissionen von Dampfkraftwerken

Bei Dampfkraftwerken wird üblicherweise die gesamte im Prozess benötigte Wärme durch Kohleverbrennung im Dampferzeuger freigesetzt und von den heißen Verbrennungsgasen auf das Wasser bzw. den Wasserdampf übertragen. Als eine der maßgebenden Einflussgrößen auf den Wirkungsgrad des Kraftwerksprozesses wird die maximale Temperatur der Wärmeübertragung durch die Werkstoffeigenschaften der Wärmeüberträgerrohre bestimmt. Die Temperaturbeschränkungen lassen sich jedoch umgehen, wenn die Wärme direkt im Dampfstrom freigesetzt wird. So können zum Beispiel bei der internen Zusatzfeuerung Erdgas oder Wasserstoff mit reinem Sauerstoff im Dampfstrom zwischen Teilturbinen oder zwischen Dampferzeuger und -turbine verbrannt werden (**Bild 1**).

Bei der Verbrennung von Erdgas mit reinem Sauerstoff entstehen als Verbrennungsprodukte Wasserdampf und CO_2, die mit dem im Kessel erzeugten Wasserdampf in der Turbine als Arbeitsmittel genutzt werden können. Wird das bei der Zusatzfeuerung entstehende Wasserdampf-CO_2-Gemisch nach der Kondensation des im Kreislauf verbleibenden Wasserdampfes im Kondensator ausgekoppelt, verdichtet und gekühlt, kondensiert der überwiegende Teil des Wasserdampfes aus. Als Rückstand verbleibt nahezu reines, gasförmiges CO_2, das verflüssigt, abtransportiert und zum Beispiel in erschöpften Öl- oder Erdgasfeldern gelagert werden kann [1; 2]. Wenn als Brennstoff Wasserstoff zum Einsatz kommt, der durch Reformierung von Erdgas hergestellt wird, kann das dabei entstehende CO_2 relativ einfach aus dem Produktgas der Reformierung abgetrennt werden. Für beide Fälle gilt, dass das CO_2 mit einem vergleichsweise geringen Energieaufwand zurückgehalten werden kann.

Der Kraftwerksprozess mit interner Erdgas-Zusatzfeuerung in der Zwischenüberhitzung zeichnet sich gegenüber dem konventionellen Kraftwerksprozess durch folgende Besonderheiten aus:

- Der Speisewasserbehälter muss an eine Anzapfung oberhalb der internen Zusatzfeuerung angeschlossen werden, um zu vermeiden, dass im gesamten Kreislauf ein Wasserdampf-CO_2-Gemisch vorliegt.
- Das Anzapfkondensat der Niederdruckvorwärmer muss aus demselben Grund in den Kondensator geleitet werden und kann nicht – wie üblich – an dem jeweiligen Vorwärmer dem Hauptkondensat zugemischt werden.

Autoren

Prof. Dr.-Ing. **Christoph Kail**, Jahrgang 1965, von 1986 bis 1991 Maschinenbaustudium an der Universität Hannover. Von 1991 bis 1999 beim Erlanger Siemens-Bereich Power Generation Gruppenleiter „Wärmekreislaufrechnung, Kaltes Ende, Kondensatoren und fortschrittliche Kraftwerkskonzepte", promovierte 1998 am Lehrstuhl für Thermische Kraftanlagen der TU München. Seit 1999 ist er Professor für Energietechnik an der FH Südwestfalen in Meschede.

Dr.-Ing. **Bert Rukes**, Jahrgang 1949, Studium des Allgemeinen Maschinenbaus an der FH Düsseldorf und des Theoretischen Maschinenbaus an der TU Berlin einschließlich Promotion von 1967 bis 1978, seit 1978 bei Siemens PG, heute Leiter für den Bereich „Prozesstechnik".

Dipl.-Ing. **Georg Haberberger**, Jahrgang 1967, Studium des Maschinenbaus von 1988 bis 1992 an der FH Würzburg-Schweinfurt, seit 1982 bei Siemens PG Gruppenleiter „Wärmekreislaufrechnung Dampfkraftwerke, Kaltes Ende, Kondensatoren".

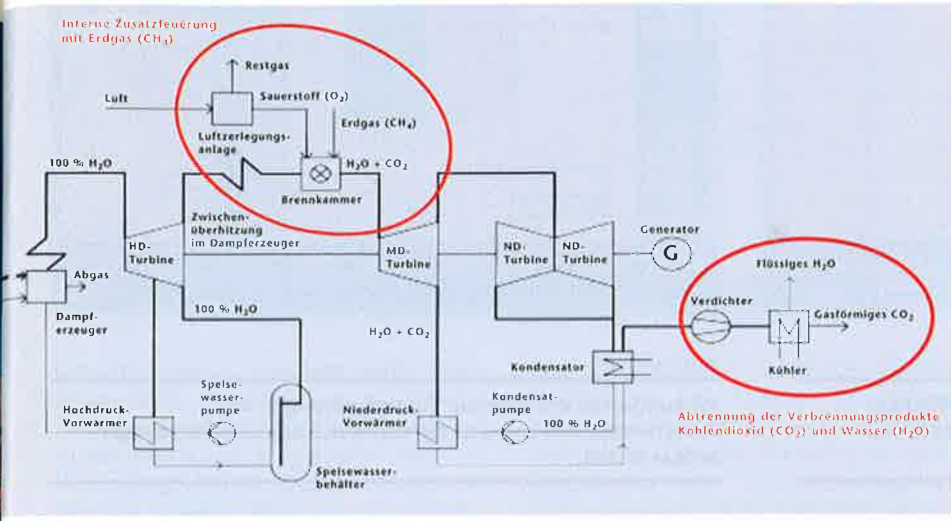

Bild 1

Schema eines Dampfkraftwerkes mit interner Zusatzfeuerung auf Erdgasbasis in der Zwischenüberhitzung.

ternen Zusatzfeuerung kann bei entsprechender Bevorratung relativ schnell zur Verfügung gestellt werden, so dass sie auch zur Abdeckung von Spitzenlastanforderungen oder zur Stützung der Netzfrequenz bei großen Belastungsschwankungen eingesetzt werden kann. Es bleibt allerdings zu prüfen, zu welchen Beschränkungen die maximal zulässigen Temperaturgradienten der Dampfturbine führen.

- Die im Vergleich zu konventionellen Dampfkraftwerken höheren Dampftemperaturen nach der internen Zusatzfeuerung ermöglichen den Einsatz eines zusätzlichen getrennten Enthitzers zur Erhöhung der Vorwärm-Endtemperatur des Speisewassers.
- Die interne Zusatzfeuerung erfordert die Neuentwicklung von einigen Komponenten des Kraftwerkes. Hier ist vor allem die mit einer Dampfkühlung versehene Brennkammer zu nennen, in der unter Anwesenheit von Wasserdampf eine stöchiometrische Verbrennung von Erdgas oder Wasserstoff mit reinem Sauerstoff stattfindet. Um zu vermeiden, dass zum Beispiel Sauerstoff oder Wasserstoff in nennenswerten Anteilen in die Turbine gelangen, sollte die Verbrennung möglichst vollständig und die Regelung der Brenngas- und Sauerstoffmenge relativ genau sein. Derartige Brennkammern wurden unter anderem von Jericha [3] und Inoue [4] untersucht. Auch die Mitteldruck-Dampfturbine, die mit einer Eintrittstemperatur bis 900 °C beaufschlagt wird, muss an diese neuen Bedingungen angepasst werden. Werden dafür Konstruktionsprinzipien und Werkstoffe aus dem Gasturbinenbau eingesetzt, sollten diese Temperaturen beherrschbar sein. Falls Dampf für die Kühlung der Turbine erforderlich ist, kann dieser aus der kalten Seite der Zwischenüberhitzung entnommen werden.
- Ferner ist zu prüfen, welche Auswirkungen das bei der Erdgas-Variante im Dampfstrom vorliegende CO_2 auf die Werkstoffe der Turbine, die Wasserchemie im gesamten Kreislauf und auf den Wärmeübergang im Kondensator und in den Speisewasservorwärmern hat. Entsprechende Untersuchungen müssen für geringe Sauerstoff-, Wasserstoff- und Kohlenmonoxidmengen durchgeführt werden. Für eine möglichst vollständige Abtrennung dieser Gase aus dem Kondensat wird voraussichtlich der Einsatz einer Kondensatreinigungsanlage notwendig sein. Zur Vermeidung von Korrosionseffekten in den Endstufen der ND-Turbine ist es unter Umständen sinnvoll, den Endpunkt der Expansion aus dem Nassdampf- in das Dampfgebiet zu verschieben. Da das Ende der Expansion bei einer Dampftemperatur von 900 °C und einem Druck von 59 bar am Austritt der internen Zusatzfeuerung ohnehin bereits nah an der Taulinie liegt, lässt sich mit einer moderaten Erhöhung der Temperatur oder einer geringfügigen Absenkung des Druckes eine Kondensation in der ND-Turbine vermeiden.
- Die zusätzliche Leistung der in-

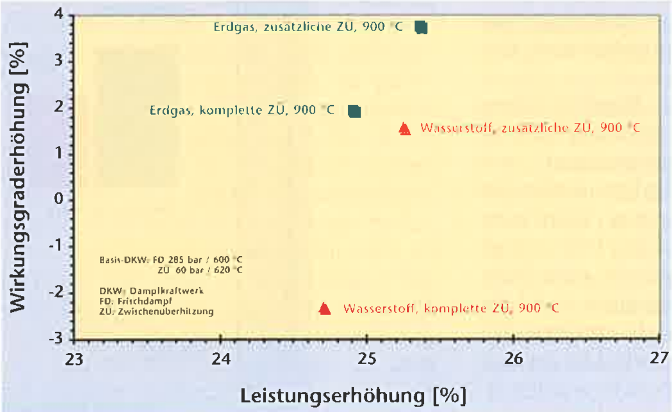

Bild 2

Wirkungsgrad- und Leistungserhöhungen durch die interne Zusatzfeuerung in der Zwischenüberhitzung.

Höhere Effizienz und Leistung bei geringerem CO_2-Ausstoß

Die Berechnung des Wirkungsgrades, der Leistung und der Kohlendioxid-Emissionen eines Dampfkraftwerks mit interner Zusatzfeuerung in der Zwischenüberhitzung wurde anhand eines steinkohlebefeuerten Dampfkraftwerkes mit einem Frischdampfzustand von 285 bar und 600 °C, einer Zwischenüber-

Technische Container-Lösungen
nach individuellem Bedarf
Ideal auch für den Einsatz als "BHKW"

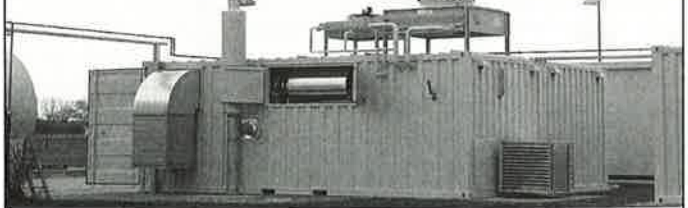

R. Thollembeek GmbH
Technische Lösungen
www.container-technik.de
Planung · Vertrieb
Postfach 2047
71010 Böblingen
Tel. 0 70 31-28 52 22
Fax 0 70 31-28 52 23
info@thollembeek.de

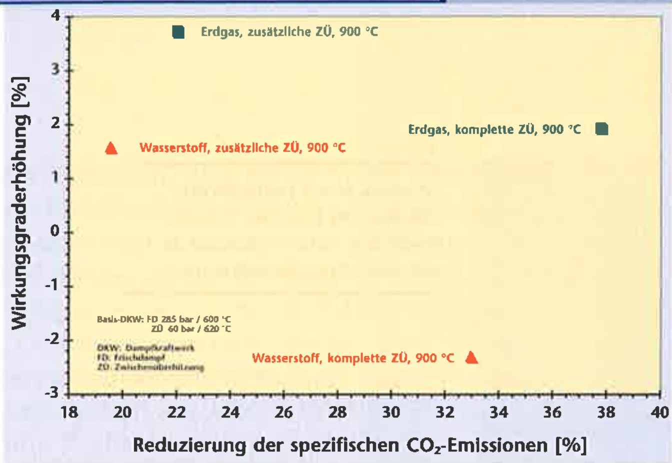

Bild 3

Wirkungsgraderhöhung und Reduktion der spezifischen CO_2-Emissionen durch die interne Zusatzfeuerung in der Zwischenüberhitzung.

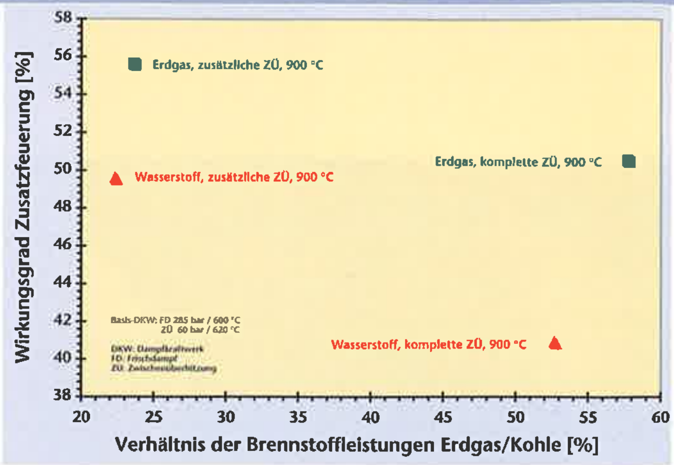

Bild 4

Wirkungsgrad der internen Zusatzfeuerung in der Zwischenüberhitzung und Verhältnis der Brennstoffleistungen Erdgas/Kohle.

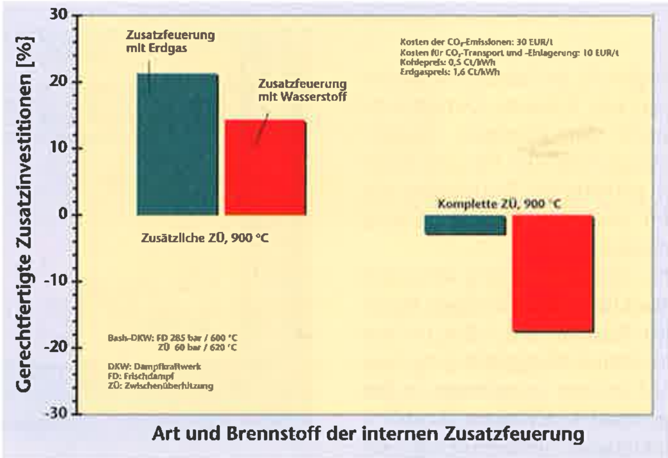

Bild 5

Gerechtfertigte Zusatzinvestitionen steinkohlebefeuerter Dampfkraftwerke mit interner Zusatzfeuerung in der Zwischenüberhitzung.

hitzung bei 60 bar und 620 °C, acht Vorwärmstufen und einem getrennten Enthitzer durchgeführt.

Bei Einsatz eines Nasskühlturms (Kondensationsdruck: 45 mbar) und bei einem Frischdampfmassenstrom von 400 kg/s erreicht das Kraftwerk ohne interne Zusatzfeuerung eine elektrische Nettoleistung von rund 510 MW und einen Nettowirkungsgrad von rund 46 %. In **Bild 2** ist die Wirkungsgrad- und Leistungserhöhung durch die interne Zusatzfeuerung in der Zwischenüberhitzung dargestellt. Alle Punkte wurden jeweils als Neuauslegung des Kraftwerkes mit gleichem Frischdampfmassenstrom berechnet. Als Brenngas wird Erdgas oder durch allotherme Reformierung von Erdgas hergestellter Wasserstoff eingesetzt. Die interne Zusatzfeuerung wird entweder als zusätzliche Zwischenüberhitzung zu der im Dampferzeuger stattfindenden Zwischenüberhitzung oder als komplette (alleinige) Zwischenüberhitzung angewendet. Die Austrittstemperatur der internen Zusatzfeuerung beträgt 900 °C.

Die maximale Wirkungsgraderhöhung wird bei einer Zusatzfeuerung mit Erdgas als zusätzliche Zwischenüberhitzung erreicht und beträgt 3,7 %. Wird anstatt des Erdgases Wasserstoff als Brennstoff eingesetzt, so ist der Wirkungsgradgewinn mit 1,6 % niedriger, da für die Herstellung des Sekundärenergieträgers Wasserstoff Energie aufgewendet werden muss. Die Leistungserhöhungen sind mit rund 25 % in beiden Fällen ungefähr gleich groß.

Die Wirkungsgraderhöhung durch die interne Zusatzfeuerung in der Zwischenüberhitzung kann zum einen auf die höhere mittlere Temperatur der Wärmezufuhr (Carnot-Faktor [5]) zurückgeführt werden. Zum anderen wird der Expansionswirkungsgrad der Niederdruckturbine durch einen höheren Dampfgehalt in den letzten Stufen verbessert. Ferner ist mit Blick auf den Wirkungsgrad zu erkennen, dass es nicht sinnvoll ist, die komplette Zwischenüberhitzung über eine interne Zusatzfeuerung zu realisieren. Dies liegt daran, dass die Kohle bei den hier vorliegenden Randbedingungen im Dampfturbinenprozess (Clausius-Rankine-Prozess) mit einem höheren Wirkungsgrad umgesetzt wird als das Erdgas im Gasturbinenprozess (Joule-Prozess). Um einen möglichst hohen Wirkungsgrad zu erreichen, sollte Kohle nicht durch Erdgas substituiert, sondern lediglich ergänzt werden.

Wird das bei der Zusatzfeuerung entstehende CO_2, wie oben beschrieben, dem Prozess entzogen, gespeichert und somit nicht der Atmosphäre zugeführt, sinken die spezifischen CO_2-Emissionen pro Kilowattstunde Elektrizität (**Bild 3**). Je mehr Brennstoff in der internen Zusatzfeuerung eingesetzt wird, umso größer ist die Emissionsreduktion. Neben dem Verhältnis der Brennstoffleistungen (Erdgas/Kohle) hängt die erzielbare CO_2-Emissionsminderung auch von dem Wirkungsgrad ab, mit dem der Brennstoff der internen Zusatzfeuerung in elektrische Energie umgewandelt wird. So sinken die spezifischen CO_2-Emissionen im günstigsten Fall einer internen Zusatzfeuerung mit Erdgas bei kompletter Zwischenüberhitzung um etwa 37,8 %. Als Wirkungsgrad der Zusatzfeuerung kann das Verhältnis der Änderung der abgegebenen elektrischen Leistung zur Änderung der zugeführten Brennstoffleistung im Vergleich zum Dampfkraftwerk ohne Zusatzfeuerung definiert werden (**Bild 4**). Dieser Wirkungsgrad kennzeichnet die Qualität eines erdgasbefeuerten Kraftwerksprozesses, bei dem das Kohlendioxid zurück-

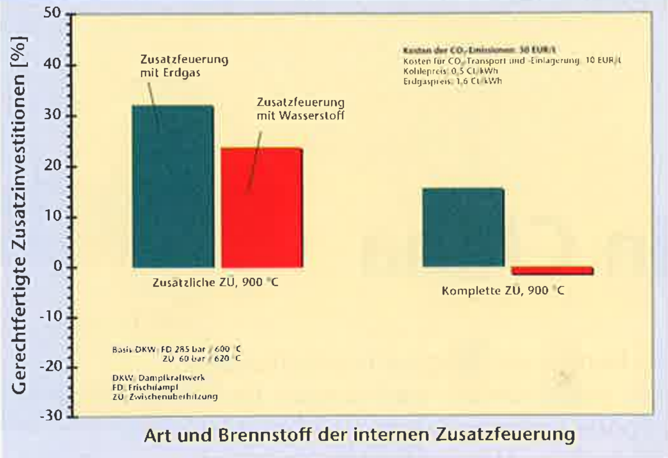

Bild 6

Gerechtfertigte Zusatzinvestitionen braunkohlebefeuerter Dampfkraftwerke mit interner Zusatzfeuerung in der Zwischenüberhitzung.

gehalten und in flüssiger Form abgegeben wird. Bei einer als zusätzliche Zwischenüberhitzung ausgeführten Zusatzfeuerung auf Erdgasbasis wird ein Wirkungsgrad von 55,7 % erzielt, ein deutlich höherer Wert als bei anderen Konzepten zur CO_2-Rückhaltung in Großkraftwerken. Bei erdgasbefeuerten GuD-Kraftwerken mit CO_2-Rückhaltung werden Wirkungsgrade von 45 bis 50 % erzielt, bei GuD-Kraftwerken mit Kohlevergasung (IGCC) Werte von 40 bis 45 % und bei kohlebefeuerten Dampfkraftwerken Werte von 30 bis 35 % [6 bis 13].

Das Verhältnis der Brennstoffleistungen Erdgas/Kohle variiert über einen weiten Bereich und beträgt hier maximal 57,8 %. Die Zusatzfeuerung bietet demnach eine gewisse Flexibilität im Hinblick auf die eingesetzte Brennstoffart und den Umfang der Kohlendioxid-Rückhaltung.

Mögliche Zusatzinvestitionen

Um einen ersten Eindruck über die Wirtschaftlichkeit von Dampfkraftwerken mit interner Zusatzfeuerung zu erhalten, werden unter der Annahme gleicher Stromerzeugungskosten die gerechtfertigten Zusatzinvestitionen gegenüber üblichen Dampfkraftwerken ermittelt. Für diese Berechnungen werden spezifische Kosten für CO_2-Emissionen von 30 €/t angenommen. Die Kosten für den Transport und die Einlagerung des zurückgehaltenen Kohlendioxids werden mit 10 €/t angenommen [14; 15]. Weitere Annahmen sind:

- Auf den Heizwert bezogener Brennstoffpreis von Steinkohle: 0,005 €/kWh,
- auf den Heizwert bezogener Brennstoffpreis von Erdgas: 0,016 €/kWh,
- Kosten für Wartung, Instandhaltung und Betriebsmittel: 0,0075 €/kWh(el.),
- spezifische Anlagenkosten des konventionellen Dampfkraftwerkes ohne interne Zusatzfeuerung: 850 €/kW(el.),
- Anzahl der äquivalenten Volllaststunden (Grundlastkraftwerk): 7 500 h/a,
- Personalkosten pro Kraftwerksblock einer 2-Block-Anlage: 2,5 Mill. €/a.

Wie in **Bild 5** zu sehen ist, betragen die gerechtfertigten Zusatzinvestitionen von mit Steinkohle befeuerten Dampfkraftwerken mit interner Zusatzfeuerung gegenüber üblichen mit Steinkohle befeuerten Dampfkraftwerken im günstigsten Fall einer Zusatzfeuerung mit Erdgas als zusätzliche Zwischenüberhitzung 21,3 % der Basis-Investition. Wird die komplette Zwischenüberhitzung durch interne Zusatzfeuerung realisiert, sind Zusatzinvestitionen nicht mehr gerechtfertigt (negative Werte), da günstige Kohle durch teures Erdgas ersetzt wird. Die Substitution von Kohle durch Erdgas erscheint bei Dampfkraftwerken also nicht nur unter thermodynamischen, sondern auch unter wirtschaftlichen Gesichtspunkten nicht sinnvoll zu sein. Im Fall einer Zusatzfeuerung mit dem Sekundärenergieträger Wasserstoff fließen die Umwandlungsverluste durch die Wasserstofferzeugung ein, so dass die gerechtfertigten Zusatzinvestitionen geringer als bei einer Zusatzfeuerung mit Erdgas ausfallen.

Bei Dampfkraftwerken auf Braunkohlebasis sind höhere Zusatzinvestitionen möglich als bei Steinkohlekraftwerken, da bei der Verbrennung von Braunkohle mehr Kohlendioxid freigesetzt wird als bei Steinkohle. Für die maximal gerechtfertigten Zusatzinvestitionen wird beim Einsatz von Braunkohle unter ansonsten gleichen Randbedingungen ein Wert von 32,1 % ausgewiesen (**Bild 6**).

Die in den Bildern 2 bis 4 dargestellten Ergebnisse, die Erhöhung von Wirkungsgrad und Leistung sowie die Reduzierung der spezifischen Kohlendioxid-Emissionen, gelten bei gleicher Qualität des Basisprozesses ohne interne Zusatzfeuerung für stein- und braunkohlebefeuerte Dampfkraftwerke.

Literatur

[1] Hanisch, C.: Nicht mehr klimawirksam – Entsorgung des Treibhausgases CO_2 im Meer geplant. Süddeutsche Zeitung vom 8. September 1998, Ressort Wissenschaft.

[2] Gas- und Ölfelder als CO_2-Lager. Energie & Management vom 15. Oktober 2002.

[3] Jericha, H. et al.: Weiterentwicklung des H_2/O_2-Dampfprozesses (Brennkammer und Hochtemperaturturbine). VGB Kraftwerkstechnik 73 (1993), Heft 9, S. 781–786.

[4] Inoue, H. et al.: Research and Development of Methane-Oxygen Combustor for Carbon Dioxide Recovery Closed-Cycle Gas Turbine. 23rd Cimac World Congress on Combustion Engine Technology for Ship Propulsion, Power Generation, Rail Traction vom 7. bis 10. Mai 2001 in Hamburg.

[5] Baehr, H. D.: Thermodynamik. Springer Verlag, Berlin, 2002.

[6] Anderson, R. E. et al.: A Power Plant Concept which Minimizes the Cost of Carbon Dioxide Sequestration and Eliminates the Emission of Atmosperic Pollutants. 4th International Conference on Greenhouse Gas Control Technologies, Interlaken, Schweiz, 1998.

[7] Edmonds, J. A. et al.: The Role of Carbon Management Technologies in Adressing Atmospheric Stabilization of Greenhouse Gases. Pacific Northwest National Laboratory, Washington.

[8] Freund, P.; Thambimuthu, K. V.: Options for Decarbonising Fossil Energy Supplies. Conference Combustion Canada '99, Calgary, Canada, 1999.

[9] Marion, J. et al.: Controlling Power Plant CO_2 Emissions: A Long Range View. First National Conference on Carbon Sequestration, U.S. Department of Energy, National Energy Technology Laboratory, 15. bis 17. Mai 2001.

[10] Marion, J. et al.: Engineering Feasibility of CO_2 Capture on an Existing US Coal-Fired Power Plant. 26th International Conference on Coal Utilization & Fuel Systems vom 5. bis 8. März 2001 in Clearwater, Florida, USA.

[11] Bolland, O.; Mathieu, P.: Comparison of two CO_2 Removal Options in Combined Cycle Power Plants. Energy Conversion and Management, 39 (16–18), pp. 1653–1663.

[12] Kvamsdal, H. M. et al.: Exergy Analysis of Gas-Turbine Combined Cycle with CO_2 Capture using Pre-Combustion Decarbonization of Natural Gas. ASME Turbo Expo 2002 vom 3. bis 6. Juni 2002 in Amsterdam, Niederlande.

[13] Göttlicher, G.: Energetik der Kohlendioxidrückhaltung in Kraftwerken. Fortschritt-Berichte VDI, Reihe 6, Nr. 421, 1999.

[14] Hendriks, C. A. et al.: Cost of Carbon Dioxide Removal by Underground Storage. 5th International Conference on Greenhouse Gas Control Technologies, Cairns, Australia, 2000.

[15] Herzog, H. J.: The Economics of CO_2 Capture. 4th International Conference on Greenhouse Gas Control Technologies, Interlaken, Switzerland, 1998.

Pre-designed steam turbines

The comprehensive Siemens product range up to 10 megawatts

SST-010

(formerly known as EPM = Expansion Power Module)

up to 110 kW

The SST-010 is a compact turbogenerator designed to expand natural gas in pressure regulating stations as a direct driving turbine in pipe installation.

Technical data

- Power output up to 110 kW
- Gas pressure up to 70 bar(a) / 1015 psi
- Gas flow rates up to 15,000 m³/h / 530,000 ft³/h
- Exhaust gas pressure up to 25 bar(a) / 363 psi
- Turbine wheel diameter 400 mm / 15.75 in

Typical dimensions

Length 1.2 m / 4 ft
Width 0.8 m / 2.6 ft
Height 0.9 m / 3 ft

Features

- Low-maintenance because of the simple design
- Extremely failure safe
- Quick-start compatible
- Casing flanged directly into the gas pipeline
- ATEX approved

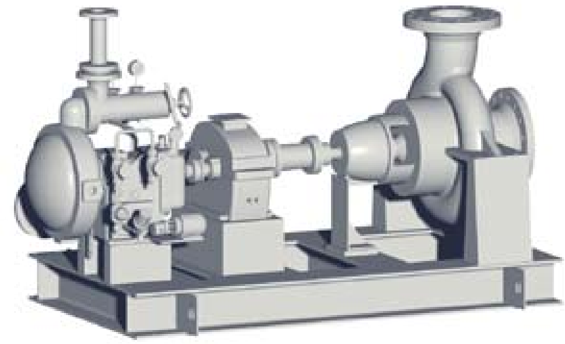

SST-050

(formerly known as AF or BF series)

up to 750 kW

The SST-050 is a single-stage, backpressure steam turbine in which the flow passes axially through the blading. It is mainly used as a power source for pumps or fans and especially as a stand-by unit with quick-start capability.

Technical data

- Power output up to 750 kW
- Inlet pressure up to 101 bar(a) / 1465 psi
- Inlet temperature dry saturated steam up to 500° C / 930° F
- Speed acc. to driven machine
- Exhaust pressure: back pressure up to 11 bar(a) / 160 psi

Typical dimensions

Length 1 m / 3.3 ft*
Width 1 m / 3.3 ft*
Height 1.3 m / 4.3 ft*

*turbine only

Features

- Low-maintenance because of the simple design
- Extremely failure safe
- Quick-start compatible
- Turbine with integral oil supply
- Meet requirements of API 611 / 612*
- ATEX version available

*if overhung design and integral gear is accepted

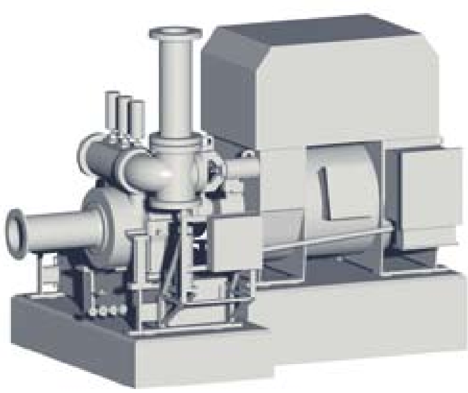

SST-060

(formerly known as AFA, CFA or CFR series)

up to 6 MW
The SST-060 stand out by their rugged design and renowned reliability even under the most severe operating conditions. They are ideal for saturated steam service. Their suitability for use as condensation or back-pressure turbines in combination with various integral gears modules opens up a broad application range.

Technical data

- Power output up to 6 MW
- Inlet pressure up to 131 bar(a) / 1900 psi
- Inlet temperature dry saturated steam up to 530° C / 985° F
- Speed acc. to driven machine
- Exhaust pressure: back pressure up to 29 bar(a) / 420 psi or vacuum

Typical dimensions

Length 1.5 m / 4.9 ft*
Width 2.5 m / 8.2 ft*
Height 2.5 m / 8.2 ft*

*turbine only

Features

- Backpressure or condensing type
- Package unit design
- Oil unit integrated in base frame
- Nozzle group control valves available
- Quick-start without pre-heating
- Tailor made
- Meet requirements of API 611 / 612*
- ATEX version available
- Suitable for ORC (Organic Rankine Cycle)
- Suitable for gas expansion

*if overhung design and integral gear is accepted

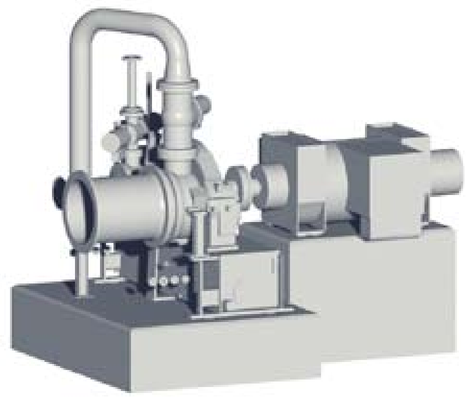

SST-110

(formerly known as TWIN version)

up to 7 MW
The SST-110 provides highest cost efficiency and high performance. It allows to reduce high heat gradients while providing a controlled extraction capability. The SST-110 is a dual casing turbine on one gearbox which can run on different steam lines.

Technical data

- Power output up to 7 MW
- Inlet pressure up to 131 bar(a) / 1900 psi
- Inlet temperature dry saturated steam up to 530° C / 985° F
- Speed acc. to driven machine
- Exhaust pressure: back pressure or vacuum

Typical dimensions

Length approx. 6 m / 20 ft (incl. generator)
Width 2.8 m / 9.2 ft
Height 3.2 m / 10.5 ft

Features

- Backpressure, extraction or condensing type
- Package unit design
- Oil unit integrated in base frame
- Nozzle group control valves available
- Quick-start without pre-heating
- Extremely compact construction
- Pressure controlled extraction
- High pressure / low pressure applications
- Meet requirements of API 611 / 612*
- ATEX version available
- Suitable for ORC (Organic Rankine Cycle)
- Suitable for gas expansion

*if overhung design and integral gear is accepted

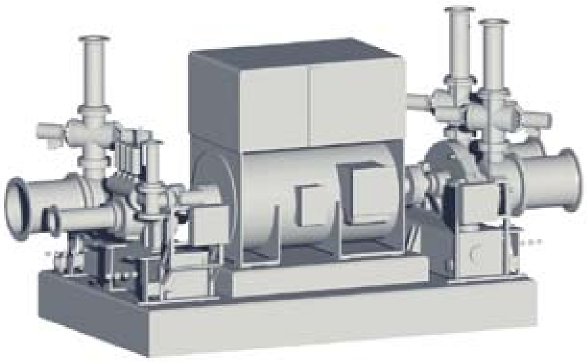

SST-120

(formerly known as Tandem version)

up to 10 MW

The SST-120 is a multi casing turbine consisting of different turbine modules on each shaft end of the generator. These can be used in parallel or serial steam flow arrangement.

Technical data

- Power output up to 10 MW
- Inlet pressure up to 131 bar(a) / 1900 psi
- Inlet temperature dry saturated steam up to 530°C / 985°F
- Speed acc. to driven machine
- Exhaust pressure: back pressure or vacuum

Typical dimensions

Length approx. 9 m / 30 ft (incl. generator)
Width 2.8 m / 9.2 ft
Height 3.2 m / 10.5 ft

Features

- Backpressure, extraction or condensing type
- Package unit design
- Oil unit integrated in base frame
- Nozzle group control valves available
- Quick-start without pre-heating
- Extremely compact construction
- Pressure controlled extraction
- High pressure- / Low pressure applications
- Meet requirements of API 611 / 612*
- ATEX version available
- Suitable for ORC (Organic Rankine Cycle)
- Suitable for gas expansion

*if overhung design and integral gear is accepted

Fields of application

Siemens industrial steam turbines increase the efficiency of power generation and improve the profitability of industrial applications.

Industries

- Chemistry
- Food & Beverage
- Independent power producers
- Manufacturing industries, producers of pumps and compressors
- Petrochemistry / Refineries
- Smelters / Steel
- Sugar / Palmoil
- Utilities
- Wood-working industry / Paper mills

Applications

- Biomass power plants
- Captive power plants
- Cogeneration / CHP
- Gas expansion
- Geothermal plants
- Heat-recovery
- Mechanical drives
- Ships / Offshore
- Solar thermal plants
- Waste incineration plants

Main advantages

- High efficiency
- High reliability / availability
- Customized proven solutions
- Compact design
- Simple installation and maintenance

Industrial steam turbines

The comprehensive Siemens product range from 2 to 250 megawatts

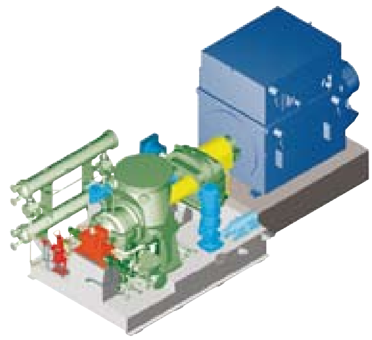

SST-100

up to 8.5 MW

The SST-100 is a single-casing turbine, geared for generator drive; pre-engineered including blading as a cost-effective solution. Mainly used for industrial applications.

Technical data

- Power output up to 8.5 MW
- Inlet pressure up to 65 bar / 945 psi
- Inlet temperature up to 480° C / 895° F
- Rotational speed up to 7,500 rpm
- Exhaust pressure (back pressure) up to 10 bar / 145 psi
- Exhaust pressure (condensing) up to 1 bar / 14.5 psi
- Exhaust area 0.22 m^2/2.4 sq. ft.

Typical dimensions

Length 8 m / 26 ft.
Width 3.7 m / 12.1 ft.
Height 3.4 m / 11.2 ft.

Features

- Back pressure / condensing type
- Package unit design
- Radial exhaust
- Simple design, rigid rotor
- Oil system integrated in base frame
- Separate oil and steam piping

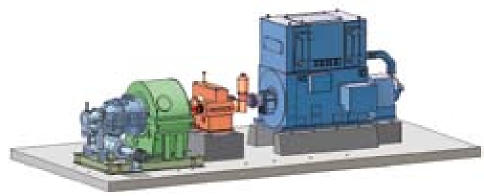

SST-150

up to 20 MW

The SST-150 is a single-casing turbine, providing geared drive to a 1,500 or 1,800 rpm generator and packaged in a skid-mounted design. For power generation, it provides high efficiency together with a very compact arrangement.

Technical data

- Power output up to 20 MW
- Inlet pressure up to 103 bar / 1,495 psi
- Inlet steam temperature up to 505° C / 940° F
- Rotational speed up to 13,300 rpm
- Bleed up to 25 bar / 365 psi
- Controlled extraction up to 16 bar / 230 psi
- Exhaust pressure (back pressure) up to 10 bar / 145 psi
- Exhaust pressure (condensing) up to 0.25 bar / 3.6 psi
- Exhaust area 0.28 – 1.6 m^2/3.0 – 17.2 sq. ft.

Typical dimensions

Length 12 m / 39 ft.
Width 4 m / 13.1 ft.
Height 5 m / 16.4 ft.

Features

- Back pressure / condensing type
- Package unit design
- Pre-engineered turbine modules, modular peripherals
- Single controlled extraction
- Radial exhaust
- Separated oil and steam piping

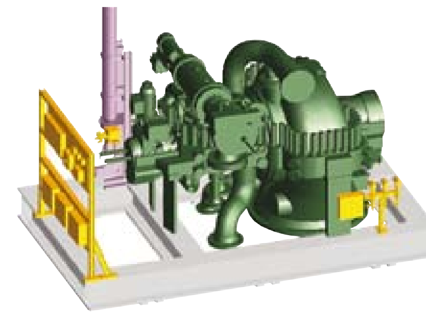

SST-200

up to 10 MW

The SST-200 is a single-casing turbine, geared or with direct drive suited to both generator and mechanical drives. Used for industry and power generation applications.

Technical data

- Power output up to 10 MW
- Inlet pressure up to 110 bar / 1595 psi
- Inlet temperature up to 520° C / 970° F
- Controlled extraction up to 16 bar / 230 psi and up to 350° C / 560° F
- Bleed up to 60 bar / 870 psi
- Exhaust pressure (back pressure) up to 16 bar / 230 psi
- Exhaust pressure (condensing) up to 0.25 bar / 3.6 psi
- Exhaust area 0.17 – 0.34 m^2/1.8 – 3.7 sq. ft.

Typical dimensions

Length 4 m / 13.1 ft.*
Width 2 m / 6.5 ft.*
Height 2.5 m / 8.2 ft.*

*turbine skid only

Features

- Back pressure / condensing type
- Package unit design
- Extensive pre-design
- High-speed, downward / upward exhaust
- Customized steam path
- Short delivery time

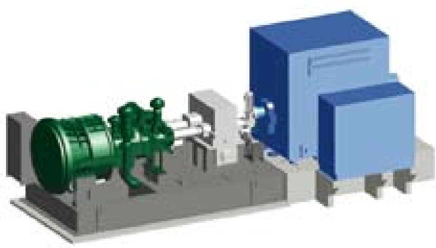

SST-300

up to 50 MW
The SST-300 is a single-casing turbine, geared for generator drive. It has a compact and flexible design with a high degree of standardization. Used for power generation applications.

Technical data

- Power output up to 50 MW
- Inlet pressure 120 bar / 1,740 psi
- Inlet temperature 520° C / 970° F
- Rotational speed up to 12,000 rpm
- Controlled extraction up to 45 bar / 655 psi and up to 400° C / 750° F
- Bleed up to 60 bar / 870 psi
- Exhaust pressure (back pressure) up to 16 bar / 230 psi
- Exhaust pressure (condensing) up to 0.3 bar / 4.4 psi
- Exhaust area 0.28 – 1.6 m^2 / 3.0 – 17.2 sq. ft.

Typical dimensions

Length 12 m / 39 ft.
Width 4 m / 13.1 ft.
Height 5 m / 16.4 ft.

Features

- Back pressure / condensing type
- Pre-engineered turbine modules, modular peripherals
- Two controlled extractions
- Radial / axial exhaust
- Adaptive stage up to 16 bar
- Package unit design
- Customized steam path

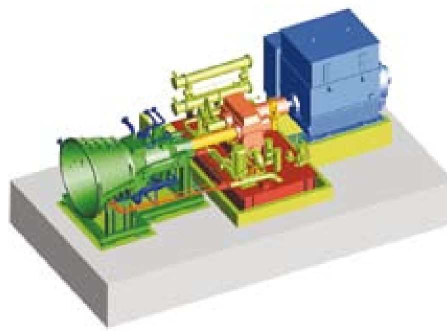

SST-400

up to 65 MW
The SST-400 is a single-casing turbine, geared for generator drive. It has a compact and flexible design with a high degree of standardization. Used for industry and power generation applications.

Technical data

- Power output up to 65 MW
- Inlet pressure up to 140 bar / 2,030 psi
- Inlet temperature up to 540° C / 1,005° F
- Rotational speed 3,000 – 8,000 rpm
- Controlled extraction up to 45 bar / 655 psi and up to 450° C / 840° F
- Bleed up to 60 bar / 870 psi
- Exhaust pressure (back pressure) up to 25 bar / 365 psi
- Exhaust pressure (condensing) up to 0.3 bar / 4.4 psi
- Exhaust area 1.3 – 3.0 m^2 / 14.0 – 32.5 sq. ft.

Typical dimensions

Length 18 m / 59 ft.
Width 8.5 m / 28 ft.
Height 5.5 m / 18 ft.

Features

- Back pressure / condensing type
- Pre-engineered turbine modules, modular peripherals
- Two controlled extractions, radial / axial exhaust
- Adaptive stage up to 16 bar
- Semi-package unit design
- Customized steam path
- Short delivery time

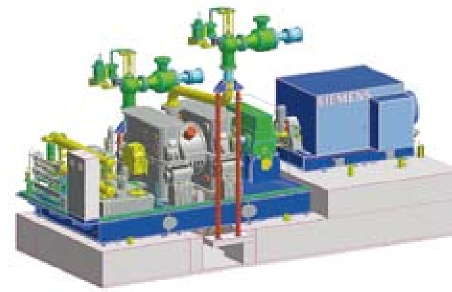

SST-500

up to 100 MW
The SST-500 is a single-casing turbine, geared or with direct drive. It is suited to both generator and mechanical drives to accommodate large volume flows. Typically used as low-pressure casing in two-cylinder applications.

Technical data

- Power output up to 100 MW
- Inlet pressure up to 30 bar / 435 psi
- Inlet temperature up to 400° C / 750° F
- Rotational speed up to 15,000 rpm
- Bleed up to 2, at various pressure levels
- Exhaust area 2 x 0.175 – 3.5 m^2 / 2 x 1.9 – 24.8 sq. ft.

Typical dimensions

Length 19 m / 62 ft.
Width 6 m / 20 ft.
Height 5 m / 16.4 ft.

Features

- Double-flow condensing turbine
- Standard turbine modules, modular peripherals
- Throttle-controlled
- Highly customized
- Customized steam path

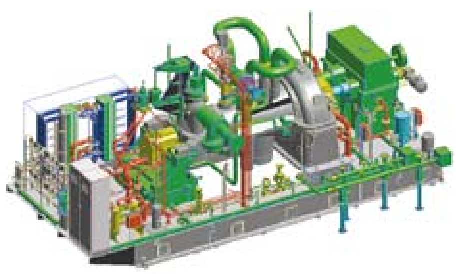

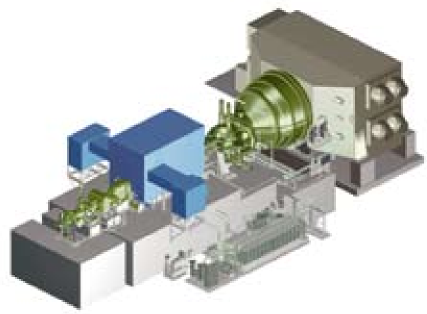

SST-600

up to 100 MW
The SST-600 is a single-casing turbine, geared or with direct drive; suited to both generator and mechanical drives. Used for tailor-made applications for most complex processes in industry and power generation.

Technical data

- Power output up to 100 MW
- Inlet pressure up to 140 bar / 2,030 psi
- Inlet temperature up to 540° C / 1,005° F
- Rotational speed 3,000 – 15,000 rpm
- Double controlled extraction up to 65 bar / 945 psi
- Bleed up to 5, at various pressure levels
- Exhaust pressure (back pressure) up to 55 bar / 800 psi
- Exhaust area 0.175 m² – 3.5 m² / 1.9 – 38 sq. ft.

Typical dimensions

Length 19 m / 62 ft.
Width 6 m / 20 ft.
Height 5 m / 16.4 ft.

Features

- Back pressure / condensing type
- Standard turbine modules, modular peripherals
- Inner casing for high steam parameters
- Second steam injection possible
- Package unit design
- Radial / axial exhaust
- Highly customized
- Customized steam path

SST-700

up to 175 MW
The SST-700 is a dual-casing turbine consisting of a geared HP module and LP module. Used for power generation applications, especially in combined cycle and solar thermal power plants. Each module can be used independently or can be combined for the optimal configuration.

Technical data

- Power output up to 175 MW
- Inlet pressure (with reheat) up to 165 bar / 2,395 psi
- Inlet temperature (with reheat) up to 585° C / 1,085° F
- Reheat temperature up to 415° C / 780° F
- Rotational speed 3,000 – 13,200 rpm
- Controlled extraction up to 40 bar / 580 psi and up to 415° C / 780° F
- Bleed up to 7; up to 120 bar / 1,740 psi
- Exhaust pressure (back pressure) up to 40 bar / 580 psi
- Exhaust pressure (condensing) up to 0.6 bar / 8.5 psi
- Exhaust pressure (district heating) up to 3 bar / 45 psi
- Exhaust area 1.7 – 11 m² / 18.3 – 118 sq. ft.

Typical dimensions

Length 22 m / 73 ft.*
Width 15 m / 59 ft.*
Height 6 m / 20 ft.*

* including condenser

Features

- Back pressure / condensing type
- Pre-engineered turbine modules
- Parallel arrangement possible
- Proven solution for solar thermal power plants
- Simple extraction in crossover pipe
- Axial / radial exhaust
- Reheat applications
- Customized steam path

SST-800

up to 150 MW
The SST-800 is a single-casing direct-drive turbine with reverse flow design for generator applications. Used for tailor-made applications for most complex processes in industry and power generation.

Technical data

- Power output up to 150 MW
- Inlet pressure up to 140 bar / 2,030 psi
- Inlet temperature up to 540° C / 1,005° F
- Rotational speed 3,000 – 3,600 rpm
- Double-controlled extraction up to 45 bar / 655 psi
- Bleed up to 6, at various pressure levels
- Exhaust pressure vacuum up to 14 bar / 205 psi
- Exhaust area 1.1 – 5.6 m²/11.8 – 60.3 sq. ft.

Typical dimensions

Length 20 m / 66 ft.
Width 8.5 m / 28 ft.
Height 6 m / 20 ft.

Features

- Back pressure / condensing type
- Standard turbine modules, modular peripherals
- Inner casing for high steam parameters
- Axial / radial exhaust
- Package unit design
- Highly customized
- Customized steam path

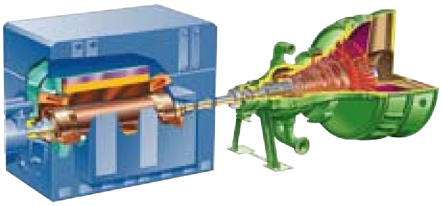

SST-900

up to 250 MW

The SST-900 is a single-casing turbine for 2-pole generators for power generation and industry. SST-900 RH is a dual-casing turbine for reheat applications.

Technical data

- Power output up to 250 MW
- Inlet pressure (with reheat) up to 165 bar / 2,395 psi
- Inlet temperature (with reheat) up to 585° C / 1,085° F
- Reheat temperature up to 580° C / 1,075° F
- Rotational speed 3,000 – 3,600 rpm; HP up to 13,200 rpm (for reheat)
- Bleed up to 7; up to 60 bar / 870 psi
- Controlled extraction up to 55 bar / 800 psi and up to 480° C / 895° F
- Exhaust pressure (back pressure) up to 16 bar / 230 psi
- Exhaust pressure (condensing) up to 0.6 bar / 8.5 psi
- Exhaust pressure (district heating) up to 3 bar / 45 psi
- Exhaust area 1.7 – 11 m^2 / 18.3 – 118 sq. ft.

Typical dimensions

Length 20.5 m / 67 ft.*
Width 11 m / 36 ft.*
Height 10 m / 33 ft.*

* including condenser

Features

- Back pressure / condensing type
- Pre-engineered turbine modules
- Two controlled extractions
- Adaptive stage up to 16 bar
- Butterfly valve up to 55 bar
- Axial / radial exhaust
- Reheat applications
- Customized steam path

Preise von Dampfturbinen lt. AE Dampfturbinenbau (2000)

Anschaffungskosten für Kondensationsturbinen

Leistung in MW	Kosten in Euro/kW
5	352
10	228
15	176
20	167
30	140
40	120
50	95

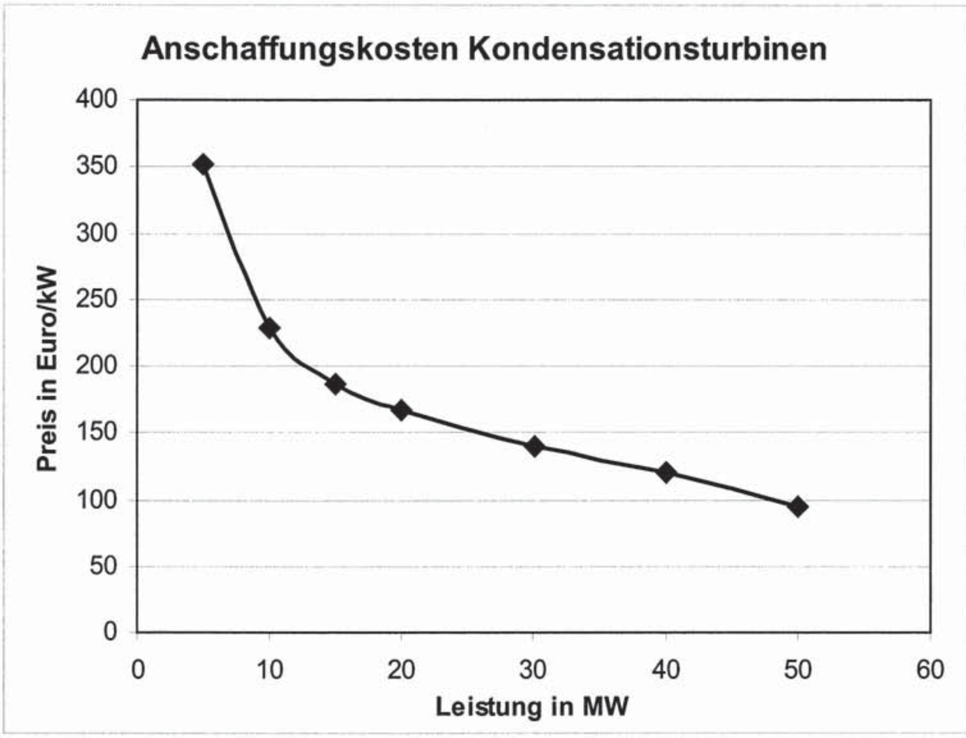

Anschaffungskosten für Gegendruckmaschinen um ca. 20 % geringer!

Inspektionen:
alle 3 Jahre: Dauer 1 Woche
alle 6 Jahre: Dauer 4 Wochen, 5 Leute, 1 Tag ca. 1000,- Euro

Organic Rankine Cycles

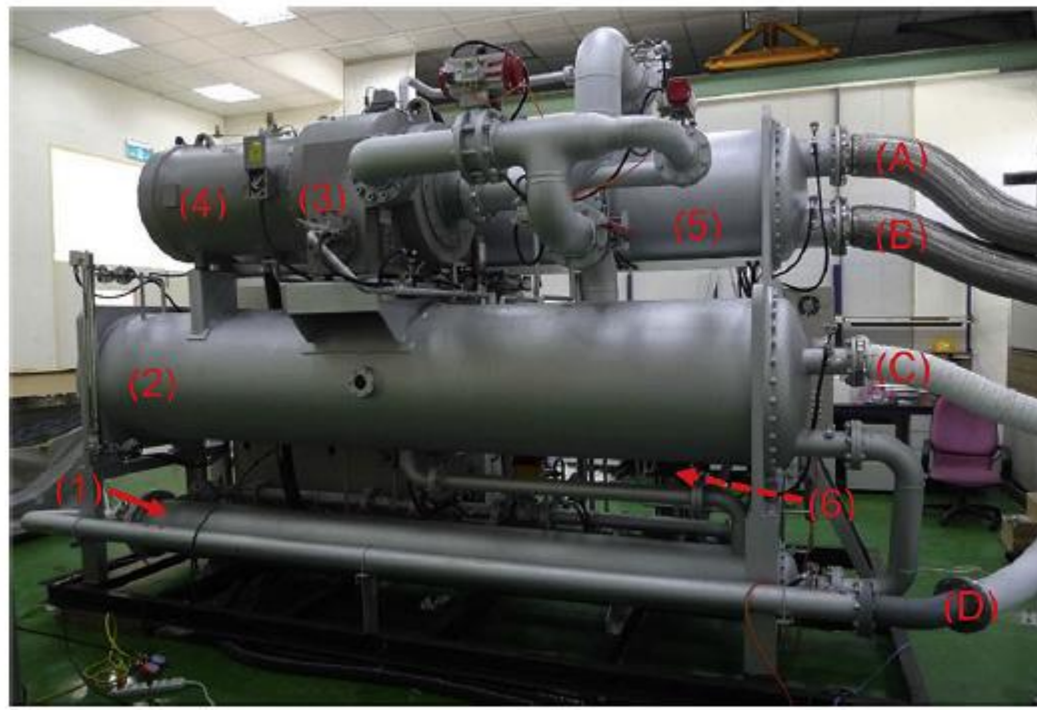

Photograph of a 250-kW ORC prototype.
(1) Preheater, (2) evaporator, (3) turbine, (4) generator,
(5) condenser, (6) pump, (A) cooling water inlet, (B) cooling water outlet, (C) hot water inlet, (D) hot water outlet.

Giovanni Manente

University of Padova

**Graz University of Technology,
April 2017**

Outline of the presentation

A geothermal Organic Rankine Cycle system (ORC)

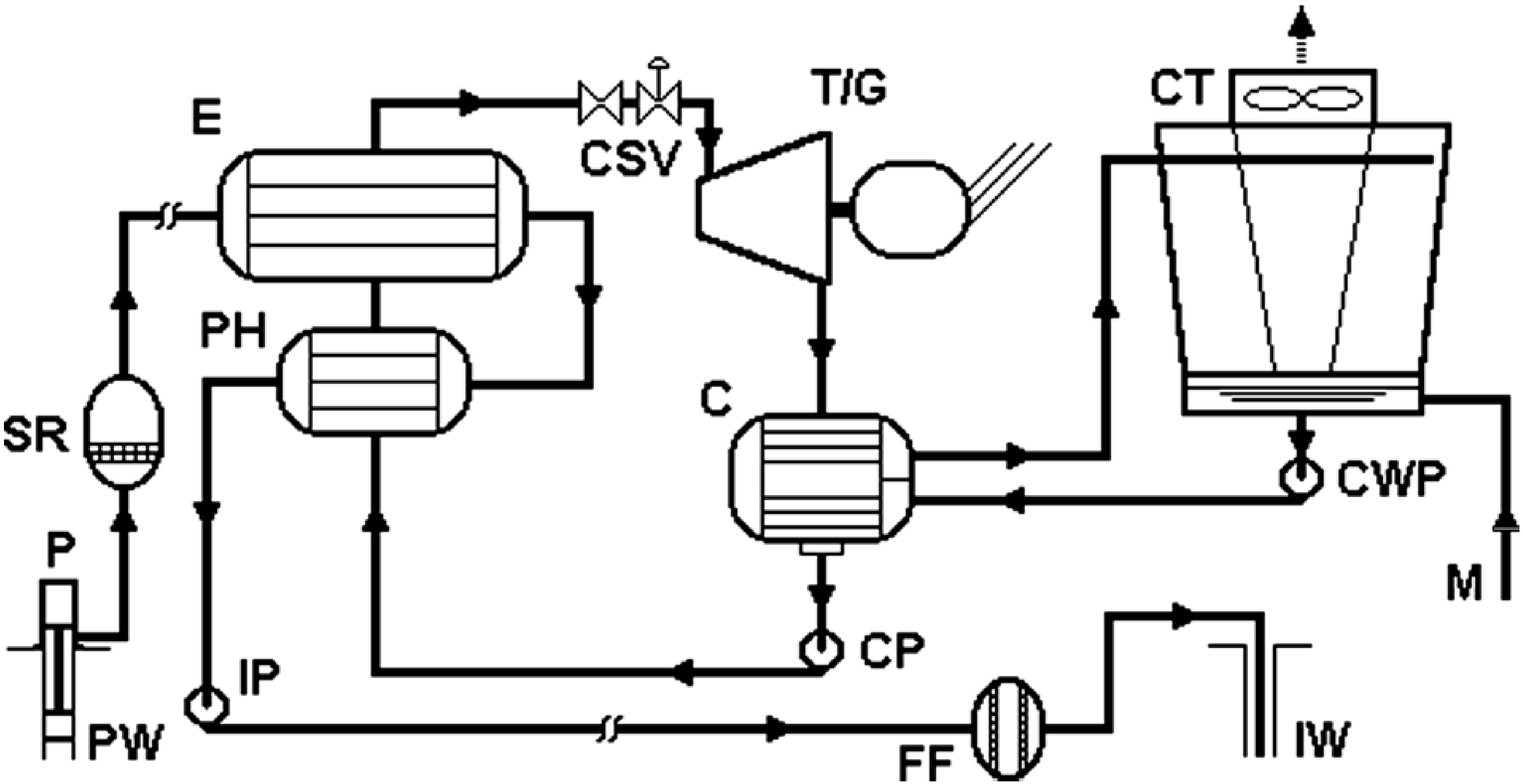

(DiPippo, Geothermal power plants, 2008)

Geofluid in the ORC

- The production wells (PW) are fitted with pumps (P) that are set below the flash depth determined by the reservoir properties and the desired flow rate
- Sand removers (SR) may be needed to prevent scouring and erosion of the piping and heat exchanger tubes
- The geofluid is everywhere kept at a pressure above its flash point and is reinjected in injection wells (IW) still in the liquid phase
- The geofluid temperature is not allowed to drop to the point where silica scaling could become an issue in the preheater and in the piping and injection wells

Working fluid in the ORC

- The working fluid, chosen for its appropriate thermodynamic properties, receives heat from the geofluid, evaporates, expands through a turbine, condenses and is returned to the evaporator by means of a feedpump
- There are two steps in the heating-boiling process, conducted in the preheater (PH) where the working fluid is brought to its boiling point and in the evaporator (E) from which it emerges as a saturated vapor

Thermodynamics of the conversion process

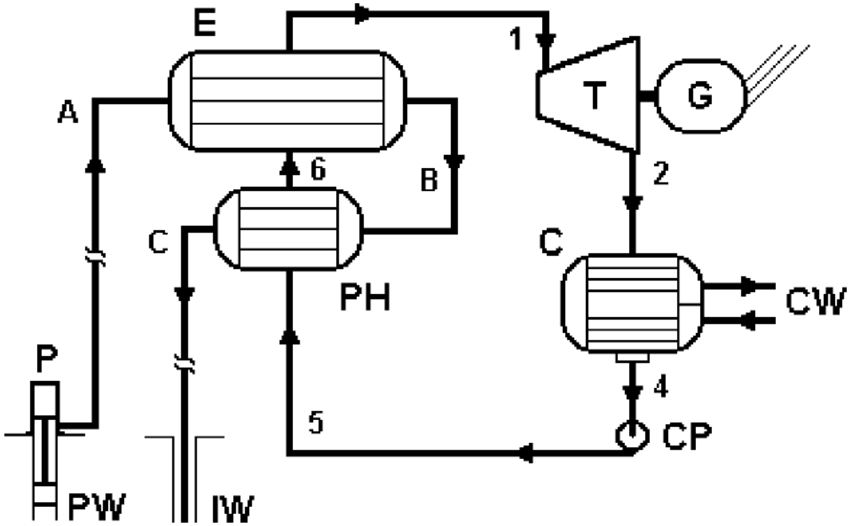

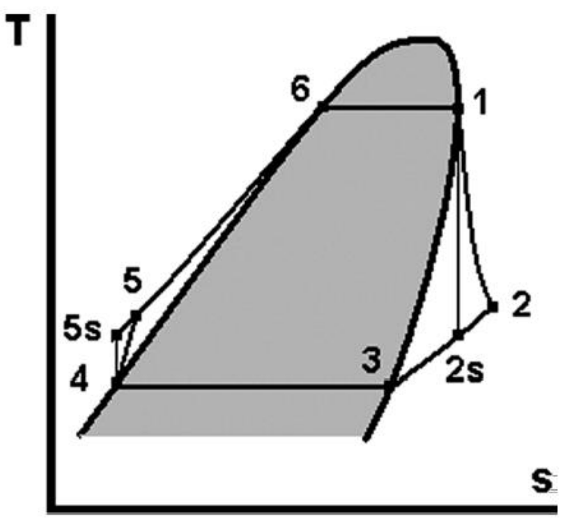

- The turbine power is the product of the mass flow rate of the working fluid and the enthalpy drop across the turbine

$$\dot{W}_t = \dot{m}_{wf} \cdot (h_1 - h_2)$$

- The power absorbed by the feed pumps is

$$\dot{W}_p = \dot{m}_{wf} \cdot (h_5 - h_4)$$

- The net power output is

$$\dot{W}_{net} = \dot{W}_t - \dot{W}_p$$

Heat exchanger analysis: preheater and evaporator

Temperature-heat transfer diagram for preheater and evaporator

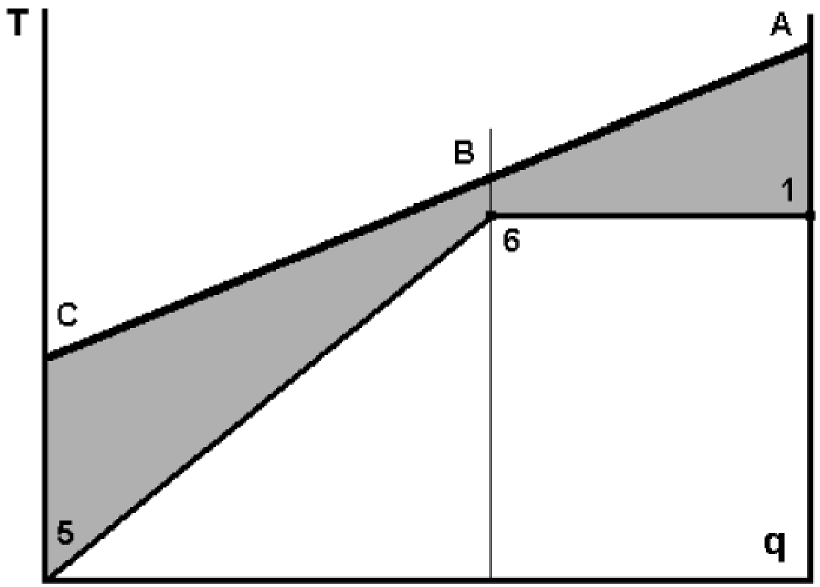

The place in the heat exchanger where the brine and working fluid experience the minimum temperature difference is called the “pinch-point”

- The pinch point temperature difference is generally set to 5°C or 10°C
- State points 5, 6 and 1 are known from the cycle specifications
- The working fluid mass flow rate (m_{wf}) can be calculated by

$$\dot{m}_{geo} \cdot c_{geo} \cdot (T_A - T_B) = \dot{m}_{wf} \cdot (h_1 - h_6)$$

- The temperature (T_C) of the geofluid leaving the plant can be obtained by

$$\dot{m}_{geo} \cdot c_{geo} \cdot (T_B - T_C) = \dot{m}_{wf} \cdot (h_6 - h_5)$$

Wet, dry and isentropic fluids

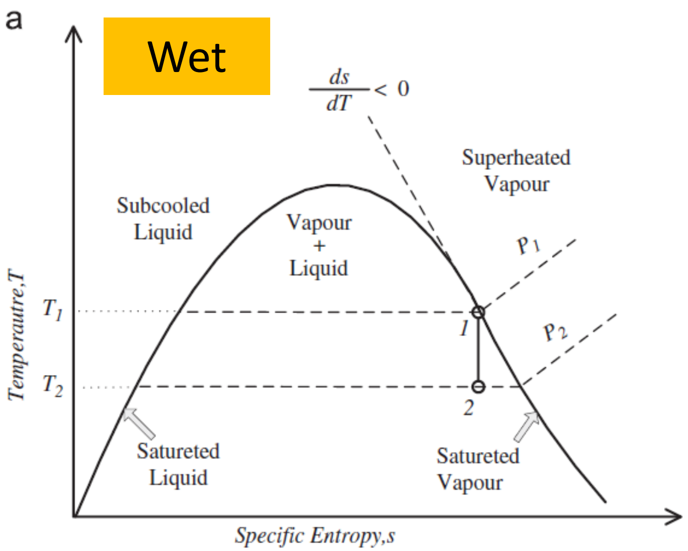

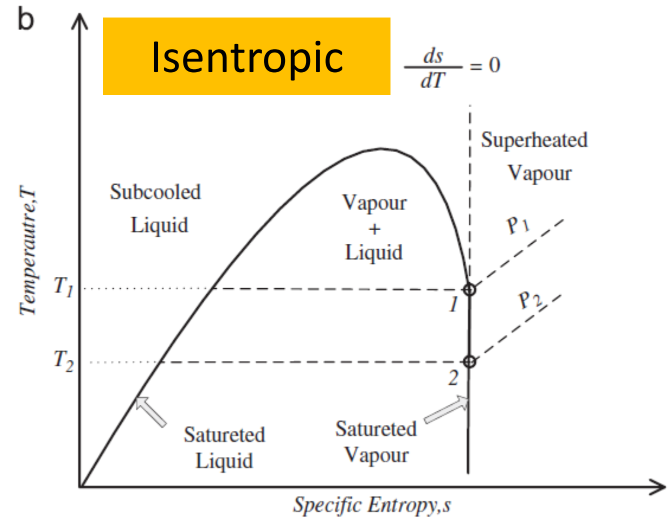

The working fluids can be classified in three categories according to the saturation vapor curve

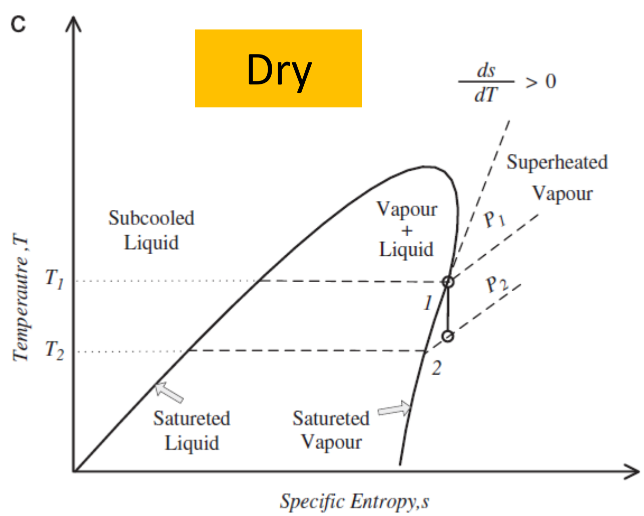

(Bao J., Renewable and Sustainable Energy Reviews, 2014)

Saturation vapor curves of organic fluids

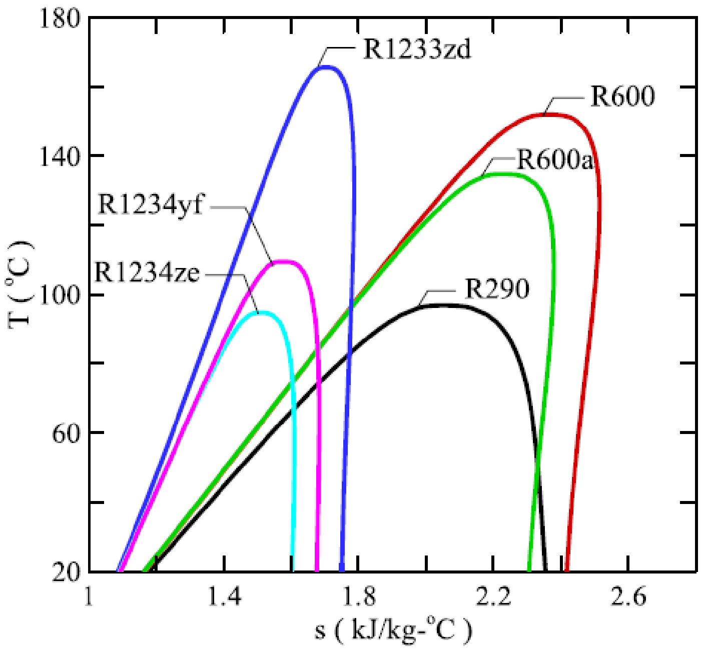

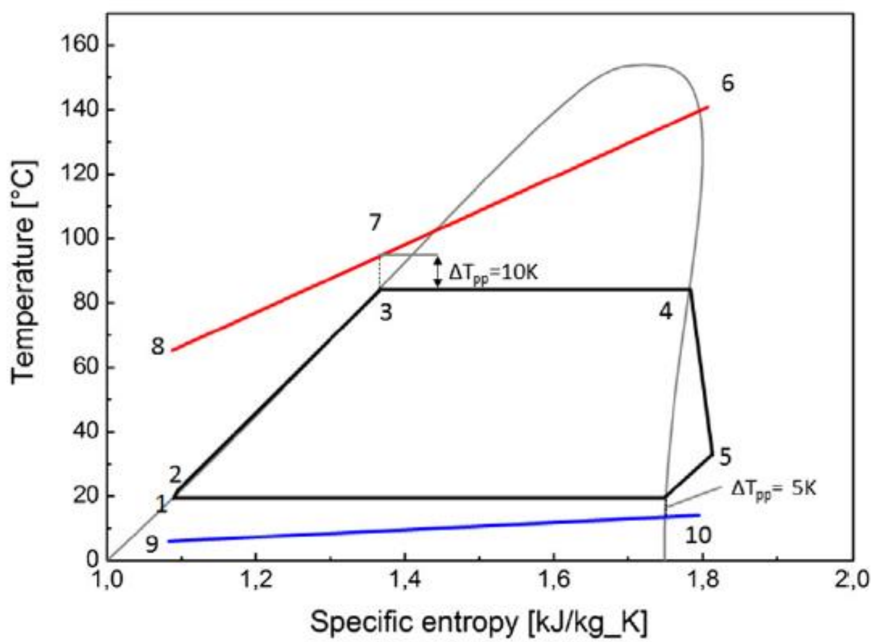

(Yang, Renewable Energy, 2016)

Saturation curves of organic fluids versus water

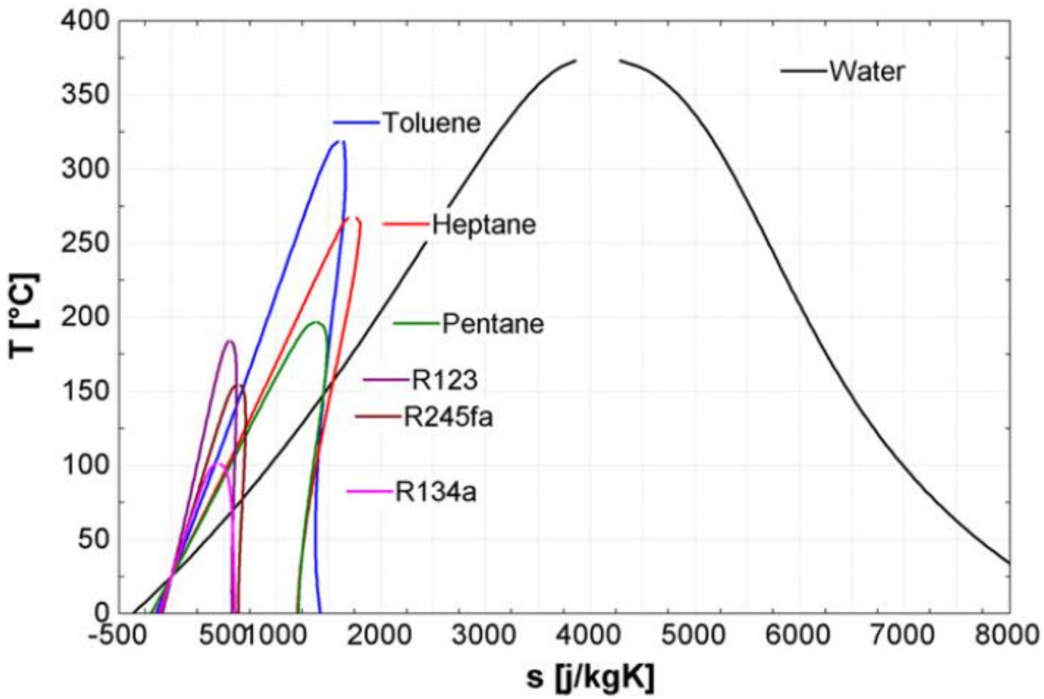

(Quoilin et al., Renewable and Sustainable Energy Reviews, 2013)

- Two main differences:

1) Positive slope of the saturated vapor curve for organic fluids → the limitation of the vapor quality at the end of the expansion process disappears → no need to superheat the vapor at turbine inlet

2) Vaporization enthalpy smaller for organic fluids → better coupling with the heat source

Effects of vaporization latent heat on the thermal matching heat source – working fluid

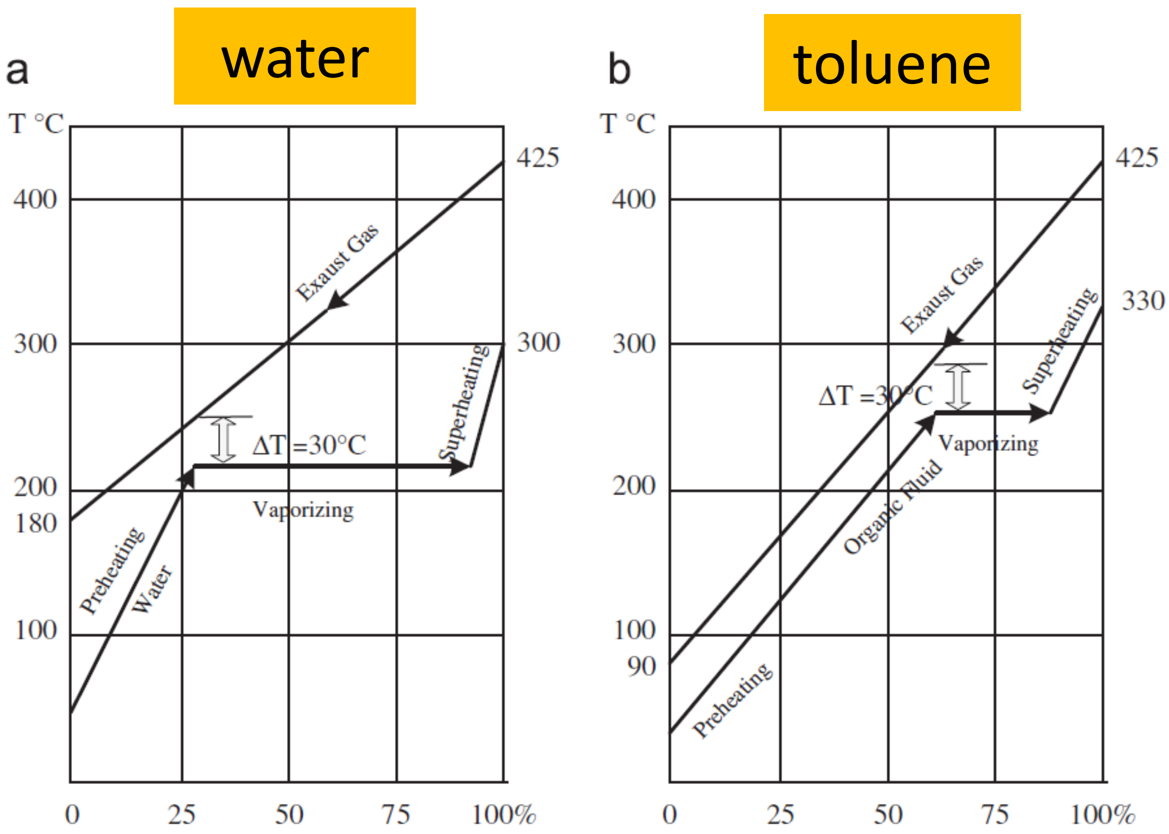

(Bao J., Renewable and Sustainable Energy Reviews, 2014)
(Larjola J., International Journal of Production Economics, 1995)

Lower vaporization heat of the working fluid causes the heat transfer process in the evaporator to occur mostly at variable temperature → the temperature profile of the working fluid in the evaporator better follows the temperature profile of the heat source → lower irreversibility in the heat transfer process

Regenerative configuration of ORC

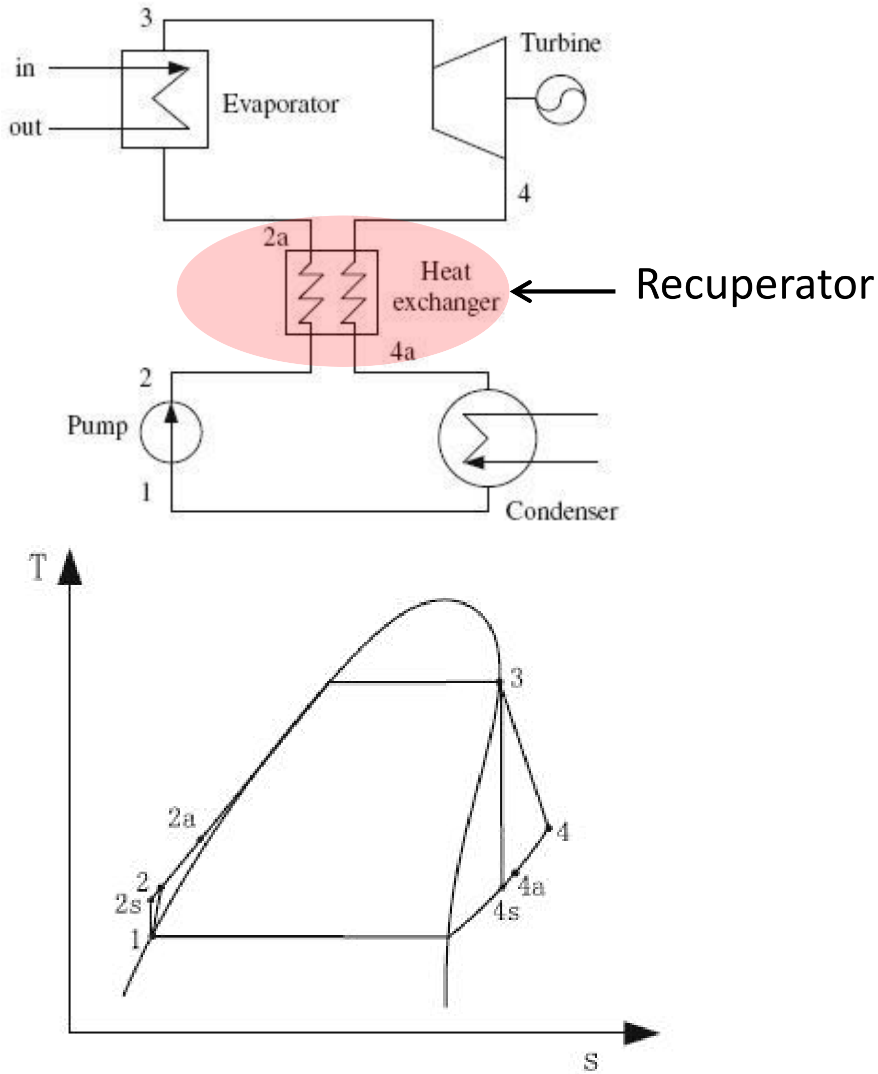

(Dai et al., Energy Conversion and Management, 2009)

- If the temperature t_4 is markedly higher than the temperature t_2, it may be rewarding to implement an internal heat exchanger (recuperator) into the cycles
- In the recuperator the vapor leaving the turbine is cooled in the process (4–4a) by transferring heat to the compressed liquid that is heated in the process (2–2a)
- In this way the thermal efficiency of the ORC increases

Optimum evaporation temperature

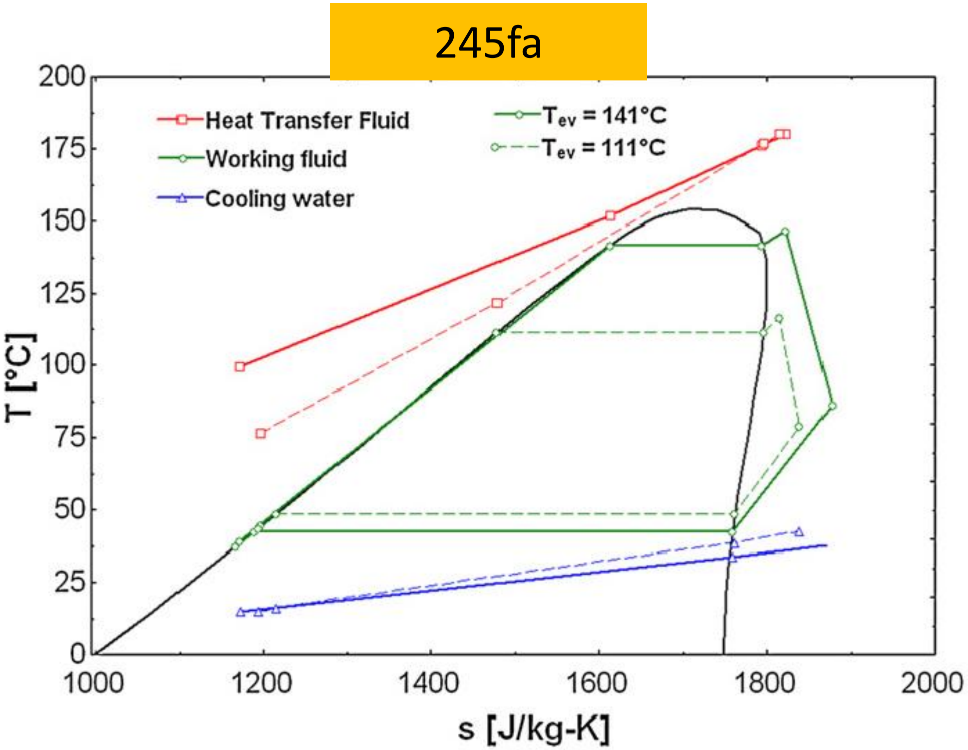

(Quoilin S. et al., Applied Thermal Engineering, 2011)

Increasing the evaporation temperature implies two effects:

1) The heat source is cooled down to a higher temperature

2) The expander specific work is increased since the pressure ratio is increased

Performance metrics

- Thermal efficiency:

$$\eta_{TH} = \frac{\dot{W}_{net}}{\dot{Q}_{in}}$$

$$\eta_{TH} = \frac{\dot{W}_{net}}{\dot{m}_{geo} \cdot (h_{in} - h_{out})}$$

- Heat recovery efficiency:

$$\phi = \frac{\dot{Q}_{in}}{\dot{Q}_{av}}$$

$$\phi = \frac{(h_{in} - h_{out})}{(h_{in} - h_0)} \approx \left(\frac{T_{in} - T_{out}}{T_{in} - T_0} \right)$$

- Total heat recovery efficiency (or "system efficiency"):

$$\eta_T = \frac{\dot{W}_{net}}{\dot{Q}_{av}}$$

$$\eta_T = \frac{\dot{W}_{net}}{\dot{m}_{geo} \cdot (h_{in} - h_0)}$$

$$\eta_T = \frac{\dot{W}_{net}}{\dot{Q}_{in}} \cdot \frac{\dot{Q}_{in}}{\dot{Q}_{av}} = \eta_{th} \cdot \phi$$

Optimum evaporation temperature – the effect of heat source temperature

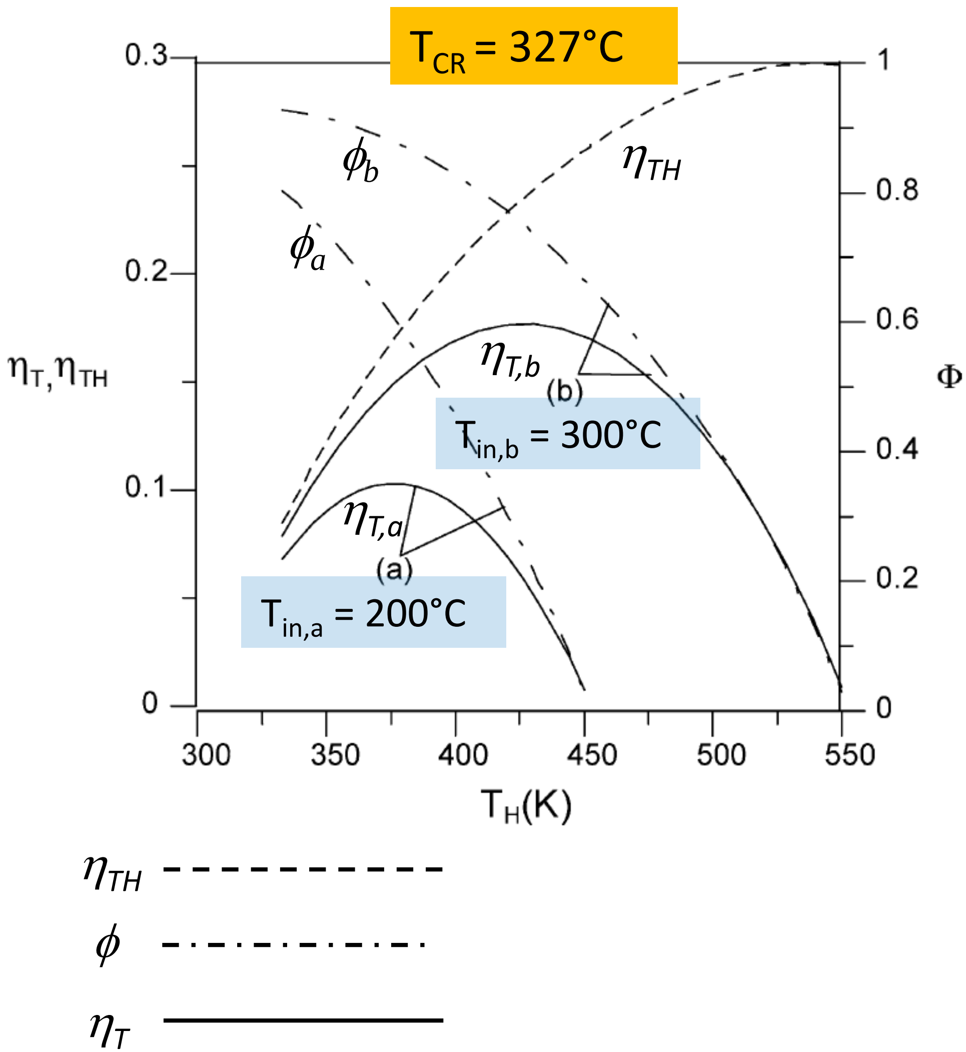

(Liu B-T et al., Energy, 2004)

- Increasing the evaporation temperature:

1) The heat recovery efficiency (ϕ) decreases
2) The thermal efficiency (η_{TH}) increases
3) The total-heat recovery efficiency (η_T) initially increases, reaches a maximum and then decreases

Optimum evaporation temperature – the effect of critical temperature

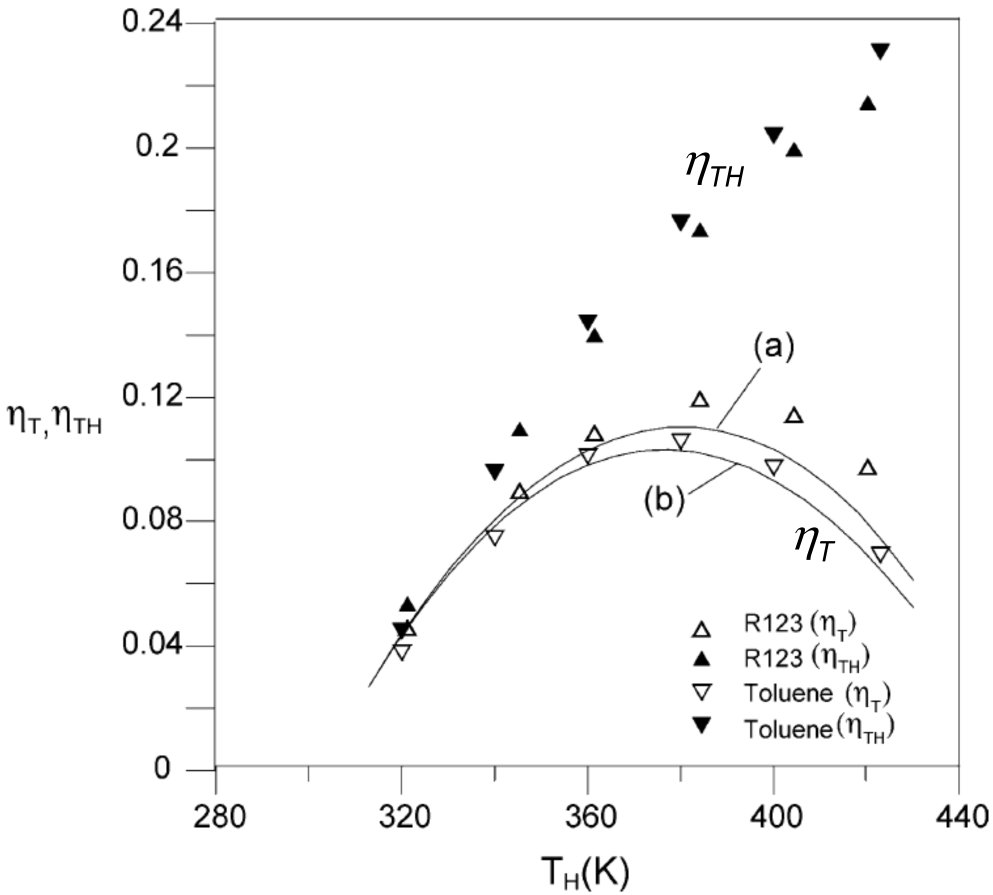

(Liu B-T et al., Energy, 2004)

- Variation of total heat recovery efficiency (η_T) and thermal efficiency (η_{TH}) versus evaporation temperature (T_H) for toluene and R123
- The critical temperature of toluene is higher than that of R123 → the thermal efficiency using toluene is higher
- However, the total heat recovery efficiency of R123 is higher

Thermal efficiency versus total heat-recovery efficiency

- Analysis of total heat-recovery efficiency is very different from the conventional analysis of fossil-fueled power plants which focused on thermal efficiency
- When the evaporation temperature (T_H) is increased, the outlet temperature of waste heat is also increased
- Therefore, although η_{TH} is increased with the increase of T_H, the heat availability ϕ is decreased, thereby showing a maximum value of η_T
- It will lead to significant difference between design of the ORC system from the viewpoints of the thermal efficiency and that based on the total heat-recovery efficiency (i.e., power output)

(Liu B-T et al., Energy, 2004)

Optimum evaporation temperature – the effect of working fluid

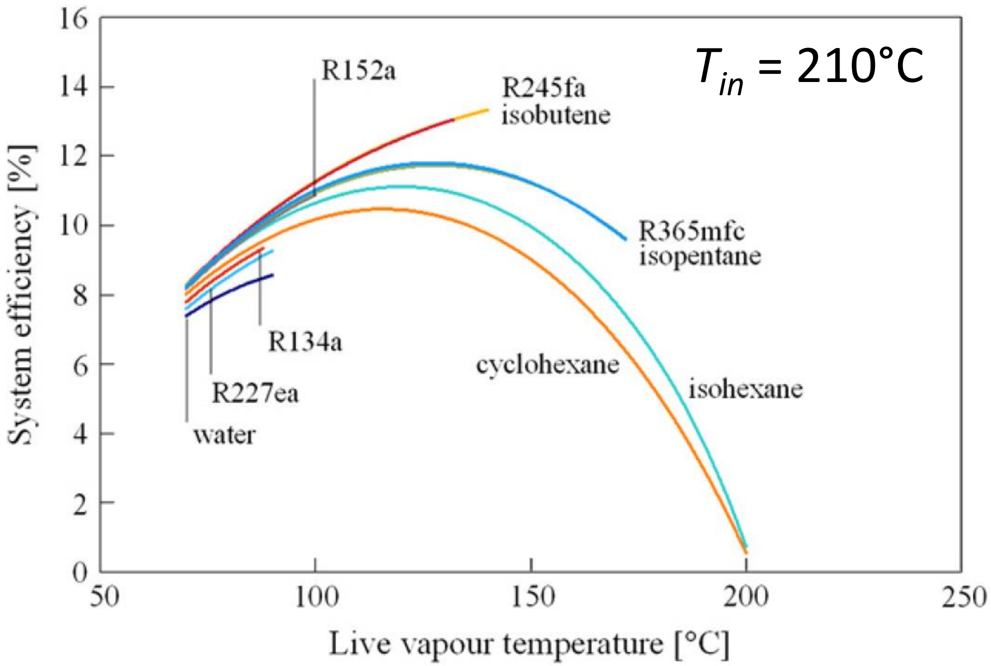

(Schuster A. et al., Energy, 2010)

- Variation of total heat recovery efficiency (also called “system efficiency”) versus evaporation temperature (+2°C of superheating) for different working fluids at subcritical state
- Heat source inlet temperature = 210°C
- The highest system efficiency is reached by R245fa and isobutene

Optimum working fluid

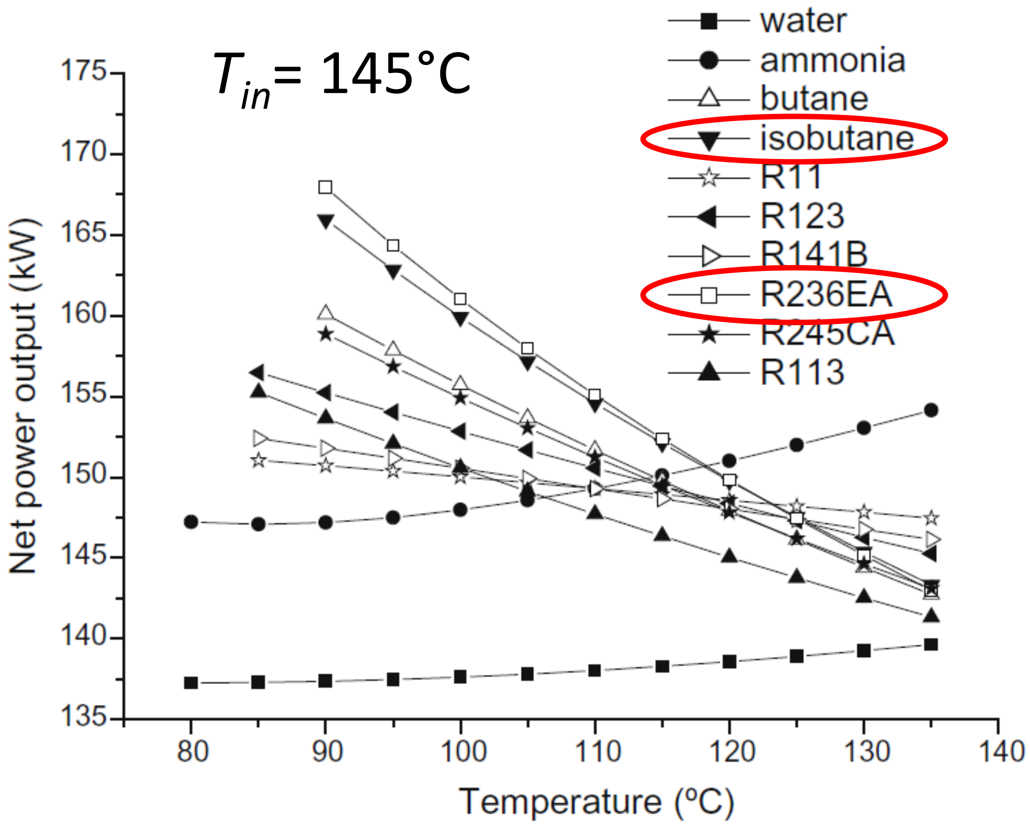

(Dai Y. et al., Energy Conversion and Management, 2009)

- The maximum power output in the utilization of waste heat at 145°C is achieved by R236ea and isobutane
- These fluids have critical temperatures slightly lower than the heat source inlet T

  T_{CR} R236ea = 139,3 °C

  T_{CR} iC4 = 134,7 °C

Optimum working fluid at different heat source temperatures

"Utilization efficiency": ratio between power output and exergy available from the geofluid

$$\eta_u = \frac{\dot{W}_{net}}{\dot{E}_{geo}}$$

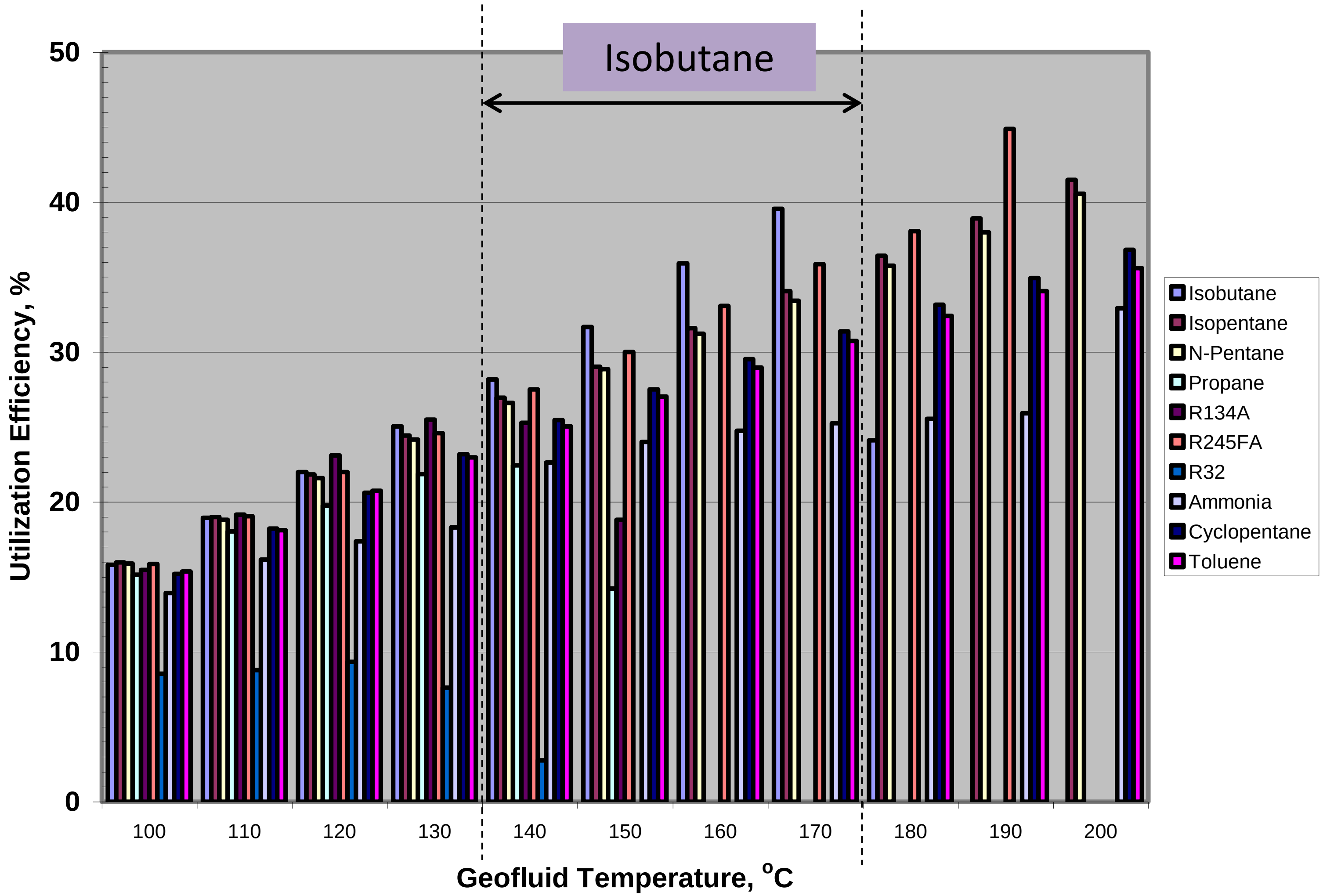

(MIT, Utilization of low-enthalpy geothermal fluids to produce electric power, Private report, 2008)

Optimum working fluid

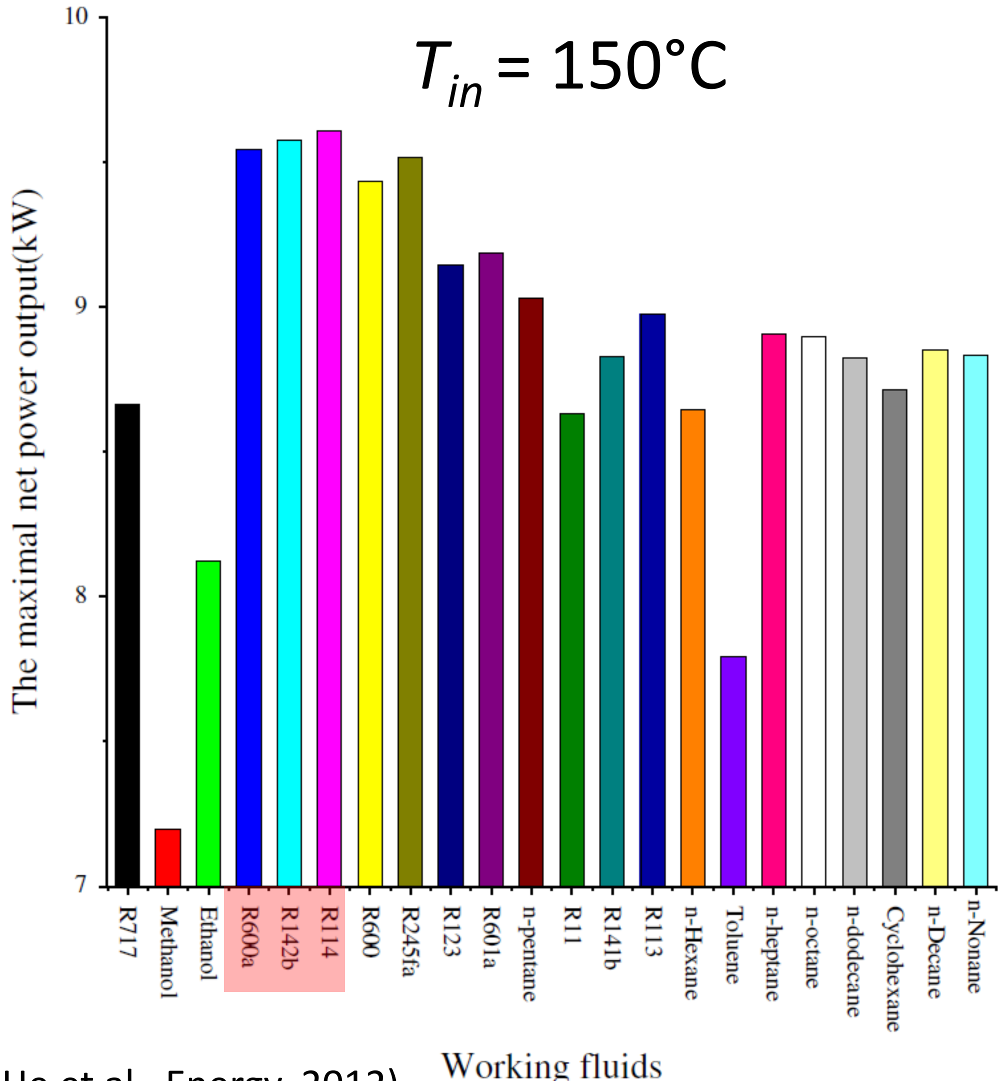

(He et al., Energy, 2012)

- The maximum power output in the utilization of waste heat at 150°C is achieved by R114, R142b and R600a (isobutane)
- These fluids have critical temperatures slightly lower than 150°C:
  $T_{CR\ \mathrm{R114}}$ = 145,8 °C
  $T_{CR\ \mathrm{R142b}}$ = 137,2 °C
  $T_{CR\ \mathrm{R600a}}$ = 134,7 °C

Guidelines for the optimum selection of working fluid

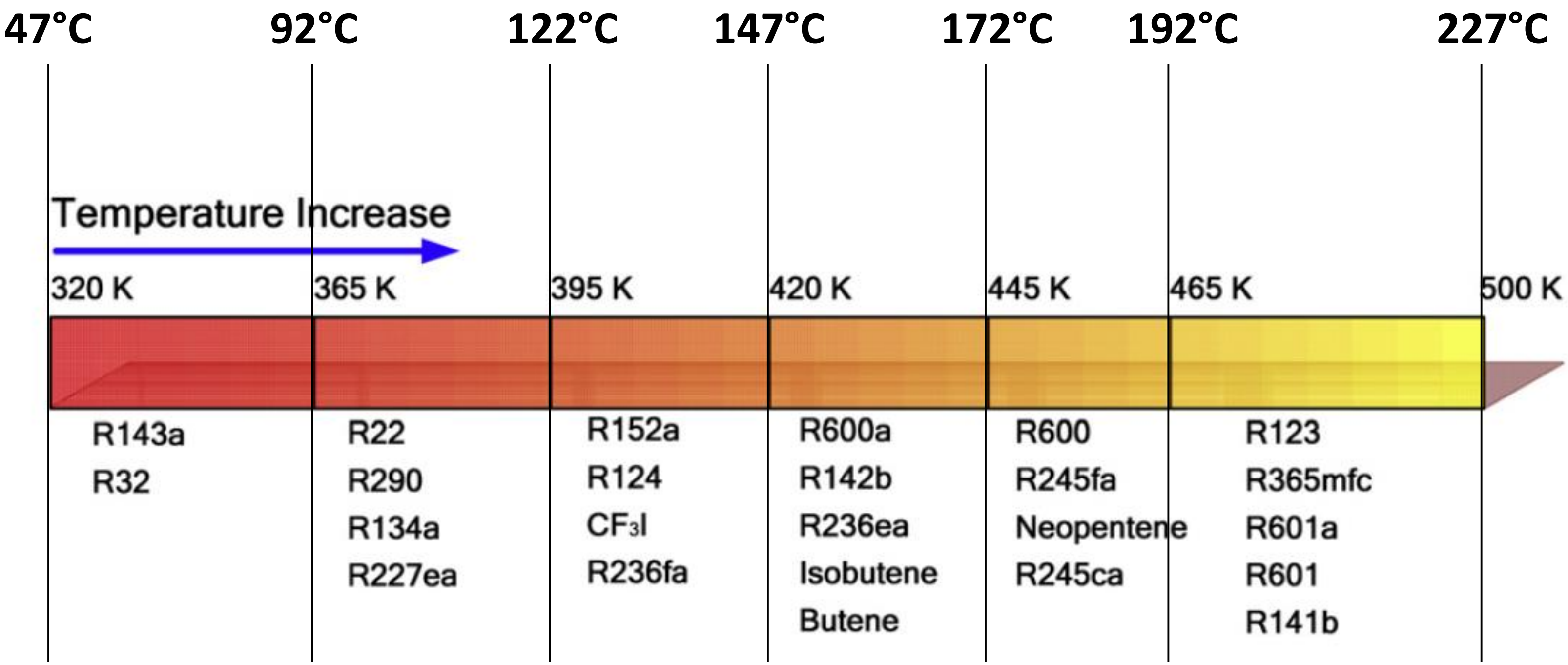

Also in this study isobutane (R600a) is suggested as promising fluid in the utilization of heat source temperatures between 147°C and 172°C

(Wang D. et al., Energy, 2013)

Subcritical vs supercritical ORC

Subcritical maximum pressure

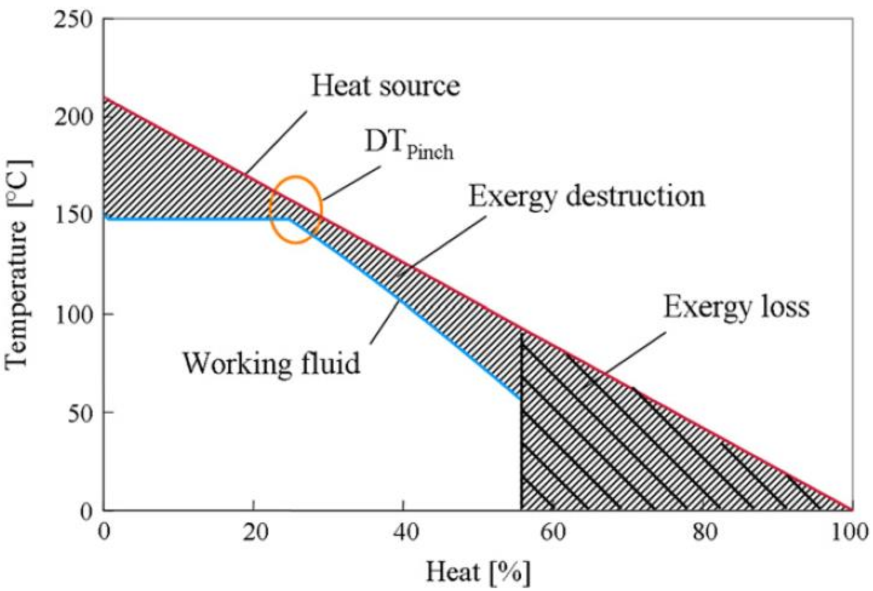

Supercritical maximum pressure

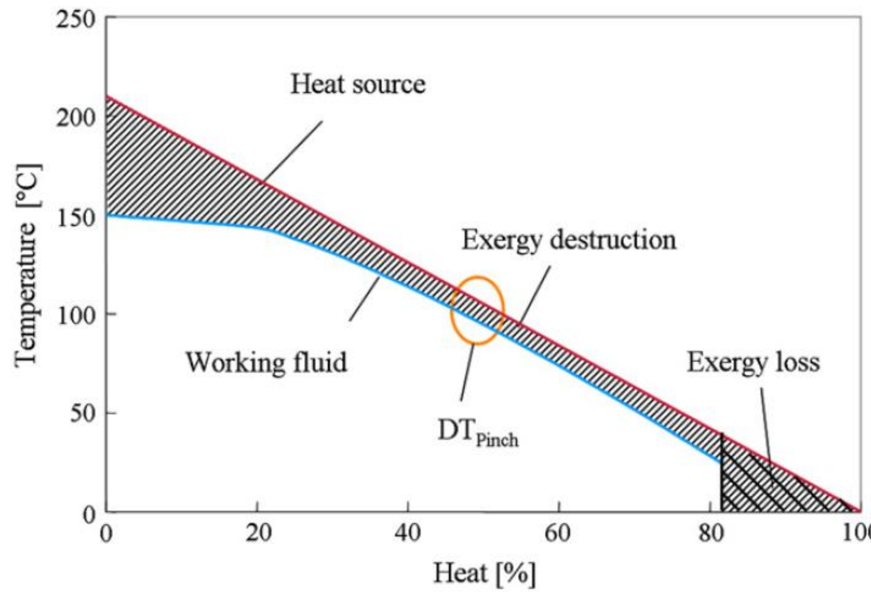

Better thermal matching between heat source and working fluid → lower exergy destruction and lower exergy loss

(Schuster A. et al., Energy, 2010)

Supercritical (or transcritical) ORC

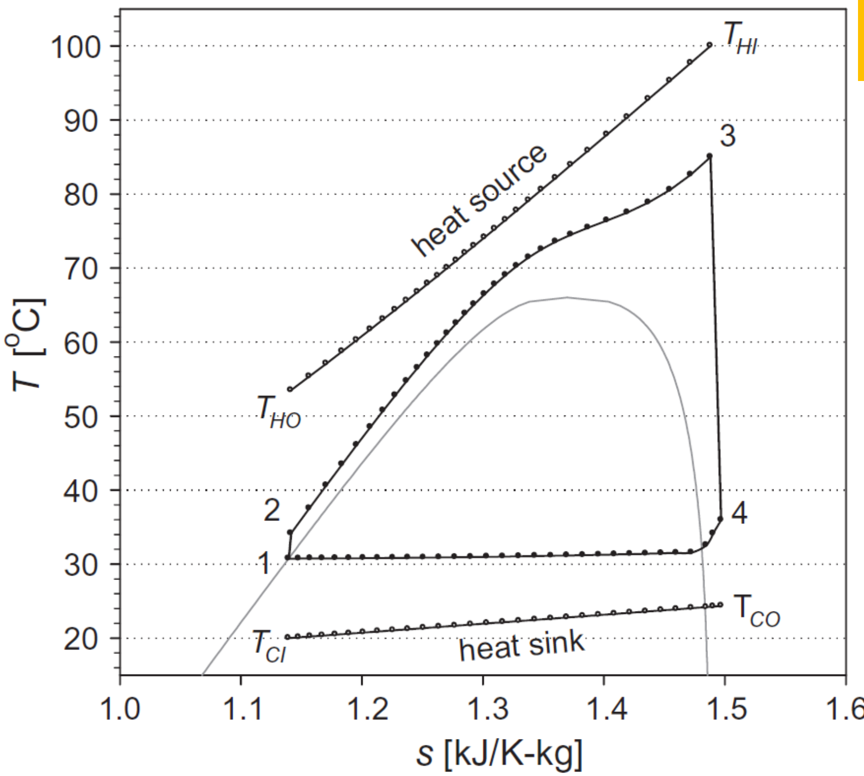

R125

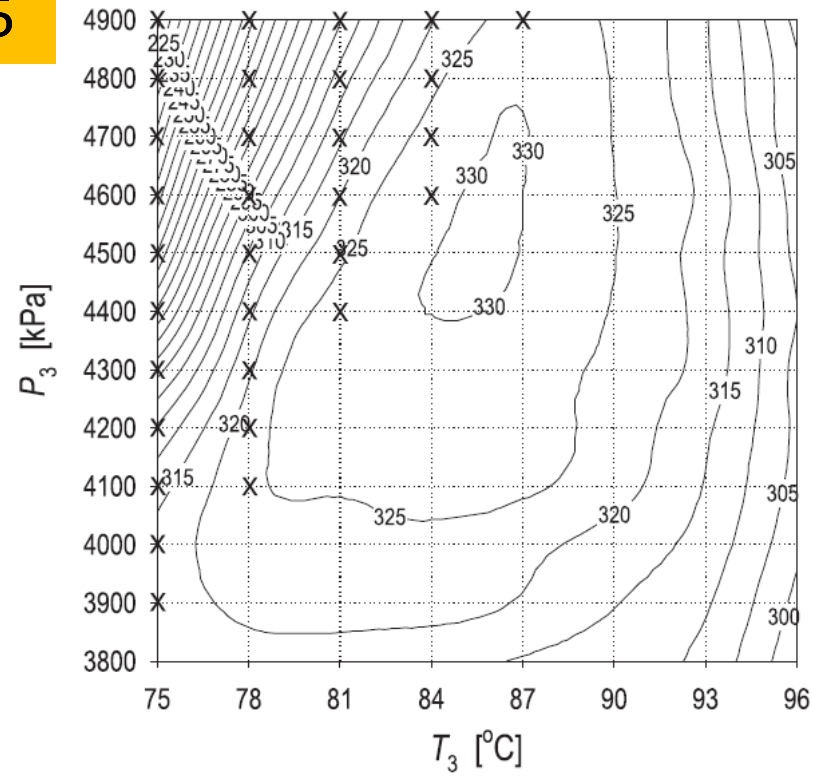

Optimum parameters	
T_3	85 °C
p_3	44.6 bar
m_{WF}	0.042 kg/s
W_{net}	330.8 W

Power output in response to changes in turbine inlet temperature (T_3) and max pressure (p_3)

(Baik et al., Applied Energy, 2011)

Supercritical (or transcritical) ORC

CO_2

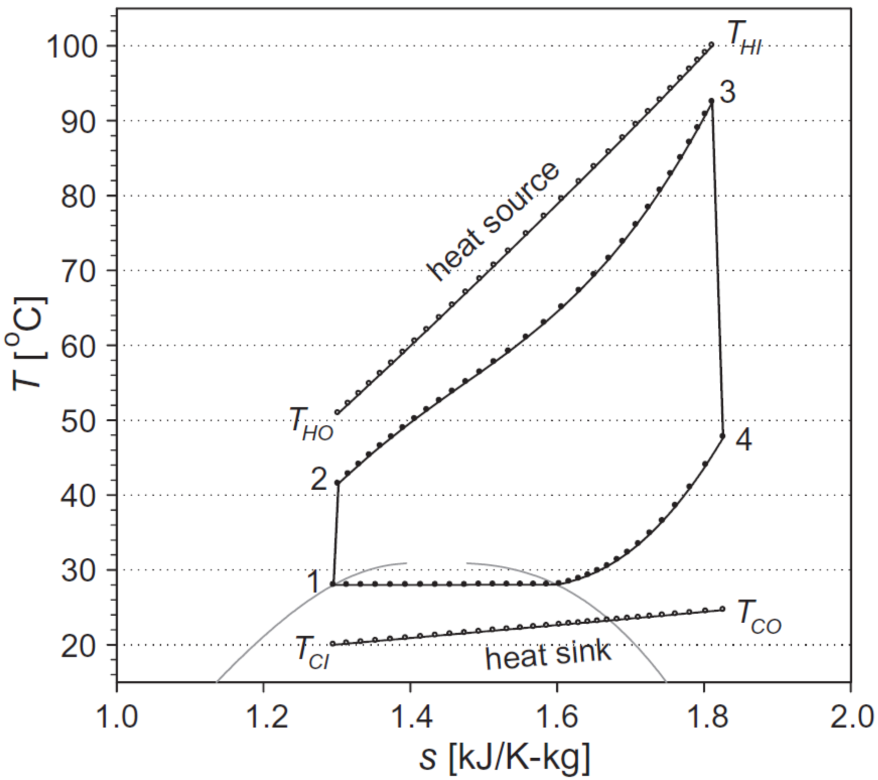

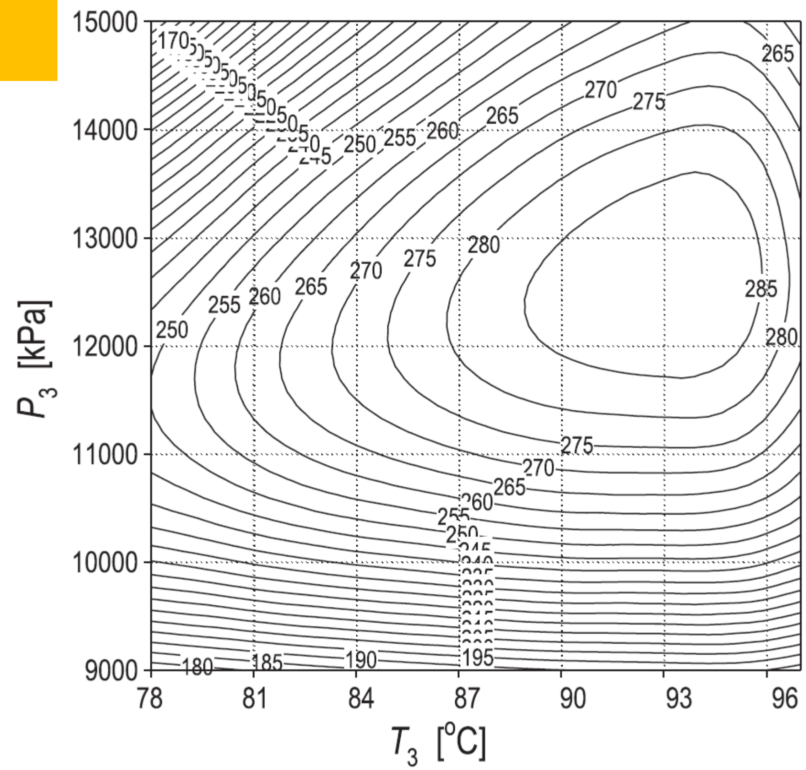

Optimum parameters	
T_3	92.5 °C
p_3	123.3 bar
m_{WF}	0.030 kg/s
W_{net}	289.8 W

(i.e., 12.5% lower than using R125)

Power output versus turbine inlet temperature (T_3) and maximum pressure (p_3)

(Baik et al., Applied Energy, 2011)

Subcritical vs supercritical ORC

T_{in}= 90°C

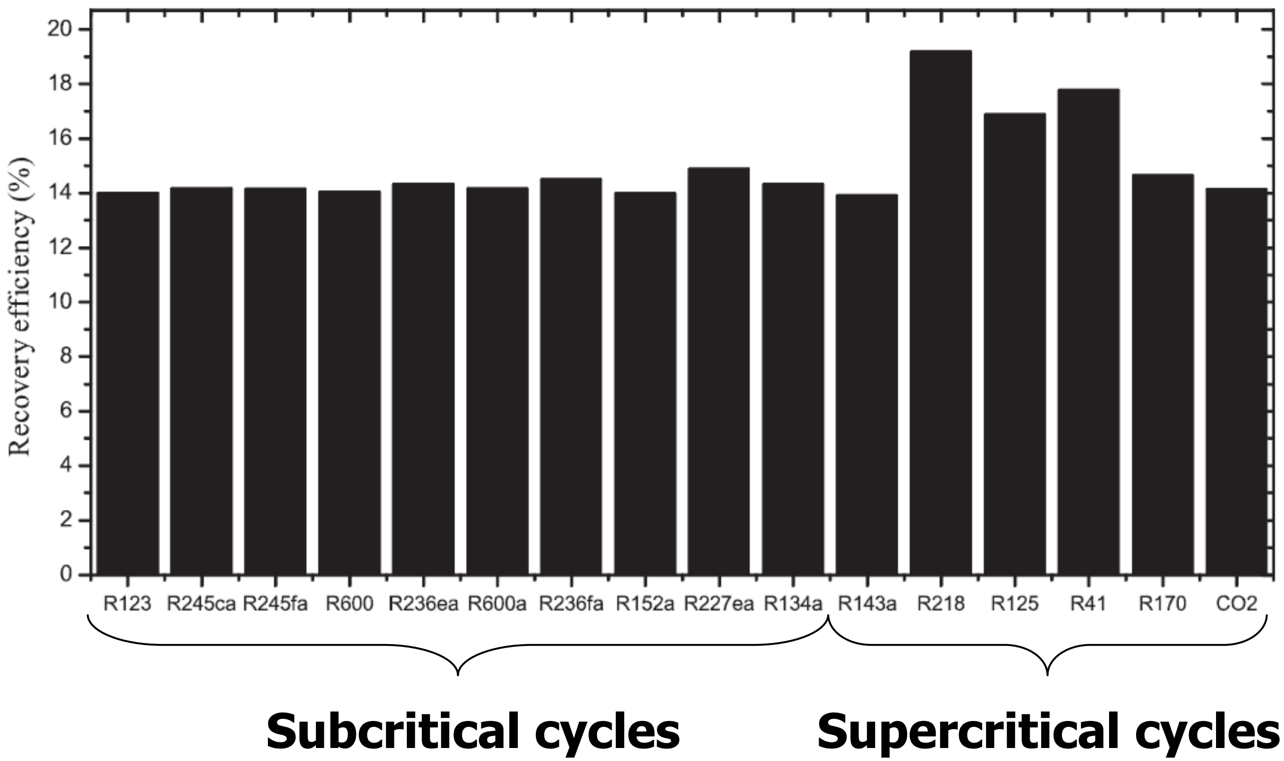

- Supercritical cycles give higher power output compared to subcritical cycles
- The highest system efficiency is obtained by R218, R41 and R125
- Also in this study R125 results in a higher power output compared to CO_2

(Shengjun Z. et al., Applied Energy, 2011)

Mixtures of organic fluids

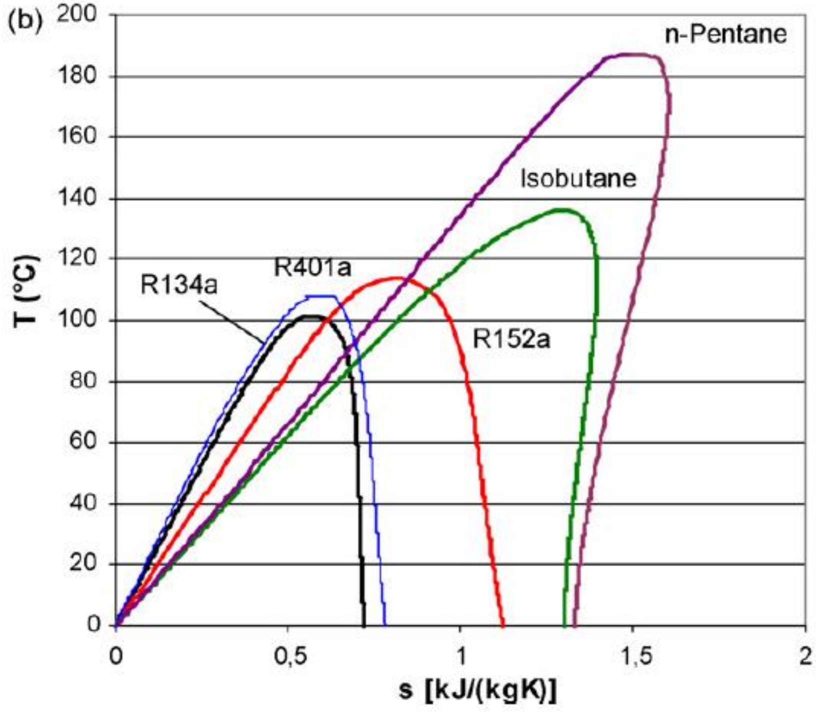

R152a
T_{CR} = 113,3 °C

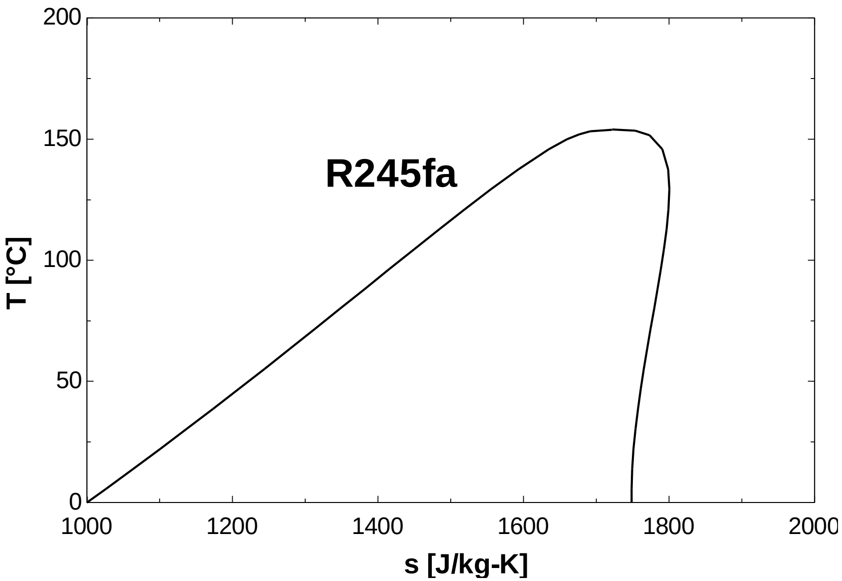

R245fa
T_{CR} = 154,1 °C

Let's consider a mixture of R152a (wet fluid, having a lower T_{CR}) and R245fa (dry fluid, having a higher T_{CR})

Mixtures of R245fa/R152a

Main advantage: evaporation and condensation at variable temperature

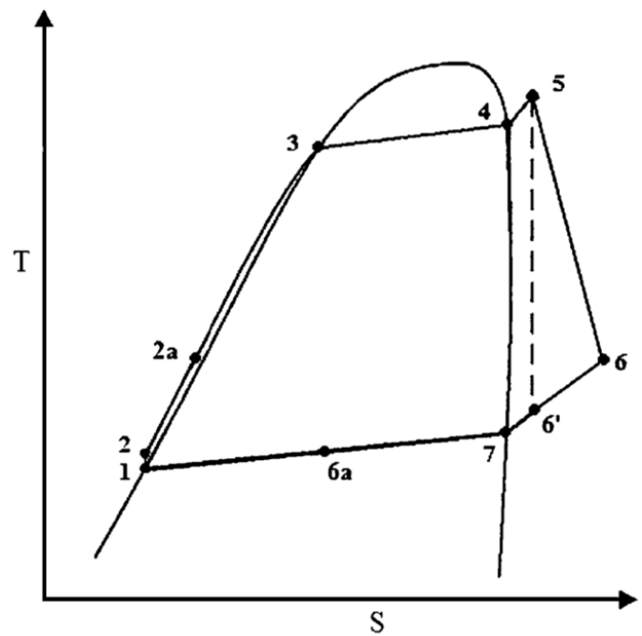

(Wang X.D. et al., Solar energy, 2009)

Three compositions of R245fa/R152a:

Ma: 0.9/0.1

Mb: 0.65/0.35

Mc: 0.45/0.55

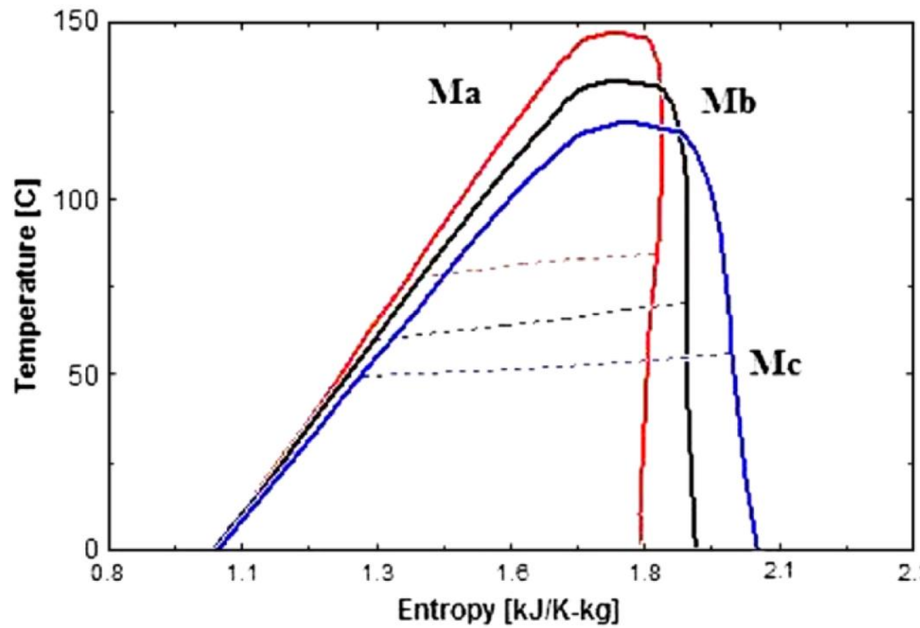

The saturated vapor curve and critical temperature of the mixture depend on the composition

Mixtures of R245fa and R227ea

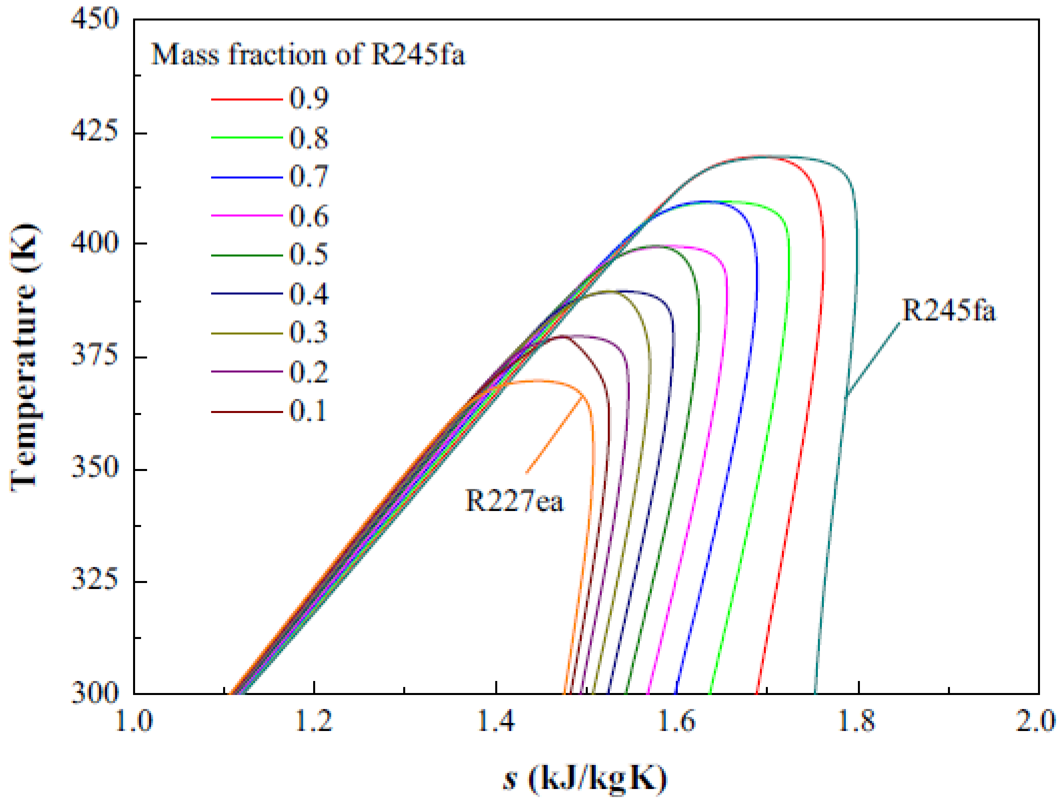

(Feng et al., Energy Conversion and Management, 2015)

Kalina cycle: mixture H_2O/NH_3

- In the Kalina cycle, geothermal heat at a low temperature is transferred to a mixture of ammonia and water

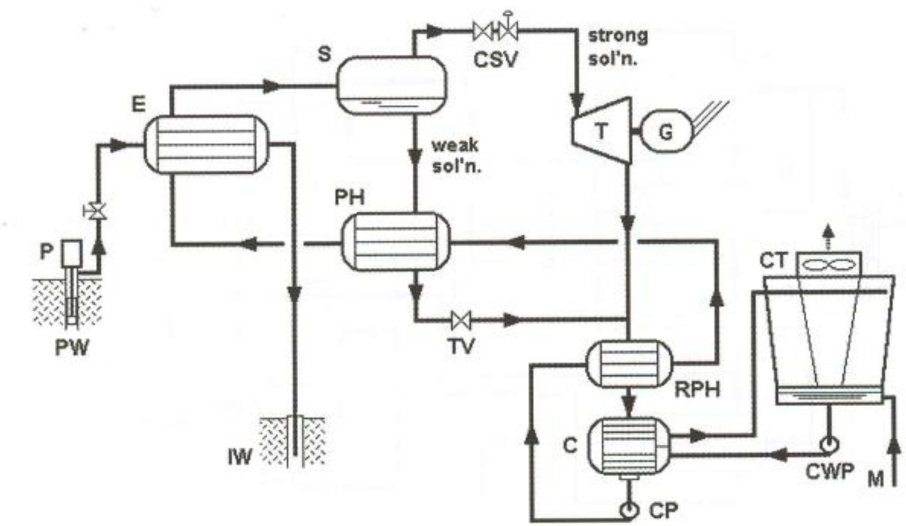

- Before the turbine, the ammonia-rich steam is separated from the liquid phase in a separator
- After the turbine, the steam and liquid phases are merged together and condensed in the condenser

- Comparison between boiling of pure water and different ammonia–water mixtures at 30 bar

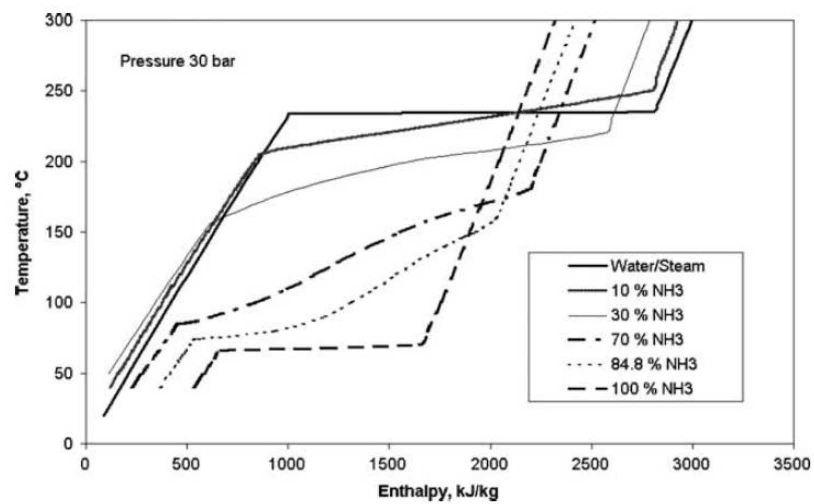

- The mixture of ammonia and water boils at a variable temperature depending on its composition
- The higher the fraction of ammonia in the mixture, the lower is its boiling temperature

Kalina power plant in Husavik (Iceland)

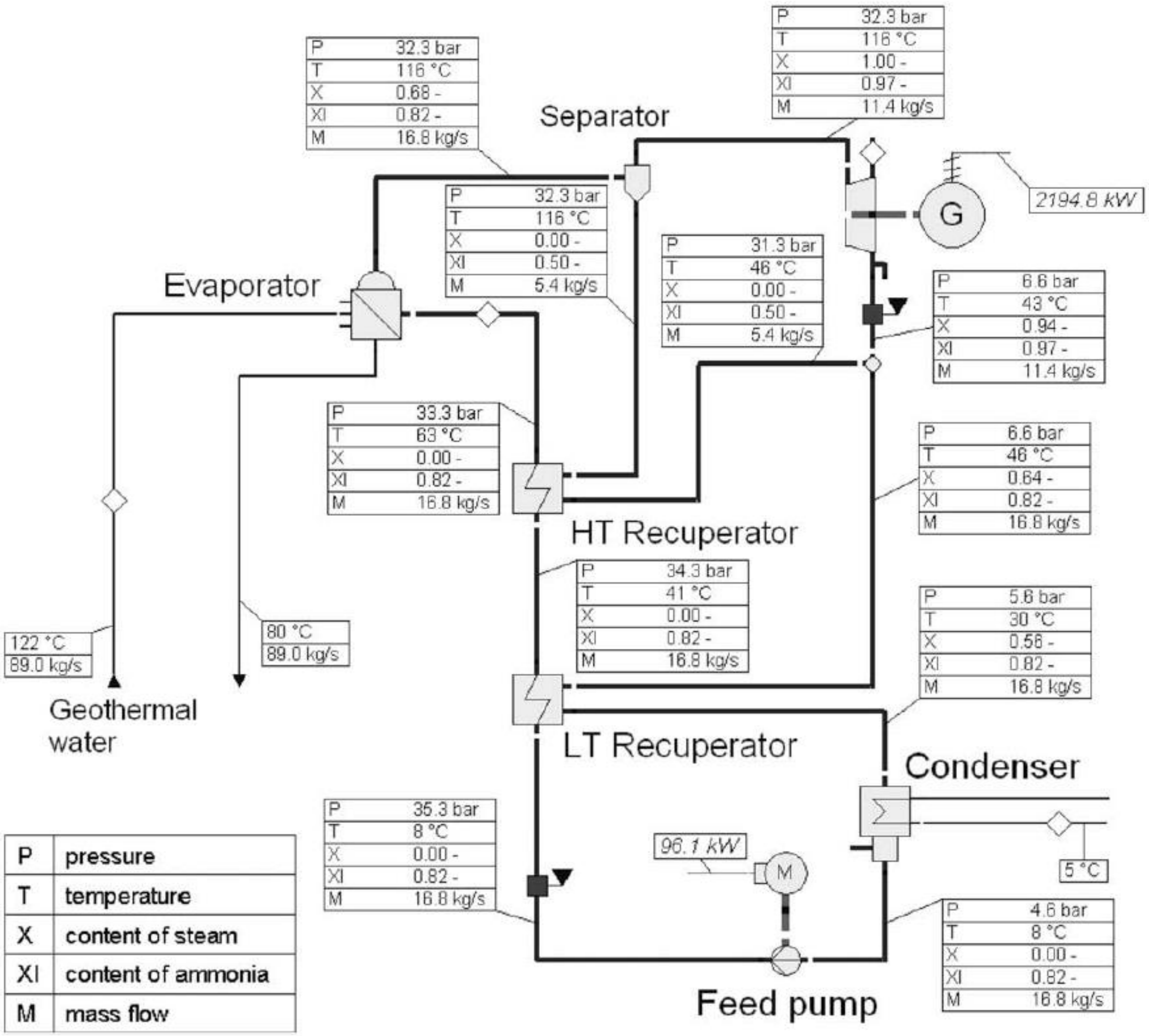

- Geofluid T_{in} = 124°C
- Mass flow rate of ammonia-water mixture to the evaporator = 16.8 kg/s
- Mass fraction of ammonia in the evaporator and condenser = 82%
- Turbine inlet pressure = 32.3 bar
- Generator power output = 2.2 MW

(Ogriseck, Applied Thermal Engineering, 2009)

Two-stage Organic Rankine Cycle coupled to ICE

Utilization of waste heat from internal combustion engines at two different temperature levels:

1) from the exhaust gases
2) from the cooling system of the combustion engine

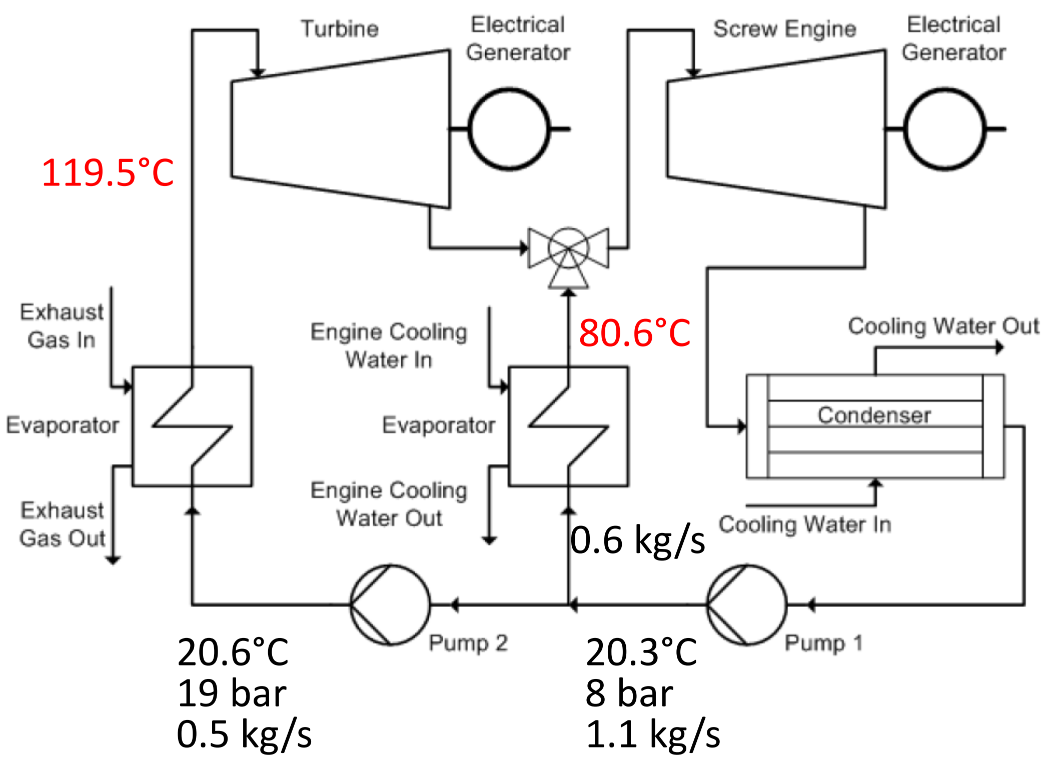

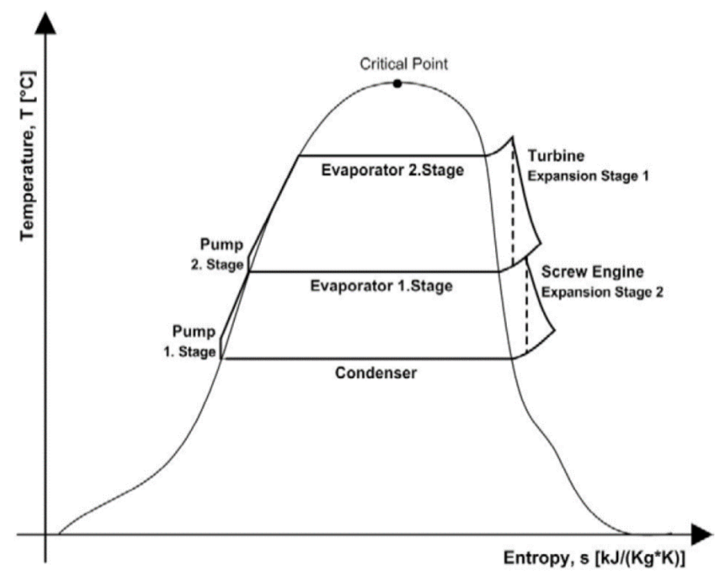

(Smolen S., Energy Science and Technology, 2011)

Dual loop ORC system combined with a Diesel engine

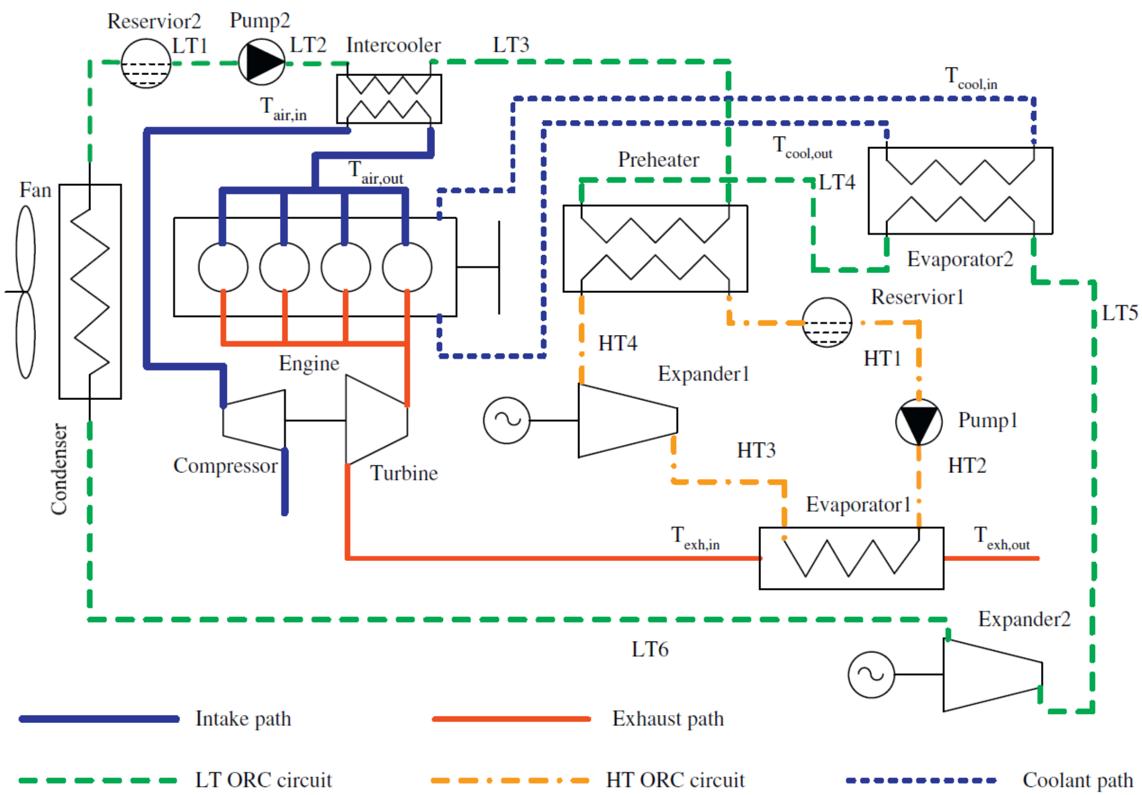

- The high temperature loop (yellow) recovers the exhausts heat
- The low temperature loop (green) recovers the residual heat of the HT loop, the waste heat of intake air in the intercooler, and the coolant waste heat
- The LT loop is coupled to the HT loop via the pre-heater, which is used as the condenser for the HT loop

(Zhang H.G., Applied Energy, 2013)

Dual loop ORC system: T-s diagrams

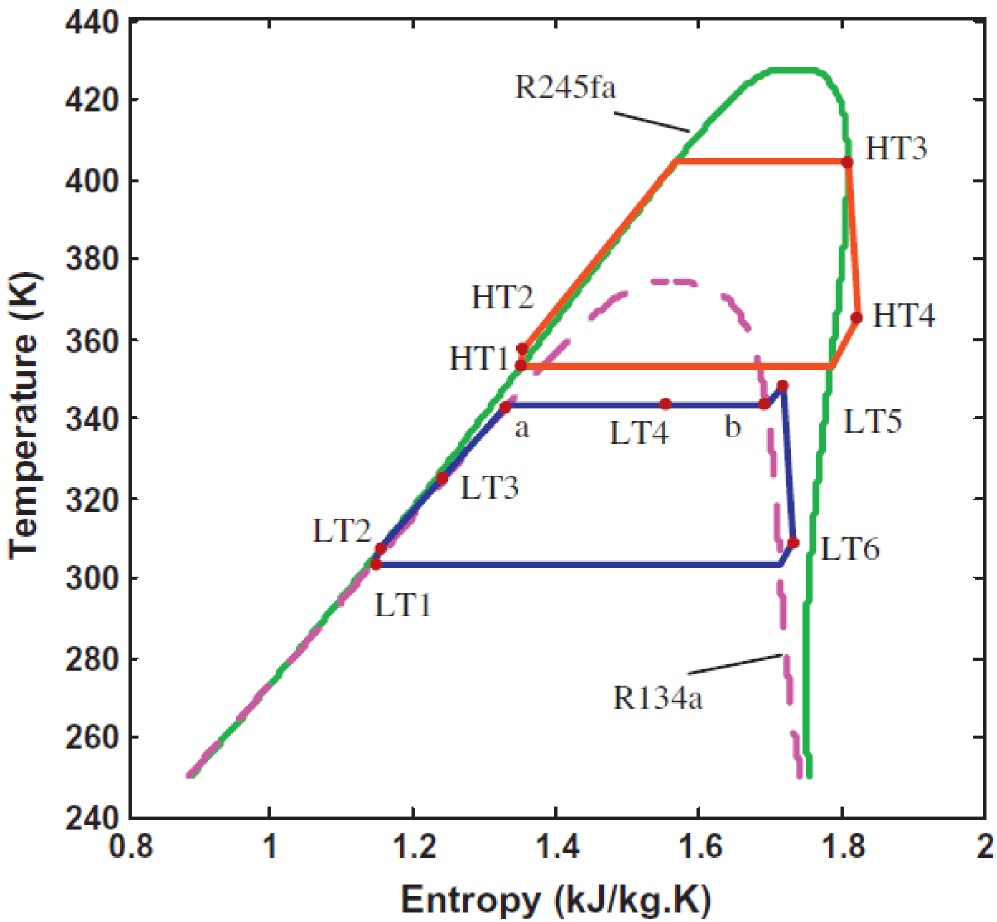

(Zhang H.G., Applied Energy, 2013)

- The working fluid in the HT loop is R245fa whereas R134a was selected for the low temperature ORC
- The saturation curves of R245fa and R134a are shown in the T–s diagram
- The upper red lines correspond to the HT loop, while the lower blue lines show the LT loop

Dual pressure ORC systems for geothermal resources

$$T_{in,geo} = 160°C$$

Optimum ORC configuration

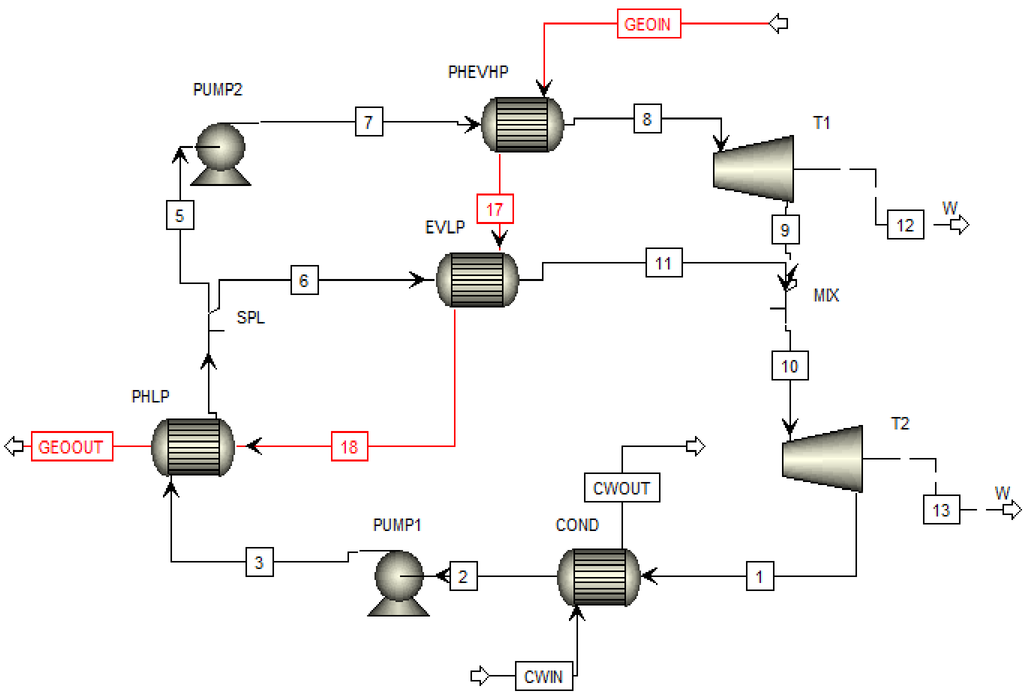

Optimum design parameters

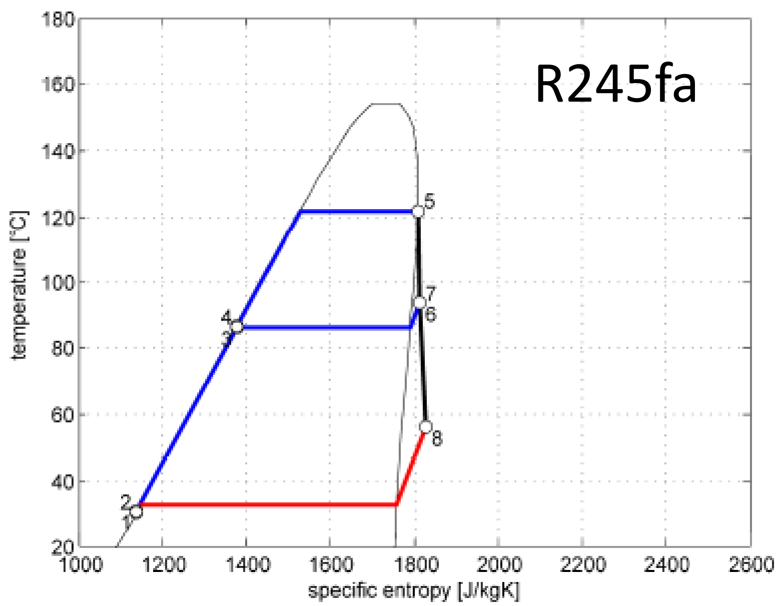

(Lazzaretto A. et al., Report ENEL-UNIPD, 2012)

Other evaluation parameters in the working fluid selection

Total heat transfer capacity when the maximum P_{net} is obtained

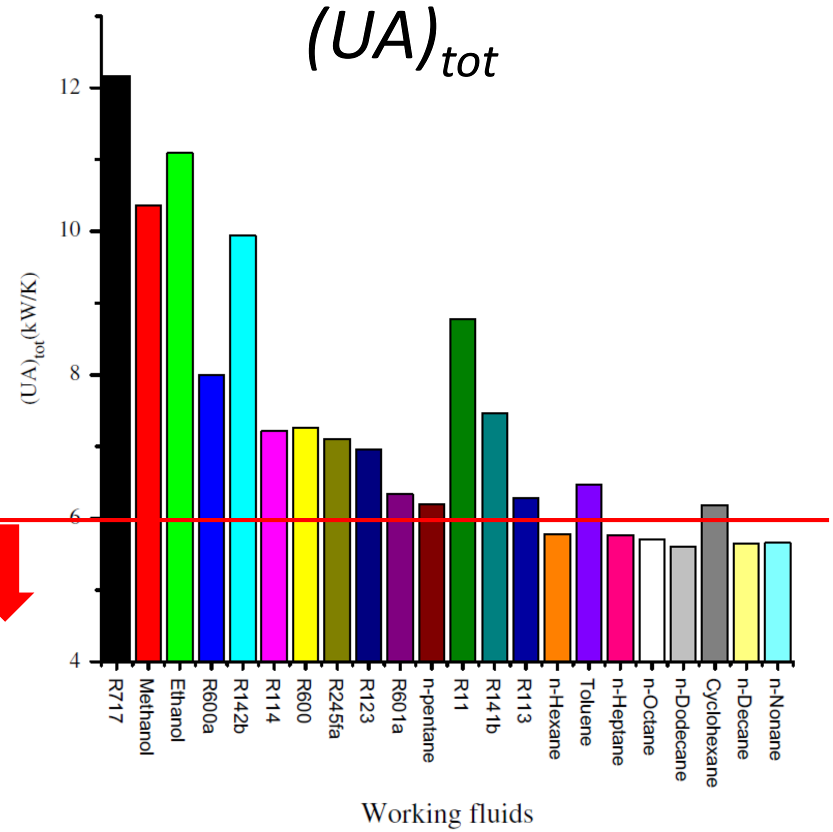

Expander size parameter when the maximum P_{net} is obtained

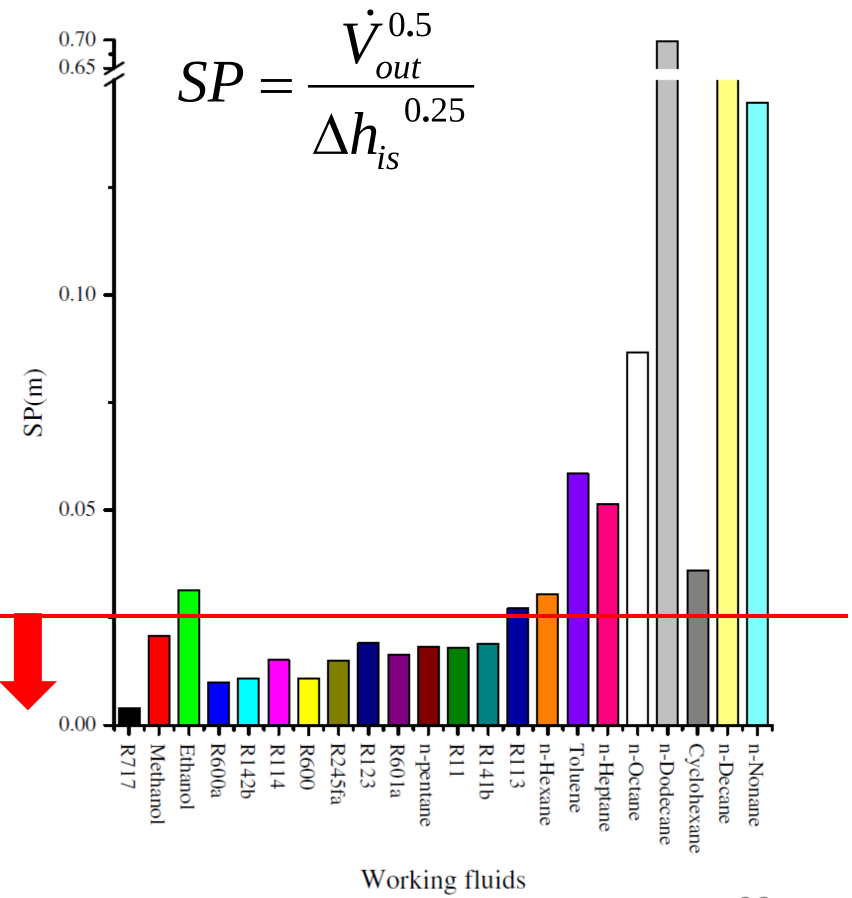

(He et al., Energy, 2012)

Economic objective functions

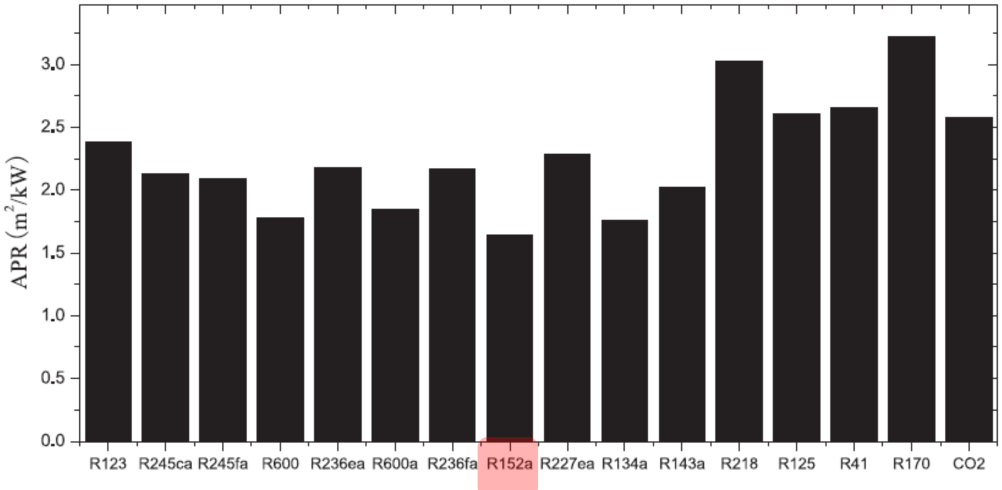

Ratio of total heat transfer area to total net power:

$$APR = \frac{A_{tot}}{\dot{W}_{net}}$$

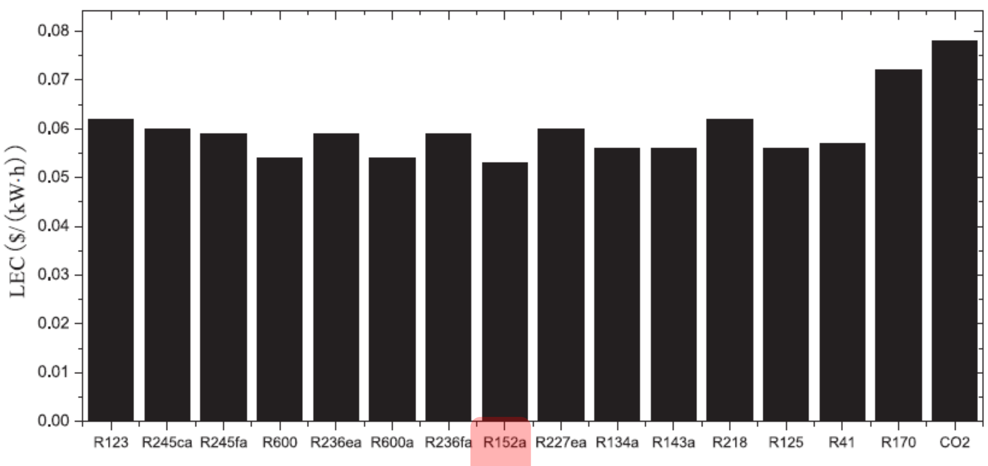

Levelized cost of electricity:

$$LEC = \frac{CC \cdot CRF + O\,\&\,M}{Annual\ \ Energy}$$

(Shengjun Z. et al., Applied Energy, 2011)

Specific investment costs of ORC systems

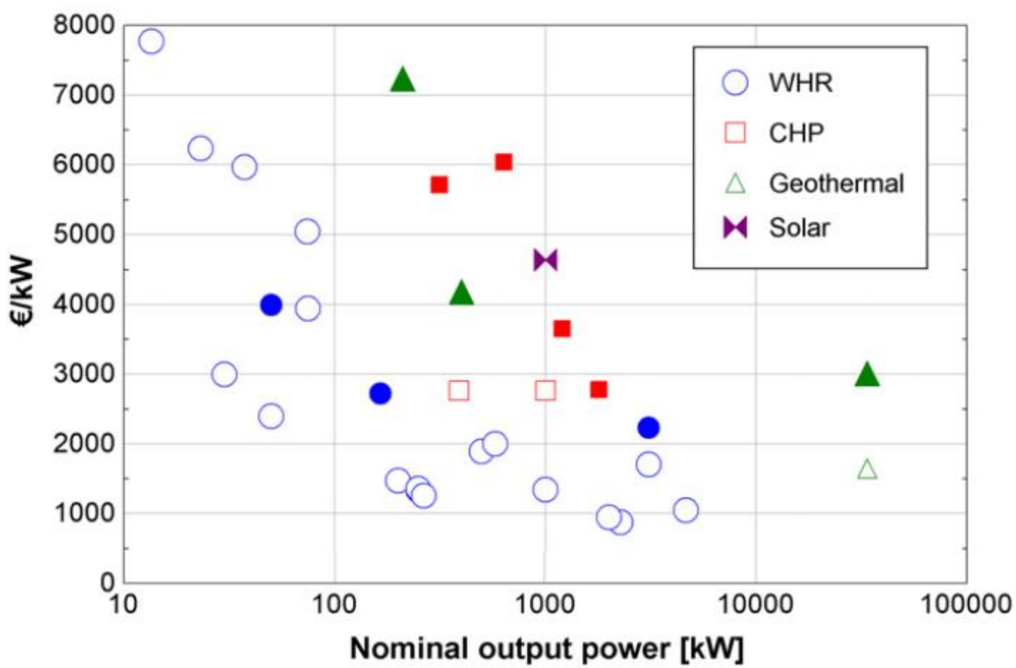

Module (empty dots) and total (plain dots) costs of ORC systems

(Quoilin et al., Renewable and Sustainable Energy Reviews, 2013)

- For a given target application, the cost tends to decrease when the output power increases
- Lowest costs are reported for waste heat recovery applications, while geothermal and CHP plants exhibit higher total cost
- "Total cost" differs from "module cost" in that it includes engineering, buildings, boiler (in case of CHP), process integration, etc., and can amount to two to three times the module cost

Optimization of a single pressure ORC

- Independent variables of the model are fixed as parameters:
  - m_{geo} = 100 kg/s
  - $T_{geo,in}$ = 130÷180°C at 10°C steps
  - $T_{geo,out} \geq$ 70°C
  - Working fluids: R600a (isobutane), R134a
  - η_P = 70%, η_T = 85%, η_{el} = 96%
  - T_{amb} = 20°C
  - $T_{air,out} = T_{cond}$ - 5°C
  - P_{ACC} = 0.15 kW per kg/s of air

- Decision variables:
  - condensation pressure (p_{cond})
  - mass flow rate of the organic fluid (m_{wf})
  - cycle maximum pressure (p_{max})
  - degree of superheating, measured in terms of specific entropy (Δs_{sup})
- Objective function:

$$\zeta_{rec} = \frac{P_{gen} - P_P - P_{ACC}}{\dot{E}_{geo}(T_{geo,in}) - \dot{E}_{geo}(T = 70\,^\circ\mathrm{C})}$$

Results for isobutane

Isobutane						
$T_{geo,in}$ (°C)	130	140	150	160	170	180
m_{WF} (kg/s)	62.4	76.0	81.8	91.6	105.6	114.5
p_{max} (bar)	14.27	15.16	18.85	23.11	35.24	44.19
$T_{T,in}$ (°C)	84.4	87.4	98.5	109.4	135.1	152.0
p_{cond} (bar)	4.375	4.345	4.376	4.376	4.396	4.381
T_{cond} (°C)	32.8	32.6	32.8	32.8	33.0	32.9
$m_{air,ACC}$ (kg/s)	2790	3490	3710	4175	4520	4995
$T_{air,out}$ (°C)	27.8	27.6	27.8	27.8	28.0	27.9
Q_{rec} (k Wt)	0	286	0	0	1288.6	2454.3
P_{gen} (kW)	2395.1	3083.9	3863.1	4868.9	6610.4	7988.1
P_{pump} (kW)	162.2	215.9	311.2	450.7	854.1	1193.7
P_{ACC} (kW)	418.6	523.6	556.6	626.5	678.1	749.2
P_{net} (kW)	1814.4	2344.4	2995.3	3791.7	5078.2	6045.3
ζ_{rec}	0.337	0.356	0.381	0.411	0.476	0.496
η_t	0.0748	0.0793	0.0909	0.1010	0.1194	0.1289

Optimum values of the decision variables

Optimum values of the objective function ζ_{rec}

- Optimum isobutane cycles are mostly subcritical with saturated vapor at turbine inlet
- At the highest brine temperatures the optimal isobutane cycles are either subcritical with slightly superheated vapor (170°C) or supercritical (180°C)

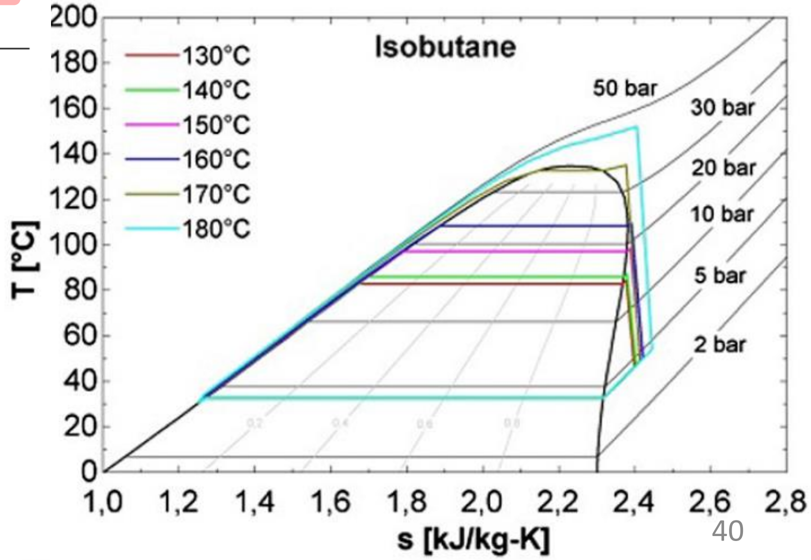

Results for R134a

R134a						
$T_{geo,in}$ (°C)	130	140	150	160	170	180
m_{WF} (kg/s)	138.2	145.0	159.5	177.4	195.0	212.1
p_{max} (bar)	40.47	45.21	47.97	52.57	58.64	66.70
$T_{T,in}$ (°C)	104.4	118.5	129.4	139.4	149.3	159.3
p_{cond} (bar)	8.475	8.454	8.323	8.319	8.308	8.286
T_{cond} (°C)	33.4	33.3	32.7	32.7	32.7	32.6
$m_{air,ACC}$ (kg/s)	2680	3130	3785	4225	4680	5170
$T_{air,out}$ (°C)	28.4	28.3	27.7	27.7	27.7	27.6
Q_{rec} (kWt)	0	0	1294.6	2672.4	3933.0	5060.0
P_{gen} (kW)	3022.7	3846.7	4822.9	5882.9	7039.9	8316.8
P_{pump} (kW)	531.1	639.6	757.0	939.3	1172.8	1478.3
P_{ACC} (kW)	402.0	469.3	567.8	634.0	702.2	775.6
P_{net} (kW)	2089.6	2737.8	3498.1	4309.6	5165.0	6062.9
ζ_{rec}	0.388	0.416	0.445	0.467	0.484	0.498
η_t	0.0826	0.0926	0.1033	0.1129	0.1215	0.1293

Optimum values of the decision variables

Optimum values of the objective function ζ_{rec}

- R134a optimum cycles are supercritical (except at 130°C)
- The exergy recovery efficiency achieved by R134a is always higher compared to that achieved by isobutane

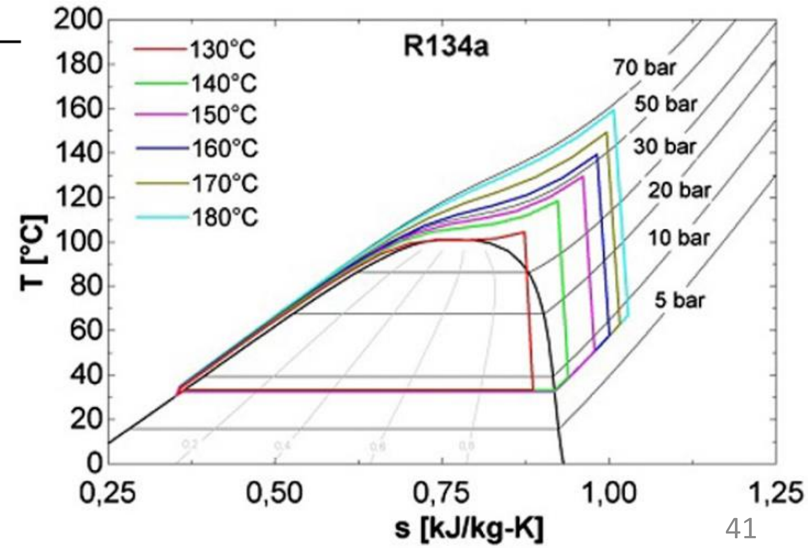

Isobutane vs R134a

Working fluid	Isobutane	R134a
$T_{geo,in}$ (°C)	150	150
m_{geo} (kg/s)	100	100
m_{WF} (kg/s)	81.8	159.5
p_{max} (bar)	18.9	48.0
$T_{T,in}$ (°C)	98.5	129.4
T_{cond} (°C)	32.8	32.7
p_{cond} (bar)	4.4	8.3
P_{gen} (kW)	3863	4823
P_{pump} (kW)	311	757
P_{ACC} (kW)	557	568
P_{net} (kW)	2995	3498
ζ_{rec} (%)	38.1	44.5
η_{th} (%)	9.1	10.3

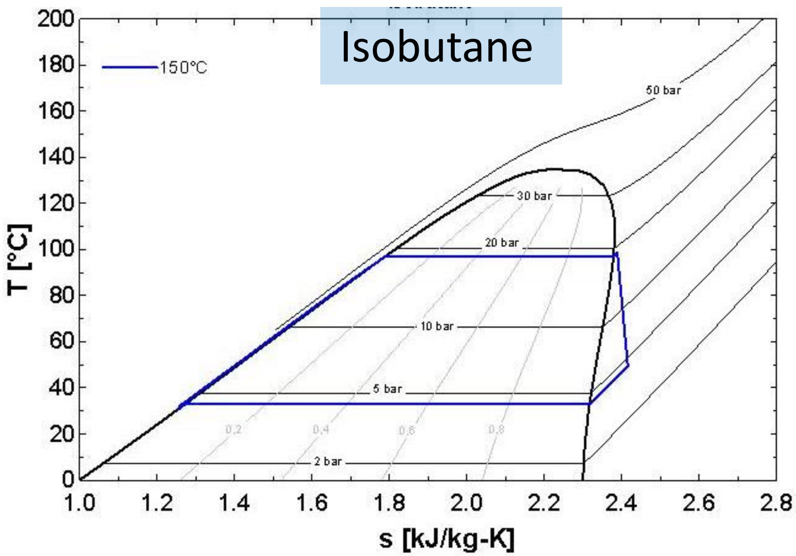

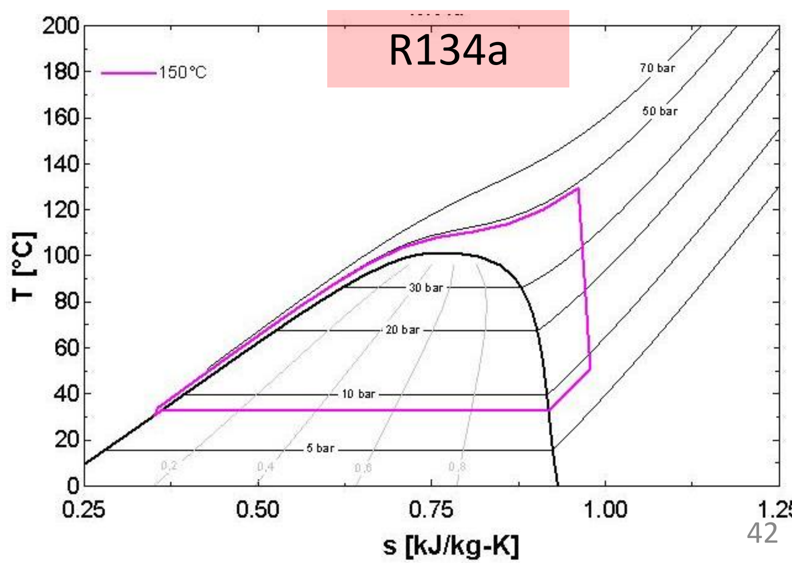

Variation of the thermodynamic objective function around the optimum

Isobutane, $T_{geo,in}$=150°C

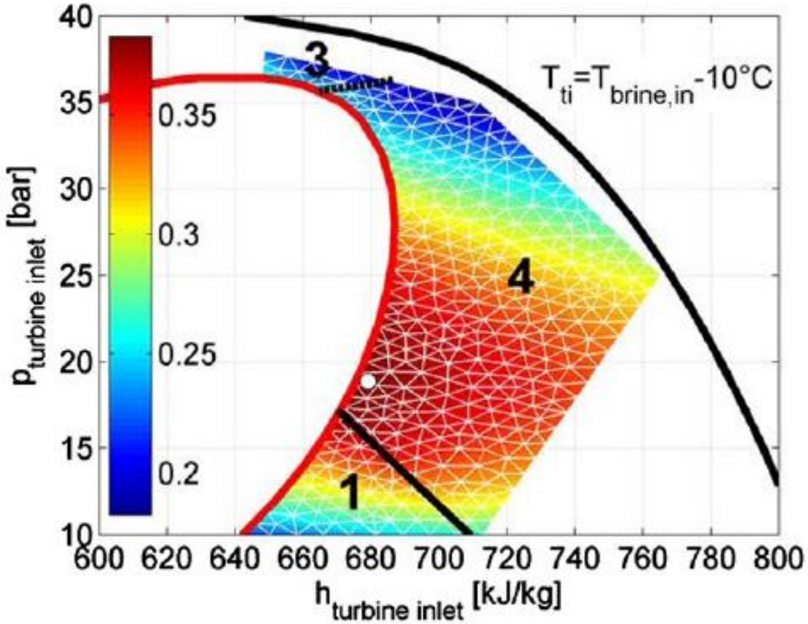

R134a, $T_{geo,in}$=150°C

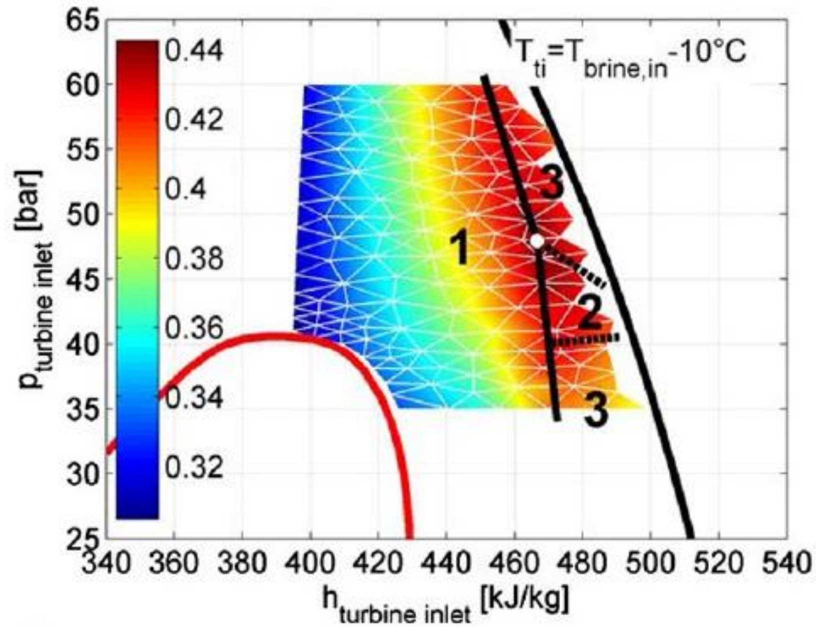

- The highest values of ζ_{rec} are obtained at turbine inlet states close to saturated vapor and maximum pressures close to the optimum pressure
- The trend of ζ_{rec} is quite flat in response to changes of the turbine inlet supercritical pressure whereas it rapidly decreases when the turbine inlet enthalpy is lowered

(Toffolo et al., Applied Energy, 2014)

Enhancement of the Electrical Efficiency of Commercial Fuel Cell Units by Means of an Organic Rankine Cycle: A Case Study

Carlo De Servi[1]
e-mail: carlo.deservi@polimi.it

Stefano Campanari
e-mail: stefano.campanari@polimi.it

Politecnico di Milano,
Department of Energy,
Via Lambruschini 4,
20156 Milano, Italy

Alessio Tizzanini
Enel Ingegneria e Ricerca SpA,
Via Mantova 24,
00198 Roma, Italy
e-mail: alessio.tizzanini@enel.com

Claudio Pietra
Turboden s.r.l.,
Via Cernaia 10,
25124 Brescia, Italy

Among the various fuel cell (FC) systems, molten carbonate fuel cells (MCFC) are nowadays one of the most promising technologies, thanks to the lower specific costs and a very high electrical efficiency (net low heating value (LHV) electric efficiency in the range 45%–50% at MW_{el} scale using natural gas as fuel). Despite this high performance, MCFC rejects to the ambient almost half of the fuel energy at about 350–400 °C. Waste heat can be exploited in a recovery Rankine cycle unit, thereby enhancing the electric efficiency of the overall system. Due to the temperature of the heat source and the relatively small power capacity of MCFC plants (from few hundred kW_{el} to 10 MW_{el}), steam Rankine cycle technology is uneconomical and less efficient compared to that of the organic Rankine cycle (ORC). The objective of this work is to verify the practical feasibility of the integration between a MCFC system (topping unit) and an ORC turbogenerator (bottoming unit). The potential benefits of the combined plant are assessed in relation to a commercial MCFC stack. In order to identify the most suitable working fluids for the ORC system, organic substances are considered and compared. The figure of merit is the maximum net power of the overall system. Finally, the economical benefits of the integration are determined by evaluating the levelized cost of electricity (LCOE) of the combined plant, with respect to the standalone MCFC system. In order to assess the economic viability of the bottoming power unit, two cases are considered. In the first one, the ORC power output is approximately 500 kW_{el}; in the latter, about 1 MW_{el}. Results show that the proposed solution can increase the electrical power output and efficiency of the plant by more than 10%, well exceeding 50% overall electrical efficiency. In addition, the LCOE of the combined power plant is 8% lower than the standalone MCFC system.
[DOI: 10.1115/1.4023119]

1 Introduction

Fuel cells (FC) are a promising technology for distributed electricity production, especially for power applications in the few hundred kW_{el} to 10-MW_{el} capacity range. They exhibit high electrical efficiency and low pollutants emissions, they can be applied to combined heat and power generation (CHP), and they can use natural gas as primary fuel as well as biogas (for instance, from wastewater treatment) or fuel blends. Despite these figures of merit, they have achieved limited penetration into the energy market, mainly due to their high specific costs compared to other conventional technologies. A possible way to improve power plant economics consists of enhancing its electrical efficiency as much as possible. Waste heat dissipated by the stack or the exhaust gases can be exploited to generate additional electricity in an organic Rankine cycle (ORC) heat recovery system [1,2]. In this paper, the potential benefits of the integration between a fuel cell power plant (topping unit) and an ORC genset (bottoming unit) are assessed in relation to a specific commercial molten carbonate fuel cell (MCFC) system [3]. This kind of fuel cell has been selected due to its well-established performance, potential competitiveness, practical availability on the market, and an exhaust gas temperature consistent with the use of a heat recovery cycle [1,2,4].

The MCFC stack releases exhaust gases at a relatively low temperature, namely about 380 °C. This heat source is particularly suitable for recovery in a bottoming unit based on ORC technology. ORC power plants are nowadays more and more applied in many fields as, for instance, in the exploitation of low enthalpy geothermal sources [5] or biomass thermal conversion. In order to identify the most suitable working fluids for the analyzed case study, different candidate substances are considered and compared in both subcritical and supercritical ORC configurations. The net power of the bottoming system is maximized by optimizing its thermodynamic parameters, the maximum pressure, and temperature of the cycle. The detailed simulations of the ORC are performed in a commercial process modeling tool [6], while an optimization algorithm implemented in an external programming environment [7] varies cycle parameters until the maximum value of the objective function is reached.

Finally, the paper presents a preliminary economic analysis in order to investigate the feasibility of the proposed solution. Thanks to the modular features of the fuel cell system, two different power capacities of the combined plant are considered (500 kW_{el} and 1 MW_{el}, respectively), in order to assess the effect of the bottoming unit capacity on the economics of the entire plant.

2 MCFC Unit

In the frame of the various FC technologies, MCFCs feature one of the lowest specific costs and a very high efficiency [8]. One of the most experienced companies in this field claims that MCFCs electricity costs are about 1.2 to 1.5 times the costs of

[1]Corresponding author.

Contributed by the International Gas Turbine Institute (IGTI) ASME for publication in the Journal of Engineering for Gas Turbines and power. Manuscript received February 29, 2012; final manuscript received October 21, 2012; published online March 18, 2013. Assoc. Editor: Piero Colonna.

Copyright © 2013 by ASME

Downloaded From: http://gasturbinespower.asmedigitalcollection.asme.org/ on 03/17/2015 Terms of Use: http://asme.org/terms

Table 1 Main performance data of the MCFC unit [10]

MCFC "DFC3000" performance data		
Power output @ BOL (beginning of life)	(kW_{el})	2800
Power output @ EOL (end of life)	(kW_{el})	2520
Efficiency (LHV)	(%)	47 ± 2
Exhaust temperature	(°C)	379 ± 10
Exhaust flow	(kg/h)	16,600
NO_x emissions	(g/MWh)	4.5
SO_x emissions	(g/MWh)	0.045
PM10	(g/MWh)	0.009
CO_2	(kg/MWh)	445

conventional power systems, such as reciprocating engines or gas turbines, depending upon the price of fuel [9]. However, in the MW_{el} capacity range, MCFCs are about 10 times cleaner in terms of NO_x emissions versus competitive conventional technologies, and they are the most fuel-efficient (net LHV electric efficiency in the range 45%–50%) and lowest CO_2 emission fossil-fuelled power generation technology available on the market [9]. For these reasons, MCFCs do qualify in many countries for government support grants and subsidies to encourage ultraclean power generation [9].

MCFC units are already commercially available, even if they have not yet achieved significant penetration into the energy market, mainly due to their specific costs (2500–2800 €/kW_{el} for the MW_{el} scale [9]), substantially higher than conventional competitive technologies. In this study, the MCFC unit is modeled according to the performance of a commercial 2.8-MW_{el} MCFC power plant [10], whose data are summarized in Table 1.

Even if the MCFC system exhibits a high efficiency, almost half of the fuel energy is rejected to the ambient. Generally, in order to improve the fuel cell power plant economy, thermal energy in the exhaust gases is recovered for CHP. However, from an economical point of view, it can be more attractive to recover waste heat in a bottoming power unit [1,2,4]. Due to the temperature of the exhaust gases ($\sim$380 ± 10 °C) and the current limited power capacity of the FC plant, this kind of heat source is particularly suitable for recovery in an ORC system. Moreover, the integration of the MCFC unit with the ORC turbogenerator requires only simple modifications to the plant layout: the addition of a counter-flow heat exchanger to heat the ORC working fluid. In principle, the implementation of the ORC turbogenerator can be designed also as a plant retrofit, which can also be technically and economically attractive.

Temperature and composition of exhaust gases vary during the useful life of the MCFC unit due to changes in efficiency of the FC system. The power output of a MCFC stack typically suffers from a progressive performance decay. This reduction is almost linear over time and is periodically recovered with a maintenance procedure based on stack replacement [3] (every five years, as generally proposed by manufacturers). Therefore, for the purpose of this study, it is possible to model the FC plant by referring to mean values of composition, temperature, and mass flow rate of the exhaust gases. As Table 2 shows, the assumed data for the MCFC system are equal to the average between the beginning of life (BOL) and the end of life (EOL) conditions.

Table 2 Exhaust flow composition, mass flow rate, and temperature for the MCFC unit [9]

Components (mol %)	BOL	EOL	Assumed value
CO_2	4.5%	4.1%	4.3%
H_2O	18.8%	17.3%	18.1%
N_2	67.5%	68.5%	68.0%
O_2	9.1%	10.2%	9.6%
Total	100.0%	100.0%	100.0%
Mass flow rate	4.61 kg/s	5.07 kg/s	4.84 kg/s
Temperature (°C)	369 °C	390 °C	379 °C

3 Thermodynamic Design of the Heat Recovery Cycle and Working Fluid Selection

One of the main steps in designing ORC processes is the selection of the working fluid. Since the exhaust gases are released from the MCFC unit at about 380 °C, the heat recovery cycle is classified as a high temperature ORC [11]. Extensive surveys about this kind of application have been already presented in literature: Angelino and Invernizzi [12] considered aromatics hydrocarbons, siloxanes, perfluorobenzene, and allied compounds for space power cycles; Angelino and Colonna di Paliano studied, in addition to the previous substances, the performance of alkanes [1] and siloxanes mixtures [2], and Drescher and Brüggemann [13] suggested the exploitation of alkylbenzenes in biomass CHP plants.

3.1 Thermal Stability. Unlike water, organic substances undergo chemical decomposition at high temperature [14]. For this reason, fluids suitable for the analyzed application must feature a high level of thermal stability, and the maximum operating temperature of the thermodynamic cycle is limited to preserve the useful life of the ORC working medium. The temperature threshold, below which thermal degradation occurs at an acceptable rate, should be assessed by experimental investigation. Testing equipments should reproduce realistic operating conditions, since fluid degradation is a complex irreversible phenomenon influenced by several aspects, such as the type of containing materials, the residence time, and the nature and quantity of impurities (moisture, lubricants, or air) [12,15]. However, such detailed data only exist for a limited number of fluids. For the others, available information is limited to laboratory tests, the results of which are sometimes ambiguous [12,16]. For example, Andersen and Bruno [17] found that toluene decomposes at 315 °C with a rate higher than that of n-pentane. On the contrary, it was successfully tested in a dynamic test loop at 400 °C [18], and it is currently used in a power cycle with a turbine inlet temperature of 325 °C [19]. These discrepancies are generally due to differences in test conditions that make the data retrieved in literature not strictly comparable [12]. In general, from literature sources [12,16,17], it can be concluded that:

- for similar substances (i.e., with the same chemical structure), the thermal stability gets worse with fluids having higher molecular weight
- branched molecules are less thermally stable than straight chains, and ring structures are the most thermally stable (e.g., benzene)
- thermal stability of organic fluids is negatively influenced by the presence of air, moisture, or other impurities in the system

For the considered case study, the constraint on the maximum temperature limits the candidate working fluids to the list reported in Table 3. Four classes of substances can be recognized: aromatic hydrocarbons, alkanes, siloxanes, and hydrofluorocarbons. Most of these fluids show good thermal stability at least up to 270 °C.

The stability thresholds (T_{stab}) of Table 3 are assessed on the basis of specific experimental investigation [14,18,20–26], if available, or of technical papers about real applications [19,27]. For thermal stability of n-butane, n-hexane, cyclobutane, and D_3, no reliable references are available in literature. Therefore, as a first approximation, these substances are supposed to behave at high temperature, as other fluids with similar molecular structure: n-butane and n-hexane as n-pentane, cyclobutane as cyclopentane, and D_3 as the other siloxanes. It is also necessary to clarify that the threshold temperature associated with cyclohexane has only a qualitative validity. According to Ref. [24], at 290 °C cyclohexane

Downloaded From: http://gasturbinespower.asmedigitalcollection.asme.org/ on 03/17/2015 Terms of Use: http://asme.org/terms

Table 3 Working fluids for high temperature ORC. For each fluid, the table shows the CAS number, the critical temperature, T_C, and pressure, P_C, the normal boiling temperature, T_B, and the molecular weight, MW, the thermal stability threshold, T_{stab}, and the global warming potential, GWP.

Substance	CAS number	T_C (°C)	P_C (bar)	T_B (°C)	MW (kg/kmol)	T_{stab} (°C)	GWP
Aromatic hydrocarbons							
Benzene	71-43-2	288.87	49.06	80.07	78.11	> 350, [17,24]	–
Toluene	108-88-3	318.60	41.26	110.60	92.14	> 350, [18,19,25]	–
p-Xylene	106-42-3	343.04	35.26	138.31	106.17	~300, [24]	–
o-Xylene	95-47-6	357.28	37.45	144.38	106.17	~300, [24]	–
m-Xylene	108-38-3	343.70	35.40	139.07	106.17	~300, [24]	–
Ethylbenzene	100-41-4	343.97	36.16	136.17	106.17	< 290, [24]	–
Propylbenzene	103-65-1	365.14	32.01	159.20	120.19	n.a.	–
Buthylbenzene	104-51-8	387.33	28.87	183.26	134.22	n.a.	–
Linear alkanes							
n-Butane	106-97-8	151.98	37.96	–0.49	58.12	270[a]	~20
n-Pentane	109-66-0	196.55	33.70	36.60	72.15	270, [27]	~20
n-Hexane	110-54-3	234.67	30.34	68.71	86.18	270[a]	n.a.
Cyclic alkanes							
Cyclobutane	287-23-0	186.85	48.40	12.53	56.11	300[b]	n.a.
Cyclopentane	287-92-3	238.54	45.15	49.25	70.13	300, [20]	11
Cyclohexane	110-82-7	280.49	40.75	80.74	84.16	< 290, [24]	n.a.
Linear siloxanes							
MM	107-46-0	245.60	19.39	100.25	162.38	> 350, [22]	–
MDM	107-51-7	290.94	14.15	152.51	236.53	> 350, [23,26]	–
MD_2M	141-62-8	326.25	12.27	194.36	310.69	> 350, [23]	–
Cyclic siloxanes							
D_3	541-05-9	281.00	16.60	135.09	222.46	> 350[c]	–
D_4	556-67-2	313.35	13.32	175.35	296.62	> 350, [22,26]	–
D_5	541-02-6	346.00	11.60	210.90	370.77	> 350, [22]	–
Hydrofluorocarbons HFC							
R125	354-33-6	66.02	36.18	–48.09	120.02	> 350, [21]	3420
R134a	811-97-2	101.06	40.59	–26.07	102.03	> 350, [21]	1370
R143a	420-46-2	72.71	37.61	–47.24	84.04	350, [14]	4180
R227a	431-89-0	101.75	29.25	–16.34	170.03	> 350, [14]	3580
R236fa	690-39-1	124.92	32.00	–1.44	152.04	> 350, [14]	9820
R245fa	460-73-1	154.10	36.51	15.14	134.05	260–300, [14,15]	1050

[a]Since no detailed data are available in the literature regarding n-butane and n-hexane, for these fluids, the same thermal stability threshold of n-pentane is assumed.
[b]Since no detailed data are available in the literature for cyclobutane, the same thermal stability threshold of cyclopentane is assumed.
[c]D_3 thermal stability has been assumed equal to that of the other siloxanes.

exhibits only a marginal stability, not adequate for industrial applications. Nevertheless, T_{stab} of cyclohexane is assumed equal to 290 °C, since (i) Ref. [24] does not describe how such a result has been obtained and (ii) there are other laboratory tests proving that a molecule of the same class, cyclopentane, features good thermal stability up to 300 °C [20], provided that no interaction with air occurs.

Looking at Table 3, it is important to consider that some of the reported values of T_{stab} are assessed in particular experimental conditions, for instance, by considering pure fluids or test lengths limited to few hours [14]. For this reason and also for precautionary considerations, these values can be higher than those applicable to a real application. Thermodynamic properties of the fluids of Table 3 are retrieved from Refs. [28] and [29], while the global warming potential (GWP) is taken from Ref. [30].

3.2 Environmental Impact and Safety Issues. Candidate substances suitable for ORC power systems should also feature a limited environmental impact. In order to evaluate this aspect, some parameters are taken into account, such as ozone depletion potential (ODP) and GWP, ASHRAE safety classification or occupational exposure limit (OEL), and the flammability level [31–33]. In the present study, the following criteria are applied:

- Fluids with ODP higher than zero have to be discarded, because they will be phased out over the next few years. For this reason, hydrochlorofluorocarbons (HCFC) are not examined.
- Substances with a GWP greater than 1370 (i.e., the GWP of R-134a, one of the most used fluids in refrigeration applications) feature an unacceptable environmental impact. Note that R-134a will be phased out of automotive air-conditioning applications in Europe due to its GWP by 2017.
- All the substances listed in Table 3, except benzene, present reasonably low toxicity characteristics.[2]
- The flammability hazard posed by each fluid is controllable by designing properly the ORC components, according to the safety precautions prescribed in the operating environment [15,34]. For instance, hydrocarbons as toluene and pentane have been successfully used at relatively high temperature [16,19,27] without posing any serious problem. However, the hazard control requirements increase the cost of the ORC installation [15].

3.3 Screening of Working Fluids. In order to identify the most suitable fluids for the investigated application, it is necessary, for each organic substance, to simulate the integration of the ORC system with the fuel cell plant and to assess the maximum

[1]The occupational exposure limit, the threshold below which a toxic substance has no effect on the health of the workers for an exposure period of 8 h per day, is 1 ppm for benzene, against 100 ppm of toluene and xylene, and 300 ppm of R245fa. Since toluene is currently employed in ORC systems and the toxicity level of the other considered aromatic hydrocarbons, when available, is comparable to that one of toluene (and also of some refrigerants), it is assumed that only benzene is affected by a level of toxicity incompatible with ORC applications.

Downloaded From: http://gasturbinespower.asmedigitalcollection.asme.org/ on 03/17/2015 Terms of Use: http://asme.org/terms

Table 4 Condensation temperature of candidate fluids (fluids which do not satisfy the environmental requirements discussed in Sec. 3.2 are not considered)

Substance	CAS number	T_{cond} (°C)
R134a	811-97-2	35.0
Cyclopentane	287-92-3	35.0
Cyclobutane	287-23-0	35.0
R245fa	460-73-1	35.0
Cyclohexane	110-82-7	35.0
n-Hexane	110-54-3	35.0
n-Pentane	109-66-0	35.0
n-Butane	106-97-8	35.0
MM	107-46-0	37.3
Toluene	108-88-3	45.3
D_3	**541-05-9**	**67.6**
Ethylbenzene	**100-41-4**	**68.0**
p-Xylene	**106-42-3**	**68.8**
m-Xylene	**108-38-3**	**69.7**
o-Xylene	**95-47-6**	**74.1**
MDM	**107-51-7**	**82.3**
D_4	**556-67-2**	**103.5**
MD_2M	**141-62-8**	**118.9**
D_5	**541-02-6**	**132.9**

achievable power. Since this operation is time consuming, it is advisable to reduce the number of candidate fluids by discarding those requiring a relatively high condensation temperature (T_{cond}).

At the condenser, two technical constraints are imposed:

(1) The minimum cycle temperature is 35 °C, because cooling water at 15 °C is assumed.
(2) The minimum condensation pressure is 100 kPa, as a precaution against excessive inward leaking of incondensable gases in the condenser, which would negatively affect conversion efficiency and the thermal stability of the working fluid [12,16]. In addition, more costly requirements would be needed in order to maintain stable vacuum conditions.

For each fluid, the ORC condensing temperature is thus prescribed by applying the more restrictive constraint (see Table 4).

In general, fluids with high T_{cond} achieve lower performance in a waste heat recovery application, since they reject thermal energy at a temperature which is higher than the prescribed minimum (35 °C). In fact, for the analyzed system, even in the case of a CHP application, it is more convenient to maximize electricity production in the ORC unit and exploit the residual thermal energy of the flue gases for cogeneration purposes. Condensation heat is not exploited for cogeneration, as usually done in biomass-fired ORC power plants, but is dissipated to the environment. For this reason, fluids demanding higher condensing temperature are

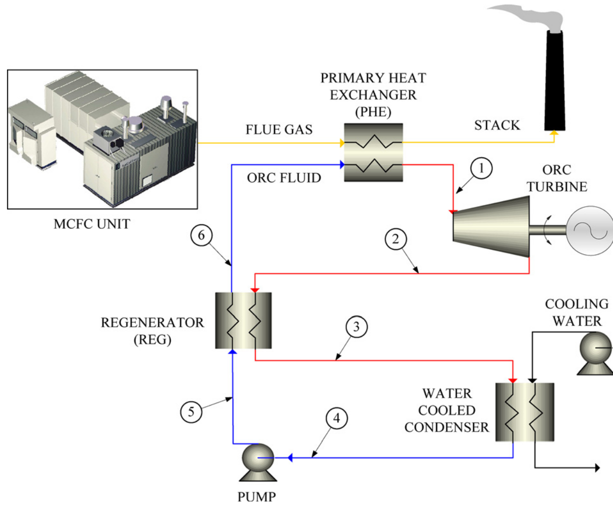

Fig. 2 Layout of the integrated plant

strongly penalized. With reference to the case study, some preliminary simulations have clearly shown that fluids characterized by a condensation temperature higher than 60 °C allow achieving, by far, the worst conversion performance. These substances, highlighted in bold in Table 4, are not further considered in the analysis.

3.4 Optimal Fluids.

For each selected substance, whose saturation curves are shown in Fig. 1, detailed simulations of the integrated power plant are carried out. Simulations require solving the mass and energy balances only for the ORC system, since data about MCFC exhaust gases (composition, temperature, and mass flow rate) are provided by the manufacturer [9]. The layout of the combined plant is shown in Fig. 2.

ORC simulations are performed using a commercial simulation tool [6], while cycle parameters are optimized by an external code implemented in a general purpose technical computing environment [7]. The optimization algorithm iteratively changes the maximum temperature (vapor temperature at turbine inlet) and the evaporation pressure of the working medium in order to maximize the objective function, namely, the net power of the ORC genset.

The main assumptions are summarized below:

- Efficiency values of turbine and feed pumps are set to the same values for all the considered fluids (values are suggested by the ORC manufacturer [35] and are reported in Table 5), even if the operating parameters, the fluid properties, and the power size have a strong influence on component

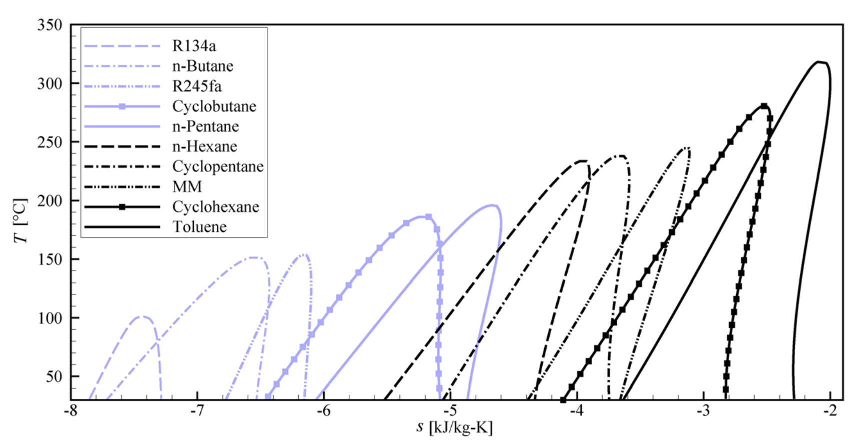

Fig. 1 Saturation curves of selected fluids

Downloaded From: http://gasturbinespower.asmedigitalcollection.asme.org/ on 03/17/2015 Terms of Use: http://asme.org/terms

Table 5 Component efficiency and operating parameters

Turbine efficiency (%)	78.7[a]
Pump efficiency (%)	75.2
Cooling water temperature (°C)	15
Cooling water maximum temperature increase (°C)	8
Minimum temperature working fluid (°C)	35
Minimum pressure working fluid (kPa)	100
$\Delta T_{p.p.}$ PHE (°C)	30
$\Delta T_{p.p.}$ REG (°C)	15

[a]Overall turbine efficiency is estimated assuming 82% isentropic efficiency and 96% mechanical efficiency.

efficiencies. However, this approximation does not compromise the identification of most suitable organic substances for the power plant [1].

- Cooling water is assumed available at 15 °C, allowing for a condensation temperature of 35° if the resulting pressure is above 100 kPa. The condensation temperature of each fluid is reported in Table 4. The maximum temperature increase of cooling water is limited to 8 °C, in compliance with typical environmental regulations.
- The minimum temperature difference, $\Delta T_{p.p.}$, in the primary heat exchanger (PHE) and in the regenerator (REG) are not taken as optimization variables, but they are fixed to 30 °C and 15 °C, respectively. Moreover, the constraint on the $\Delta T_{p.p.}$ in the PHE univocally defines the mass flow rate of the ORC working fluid.
- The regenerator is included in the ORC plant layout for each of the candidate fluids.

The last assumption is motivated by the fact that regeneration reduces heat recovery (due to the higher inlet temperature of the working fluid in PHE), but, depending on the working medium and operating conditions, does not affect or allows for an increase of the ORC power output [36]. The two following arguments can explain this result. Suppose that the optimal value of turbine inlet temperature and cycle pressure have been found, and consider the composite temperature thermal power curve (T-Q curve) of the exhaust gases and the working medium reported in Fig. 3. Once the cycle parameters are fixed, the pinch point position in the PHE occurs at a certain point along the T-Q curves, depending on the exhaust gases inlet temperature and heat capacity. The mass flow rate of the generated vapor is defined by the thermal power recoverable between the exhaust inlet and the pinch point of the PHE. If fluid regeneration is not performed, the pinch point position and mass flow rate of vapor do not change. Therefore, since the outlet and inlet condition of turbine and feed pump are fixed (points 1, 2, 4, and 5 in Fig. 2), the net power of the cycle remains constant (if variations in the pressure drops across the heat exchangers of the ORC unit are neglected). In this case, it comes out that regeneration has no influence on ORC net power production.

Now consider the case of Fig. 4. The pinch point position is at the inlet of PHE. At the same turbine inlet temperature and cycle pressure, without regeneration, the pinch point moves at a lower temperature and then the vapor mass flow rate decreases (it can be deduced by observing the increase in the slope of the composite curve of the working fluid in the T-Q diagram), penalizing the net power output. In general, a new optimization of the cycle parameters does not improve the solution as much as obtained with fluid regeneration. In this circumstance, the regenerator positively affects the electricity production, since it enhances the matching between the hot and cold composite curves in the PHE.

Moreover, for the analyzed case study, regeneration entails two benefits:

(1) Due to the higher temperature of exhaust gases at the PHE outlet, the remaining thermal energy can be exploited for a cogeneration purpose.
(2) Since the maximum temperature increase of cooling water is 8 °C, regeneration permits reducing the power consumption of the condenser pump, thus increasing the net electricity production of the plant. On the contrary, this effect does not occur when the $\Delta T_{p.p.}$ of the condenser is instead kept constant.

A crucial aspect for the validity of ORC simulations is the selection of a reliable equation of state (EOS) for the estimation of the thermodynamic properties of the working fluid. Reference or technical equations of state (REOS) have been developed by the National Institute of Standards and Technologies (NIST) for a number of organic substances [28], among which most of the fluids are used in refrigeration. The adopted simulation tool provides the option of estimating fluid properties with REOS only for a limited set of fluids. In case of MM, cyclopentane, and cyclobutane, therefore, a simpler and less accurate thermodynamic model has been employed, namely the Peng–Robinson

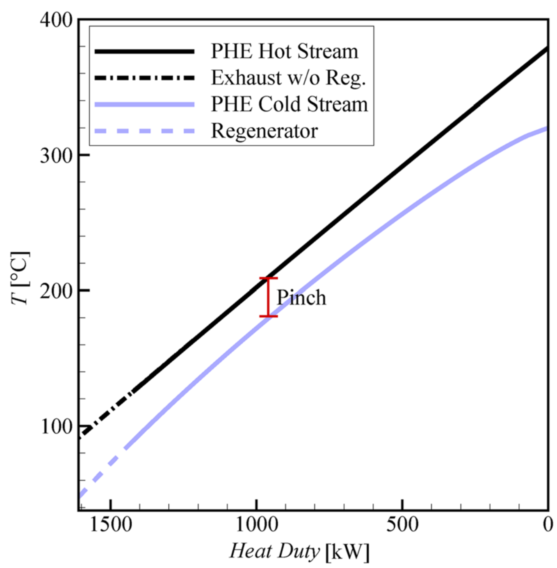

Fig. 3 The composite temperature thermal power curve (T-Q curve) of the exhaust gases and the working medium. Pinch point does not occur at the ends of PHE.

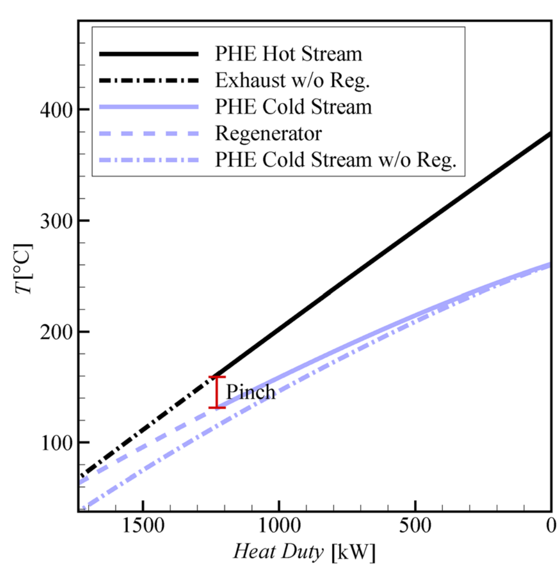

Fig. 4 Composite temperature thermal power curve (T-Q curve) of the exhaust gases and of the working medium. Pinch point occurs at the inlet of the working fluid in PHE.

Downloaded From: http://gasturbinespower.asmedigitalcollection.asme.org/ on 03/17/2015 Terms of Use: http://asme.org/terms

cubic equation of state. This approximation does not compromise the comparison among the various simulated heat recovery units adopting different working fluids, because the error introduced by Peng–Robinson EOS is expected to be within the total uncertainty of the overall model of the ORC system.

The solution found by the optimization procedure should also satisfy physical and technical constraints typical of the ORC process. An arbitrary combination of the cycle parameters can be unfeasible, for instance, yielding a two-phase fluid at the outlet of the evaporator or a wet expansion in the turbine. Therefore, process constraints are embedded in the optimization algorithm, returning an objective function equal to $-\infty$ if any constraint is violated. This procedure has the following advantages:

(a) explicit relationships to describe technical and physical constraints of ORC are not needed
(b) the original constrained problem is transformed into an unconstrained one
(c) the optimization procedure is robust with respect to simulation errors

On the other hand, this approach has the drawback that the objective function is not continuously differentiable, so that tackling this optimization problem requires a robust derivative-free method. For our problem, the complex method [37] is preferred due to its robustness and relative simplicity.

The results of the optimization procedure are reported in Table 6.

The organic substance allowing for the best performance is cyclohexane: more than 80% of the MCFC exhaust energy can be converted into electricity, and this simulated ORC system features also the highest thermal efficiency, namely, 26%. This result is achievable, thanks to the almost perfect matching between the hot and cold composite curves in the primary heat exchanger, as shown in Fig. 5. The regenerator improves the performance of the ORC, because the pinch point position is located at the inlet of the working fluid in the PHE. The cycle is supercritical, and this is the case for all other working fluids, except toluene, which allows achieving the maximum performance at relatively low pressure (17 bar). In comparison to the cyclohexane ORC system, the adoption of toluene as the working fluid provides several advantages:

(a) Fluid regeneration is not necessary, unless cogeneration is exploited, since the pinch point position is not affected by the temperature of the working medium at the inlet of the PHE (see Fig. 6).
(b) The volume flow ratio (VFR) of the turbine is more favorable (high VFR demands for a complex and large turbine and, consequently, the cost of the system is bound to be greater) [1].

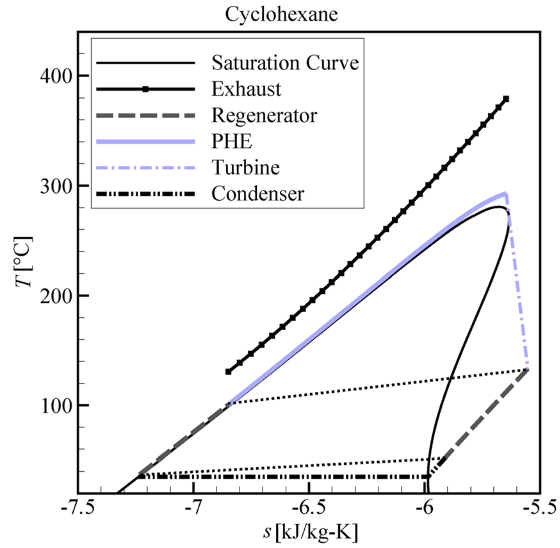

Fig. 5 Temperature–entropy diagram for cyclohexane

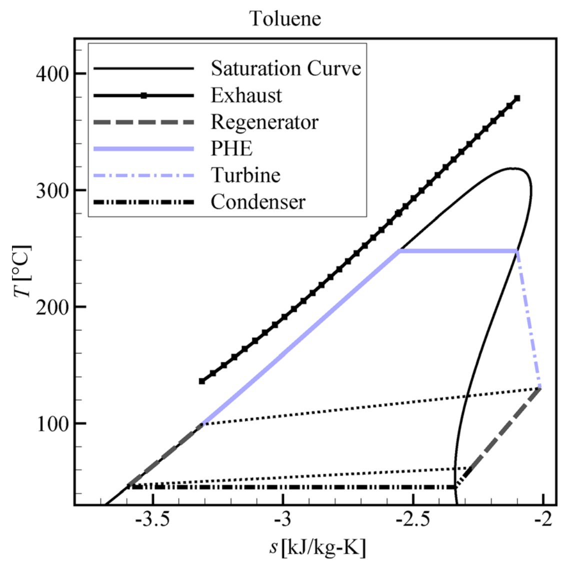

Fig. 6 Temperature–entropy diagram for toluene

Table 6 Simulated ORC performance for each candidate working fluid. The net power is scaled assuming 1 MW of recoverable thermal energy from the fuel cell plant, which corresponds to an exhaust temperature at stack of 85 °C. Table rows in bold characters represents the three cases considered in the economic analysis.

Substance	EOS	ORC Net power[a] (kW_{el})	Tin turbine (°C)	Cycle pressure (bar)	Vout/Vin turbine	η_{el}	η_{II}	χ[b]	Tout exhaust (°C)	Cycle type
Cyclohexane	**Refprop**	**221.83**	**290.00**	**48.51**	**574**	**26.15%**	**42.66%**	**84.83%**	**130.61**	**Supercritical**
Cyclopentane	Peng Rob.	219.11	290.70	89.00	214	25.01%	42.14%	87.61%	122.22	Supercritical
Cyclobutane	Peng Rob.	208.87	300.00	143.00	70	24.65%	40.17%	84.72%	130.94	Supercritical
Toluene	**Refprop**	**206.24**	**247.85**	**17.00**	**175**	**24.86%**	**39.66%**	**82.95%**	**136.24**	**Saturated**
n-Hexane	Refprop	201.15	270.00	53.00	354	24.38%	38.68%	82.51%	137.58	Supercritical
n-Pentane	Refprop	193.98	270.00	80.99	120	23.84%	37.31%	81.36%	141.04	Supercritical
R245fa	Peng Rob.	186.16	290.42	142.87	64	23.91%	35.80%	77.86%	151.53	Supercritical
n-Butane	Refprop	182.55	270.00	117.00	39	22.89%	35.11%	79.76%	145.82	Supercritical
MM	**Peng Rob.**	**181.25**	**260.96**	**30.04**	**754**	**24.28%**	**34.86%**	**74.64%**	**161.16**	**Supercritical**
R134a	Peng Rob.	174.10	301.57	185.00	17	23.35%	33.48%	74.56%	161.40	Supercritical

[a]ORC net power is computed as the difference between the electrical power of the turbogenerator and the consumption of the feed pump and the cooling water pump.
[b]Heat recovery factor.

Downloaded From: http://gasturbinespower.asmedigitalcollection.asme.org/ on 03/17/2015 Terms of Use: http://asme.org/terms

(c) The cycle pressure is lower, which implies a lower capital expenditure (CAPEX) for the bottoming unit, since cycle pressure influences specific costs of piping and heat exchangers, one of the major cost items of ORC power plants [38].

For these reasons, the toluene ORC unit, as well as the cyclohexane one, is selected for the economic comparison with the standalone MCFC power plant. In addition, an ORC system featuring a nonhydrocarbon fluid is also considered in order to extend the analysis. Simulated heat recovery units employing MM and R245fa as working fluids result in similar performance. The system with MM as working fluid is selected for inclusion in the economic analysis; even its performance is slightly lower, due to the following attractive features:

(a) the low cycle pressure, overall less than half of the cyclohexane cycle pressure
(b) the lower cost of the fluid compared to R245fa
(c) the higher temperature of the exhaust gases at the PHE outlet, an aspect which promotes the exploitation of the remaining heat for cogeneration

Furthermore, the choice of MM is also supported by the fact that state-of-the-art high-temperature ORC currently employs mainly siloxanes as working fluids [11].

Finally, it is worth noting that, in each optimized cycle, the vapor superheating is limited to the amount strictly required in order to avoid that liquid droplets enter the turbine. As shown in Ref. [33], superheating negatively affects cycle efficiency in case the working fluid features a positive slope (dT/ds) of the saturation vapor curve in the T–s diagram. In the MM and cyclohexane cycles (see Figs. 5 and 7), it occurs that some thermodynamic states in the expansion are very close to the saturation curve. As it is well known that liquid droplets formation in the turbine can affect negatively its efficiency and reliability, this aspect should be further investigated.

4 Economic Analysis of the Combined Plant

For each of the selected optimized ORC systems, four different configurations are examined, in order to point out the influence of scale effects and of the cogeneration option on the economics of the combined plant. As far as the plant scale is concerned, two different power capacities of the bottoming system are analyzed:

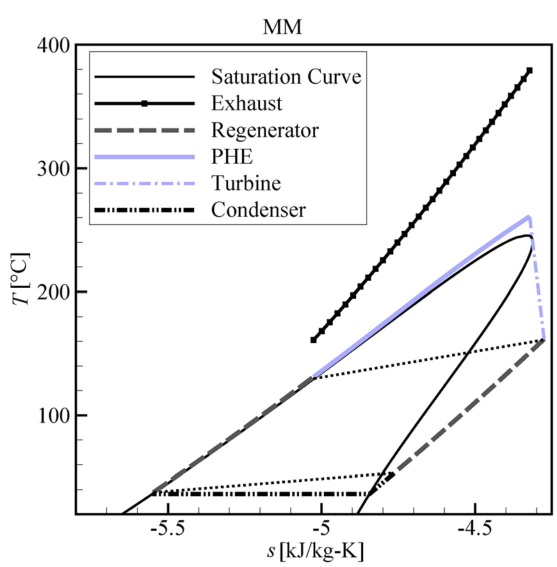

Fig. 7 Temperature–entropy diagram for MM

Table 7 Configurations examined in the economic analysis

Case	ORC size	Cogeneration	Regenerator	MCFC modules
1	500–700 kW_{el}	–	–	2×2.8 MW_{el}
2	500–700 kW_{el}	Yes	Yes	2×2.8 MW_{el}
3	1–1.4 MW_{el}	–	–	4×2.8 MW_{el}
4	1–1.4 MW_{el}	Yes	Yes	4×2.8 MW_{el}

(1) the combined plant employs two MCFC modules, resulting in an electrical power of the ORC unit between 500–700 kW_{el}, depending on the considered working fluid
(2) the combined plant consists of four MCFC modules and of an ORC genset with a net power output above 1 MW_{el}

In the following, these two plant configurations are referred to as the 500 kW_{el} and 1 MW_{el} cases.

When the exploitation of the remaining heat in the flue gases for cogeneration purposes is also investigated, a counter-flow heat exchanger is added to the plant layout before the stack, such that it can generate hot water for a heating network.

In contrast to the procedure followed for the selection of the optimal fluids, for all cases without cogeneration, the regenerator is not employed, even if this implies, especially for an MM ORC system, a loss in electricity production. This choice puts into evidence the impact of the regenerator on the plant capital cost. The analyzed configurations are summarized in Table 7.

4.1 Assumptions for the Computation of the LCOE. The economic benefits due to the integration of the technologies are assessed by evaluating the levelized cost of electricity (LCOE) of the combined plant with respect to the standalone MCFC system.

MCFC Unit. In the case of the standalone MCFC unit, the LCOE is equal to 11.5 c€ per kW_{el} installed, assuming 15 years of service life of the plant and a cost of natural gas slightly higher than 5 €/GJ [3,9]. In order to obtain conservative results, a cogenerative configuration is analyzed, considering the use of waste thermal energy in the flue gases to supply a heating network. Thus, the LCOE of the FC plant decreases about 2.3% (LCOE DFC3000 with cogeneration = 11.24 €c/kWh). The revenue related to cogeneration is obtained on the basis of the following hypotheses:

(a) The minimum temperature of the exhaust gases at the stack is 85 °C (this value corresponds to a return temperature of the water of heating network equal to 70 °C).
(b) The thermal load of the heating system is 2000 equivalent hours per year (which corresponds to the typical load of a heating system at midlatitudes).
(c) A heat price equal to 25 €/MWh. This value is a conservative assumption according to the fuel cost stipulated for the power plant, although heat prices for civil users can be remarkably higher, due to lower consumption volumes and different fuel taxation.

These assumptions, summarized in Table 8, are also used for the cogenerative cases of the combined plant.

Table 8 MCFC LCOE assumptions

Life of the power plant	(year)	15
Fuel cost	(€/GJ)	5.1
O&M cost	(c€/kWh)	2.86
Average power produced	(kW_{el})	2660
Availability	(hour/year)	8000
Specific cost	(€/kW_{el})	2450
Thermal power cogenerated for each module	(kW_{el})	1640
Cogeneration time	(hour/year)	2000
Heat price	(€/MWh)	25

Downloaded From: http://gasturbinespower.asmedigitalcollection.asme.org/ on 03/17/2015 Terms of Use: http://asme.org/terms

It is worth noting that, in the evaluation of the LCOE, a low cost of natural gas is considered; this is a conservative hypothesis, because it reduces the abatement of LCOE achievable by integrating the two technologies.

ORC Unit. Costs of ORC systems are estimated on the basis of the commercial experience of one of the major companies in the field of ORC manufacturing [35], considering a turnkey supply. In particular, the cost evaluation procedure can be summarized as follows:

(a) The turbine cost depends on its number of stages, mean diameter, and maximum allowable operating pressure.[3] The number of stages is three (for each considered substance) and the speed of revolution is 3000 rpm, in order to allow direct coupling with the asynchronous generator. With these assumptions, the preliminary estimate of the axial turbine size is performed according to the mean line design procedure described by Macchi [39] and Lozza et al. [40]. This method permits the optimization of the basic turbine design variables (including mean diameter, isentropic degree of reaction of stages, all relevant blade geometric parameters, and pressure drop subdivision among stages), using the Craig and Cox loss correlation [41] to predict turbine performance.

(b) The cost of heat exchangers is assumed proportional to the weight of the materials (carbon steel), according to an empirical correlation, developed, analyzing commercial proposals of different manufacturers. The design of these components is carried out by an in-house tool, having set the heat exchanger type, the inlet conditions of the streams, and the temperature difference at the pinch point.
For the evaporator of the ORC unit, a kettle-type shell and tube heat exchanger is considered for the subcritical cycle, while, for the supercritical cycles, a once through heat exchanger is designed.

(c) The fluid cost is proportional to the mass (about 3 €/kg for hydrocarbons, 5 €/kg for siloxanes) of the working medium in the closed loop. The fluid quantity is estimated, considering the volume occupied by the liquid in the heat exchangers, increased 20% to take into account the capacity of the pipes.

(d) Pumps are selected on the basis of the fluid type, mass flow rate, and total head, considering an overhead of 10% with respect to the nominal condition as an operating margin. Prices are then retrieved from manufacturer's lists.

(e) The cost of other components, as piping, control system, measuring devices, lubrications systems, wirings, electronic power conditioning systems, etc., represents a fixed percentage ($\sim$15%) of the total expenditure. This percentage decreases as the capacity of the ORC system increases.

In general, the most expensive component of the cycle is the turbine, which represents 35% of the total capital investment. The shares of the other cost items are: 30% for the heat exchangers, 10% for the working fluid, and 25% for other components. In the cost estimation procedure, the results of which are reported in Fig. 8, effects related to production volume are not taken into account.

The genset affected by the high specific cost is the one employing cyclohexane as the working fluid, even if the estimated power output is the largest of all the considered ORC power plants. This is due to the high cycle evaporation pressure, which is one of the key variables influencing the specific cost: as it can be observed in Fig. 8, after cyclohexane, the system with the highest capital costs is the MM ORC unit, which is characterized by a cycle pressure greater than the one of the toluene genset. It is also worth noting that, doubling the ORC power, the specific capital cost is reduced by 30%.

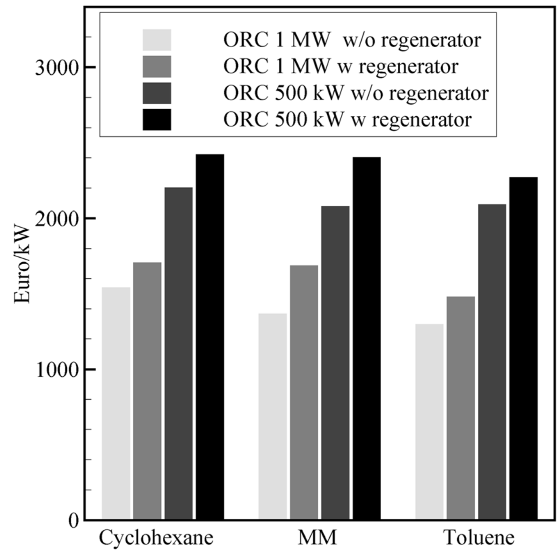

Fig. 8 ORC capital cost (€/kW)

The ORC LCOE, shown in Fig. 9, is evaluated on the basis of the assumptions summarized in Table 8 and considering an O&M cost of 0.5 c€/kWh. It is also important to observe that, in the computation of the ORC LCOE (i) the lifetime of the bottoming unit is shorter than that usually considered for these power plants (15 years versus about 20 years [42]) and (ii) the value of the interest rate (5%) is relatively high [43]. These are conservative hypotheses, because they reduce the abatement of the LCOE achievable by the integration of the two technologies.

4.2 Combined Plant Economy. Energy and economic performance of the combined plant are summarized in Table 9. Adding an ORC unit downstream from a MCFC system allows for an increase of power and efficiency of more than 10%, except for the MM cases without the regenerator. However, all the considered configurations well exceed 50% of efficiency, which is the best performance with respect to any competitive technology (like large stationary or marine diesel engine) in this power capacity range. On the contrary, the LCOE reduction (see Fig. 10) achieves

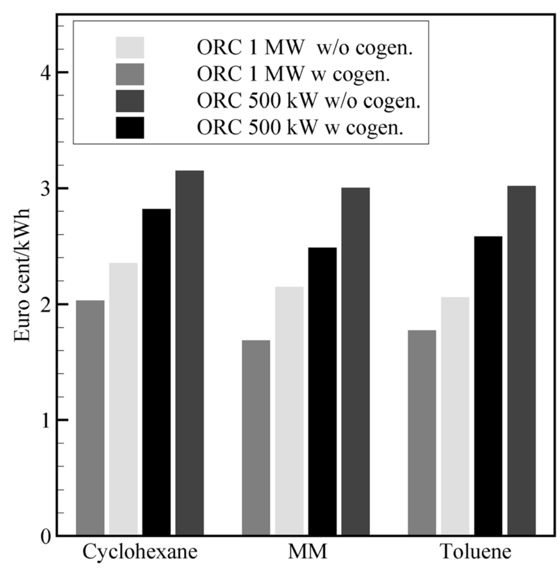

Fig. 9 ORC LCOE

[2]The maximum allowable operating pressure of the turbine is calculated as the nominal operating pressure plus a safety margin of 3 bar.

Downloaded From: http://gasturbinespower.asmedigitalcollection.asme.org/ on 03/17/2015 Terms of Use: http://asme.org/terms

Table 9 **Energy and economic performance of the integrated plant for the different analyzed configurations**

Analyzed cases	W_{el} (MW_{el})	$Q_{cogen.}$ (MW_{th})	η_{el} (%)	LCOE	$\Delta\eta_{el}$[a] (%)	ΔLCOE* (%)
Cyclohexane						
500 kW_{el} w/o cogen.	5.99	–	52.93	10.53	12.62	–6.32
500 kW_{el} w. cogen.	6.00	0.67	53.00	10.49	12.77	–6.66
1 MW_{el} w/o cogen.	12.06	–	53.27	10.39	13.35	–7.60
1 MW_{el} w. cogen.	12.07	1.24	53.34	10.35	13.49	–7.96
Toluene						
500 kW_{el} w/o cogen.	5.94	–	52.51	10.58	11.73%	–5.91%
500 kW_{el} w. cogen.	5.97	0.68	52.75	10.53	12.24%	–6.34%
1 MW_{el} w/o cogen.	11.96	–	52.82	10.42	12.38%	–7.27%
1 MW_{el} w. cogen.	11.97	1.29	52.86	10.39	12.48%	–7.56%
MM						
500 kW_{el} w/o cogen.	5.82	–	51.39	10.73	9.34%	–4.53%
500 kW_{el} w. cogen.	5.89	0.85	52.01	10.60	10.65%	–5.66%
1 MW_{el} w/o cogen.	11.69	–	51.65	10.61	9.89%	–5.59%
1 MW_{el} w. cogen.	11.83	1.67	52.27	10.48	11.21%	–6.75%

[a]With reference to the standalone MCFC plant.

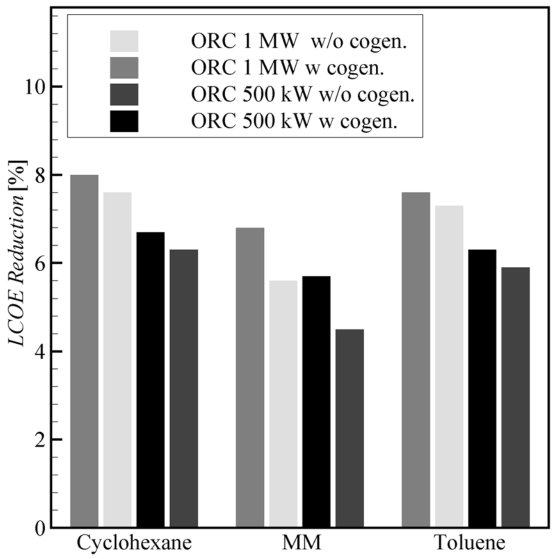

Fig. 10 LCOE reduction obtained by implementing the ORC unit

lower improvements, approximately half of those related to the energy performance of the combined plant. This is due to the fact that ORC LCOEs (see Fig. 9) represent about 20% of the standalone MCFC LCOE, while the ORC electricity production is about 9% of the total electricity production.

The best LCOE reduction is obtained in the case of cyclohexane systems, despite the highest capital cost of the ORC genset. In fact, since the specific cost of the bottoming unit is significantly lower than that of the MCFC system, the LCOE of the combined plant is more influenced by the energy production of the ORC unit than by its cost. For this reason, in the MM case, the quite high additional costs arising from the implementation of the regenerator are more than offset by the increase in electricity production. Due to the cogeneration and the regenerative configuration, the ORC power plant employing MM as the working fluid approaches the economic result of the ORC systems employing the two hydrocarbons.

5 Conclusions

This work investigates the major aspects of the practical feasibility of the integration between a MCFC power plant and an organic Rankine cycle system by assessing the influence of all main parameters affecting the integration, both from the technical and economical point of view. The adopted method is as follows: (i) selection of the more promising working fluids and of the more profitable plant layouts for the ORC unit; (ii) optimization of thermodynamics parameters of the heat recovery system in order to maximize the electricity production of the combined plant; and (iii) economic analysis of the most promising configurations.

In particular, after a preliminary screening of the organic substance suitable for high-temperature ORC systems, ten candidate fluids are selected. For each of them, detailed simulations of the ORC are performed using a commercial process modeling tool, while the optimization of the cycle parameters (cycle maximum temperature and evaporation pressure) is obtained by an optimization algorithm implemented in an external programming environment. The ORC layout considered in the optimization procedure includes a regenerator, since simple considerations demonstrates that regeneration, even if it reduces heat recovery, impacts positively on the ORC net power.

Results of the optimization procedure show that the best working fluids for the analyzed application are cycloalkanes, especially cyclohexane and cyclopentane. Even if the simulations of systems using MM and toluene as the working fluids result in a lower power output, these working media have some favorable features, namely, a lower cycle pressure and turbine VFR, which reduce the capital costs of the ORC unit. For this reason, the following economic analysis considers these two working fluids as well as cyclohexane. For each selected substance, four different configurations are examined, in order to point out the influence of the ORC power capacity and the cogeneration option on the economy of the combined plant. The benefits of the integration are assessed on the basis of the LCOE.

The study results show that the addition of an ORC unit to the MCFC system increases the electrical efficiency of the FC plant from 47% to more than 53%. Using conservative assumptions with commercial data provided by experienced companies in the fields of FC and ORC systems, it is demonstrated that this efficiency enhancement allows reducing the LCOE by a value of about 6%–8%. The highest performance is obtained with cyclohexane as the ORC system's working fluid, which, in the best case (with cogeneration and an ORC power size greater than 1 MW_{el}), allows reducing the MCFC LCOE by 8%. However, similar results are obtained for toluene and the linear siloxane MM.

The economic feasibility of the combined plant is also demonstrated for relatively smaller capacity (~500 kW_{el}) of the ORC unit, and it becomes particularly attractive for multi-MW MCFC plants, implementing at least two modules of 2.8 MW_{el} each, where both efficiency and LCOE reach their best values. These performance improvements can be achieved, implementing

Downloaded From: http://gasturbinespower.asmedigitalcollection.asme.org/ on 03/17/2015 Terms of Use: http://asme.org/terms

already well-established technology with clearly predictable costs, and without penalizing the reliability of the plant. This may result attractive with respect to more complex solutions, such as the hybrid MCFC-gas turbine cycles, which offer higher performances, but involve a much more critical development of dedicated turbomachinery, and a more difficult plant integration [4].

Nomenclature

Acronyms

BOL = beginning of life of MCFC stack
CAPEX = capital expenditure
EOL = end of life of MCFC stack
EOS = equation of state
FC = fuel cell
GWP = global warming potential
HFC = hydrofluorocarbons
LCOE = levelized cost of electricity
LHV = low heating value
MCFC = molten carbonate fuel cell
MW = molecular weight
ODP = ozone depletion potential
ORC = organic Rankine cycle
PHE = primary heat exchanger
REG = regenerator
REOS = reference equation of state
VFR = volume flow ratio

Symbols

P_C = critical pressure
Q = heat power
T_b = boiling temperature
T_C = critical temperature
T_{cond} = condensing temperature
T_{stab} = thermal stability threshold of the organic fluid
V = volume flow
W = electrical power
s = entropy

Subscripts

el = electrical
in = inlet condition
out = outlet condition
p.p. = pinch point

Greek Letters

η = efficiency
χ = recovery factor

References

[1] Angelino, G., and Colonna di Paliano, P., 2000, "Organic Rankine Cycles (ORCs) for Energy Recovery From Molten Carbonate Fuel Cells," Proceedings of the 35th Intersociety Energy Conversion Engineering Conference, Las Vegas, NV, July 24–28.
[2] Angelino, G., and Colonna di Paliano, P., 2000, "Air Cooled Siloxane Bottoming Cycle for Molten Carbonate Fuel Cells," Fuel Cell Seminar, Portland, OR, October 30–November 2.
[3] Remick, R. J., Wheeler, D., and Singh, P., "MCFC and PAFC R&D Workshop Summary Report," U. S. DOE, January 2010, http://www1.eere. energy.gov/
[4] Campanari, S., Iora, P., Macchi, E., and Silva, P., 2007, "Thermodynamic Analysis of Integrated MCFC/Gas Turbine Cycles for Sub-MW and Multi-MW Scale Power Generation," ASME J. Fuel Cell Sci. and Technol., **4**, pp. 308–316.
[5] Di Pippo, R., 2005, *Geothermal Power Plants: Principles, Applications and Case Studies*, Elsevier, New York.
[6] Aspen Technology Inc., 2011, ASPEN PLUS v. 7.3, Burlington, MA.
[7] The MathWorks Inc., 2011, MATLAB 7.12, Natick, MA.
[8] Moreno, A., McPhail, S., and Bove, R., 2008, "International Status of Molten Carbonate Fuel Cell (MCFC) Technology," Joint Research Centre–Institute for Energy, JRC Scientific and Technical Report EUR 23373 EN, European Commission, Luxembourg.
[9] FuelCell Energy, 2011, private communication.
[10] FuelCell Energy, 2010, *DFC3000: Direct FuelCell Power Plant Applications Guide*, FuelCell Energy, Danbury, CT.
[11] Lai, N. A., Wendland, M., and Fischer, J., 2011, "Working Fluids for High-Temperature Organic Rankine Cycles," Energy, **36**, pp. 199–211.
[12] Angelino, G., and Invernizzi, C. M., 1993, "Cyclic Methylsiloxanes as Working Fluids for Space Power Cycles," ASME J. Sol. Energy Eng., **115**, pp. 130–137.
[13] Drescher, U., and Brüggemann, D., 2007, "Fluid Selection for the Organic Rankine Cycle (ORC) in Biomass Power and Heat Plants," Appl. Therm. Eng., **27**, pp. 223–228.
[14] Angelino, G., and Invernizzi, C., 2003, "Experimental Investigation on the Thermal Stability of Some New Zero ODP Refrigerants," Int. J. Refrig., **26**(1), pp. 51–58.
[15] Zyhowski, G. J., "Honeywell Refrigerants Improving the Uptake of Heat Recovery Technologies," http://www.honeywell-orc.com/wp-content/uploads/2011/09/Honeywell-Refrigerants-Improve-Uptake-Heat-Recovery-Technologies.pdf
[16] Schroeder, D. J., and Leslie, N., 2010, "Organic Rankine Cycle Working Fluid Considerations for Waste Heat to Power Applications," ASHRAE Trans., **116**(Part 1), pp. 525–533.
[17] Andersen, A., and Bruno, T., 2005, "Rapid Screening of Fluids for Chemical Stability in Organic Rankine Cycle Applications," Ind. Eng. Chem. Res., **44**, pp. 5560–5566.
[18] Havens, V. N., Ragaller, D. R., Silbert, L., and Miller, D., 1987, "Toluene Stability Space Station Rankine Power Systems," Proceedings of the 22nd Intersociety Energy Conversion Engineering Conference (IECEC), Philadelphia, PA, August 10–14.
[19] van Buijtenen, J. P., 2009, "The Tri-O-Gen Organic Rankine Cycle: Development and Perspectives," Power Eng., **13**(1), pp. 4–12.
[20] Ginosar, D. M., Petkovic, L. M., and Guillen, D. P., 2011, "Thermal Stability of Cyclopentane as an Organic Rankine Cycle Working Fluid," Energy Fuels, **25**(9), pp. 4138–4144.
[21] Calderazzi, L., and Colonna, P., 1997, "Thermal Stability of R-134a, R-13I1, R-7146, R-125 Associated With Stainless Steel as a Containing Material," Int. J. Refrig., **20**, pp. 381–389.
[22] Colonna, P., Nannan, N. R., Gurdone, A., and Lemmon, E. W., 2006, "Multiparameter Equations of State for Selected Siloxanes," Fluid Phase Equilib., **244**, pp. 193–211.
[23] Colonna, P., Nannan, N. R., and Gurdone, A., 2008, "Multiparameter Equations of State for Siloxanes: $[(CH3)_3\text{-}Si\text{-}O_{1/2}]_2\text{-}[O\text{-}Si\text{-}(CH_3)_2]_{i=1,\ldots,3}$, and $[O\text{-}Si\text{-}(CH_3)_2]6$," Fluid Phase Equilib., **263**(2), pp. 115–130.
[24] Prabhu, E., 2006, "Solar Trough Organic Rankine Electricity System. Stage 1: Power Plant Optimization and Economics," Subcontract Report No. NREL/SR-550-39433.
[25] Angelino, G., Invernizzi, C., and Macchi, E., 1991, "Organic Working Fluid Optimization for Space Power Cycles," *Modern Research Topics in Aerospace Propulsion*, Springer-Verlag, New York.
[26] Colonna di Paliano, P., 1996, "Fluidi di Lavoro Multi Componenti Per Cicli Termodinamici di Potenza (Multicomponent Working Fluids for Power Cycles)," Ph.D. thesis, Politecnico di Milano, Milano, Italy.
[27] Leslie, N. P., Zimron, O., Sweetser, R. S., and Stovall, T. K., 2009, "Recovered Energy Generation Using an Organic Rankine Cycle System," ASHRAE Trans., **115**(Part I), pp. 220–230.
[28] Lemmon, E. W., Huber, M. L., and McLinden, M. O., 2010, "NIST Standard Reference Database 23: Reference Fluid Thermodynamic and Transport Properties-REFPROP, Version 9.0", National Institute of Standards and Technology, Standard Reference Data Program, Gaithersburg, MD.
[29] "NIST Chemistry WebBook," NIST, http://webbook.nist.gov/chemistry/
[30] Calm, J. M., and Hourahan, G. C., 2011, "Physical, Safety and Environmental Data for Current and Alternative Refrigerants," Proceedings of 23rd International Congress of Refrigeration (ICR2011), Prague, Czech Republic, August 21–26.
[31] Papadopoulos, A. I., Stijepovic, M., and Linke, P., 2010, "On the Systematic Design and Selection of Optimal Working Fluids for Organic Rankine Cycles," Appl. Therm. Eng., **30**, pp. 760–769.
[32] Maizza, V., and Maizza, A., 1996, "Working Fluids in Non-Steady Flows for Waste Energy Recovery Systems," Appl. Therm. Eng., **16**(7), pp. 579–590.
[33] Chen, H., Goswami, D. Y., and Stefanakos, E. K., 2010, "A Review of Thermodynamic Cycles and Working Fluids for the Conversion of Low-Grade Heat," Renewable Sustainable Energy Rev., **14**, pp. 3059–3067.
[34] Marciniak, T. J., Krazinski, J. L., Bratis, J. C., Bushby, H. M., and Buyco, E. H., "Comparison of Rankine-Cycle Power Systems: Effects of Seven Working Fluids," Argonne National Laboratory Report No. ANL/CNSV-TM—87.
[35] Turboden s.r.l., http://www.turboden.eu
[36] Martelli, E., Nord, L. O., and Bolland, O., 2012, "Design Criteria and Optimization of Heat Recovery Steam Cycles for Integrated Reforming Combined Cycles With CO_2 Capture," Appl. Energy, **92**, pp. 255–268.
[37] Box, M. J., 1965, "A New Method for Constraint Optimization and a Comparison With Other Methods," Comput. J., **8**, pp. 42–52.

Downloaded From: http://gasturbinespower.asmedigitalcollection.asme.org/ on 03/17/2015 Terms of Use: http://asme.org/terms

[38] Stijepovic, M. Z., Linke, P., Papadopoulos, A. I., and Grujic A. S., 2012, "On the Role of Working Fluid Properties in Organic Rankine Cycle Performance," Appl. Therm. Eng., **36**, pp. 406–413.
[39] Macchi, E., 1977, "Design Criteria for Turbines Operating With Fluids Having a Low Speed of Sound in Closed Cycle Gas Turbines," Lecture Series 100 on Closed Cycle Gas Tubines, Von Karman Institute for Fluid-Dynamics, Bruxelles.
[40] Lozza, G., Macchi, E., and Perdichizzi, A., 1982,"On the Influence of the Number of Stages on the Efficiency of Axial-Flow Turbines," 27th International Gas Turbine Conference and Exhibition, London, April 18–22.
[41] Craig, H. R. M., and Cox, H. J. A., 1970, "Performance Estimation of Axial Flow Turbines," Proc. Inst. Mech. Eng., **185**, pp. 407–424.
[42] Bronicki, L. Y., 1999, "Organic Rankine Cycle Power Plant, for Waste Heat Recovery," 13th Symposium on Industrial Applications of Gas Turbines, Banff, Alberta, Canada, October.
[43] "Costi di Produzione di Energia Elettrica da Fonti Rinnovabili," Rapporto Commissionato da AEEG al Politecnico di Milano - Dipartimento di Energia, Dicembre 2010, http://www.autorita.energia.it/allegati/docs/11/103-11arg_rtalla.pdf

Downloaded From: http://gasturbinespower.asmedigitalcollection.asme.org/ on 03/17/2015 Terms of Use: http://asme.org/terms

Kapitel 6: Kombiprozeß

1. Beschreibung des Kombiprozesses
2. Q-T-Diagramm des AHK
3. A Comparative Evaluation of Advanced Combined Cycle Alternatives
4. Ertüchtigung bestehender Dampfkraftwerke durch Gasturbinen
5. Combined Cycle Pricing

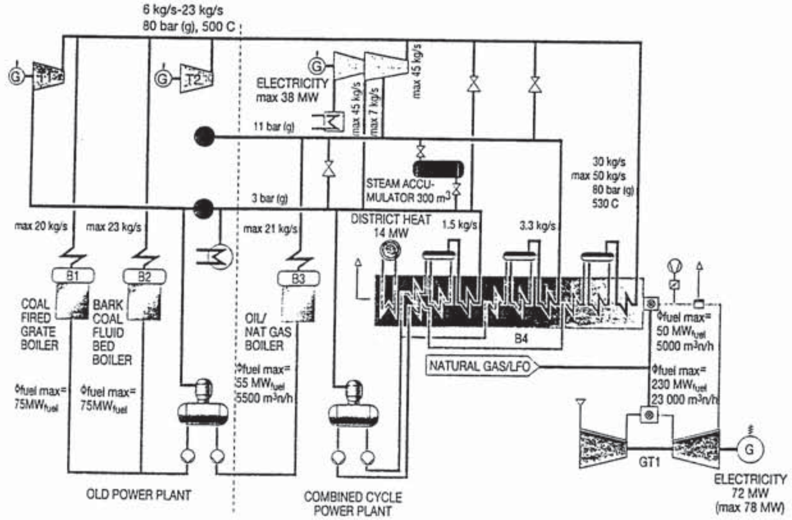

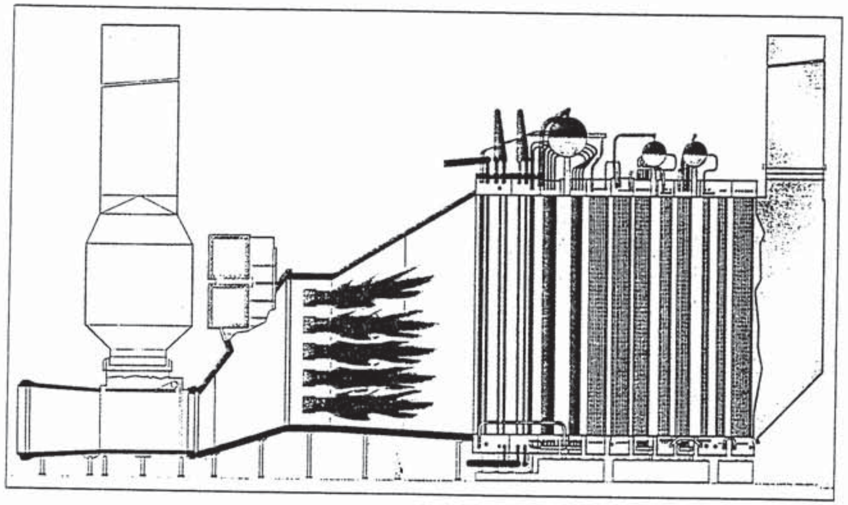

Figure 6. Cross section through the heat recovery steam generator

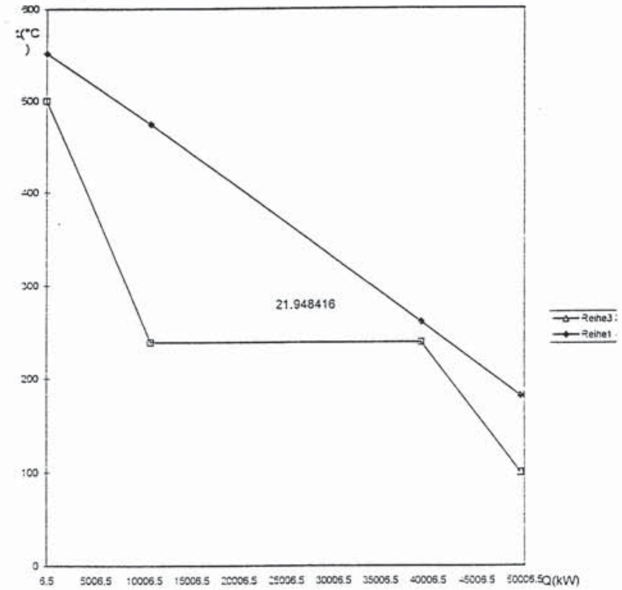

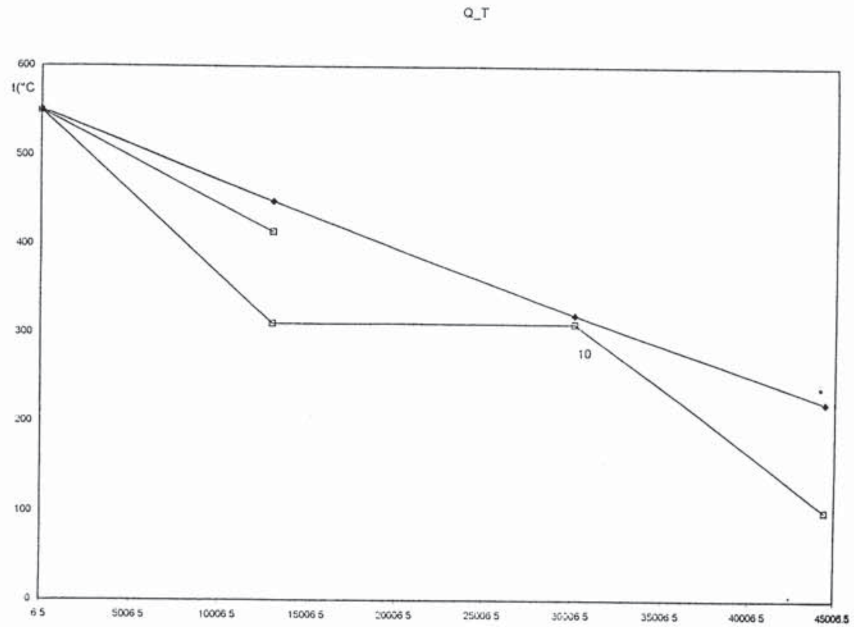

A Comparative Evaluation of Advanced Combined Cycle Alternatives

O. Bolland
Thermal Energy Division,
Department of Mechanical Engineering,
The Norwegian Institute of Technology,
7034 Trondheim, Norway

This paper presents a comparison of measures to improve the efficiency of combined gas and steam turbine cycles. A typical modern dual pressure combined cycle has been chosen as a reference. Several alternative arrangements to improve the efficiency are considered. These comprise the dual pressure reheat cycle, the triple pressure cycle, the triple pressure reheat cycle, the dual pressure supercritical reheat cycle, and the triple pressure supercritical reheat cycle. The effect of supplementary firing is also considered for some cases. The different alternatives are compared with respect to efficiency, required heat transfer area, and stack temperature. A full exergy analysis is given to explain the performance differences for the cycle alternatives. The exergy balance shows a detailed breakdown of all system losses for the HRSG, steam turbine, condenser, and piping.

Introduction

In the past two decades, combined gas and steam turbine cycle (CC[1]) plants have successfully been put into operation with very good fuel utilization compared to other types of thermal power plants. CC plants can either be used for the generation of electricity only, or for the generation of electricity and heat. Among thermal power plants that are commercially available, the CC is the type that generates electricity with the highest efficiency. The future outlook for CC plants in Europe is very good. A number of such plants are expected to be built during the 1990s. In Great Britian and the Netherlands, CC plants are becoming very popular.

In the early seventies, CCs were built with typical electrical efficiencies of about 40 percent. Recently, CCs have been built with electrical efficiencies above 50 percent. Two plants are worth mentioning in this respect: Pegus 12 (220 MW) in Utrecht, the Netherlands, which was being put into operation in Feb. 1989 (Frutschi and Plancherel, 1989), and a 1350 MW plant, which is being built in Ambarli, Turkey (Hamann and Joyce, 1989). For both plants the guaranteed net efficiency based on the lower heating value is above 51 percent, which can be regarded as 1989 "state of the art" for CCs.

The increase in the electrical efficiency of CCs in the last few years has mainly been caused by gas turbine improvements. Increased firing temperatures have been introduced for gas turbines with relatively moderate pressure ratios, which has resulted in exhaust gas temperatures above 500°C. This type of gas turbine improvement has a positive influence on the electrical efficiency of the steam cycle.

[1]The terms GuD (Gas und Dampf) and STAG (STeam And Gas) are also commonly used.

Contributed by the International Gas Turbine Institute and presented at the 35th International Gas Turbine and Aeroengine Congress and Exposition, Brussels, Belgium, June 11–14, 1990. Manuscript received by the International Gas Turbine Institute January 17, 1990. Paper No. 90-GT-335.

This paper deals with the potential for improving the steam cycle efficiency in a large CCs (> 400 MW), and thereby increasing the CC electrical efficiency. The steam cycle can be improved by, among other things, decreasing the temperature differences in the heat recovery steam generator (HRSG) and by lowering the condenser pressure. This paper concentrates on another alternative: increasing the CC electrical efficiency for a given gas turbine, by improvements in the *steam cycle configuration*.

Why is it necessary to improve the efficiency of the CC? Modern CCs already have a very high efficiency and most improvements in efficiency have disadvantages with respect to investment costs, complexity, and reliability. The economics of a power plant govern how the plant should be built. In this respect there are four main factors to be considered: fuel costs, capital costs, time of construction, and environmental issues. The motivation for further improvements in CC efficiencies is an expected growth in energy prices and environmental aspects. The latter are becoming more and more important, and improved fuel utilization is one measure to reduce emissions from thermal power plants.

Table 1 Performance data for the selected gas turbines

	V94.2	V94.3[2]	
Net power output	144.3	189.5	MW
Net efficiency	32.5	> 35	%
Exhaust gas mass flow	504.0	565.2	kg/s
Exhaust gas temperature	553.1	563.4	°C
Pressure ratio	10.7	16.0	-

[2]According to Siemens, performance data for the V94.3 are preliminary.

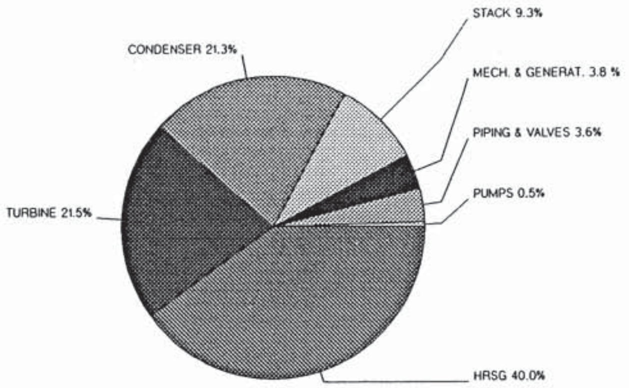

Fig. 1 Breakdown of exergy losses in a dual pressure steam cycle

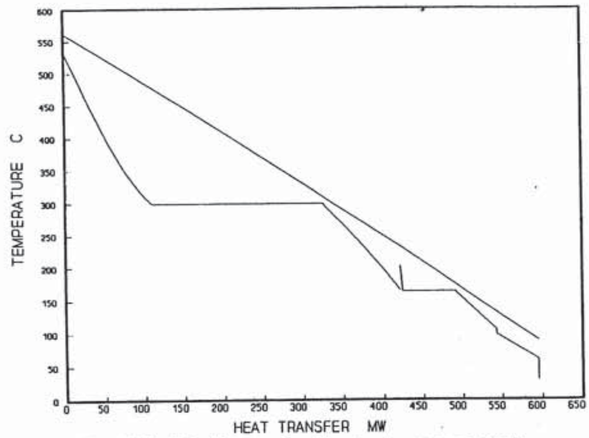

Fig. 2(*b*) TQ diagram for the dual pressure cycle

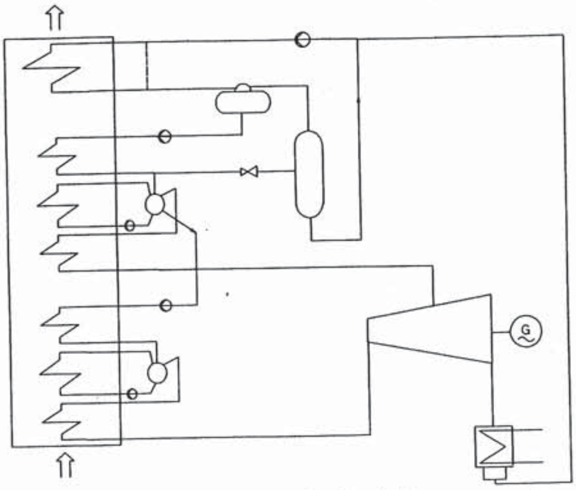

Fig. 2(*a*) Flowsheet diagram for the dual pressure cycle

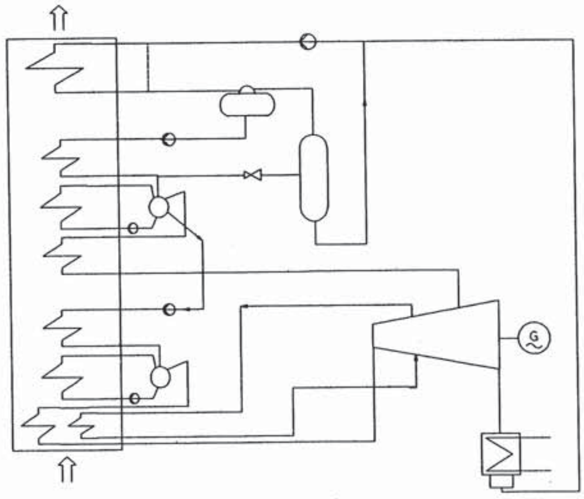

Fig. 2(*c*) Flowsheet diagram for the dual pressure reheat cycle

Gas Turbines Used in the Study

Two gas turbines were used for the study: Siemens V94.2 and Siemens V94.3. The former of these is at present one of the largest gas turbines in operation anywhere in the world, and is a representative choice for a modern CC gas turbine. The latter is an improved model from Siemens, with a high firing temperature. This machine represents a new generation of gas turbines now being introduced to the market. This new generation consists of machines like the 150 MW class Fr 7F and the 210 MW Fr 9F from General Electric and Alsthom; Westinghouse and Mitsubishi with the 15 MW MF-111 and 150 WM W501F; Siemens with the 60 MW V64.3, 155 MW V84.3, and the 190 MW V94.3. ABB is probably going to make the 200 MW Type 15.

The two gas turbines selected for this study are calculated at ISO conditions with inlet/outlet pressure drops of 10/40 mbar. The thermodynamic cycle data are given in Table 1 (Rukes, 1990).

Steam Cycle Configurations

Large modern CCs are normally built with a dual-pressure steam bottoming cycle. Figure 1 shows a typical distribution of losses of available work[3] for such a steam cycle. Obviously,

[3]The terms "availabe work," "availability," and "exergy" are synonymous and are going to be used interchangeably.

Nomenclature

- A = heat transfer area, m^2
- $\tilde{A}$ = nondimensional heat transfer area, see equation (16)
- c = efficiency moisture correction factor
- CC = Combined Cycle
- C_P = specific heat, kJ/kg/K
- e = specific exergy, kJ/kg/s
- E = exergy, kJ/s, kW
- H = specific enthalpy of exhaust, kJ/kg
- h = specific enthalpy of H_2O, kJ/kg
- HP = high pressure
- IP = intermediate pressure
- LHV = lower heating value, kJ/kg
- LP = low pressure
- m = mass flow, kg/s
- p = pressure, bar
- Q = heat flow, kJ/s, kW
- R = gas constant, kJ/kg/K
- RH = reheat pressure
- s = specific entropy, kJ/kg/s
- t = temperature, °C
- T = temperature, K
- U = total heat transfer coefficient, $kW/m^2/K$
- W = work, kW
- x = steam quality, kg/kg
- η = efficiency

Subscripts

- a = ambient
- aux = auxiliary
- C = cold
- CC = combined cycle
- ex = exhaust gas
- f = fuel
- GT = gas turbine
- H = hot
- HRSG = heat recovery steam generator
- pp = pinch-point temperature difference
- reh = reheat
- SC = steam cycle
- st = steam
- 1, 2, 3 = cycle state points in Fig. 3

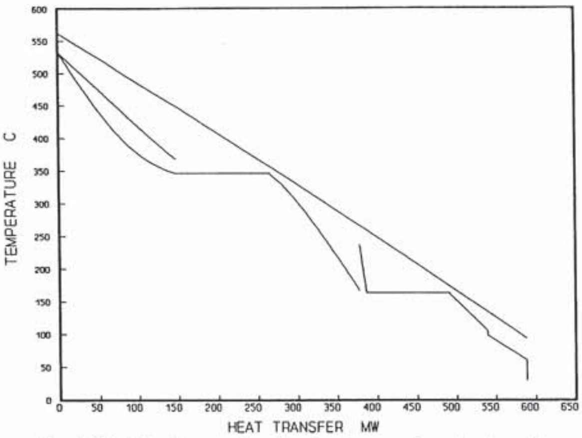

Fig. 2(*d*) TQ diagram for the dual pressure reheat cycle

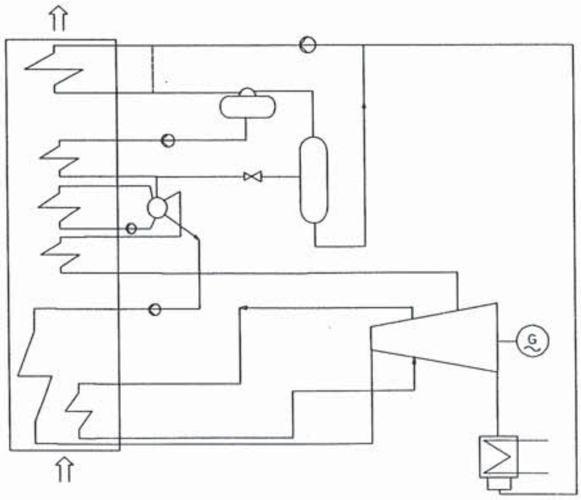

Fig. 2(*e*) Flowsheet diagram for the dual pressure supercritical reheat cycle

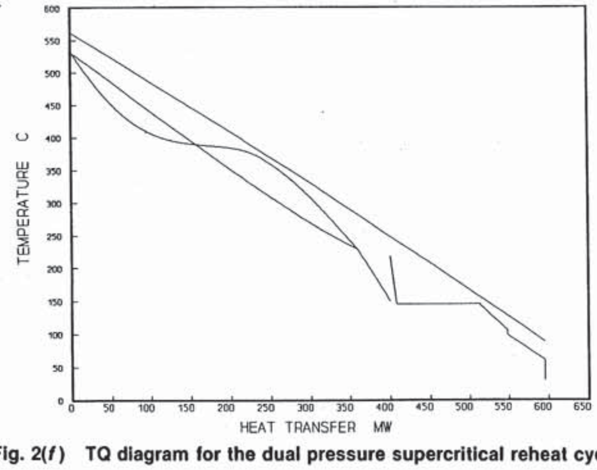

Fig. 2(*f*) TQ diagram for the dual pressure supercritical reheat cycle

the HRSG losses constitute a main share (≈ 40 percent) of the steam cycle loss of available work. Figures 2(*a–l*) show TQ diagrams and the cycle flowsheet for proposed changes in configuration to decrease loss of available work and thereby improve the steam cycle efficiency. The following cycle configurations are shown in Figs. 2(*a–l*):

2(*a*, *b*) Dual pressure cycle
2(*c*, *d*) Dual pressure reheat cycle
2(*e*, *f*) Dual pressure supercritical reheat cycle
2(*g*, *h*) Triple pressure cycle
2(*i*, *j*) Triple pressure reheat cycle
2(*k*, *l*) Triple pressure supercritical reheat cycle

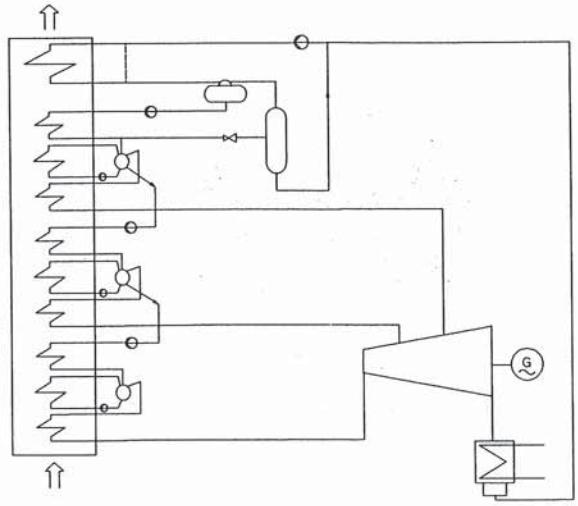

Fig. 2(*g*) Flowsheet diagram for the triple pressure cycle

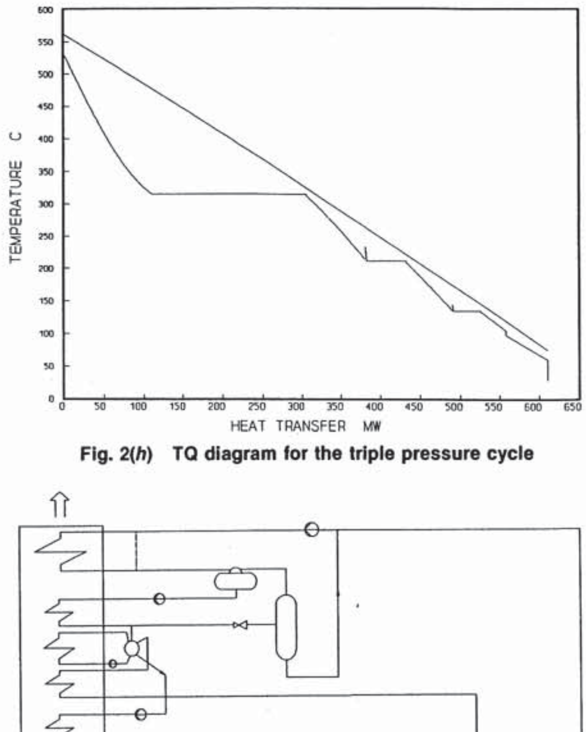

Fig. 2(*h*) TQ diagram for the triple pressure cycle

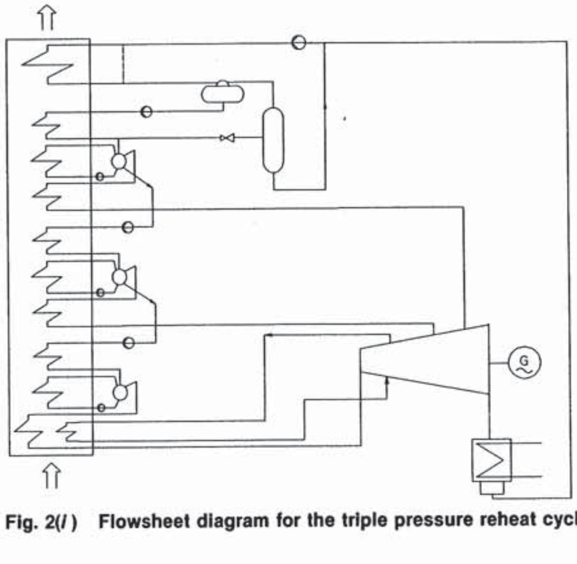

Fig. 2(*l*) Flowsheet diagram for the triple pressure reheat cycle

The choice of preheating and deaeration system needs to be explained. The steam for deaeration is generated in a flashtank outside the HRSG. Hot pressurized water from the LP economizer is throttled before entering the flashtank. The steam that is flashed off goes to the deaerator, and the water leaving the flashtank is used to preheat the feedwater coming from the condenser. To prevent the exhaust gas moisture from condensing, the feedwater should be heated up to a temperature above the dewpoint of the exhaust gas. This is done in the

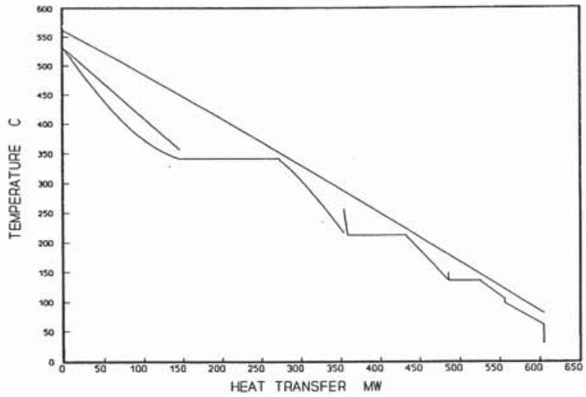

Fig. 2(*j*) TQ diagram for the triple pressure reheat cycle

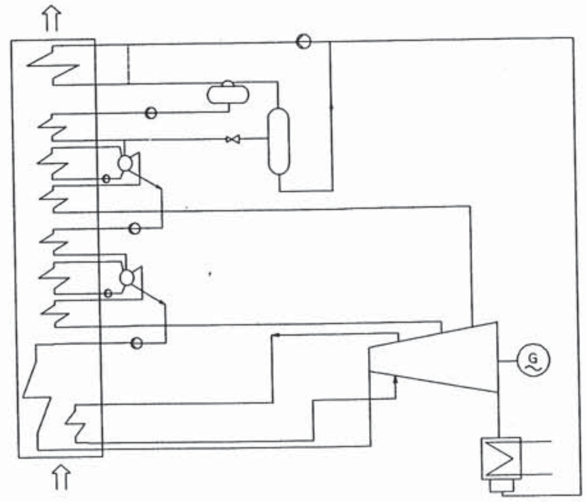

Fig. 2(*k*) Flowsheet diagram for the triple pressure supercritical reheat cycle

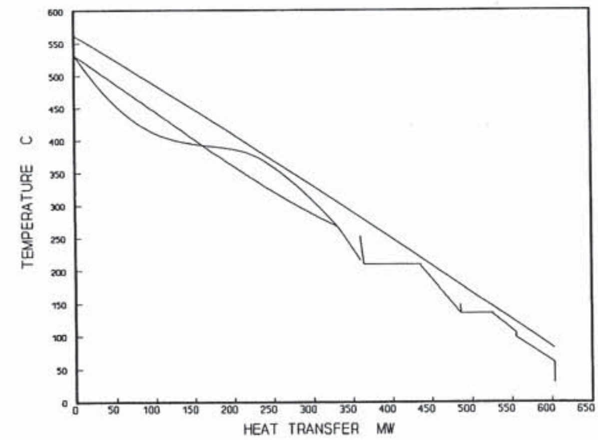

Fig. 2(*l*) TQ diagram for the triple pressure supercritical reheat cycle

feedwater preheater with a circulation loop (dashed line in flowsheet figures). The circulation ratio is such that the feedwater temperature entering the HRSG is above the dewpoint of the exhaust gas. In this study the feedwater temperature entering the HRSG is set to 60°C, which is well above the dewpoint of the exhaust gas, normally about 40°C.

Computational Model

The HRSG model is separated into two basic types of computational model: the subcritical pressure stage and the supercritical pressure stage. The former consists of an economizer, an evaporator with forced circulation, and a superheater. The

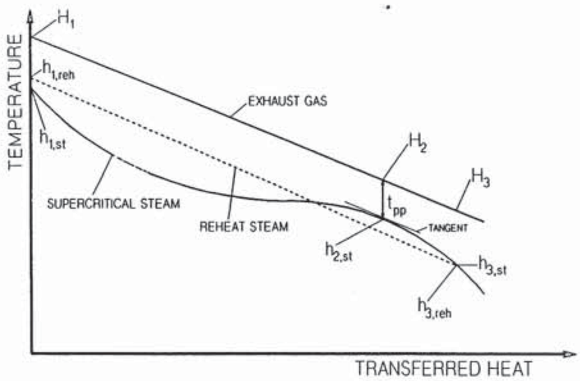

Fig. 3 TQ diagram for supercritical pressure stage

latter consists of a once-through heat exchanger. For the HRSG calculations, the exhaust-gas/live-steam approach temperature difference, pinch-point temperature difference, economizer approach temperature difference, live-steam pressure, and pressure drops are given as input. For the subcritical pressure stage the computational procedure is quite straightforward. The procedure applied in this study is similar to the method presented by Chin and Elmasri (1987). The computational procedure for the supercritical pressure stage is more complex since the steam[4] is not undergoing any sudden change of phase and there is no distinct "pinch point." The steam temperature at the pinch point is therefore not as easily found as for the subcritical case. Figure 3 shows a TQ diagram for a supercritical pressure stage. Obviously, the slopes of the two curves have to be equal at the pinch point. Further, the distance between the two curves has to be the specified pinch-point temperature difference, and there must be a heat transfer balance between exhaust gas and steam. With these three requirements formulated in equations (1)–(3), the steam temperature ($t_{2,st}$) at the pinch point can be found

$$m_{st} \cdot C_{P\,2,st} = m_{ex} \cdot C_{P\,2,ex} \tag{1}$$

$$m_{st} \cdot (h_{1,st} - h_{2,st}) = m_{ex} \cdot (H_1 - H_2) \tag{2}$$

$$t_{2,st} = t_{2,ex} - t_{pp} \tag{3}$$

If constant specific heat is assumed for the exhaust gas, the steam temperature at the pinch point can be found more easily

$$t_{2,st} = t_{1,ex} - t_{pp} - \frac{h_{1,st} - h_{2,st}}{C_{P\,2,st}} \tag{4}$$

However, for this study the formulation for variable specific heat is applied. It should be noted that when applying equation (1) caution must be made when evaluating the specific heat ($C_{P\,2,st}$) for steam near the critical temperature. The specific heat changes very rapidly as function of temperature above and near the critical point. For a supercritical stage with reheating, the same procedure can be applied except for equation (2), which has to be rewritten, and an extra heat balance equation needs to be added (equation (6))

$$(h_{1,st} - h_{2,st}) \cdot (H_1 - H_3) = (H_1 - H_2) \cdot (h_{1,st} - h_{3,st}) \tag{5}$$

$$m_{ex} \cdot (H_1 - H_3) = m_{st} \cdot (h_{1,st} - h_{3,st}) + m_{\mathrm{reh}} \cdot (h_{1,\mathrm{reh}} - h_{3,\mathrm{reh}}) \tag{6}$$

The HRSG heat transfer area calculation is carried out by an integration method for each type of heat exchanger (superheater, evaporator, economizer, and preheater). A counterflow heat exchanger model is applied. The integration model ensures that the effect of variable specific heat capacities is taken into account. This is important for high-pressure superheated steam and water near saturation. A counterflow heat exchanger model may not be accurate in all cases, but when comparing heat transfer areas as in this study, such a model should be sufficient.

[4]Water at supercritical pressure can hardly be defined as either water or steam, but it is here referred to as steam.

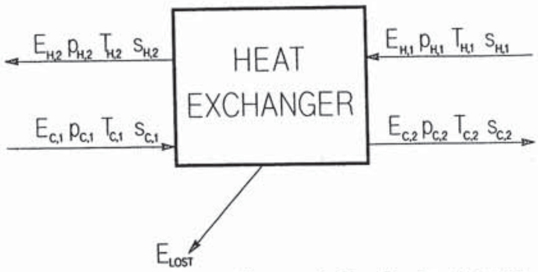

Fig. 4 Exergy balance of a counterflow heat exchanger

The steam turbine expansion is broken into a number of sections, which correspond to the number of HRSG pressure stages. Each section is computed by an individual dry isentropic step efficiency. The efficiency for the LP section is corrected for moisture if the expansion crosses into the wet region. The LP expansion is broken into steps, and the efficiency for each step is corrected for moisture when the exit quality is below that for the onset of condensation. This "Wilson line" quality is normally between 0.95 and 0.98. The efficiency degradation is assumed to be an exponential function (7) of mean step steam quality

$$\eta_{\text{step}} = \eta_{\text{dry}} \cdot (1 - (1 - x_{\text{step,mean}})^c) \tag{7}$$

The exponent c is typically in the range 1.0–1.3, and is chosen to be 1.15 for this study. That means the penalty for moisture is a decrease in isentropic efficiency with a factor typically in the range 0.63–0.75 for every extra percent of moisture. The steam turbine model also takes into account a throttle valve loss, steam leakages through the steam turbine seals, LP section leaving loss, and steam turbine and generator auxiliary power requirements.

The condenser model is a water-cooled counterflow heat exchanger. The cooling water pressure drop and the required pump work are calculated.

Heat and exergy balances are carried out for *all components* in the model. To ensure that there are no errors in the model, an overall system heat balance is carried out, as well as an overall exergy balance.

The net efficiency of the CC is here defined as

$$\eta_{CC} = \frac{W_{GT} + W_{SC} - W_{\text{AUX}}}{m_f \cdot \text{LHV}} \tag{8}$$

W_{GT}, W_{SC} = power output at the generator terminals
W_{AUX} = auxiliary power demand and pump work

Exergy Analysis

Traditional first-law cycle analysis based upon component performance characteristics coupled with energy balances invariably lead to a correct final answer. However, such analysis cannot locate and quantify the sources of loss that lead to that result. This is because the first law embodies no distinction between work and heat, no provision for quantifying the *quality of energy*. These limitations are not a serious drawback when dealing with familiar systems, since an intuitive understanding of the different parametric influences on system performance and a second-law qualitative appreciation of "grade-of-heat" and effect of pressure loss can be developed. When analyzing novel and complex thermal systems, however, such an understanding must be supplemented by more rigorous quantitative methods. Second-law analysis, or exergy analysis, provides these tools. Second-law analysis is no substitute for first-law analysis; it is, rather, a supplement.

The quantity energy can be split into exergy and anergy:

$$\text{Energy} = \text{Exergy} + \text{Anergy}$$

Anergy is energy in equilibrium with the ambient conditions and cannot be converted to work, while exergy is the proportion

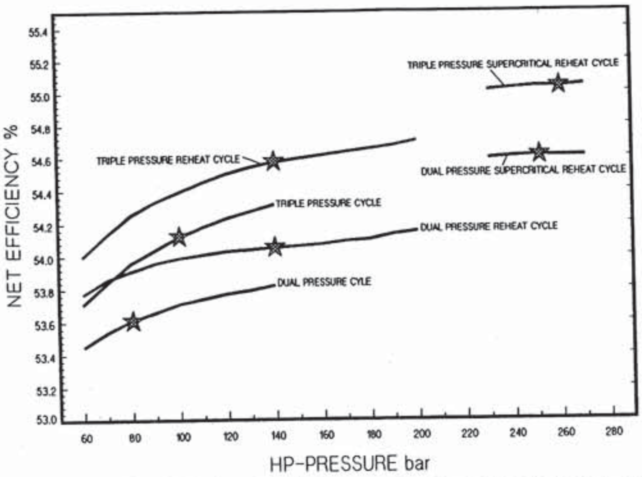

Fig. 5 Combined Cycle net efficiency as function of HP pressure for the V94.3 gas turbine

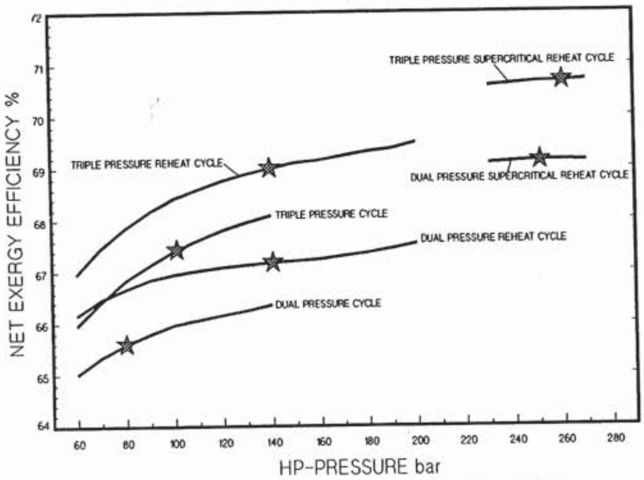

Fig. 6 Steam cycle net exergy efficiency as function of HP pressure for the V94.3 gas turbine

of energy that theoretically can be converted to work. The exergy of a flow stream for a given pressure p_1 and temperature t_1 can be computed by the following expression:

$$e(p_1, t_1) = (h_1 - h_a) - T_a \cdot (S_1 - S_a) \tag{9}$$

where

$$h_a = h(p_a, t_a) \qquad h_1 = h(p_1, t_1)$$
$$s_a = s(p_a, t_a) \qquad s_1 = s(p_1, t_1)$$

For an ideal gas, the term $s_1 - s_a$ can be written

$$s_1 - s_a = \int_a^1 C_P(T)/T \cdot dT - R \cdot \int_a^1 dp/p \tag{10}$$

To quantify the loss of exergy for a component, an exergy balance is applied. Figure 4 shows a counterflow heat exchanger and the quantities related to an exergy balance. The loss of exergy for the heat exchanger is

$$E_{\text{lost}} = E_{\text{in}} - E_{\text{out}} = E_{H,1} + E_{c,1} - E_{H,2} - E_{c,2} \tag{11}$$

The steam cycle is a closed loop. Exergy in a steam leaving a component is transferred to the next component, and is therefore not lost from the system. The exception is at points where exergy is deliberately rejected from the system, such as the HRSG stack and the condenser cooling water. The loss of exergy for all other components in the steam cycle can be calculated in a similar way as shown in the above example. When adding up all losses of exergy plus the generated work, this should equal the exergy of the gas turbine exhaust gas entering the HRSG. At this point the *exergy efficiency* can be defined

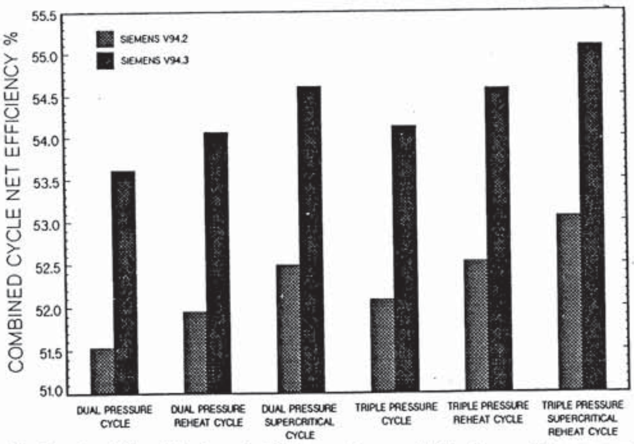

Fig. 7 Combined Cycle net efficiency for specially chosen HP pressure for the V94.2 and V94.3 gas turbines

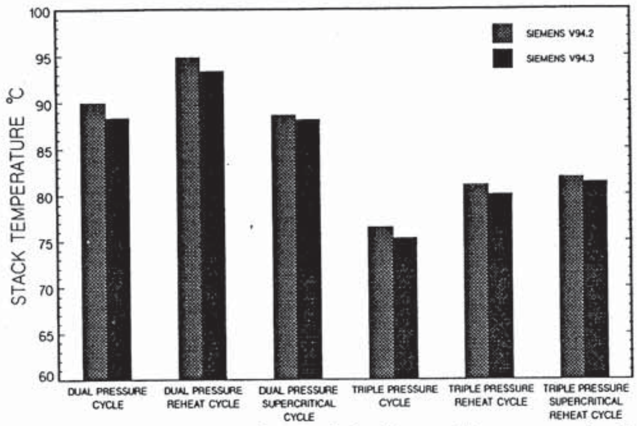

Fig. 8 Stack temperature for specially chosen HP pressures for the V94.2 and V94.3 gas turbines

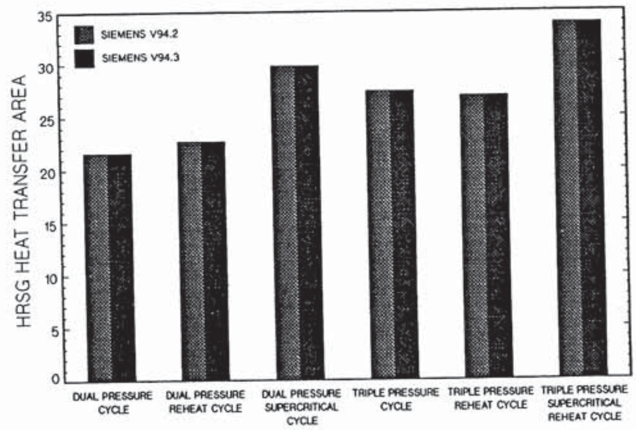

Fig. 9 HRSG relative heat transfer areas for the V94.2 and V94.3 gas turbines

$$\eta_{\text{exergy}} = \frac{W_{\text{net,out}}}{E_{\text{HRSG,in}}} = \frac{E_{\text{HRSG,in}} - \Sigma E_{\text{loss}}}{E_{\text{HRSG,in}}} \tag{12}$$

and further, the *maximum thermal efficiency* referred to the exhaust gas is given by

$$\eta_{\text{thermal,max}} = \frac{E_{\text{HRSG,in}}}{Q_{\text{HRSG,in}}} \tag{13}$$

where

$$Q_{\text{HRSG,in}} = m_{ex} \cdot (H_{\text{HRSG,in}} - H_a) \tag{14}$$

and $H_{\text{HRSG,in}}$ is referred to ambient conditions, which means

$$H_a = 0$$

The maximum thermal efficiency describes the thermodynamic limitation for the conversion of heat to work. The exergy efficiency accounts for internal steam cycle "imperfections," such as heat exchanger temperature differences, "mismatched" heat exchanger temperature profiles, heat losses, pressure losses, mixing losses, mechanical losses, generation of entropy in compression and expansion processes and rejection of exergy to the surroundings. By combining equations (12) and (13) a relation between work and heat is obtained

$$W_{\text{net,out}} = Q_{\text{HRSG,in}} \cdot \eta_{\text{thermal,max}} \cdot \eta_{\text{exergy}} \tag{15}$$

Results and Discussion

Parametric studies were carried out for combined cycles using the Siemens V94.2 and V94.3 gas turbines (representing current "state of the art" and advanced technology, respectively). Thermodynamic cycle data for the gas turbines were presented earlier, and the Appendix contains additional particulars for the various cycle components.

Net exergy efficiencies (equation (12)) and net combined cycle efficiencies (equation (8)) were calculated for the various combined cycles. These efficiencies are presented in Figs. 5 and 6 as functions of the design HP pressure for the HRSG, using the V94.3. At each HP pressure the other live-steam pressures (RH, IP, LP) are optimized with respect to cycle efficiency. Figures 7-9 compare the effects of the two gas turbines on net cycle efficiency, stack temperature, and the required HRSG heat transfer area in each of the cycles.

Introducing reheat improves the efficiency by 0.2–0.4 percentage points compared to the nonreheat cycles, for both the dual and triple pressure cycles. The difference in efficiency between dual and triple pressure cycles is about 0.5–0.6 percentage points, except for smaller HP pressures, where this difference tends to decrease. Supercritical reheat cycles give a higher efficiency than the subcritical cycles. There is also a significant difference in efficiency between the dual and triple pressure supercritical reheat cycles, about 0.5 percentage point.

The variation in exergy efficiency is from 65 percent for the dual pressure cycle at 60 bar HP pressure and up to nearly 71 percent for the triple pressure supercritical reheat cycle. The differences in exergy efficiency correspond, of course, to what has been explained for Fig. 5. It is interesting here to make a comparison between the steam cycle and the Kalina cycle, where in the latter cycle a mixture of ammonia and water is used as working fluid. For the Kalina cycle, Stecco and Desideri (1989) have calculated the exergy efficiency to be 63.2 percent when utilizing exhaust gas heat at 577°C. It should be emphasized, however, that the assumptions used in the present work differ from those of Stecco and Desideri.

In Figs. 5 and 6 the graphs are marked in order to represent a "reasonable" choice of HP pressure for each type of cycle. These choices are mainly based on the steam turbine exit quality for the nonreheat cycles. For the subcritical reheat cycles the HP pressures are chosen to be 140 bar. Increased live-steam pressure normally implies higher HRSG cost, but for the subcritical reheat cycles the HRSG HP stage has a smaller mass flow and also a smaller volumetric flow compared to the nonreheat cycles. The increased tube thickness (and weight) due to higher pressure will be opposed by smaller tube diameters. Table 2 summarizes the results from the calculations with the chosen HP pressures, which are marked in Figs. 5 and 6.

Figures 7-9 are graphic presentations of the data in Table 2. When comparing the CC performance with respect to gas turbine technology (V94.2 versus V94.3), the differences in efficiency (Fig. 7) are about 2.0–2.1 percentage points. These differences are larger than any of the differences between the cycles with a given gas turbine. The potential for CC efficiency improvement therefore mainly relies on gas turbine developments. With the new generation of gas turbines, in this study represented by the Siemens V94.3, it is likely to have CC net efficiencies reaching 54–55 percent.

Figure 8 shows the stack temperature for the different cycles. As can be seen there are only minor differences in stack temperatures when comparing the two types of gas turbine. There is no obvious connection between the stack temperature and efficiency. This means that the CC efficiency is not solely dependent on *how much* of the exhaust gas energy, is utilized, but it is also a question of *how* the exhaust gas energy is utilized.

In Fig. 9 and Table 2 the HRSG heat transfer areas are given in a nondimensional form, which is

$$\tilde{A}_{\mathrm{HRSG}} = U \cdot A \cdot T_a / W_{SC} \tag{16}$$

where W_{SC} $[W]$ is the steam cycle net power output. T_a is a constant for all cases. Equation (16) defines a parameter relating the required UA to the net power output of the steam cycle. Figure 9 shows that there is very little difference in the HRSG heat transfer area between the two gas turbines. As can be seen when comparing Figs. 7 and 9, increased efficiency comes at the expense of a larger heat transfer area. The supercritical cycles, especially, require a large heat transfer area for a given gain in efficiency. It is interesting to note that the triple pressure subcritical reheat cycle requires less heat transfer area than the triple pressure nonreheat cycle. The reason for this is that the reheat results in less mass flow going through the HP economizer and HP evaporator, which constitute most of the heat transfer area for a nonreheat cycle. Besides, the condensate flow rate is less for a reheat cycle compared to a nonreheat cycle, which means less heat transfer and heat transfer area at the cold end of the HRSG.

The effect of supplementary firing in front of the HRSG for three different types of cycles is shown in Fig. 10. The selected cycles are the dual pressure cycle, the triple pressure reheat cycle, and the dual pressure supercritical reheat cycle. All three cycles are calculated with the V94.3 gas turbine. The two subcritical cycles are calculated with different HP pressures along with an optimization of the other live-steam pressures. As can be seen from Fig. 10 supplementary firing does not improve the efficiency of the subcritical cycles irrespective of the HP pressure within the range stated in Fig. 10. On the other hand, the efficiency is slightly improved by the supplementary firing of the dual pressure supercritical cycle.

The difference among the cycles with respect to efficiency is described by means of a first-law method of analysis. A

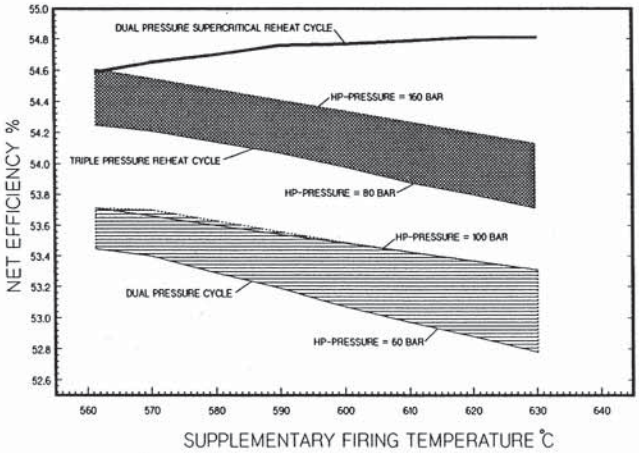

Fig. 10 Combined Cycle net efficiency as a function of supplementary firing temperature

Table 2 Cycle performance

Type of cycle	V94.2 η_{CC}	V94.3 η_{CC}	V94.2 W_{cc}	V94.3 W_{cc}	V94.2 $\bar{A}_{HRSG}$	V94.3 $\bar{A}_{HRSG}$	V94.2 t_{STACK}	V94.3 t_{STACK}
Dual pressure	51.53	53.61	687.7	577.3	21.76	21.59	90.0	88.4
Dual pressure reheat	51.95	54.06	693.3	582.2	22.81	22.70	94.9	93.4
Dual pressure supercritical reheat	52.49	54.60	700.5	588.0	29.90	29.79	88.6	88.1
Triple pressure	52.08	54.12	695.2	582.8	27.55	27.36	76.5	75.3
Triple pressure reheat	52.52	54.57	701.0	587.6	27.14	26.88	81.0	80.0
Triple pressure supercritical reheat	53.05	55.03	708.0	592.7	34.09	33.90	81.8	81.3

W_{cc} [MW], $\bar{A}$ [-], t [°C]

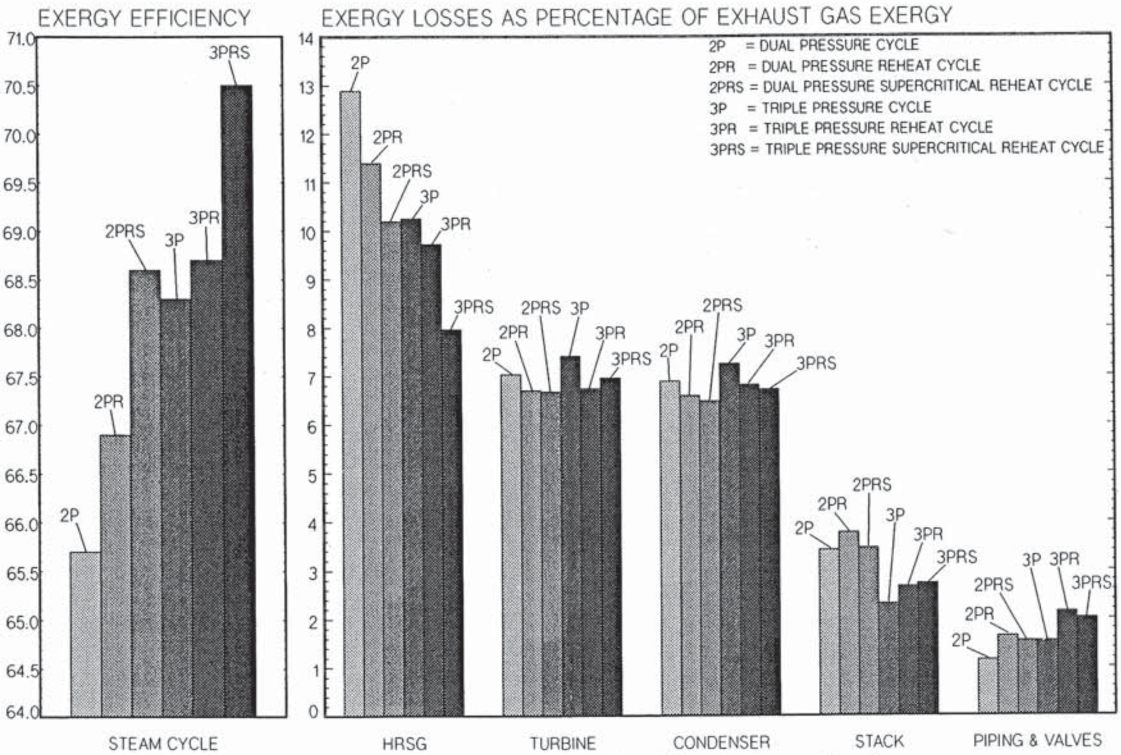

Fig. 11 Exergy efficiency and exergy loss breakdown for the considered cycles

second-law or exergy analysis provides information about *why* there are differences in cycle performance. Figure 11 shows a breakdown of exergy losses for different components in the steam cycle with the V94.2 gas turbine, as well as the steam cycle net exergy efficiencies. The main reason for differences in efficiency between the cycles is the decrease in HRSG exergy losses. The steam turbine exergy losses do not differ significantly between the cycles. The variations can be explained by the fact that different mass flows are expanded in the turbines and the efficiencies vary because of differences in exit quality, especially between reheat and nonreheat cycles. The condenser has also rather small variations in exergy losses, but the reheat cycles have slightly lower condenser losses. Even if reheat cycles have a higher steam turbine exit quality, the reduction in condenser steam mass flow implies a smaller loss of exergy. The stack exergy loss is a function of stack temperature, and as can be seen the triple pressure cycles have much smaller losses than the dual pressure cycles. The exergy losses from pipes and valves shown in Fig. 11 are obviously a function of cycle complexity and steam mass flow.

Conclusions

The combination of the first-law and second-law approaches provides a good tool for the analysis of power cycles. The exergy balance method of analysis enables all loss sources to be *located* and *quantified*. When different steam cycle configurations are compared, the exergy analysis gives a very useful understanding of *why* thermodynamic performance differs from one type of cycle to another.

The triple pressure supercritical reheat steam cycle gives the largest increase in efficiency compared to a "state-of-the-art" dual pressure subcritical steam cycles. On the other hand, the increase in required heat transfer area is large compared to the gain in efficiency. The triple pressure subcritical reheat steam cycle seems to be very interesting. Compared to the dual pressure nonreheat cycle, the increase in efficiency is approximately on percentage point. Supplementary firing is not very interesting as a measure to increase CC efficiency with the types of gas turbine used in this study, except for the supercritical cycles. However, supplementary firing provides flexibility with respect to load control, and from a design point of view, flexibility is added to power output without having to make significantly less efficient cycles.

When comparing the CC efficiency of the two gas turbines used in this study, it is obvious that the new generation of gas turbines now being introduced to the market will increase the CC efficiency by about 2 percentage points. This new generation of gas turbines together with some of the proposed steam cycle configurations will make it possible to reach net efficiencies in the range of 54–55 percent for large combined cycles.

Acknowledgments

The discussions held with Dr. Maher Elmasri were invaluable during the course of this work.

References

Bolland, O., 1987, *GuD Power Plant Alternatives for Norwegian Boundary Conditions*, Siemens (KWU) report, Erlangen, Federal Republic of Germany.

Bolland, O., and Loken, P. A., 1987, *Potentials to Improve the Steam Cycle Efficiency in an Unfired Combined Cycle*, SINTEF report STF15 A87053, Trondheim, Norway.

Chin, W. W., and Elmasri, M. A., 1987, "Exergy Analysis of Combined Cycles: Part 2—Analysis of Two-Pressure Steam Bottoming Cycle," ASME JOURNAL OF ENGINEERING FOR GAS TURBINES AND POWER, Vol. 109, pp. 237–243.

Engelke, W., 1989, *Dampfturbinen für GuD-Kraftwerke*, BWK, Vol. 41, No. 7/8, July/Aug., pp. 335–342.

Frutschi, H. U., and Plancherel, A., 1988, "Comparison of Combined Cycles With Steam Injection and Evaporisation Cycles," IGTI-Vol. 3, ASME Cogen-Turbo, pp. 137–145.

Hamann, B., and Joyce, J. S., 1989, "World's Largest Gas Turbines for Ambarli Combined Cycle," *Modern Power Systems*, pp. 61–74, May.

Horlock, J. H., 1987, *Cogeneration—Combined Heat and Power (CHP), Thermodynamics and Economics*, Pergamon Press, New York.

Johnson, D. G., 1982, "Möglichkeiten der Kombi-Kraftwerke mit Hochtemperatur-Gasturbinen," *VGB Kraftwerkstechnik 62*, pp. 167–173, Mar.

Kehlhofer, R., et al., 1984, "Gasturbinenkraftwerke, Kombikraftwerke, Heizkraftwerke und Industriekraftwerke," *Handbuchreihe Energie Technischer Verlag Resch*, Verlag TUV Rheinland, Band 7, Chap. 2.

Kotas, T. J., 1985, *The Exergy Method of Thermal Plant Analysis*, Butterworths, London.

Rukes, B., 1990, Head of Department for Calculating of Heat Cycles and Heat Removal Systems, Siemens AG-KWU Group, The Federal Republic of Germany, Private Communication.

Stecco, S. S., and Desideri, U., 1989, "A Thermodynamic Analysis of the Kalina Cycles: Comparisons, Problems and Perspectives," ASME Paper No. 89-GT-XX.

APPENDIX

Inputs not mentioned in the body of the paper but used in the calculations cited are:

Gas Turbines

- Ambient temperature = 15 [°C]
- Ambient pressure = 1.013 [bar]
- Relative humidity = 60 [percent]
- Inlet pressure drop = 10 [mbar]
- Outlet (HRSG) pressure drop = 40 [mbar]
- Auxiliary power for each gas turbine = 400 [kW]

HRSG

- Pinch point = 10 [K]
- Minimum steam/exhaust approach temperature = 30 [K]
- Economizer approach temperature = 2 [K]
- Pressure drop live-steam pipes:
  Subcritical cycles HP = 5, RH = 7, IP = 7, LP = 10 [percent]
  Supercritical cycles HP = 4, RH = 7, IP = 7, LP = 10 [percent]
- Heat loss live-steam pipes = 1 [K]
- Pressure drop superheaters = 5 [percent]
- Pressure drop evaporators = 5 [percent]
- Pressure drop economizers = 5 [percent]
- Pressure drop feedwater preheater = 4 [bar]
- Deaerator pressure = 1.2 [bar]
- Exhaust gas duct heat loss = 2 [K]
- Maximum steam temperature: HP = 540, RH = 560 [°C]

Steam Turbine

- Pressure drop throttle valves = 2 [percent]
- Pressure drop reheat return pipe = 3 [percent]
- Isentropic efficiencies: HP = 92, RH = 92, IP = 92, LP = 89 [percent] (subcritical)
- Isentropic efficiencies: HP = 91, RH = 92, IP = 92, LP = 89 [percent] (supercritical)
- Steam leakages through seals: HP = 0.2, RH = 0.2, IP = 0.2, LP = 0.2 [percent]
- LP section leaving loss = 30 [kJ/kg]
- "Wilson line" quality = 0.975
- Auxiliary power fraction = 0.25 [percent] (pump work not included)
- Mechanical/generator efficiency = 98.2 [percent]

Condenser

- Condenser pressure = 0.04 [bar]
- Cooling water temperature = 15 [°C]
- Allowed cooling water temperature increase = 9 [K]
- Cooling water pressure drop = 1 [bar]

Pumps

- Mechanical efficiency = 92 [percent]
- Isentropic efficiency = 80 [percent]

Gasturbinen sind ein ausgezeichnetes Instrument, bei bestehenden Dampfkraftwerken die Leistung zu vergrößern, den Block-Wirkungsgrad zu steigern, die Flexibilität des Betriebes zu verbessern und eventuell die Lebensdauer des Blockes zu verlängern. Dabei kann die Infrastruktur des bestehenden Kraftwerkes voll genutzt werden, ein Aspekt, der vor allem die Genehmigungsfähigkeit und die Wirtschaftlichkeit der Nachrüstung positiv beeinflusst.
Für die Nachrüstung gibt es verschiedene Möglichkeiten der Anbindung der Gasturbine. Die umfassendste Rekonstruktion stellt das „Full Repowering" dar. Dabei wird der Dampferzeuger einer bestehenden Anlage vollständig durch eine oder mehrere Gasturbinen und die zugehörigen Abhitzedampferzeuger ersetzt.

Ertüchtigung bestehender Dampfkraftwerke durch Gasturbinen

Günter Bauer

Bild 1 | Erforderliche Neuausrüstung eines kohlegefeuerten Dampferzeugers beim „Topping": eine Gasturbine liefert teilweise oder vollständig den Sauerstoff für die Feuerung.

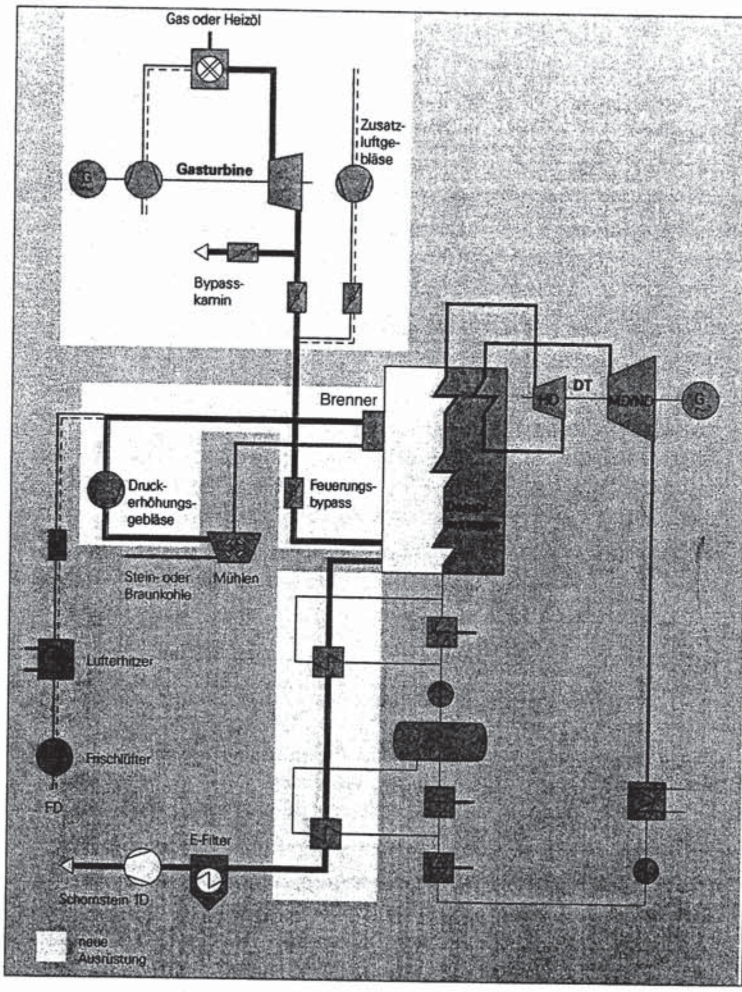

Dipl.-Ing. *Günter Bauer*, Jahrgang 1956, studierte Maschinenbau mit dem Schwerpunkt Energietechnik an der Fachhochschule Regensburg. Seit 1981 bei Siemens/KWU tätig im Bereich Projektierung und Abwicklung von fossil gefeuerten Dampferzeugern, ist er heute verantwortlich für die Optimierung der Komponentenauslegung im Bereich Dampferzeuger und Rauchgasweg sowie die Erarbeitung von verbesserten Schaltungskonzepten zur Wirkungsgradsteigerung von Dampfkraftwerken.

Für die Nachrüstung von Dampfkraftwerken gibt es verschiedene Möglichkeiten der Anbindung einer Gasturbine (GT): Bei der „Topping"-Variante dient das Gasturbinenabgas ganz oder teilweise als Sauerstoffträger für die Verbrennung des Brennstoffes im gefeuerten Dampferzeuger (DE). Das ermöglicht die bessere Ausnutzung des Restsauerstoffgehaltes und des hohen Wärmeinhaltes des GT-Abgases im Dampferzeuger. Ein Teil der sonst notwendigen Brennstoffwärme wird ersetzt, und der Wirkungsgrad des Blockes steigt an.

Ein vergleichbarer Zuwachs an Leistungs- und Wirkungsgradsteigerung kann durch eine „Parallel Repowering"-Variante erzielt werden. Hierbei wird die Abgaswärme der Gasturbine in einem Abhitzedampferzeuger (AHDE) zur Erzeugung von Dampf in einer oder mehreren Druckstufen genutzt und dieser der bestehenden Dampfturbine des zu ertüchtigenden Blockes zugeführt.

Eine Untervariante des „Parallel Repowering" ist das „Boosting". Hierbei wird mit dem GT-Abgas jeweils ein Teilstrom des Speisewassers und des Kondensates erwärmt und damit die Anzapfdampfentnahme aus der Dampfturbine reduziert.

Eine sehr umfassende Rekonstruktion stellt das „Full Repowering" dar. Dabei wird der Dampferzeuger einer bestehenden Anlage vollständig durch eine oder mehrere Gasturbinen und den zugehörigen Abhitzedampferzeugern ersetzt.

Topping

Topping bezeichnet die Umwandlung eines konventionellen Dampfkraftwerkes (DKW) in einen DKW-Prozeß, bei dem eine Gasturbine teilweise oder vollständig den Sauerstoff für die Feuerung des Dampferzeugers liefert. Durch den hohen Energieinhalt des Gasturbinenabgases wird der Brennstoffbedarf des Dampferzeugers ge-

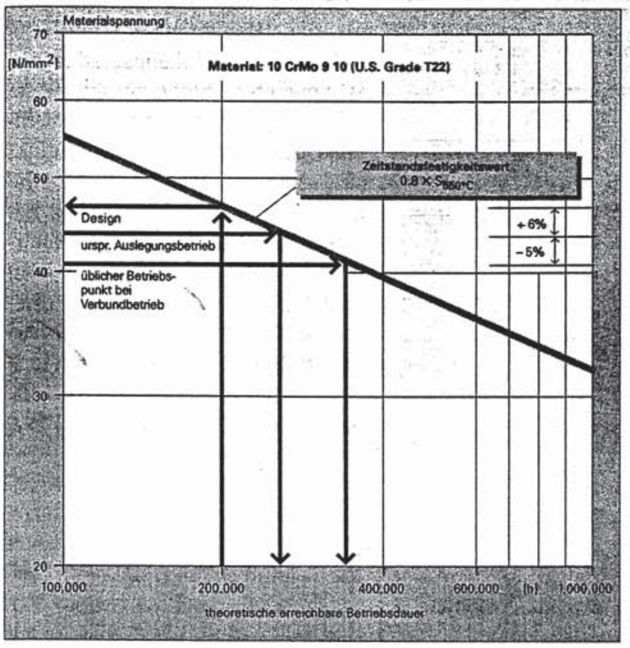

Bild 2 | Verlängerung der theoretischen Lebensdauer hochbelasteter Bauteile beim „Parallel Repowering". Durch die geänderte Dampfverteilung in der Dampfturbine und die niedrigen Rohrleitungsdruckverluste reduziert sich der Systemdruck am Dampferzeugeraustritt und damit im gesamten Dampferzeuger-Hochdrucksystem.

senkt. Bei der Verbrennung mit GT-Abgas wird aufgrund des geringeren O_2-Gehaltes ein spezifisch höherer (bis zu 40 %) Rauchgasvolumenstrom erzeugt als bei der Verbrennung mit Luft. Dieser Effekt wird teilweise kompensiert durch den geringeren Brennstoffbedarf des Dampferzeugers. Kann die Rauchgasgeschwindigkeit wegen der Gefahr der Heizflächenerosion (Aschegehalt) oder wegen des Druckverlustes (Festigkeitsauslegung, Gegendruck GT, Leistungsgrenze Saugzug, Auslegung der Komponenten des Rauchgasweges) nicht erhöht werden, muß die Dampferzeugerleistung und damit die Leistung der Dampfturbine gesenkt werden.

„Topping" erfordert umfangreiche Anpassungen des Dampferzeugers (**Bild 1**). Wegen der hohen GT-Abgastemperatur und des deutlich höheren Volumenstromes müssen das gesamte Luftkanalsystem und die Brenner erneuert werden.

Da wegen der geringen Verbrennungsluftmenge der Luftvorwärmer meist komplett entfällt, werden für die Abkühlung der Rauchgase an dessen Stelle Teilstromspeisewasser- und Teilstromkondensatheizflächen installiert. Bei der Bemessung letzterer ist darauf zu achten, daß die Heizflächentemperatur immer oberhalb des Schwefelsäuretaupunktes des Rauchgases gehalten wird, um Heizflächenkorrosion zu vermeiden.

Für die Teillastfahrweise wird ein Teilbypass des GT-Abgases erforderlich, durch den überschüssiges GT-Abgas an der Feuerung vorbei direkt in den Konvektionszug des Dampferzeugers, üblicherweise vor den ZÜ1, geleitet werden kann.

Nachdem bei der Verbrennung mit GT-Abgas trotz Rückgang des Brennstoffbedarfes ein höherer Rauchgasstrom erzeugt wird und die Brennkammertemperatur sinkt, ist es unter Umständen erforderlich, die Heizflächen an die neue Wärmeverteilung im Dampferzeuger anzupassen. Auch die Komponenten des Rauchgasweges wie E-Filter, REA und vor allem der Saugzug sind auf ihre Auslegungsreserven zu überprüfen und gegebenenfalls zu ertüchtigen.

Siemens betreibt die Entwicklung von Konzepten, Gasturbinen an die Feuerung eines Dampferzeuger anzubinden, seit 1965. So sind 17 Gasturbinen von Siemens in dieser Anordnung in Europa im Einsatz, zum Beispiel im 750-MW-Kohleblock in Werne oder im 700-MW-Gasblock Eemscentrale.

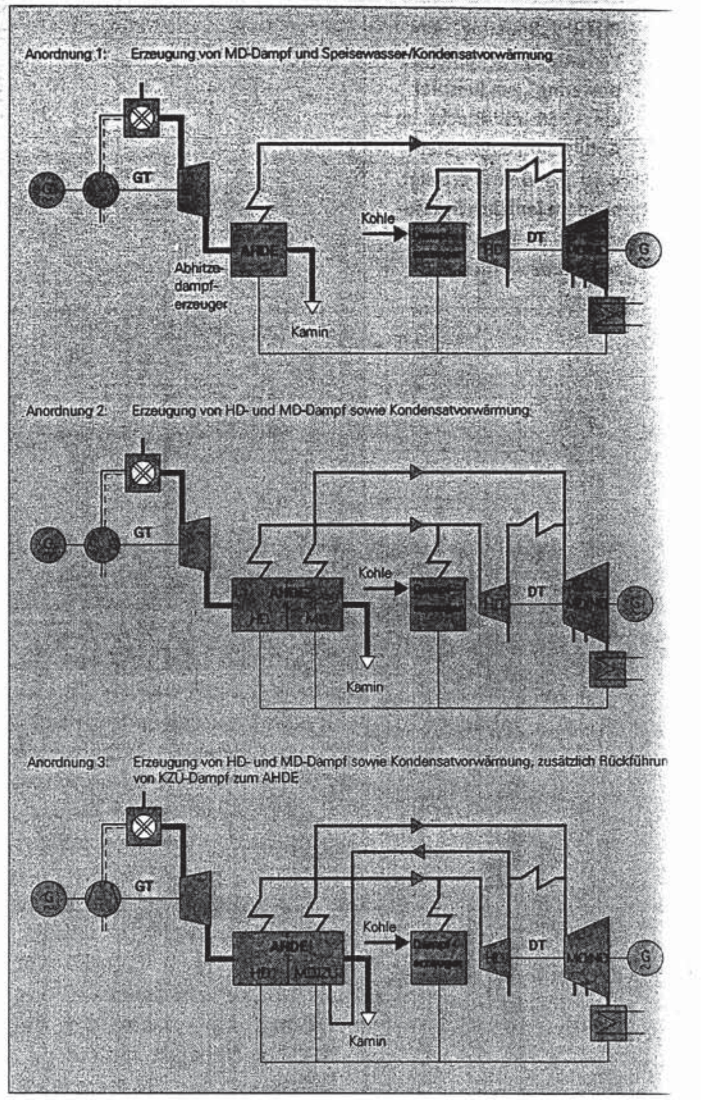

Bild 3 | „Parallel Repowering" (Verbund); Unterschiede der wichtigsten Varianten.

Parallel Repowering (Verbund)

Wie die Bezeichnung schon ausdrückt, wird bei einem „parallel powered"- oder Verbund-Kraftwerk die Dampfturbine von zwei parallel arbeitenden Dampferzeugern mit Dampf versorgt. Der gefeuerte Dampferzeuger kann mit jedem beliebigen Brennstoff beheizt werden, und auch die Art der Feuerung unterliegt keinerlei Einschränkungen. Die zweite Dampfquelle stellt ein der Gasturbine nachgeschalteter Abhitzedampferzeuger dar.

Der große Vorteil des „Parallel Repowering"-Prinzips sind die Vielseitigkeit und Freiheit bei der Wahl

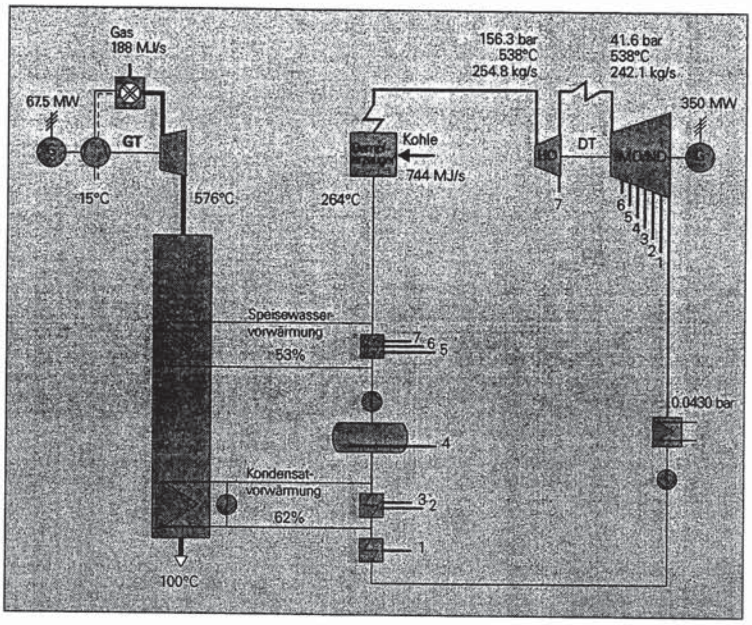

Bild 4 | **„Boosting", eine Variante des „Parallel Repowering", am Beispiel eines 350-MW-Blocks. Im Abhitzenutzungssystem wird kein Dampf erzeugt, sondern lediglich Speisewasser- und Kondensatteilströme werden erwärmt.**

der Gasturbinenleistung, der Art der Dampfeinbindung, des Brennstoffes für den gefeuerten Dampferzeuger, die flexible Betriebsweise und vor allem die einfache Anbindung der neuen Komponenten GT und Abhitzedampferzeuger an den bestehenden Block. Die Leistung der einzusetzenden Gasturbine kann bis zu einem maximalen GT/Blockleistungs-Verhältnis von 1:1,5 frei gewählt werden. Gas- und Dampfturbine lassen sich unabhängig voneinander betreiben.

Da die Abgase des gefeuerten und des Abhitze-Dampferzeugers nicht gemischt werden, entsteht auch keine Leistungseinschränkung durch Komponenten des Rauchgasweges oder die Notwendigkeit zu deren Ertüchtigung oder Austausch. Außerdem wird der gefeuerte Dampferzeuger im Verbundbetrieb bei unveränderter Dampfturbinenleistung in Teillast gefahren.

Bild 5 | **Neue Komponenten beim „Full Repowering": Gefeuerte Dampferzeuger, die ihre Lebensdauer erreicht haben, werden durch eine oder mehrere Gasturbinen-/AHDE-Einheiten ersetzt.**

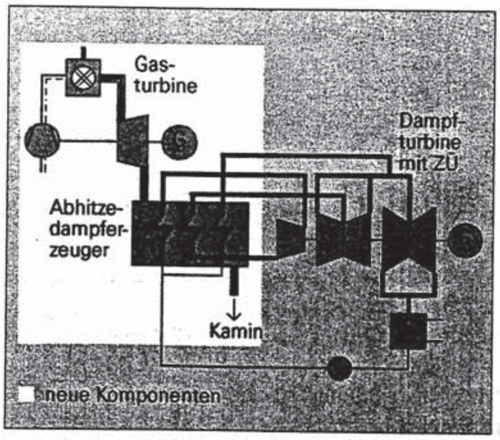

Durch die geänderte Dampfverteilung in der Dampfturbine und die niedrigeren Rohrleitungsdruckverluste reduziert sich der Systemdruck am Dampferzeugeraustritt und damit im gesamten Dampferzeuger-Hochdrucksystem. Daraus ergibt sich eine spürbare Verlängerung der theoretischen Restlebensdauer der Bauteile, die der Zeitstandserschöpfung unterliegen (**Bild 2**).

Die wichtigsten Verbundvarianten sind in **Bild 3** schematisch dargestellt. Variante 1 zeigt den MD-Verbund, bei dem im Abhitzedampferzeuger Dampf in der Druckstufe der Mitteldruckteilturbine erzeugt und dem heißen ZÜ-Dampfstrom des gefeuerten Dampferzeugers zugeführt wird. Die weitere Abkühlung der GT-Abgase auf eine wirtschaftliche Abgastemperatur erfolgt in den Teilstromspeisewasser- und -kondensatheizflächen. Die Vorteile dieser Anordnung sind die einfache Ausführung des Abhitzedampferzeugers, die problemlose Anbindung an den bestehenden Block und daß der gefeuerte Dampferzeuger nicht angepaßt werden muß.

Bei der Variante 2 liefert ein Zweidruck-Abhitzedampferzeuger Dampf mit den Parametern des Frischdampfes und der heißen ZÜ-Stufe. Zur Restabkühlung des GT-Abgases dient ein Teilstromkondensatvorwärmer. Die Dampfströme werden jeweils vor der Dampfturbine den Hauptdampfströmen zugeführt. Der Wirkungsgradgewinn ist bei dieser Anordnung sehr hoch, da sehr viel Wärme auf hohem Niveau übertragen wird. Allerdings sind Anpassungen der ZÜ-Heizflächen des gefeuerten Dampferzeugers erforderlich, weil der im Abhitzedampferzeuger gebildete Frischdampfstrom im ZÜ-System des gefeuerten Dampferzeugers zusätzlich mit wiederaufgeheizt werden muß. Für den DKW-Betrieb ohne Gasturbine ist das ZÜ-Einspritzsystem zu ertüchtigen.

Die Variante 3 unterscheidet sich von der vorherigen nur in der Rückführung eines kZÜ-Teilstromes zum Abhitzedampferzeuger. Um den Nachteil der DE-Anpassung zu vermeiden wird so viel kZÜ-Dampf zum Abhitzedampferzeuger zurückgeführt, wie in dessen Hochdruckstufe Frischdampf erzeugt wurde. Damit bleiben die Verhältnisse im gefeuerten Dampferzeuger bestehen. Diese Anordnung ist zwar sehr aufwendig in der Konstruktion des AHDE und der Anbindung an das bestehende System, hat aber den Vorteil des höheren Wirkungsgradgewinnes als die MD-Variante und erlaubt die flexibelste Betriebsweise des Gesamtblockes.

Für alle Varianten gilt, daß mit steigendem GT/Blockleistungsverhältnis auch der Wirkungsgradgewinn zunimmt. Begrenzend wirken dabei gegebenenfalls die einseitige Belastung der Dampfturbine, der nutzbare Teillastbereich des gefeuerten Dampferzeugers und eventuell auch eine Wirtschaftlichkeitsbetrachtung in bezug auf die Brennstoffkosten (Erdgas/Kohle o.ä.).

Ein Beispiel für „Parallel Repowering" ist der 160-MW-Gas-Block von Mussalo, Finnland. Dieser wurde 1994 mit einer Siemens-Gasturbine V64.3 in der MD-Verbund-Variante nachgerüstet. Die Blockleistung konnte dabei zusätzlich zu den rund 64 MW der GT um 25 MW an der Dampfturbine gesteigert werden, wodurch sich eine neue Gesamtleistung von fast 250 MW ergab. Der Wirkungsgrad des Blockes stieg um rund 4%-Punkte.

Boosting

Das „Boosting" ist prinzipiell eine Variante des „Parallel Repowering". Im neu zu erstellenden Abhitzenutzungssystem wird aber kein Dampf erzeugt, sondern lediglich Speisewasser- und Kondensatteilströme werden erwärmt (**Bild 4**). Die dadurch eingesparten Dampfturbinen-Anzapfdampfströme steigern entweder die Dampfturbinenleistung oder der gefeuerte Dampferzeuger wird in Teillast gefahren. Die optimale Wirkungsgradsteigung wird erzielt, wenn möglichst viel GT-Abgaswärme zur Speisewasservorwärmung genutzt wird. Eine günstigere Betriebsweise erreicht man aber durch eine etwa 50%/50%-Aufteilung der Abgaswärme zur Speisewasser -und Kondensaterwärmung. In diesem Fall kann die Gasturbine in einem breiten Band der Blockteillast in Vollast betrieben werden.

Full Repowering

Da die Lebensdauer von Dampfturbinen länger ist als die des gefeuerten Dampferzeugers, bietet es sich bei Anlagen, deren Dampferzeugerlebensdauer verbraucht ist, an, diesen durch eine oder mehrere Gasturbinen-/Abhitzedampferzeuger-Einheiten zu ersetzen, **Bild 5**. Die AHDEs müssen dann so ausgelegt werden, daß die Dampfparameter und -massenströme den ursprünglichen entsprechen. Die Investition für die neuen Gasturbinen, Abhitzedampferzeuger, verbindende Systeme und Leittechnikerneuerung ist sehr niedrig, besonders im Hinblick auf den Anstieg der Gesamtleistung des Blokkes. Da das Leistungsverhältnis GT/DT bei GuD-Anlagen etwa 2:1 beträgt, steigt die Blockleistung bei Wiederherstellung der ursprünglichen DT-Leistung auf bis zum maximal dreifachen Wert. Aufgrund der kompakten Bauweise der GT/AHDE-Einheiten ist deren Anordnung an der Stelle des zu ersetzenden Dampferzeuger normalerweise problemlos möglich. Lediglich die Stromableitungssysteme sind an die neue Blockleistungsgröße anzupassen.

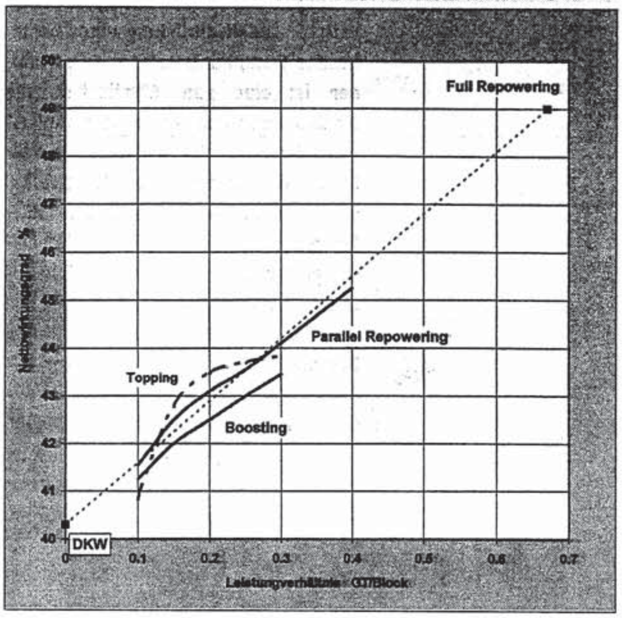

Bild 6 | Wirkungsgradgewinn durch GT-Nachrüstung. Die Höhe ist abhängig von der Art der Gasturbinenanbindung und vom Leistungsverhältnis P_{GT}/P_{Block}.

In USA wurden acht Gasturbinen vom Typ Siemens V84.2 zur Nachrüstung von Dampfkraftwerken in

Suchen Sie Problemlösungen?

Tips und Anregungen erhalten Sie aus Anzeigen – weitgehende Informationen direkt von den Inserenten. Lassen Sie sich beraten. Unsere Inserenten freuen sich auf Ihren Anruf.

Springer VDI Verlag
Verlag für technische Zeitschriften

Postfach 10 10 22, 40001 Düsseldorf, Telefon 02 11/61 03-0, Telefax 02 11/61 03-3 00

Fazit **Die Nachrüstung eines bestehenden Dampfkraftwerks mit Gasturbinen ist eine gute Möglichkeit, die Blockleistung und den Blockwirkungsgrad zu steigern. Das gilt besonders für Länder und Standorte, wo Kraftwerksneubauten schwer zu realisieren sind.**

Die maximale Wirkungsgrad- und Leistungssteigerung ist mit der „Full Repowering"-Variante möglich. Dabei ist aber zu beachten, daß durch die Dampferzeugung ausschließlich mit GT-Abgasen der Einsatz von festen Brennstoffen in der Regel nicht mehr möglich ist. Der Einfluß der Brennstoffpreise ist in einer Wirtschaftlichkeitsbetrachtung zu untersuchen. Ebenso ist zu prüfen, ob die erforderliche Menge an GT-Brennstoff (normalerweise Erdgas) am Standort überhaupt zur Verfügung gestellt werden kann.

Bei den anderen Varianten wird in der Regel je Block nur eine Gasturbine zusätzlich zu den vorhandenen Einrichtungen eingesetzt. Somit ist die Nutzung des ursprünglichen Brennstoffes weiterhin möglich, nur der Verbrauch wird reduziert. Einschränkungen können sich hierbei eventuell bei der „Topping"-Variante ergeben, da dort die Verbrennung bei niedrigem O_2-Gehalt des Sauerstoffträgers abläuft. Diese Einschränkung, das enge Band des sinnvollen GT-/Blockleistungsverhältnisses und die relativ höheren Investitionen machen diese Lösung für Nachrüstungen weniger attraktiv.

Die Verbundlösungen sind für die Ertüchtigung bestehender Kraftwerksblöcke gut geeignet, da diese einen wirtschaftlichen Kompromiß aus Leistungssteigerung, Wirkungsgradgewinn, Brennstoffwahl und -einsatz darstellen und eine flexible Betriebsweise erlauben.

dieser Variante eingesetzt. Im Kraftwerk Bergen, New Jersey, wurde eine Dampfturbine mit einer Leistung von 285 MW, die seit der Inbetriebnahme 1960 rund 200 000 Betriebsstunden erreichte, mit vier Gasturbinen V84.2 und Dreidruck-Abhitzedampferzeugern nachgerüstet. Die Restlebensdauer der Dampfturbine wurde durch Absenkung der Dampfparameter verlängert. Bei diesen Randbedingungen erhöhte sich die Blockleistung von original 285 MW auf 650 MW. Trotz der niedrigeren Dampfparameter erhöhte sich der Nettowirkungsgrad auf rund 49 %. Durch die Wirkungsgraderhöhung und den Einsatz von Erdgas verringerten sich die Emissionen deutlich. Die NO_x-Emissionskonzentration liegt nach der Ertüchtigung unter 9 ppm (trockenes Rauchgas, 15 % O_2), CO und Kohlenwasserstoff bewegen sich im Bereich der Nachweisgrenze.

Wirkungsgradgewinn

Die Höhe des Wirkungsgradgewinns ist grundsätzlich abhängig von der Art der Gasturbinenanbindung und vom Leistungsverhältnis P_{GT}/P_{Block} (**Bild 6**). Während beim „Topping" der beste Wirkungsgrad erreicht ist, wenn das GT-Abgas genau soviel Sauerstoff liefert wie für die Verbrennung des Brennstoffes im gefeuerten Dampferzeuger notwendig, steigt der Wirkungsgradgewinn bei „Parallel Repowering" und „Boosting" mit dem Leistungsverhältnis P_{GT}/P_{Block} stetig an. Begrenzend wirken dabei nur betriebliche Aspekte wie minimale Teillast des Dampferzeuger, Dampfverteilung in der Dampfturbine und Kondensatorschluckvermögen.

Den größten Sprung erreicht die Variante „Full Repowering". Da die Dampfparameter und DT-Beaufschlagung bei Nachrüstung aber nicht für den GuD-Betrieb optimiert sind, liegt der erzielbare Blockwirkungsgrad niedriger als bei Neubau-GuD-Kraftwerken.

Investionskosten

Die anfallenden Investionskosten setzen sich bei den verschiedenen Ertüchtigungsvarianten unterschiedlich zusammen.

Beim Vorschalten der Gasturbine an den Dampferzeuger (Topping) fallen neben den Aufwendungen für die Gasturbine, E- und L-Technik und Baumaßnahmen umfangreiche Umbaumaßnahmen am Dampferzeuger an. Diese betreffen insbesondere das Verbrennungsluftsystem, die Brenner inklusive Rohrwandausbiegungen, die bestehenden Heizflächen, Anbindungen eines GT-Abgasteilbypasses, zusätzliche Teilstromheizflächen für Speisewasser- und Kondensatvorwärmung und Ertüchtigung der Komponenten im Rauchgassystem.

Die Verbundvarianten (Parallel Repowering, Boosting) erfordern üblicherweise keine Modifikationen des bestehenden Blockes. Die notwendigen Kosten beschränken sich auf die Neuanschaffung der Gasturbine, des Abhitzedampferzeugers sowie der zugehörigen E-, L- und Bautechnik. Die Anbindung an den Block ist durch die einfach zu verlegenden Wasser- und Dampfleitungen sehr variabel und wenig aufwendig.

Beim vollständigen Ersatz des Dampferzeugers durch GT/AHDE-Einheiten (Full Repowering) muß der Bewertungsmaßstab angepaßt werden, da bei dieser Variante die Blockleistung erheblich höher steigt als bei den anderen Varianten. Neben der Demontage des Dampferzeugers sowie der zugehörigen und verbindenden Systeme werden zur Beibehaltung der ursprünglichen Dampfturbinenleistung eine größere Anzahl von Gasturbinen, Abhitzedampferzeuger und Rohrleitungsystemen erforderlich. Ebenso steigt der absolute Aufwand für E-, L- und Bautechnik an. Ein objektiver Vergleich ist daher nur unter Bezug auf die zusätzliche oder die Gesamtblockleistung möglich.

Setzt man die so ermittelten relativen Kosten der Topping-Variante zu 100 %, betragen die spezifischen Kosten der Verbund-Varianten und des Full Repowering etwa 80 % und die des Boosting 70 bis 75 %.

Combined Cycle Prices

Prices up 20% on average for 18-24 months delivery wait

The 'equipment-only' budget prices for turnkey combined cycle projects are FOB the factory in year 2008 U.S. dollars referenced to a standardized OEM reference plant design.

This year's plot of total plant equipment costs versus power output shows the classic slope of decreasing price with increasing size -- but the change in price is more gradual than for simple cycle units.

This is attributed to the increased engineering development and manufacturing costs for advanced technology gas turbine designs (F+, G and H models) specially developed for combined cycle power generation and associated increase in the cost of more advanced steam turbine cycle equipment.

On the gas turbine side, new materials and coatings developed for the buckets and nozzles (to withstand high temperature) are more expensive and the process required to manufacture them is more costly.

Scope of supply

Basic equipment for an operational combined cycle package includes gas turbines, heat recovery steam generators, steam turbine, electric generators and associated balance-of-plant systems:

• ***Gas turbine.*** Skid mounted single fuel design with acoustically treated enclosure for outdoors installation and with standard starting and control systems. No inlet air heating or chilling.

• ***Steam turbine.*** Condensing subcritical designs, with single or dual-pressure levels for small plants, triple-pressure levels with reheat for large plants. Axial or radial exhaust and water-cooled heat rejection.

• ***Unfired HRSG.*** Outdoors mounted heat recovery steam generator, with ductwork but no bypass damper, short exhaust stack. Dual-pressure level design or triple pressure units with reheat. Catalytic sections are optional add-on (expensive).

Combined Cycle Plant Prices 2007. Here again, plant prices vary considerably, depending on design integration of the gas turbine, HRSG and steam turbine. In the larger unit sizes, the lower $ per kW prices reflect economy of scale in the equipment design and manufacture.

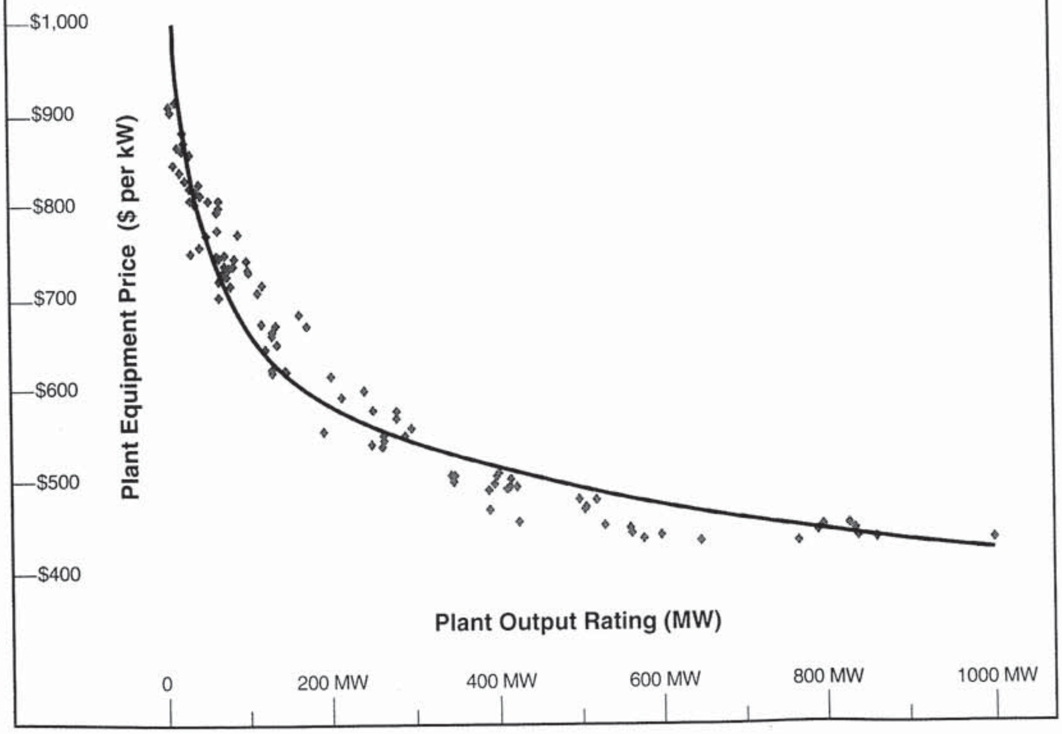

• ***Electric generators.*** Generally air-cooled for small machines and hydrogen cooled on large units. Main step-up transformer, neutral grounding cubicle, and non-segregated bus included.

• ***Balance of plant.*** Standard plant controls and auxiliary systems. It does not include substation, water treatment facility, special tools, replacement spare parts, black start generator sets, fuel conditioning and compression equipment, etc.

$ per kW

Prices are referenced to net plant output, with allowance for HRSG losses, measured across the electric generator terminals, at 59°F (15°C) sea level site conditions on natural gas fuel.

As to be expected, reference plants designed around integrated high efficiency gas turbine and steam turbine cycles are priced higher than less efficient plants.

Steam turbines developed especially for combined cycle operation, for example, cost more than earlier generation designs.

Triple-pressure HRSGs (with reheat) and matching multi-casing steam turbines increase plant costs but generate more power because they are more efficient.

High efficiency hydrogen-cooled electric generators are also considered as standard equipment for large combined cycle plants.

Lately, however, advanced air-cooled generator designs have become more common because they provide almost the same level of efficiency at much lower cost.

Higher fuel costs are driving efficiency

In recent years several owner-operators have been driven to shut down combined cycle assets because natural gas fuel costs were higher than the value of the electricity generated.

For combined cycles in base load service, fuel is said to represent up to 70% of total plant costs including acquisition, owning and operating costs, and debt service.

It has always been the biggest single cost of plant ownership and operation, even when natural gas was selling for US $2-3 per MMBtu. This is why efficiency is so important.

For a combined cycle plant in the 400-500 MW range, burning $7 to $8 MMBtu gas, a difference of one or two percentage points in plant efficiency can be critical.

Depending on utilization and average fuel price, even a single percentage point improve-

Combined Cycle Heat Rates 2007. As shown, heat rates vary all over the place, depending on HRSG and steam turbine design, and on whether or not the gas turbine design is optimized for combined cycle application.

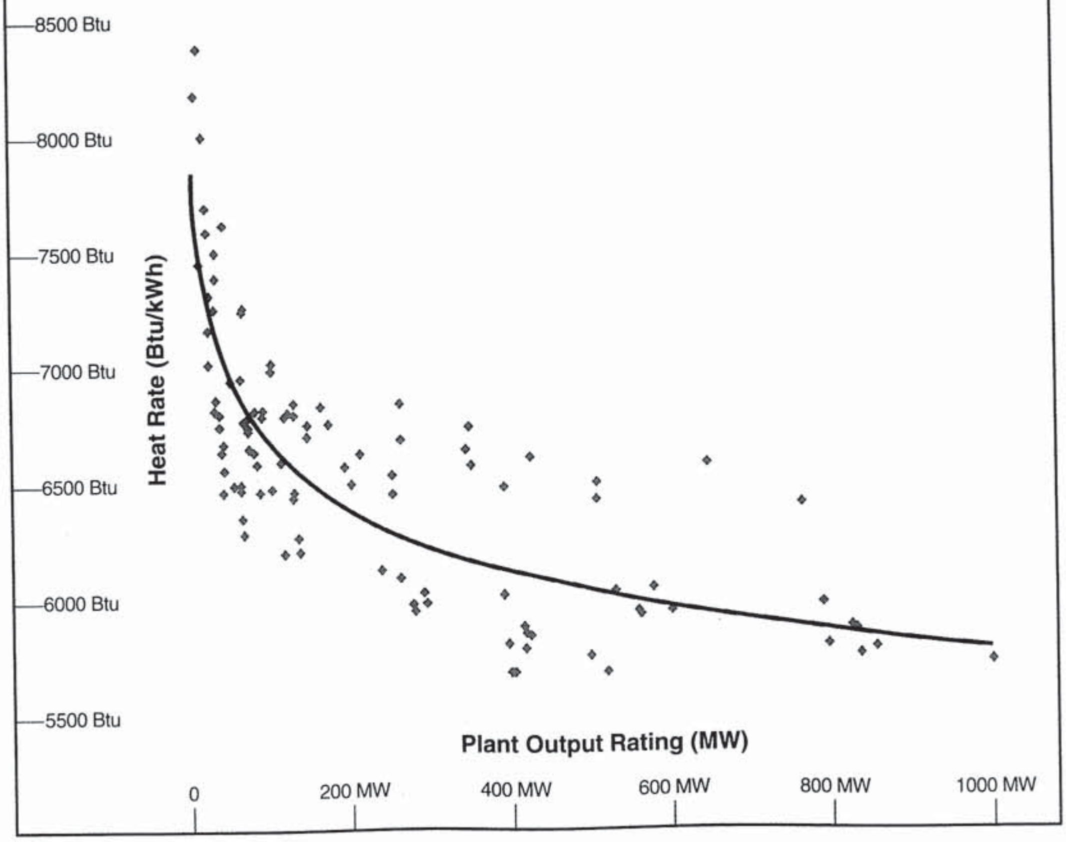

ment in efficiency can reduce operating costs by several million dollars a year.

It is hard to generalize about savings because the relative value of efficiency hinges on many factors with design performance, fuel price, plant size and operational profile topping the list.

Growing demand for combined cycles

A fast growing market is forecast for natural gas-fired combined cycle power generation projects in the United States in the next few years.

This has largely been brought about by the growing concern over global warming due to greenhouse gas emissions (carbon dioxide in particular) generated by pulverized coal steam plants.

Many supercritical pulverized coal plants proposed during 2006 and early 2007 have been cancelled because the design cost of building them with CO2 capture has doubled original estimates.

The same has happened to utilities and IPPs considering coal-based integrated gasification combined cycle (IGCC) plants with syngas-compatible gas turbines.

Although carbon capture is less expensive (than for pulverized coal steam plants) it increases the already high cost estimates for IGCC plants by 50 per cent.

Existing natural gas fired combined cycle plants would have to retrofit their gas turbines to burn the syngas but, according to power plant engineers, this can be done on-site at reasonable cost.

Near term however, OEMs expect the boom in combined cycle plants to be fueled by natural gas and, increasingly, by LNG to make up for shortages in natural gas availability as demand outgrows the supply.

OEM modular reference plants

Engineering firms and OEMs have been working to shrink construction schedules by developing standardized, pre-engineered and easily replicated modular combined cycle packages.

Computer design allows a complete plant, down to the piping and wiring routing, to be designed and reviewed before any earth is moved — so that there are no site surprises or delays when the plant is being built.

A standardized 1x1 combined cycle configuration is made up of about ten key modules: gas turbine, electric generator(s), steam turbine, HRSG, condenser, lube oil and fuel skids, controls package, water treatment system, and one or two others.

Currently, despite a growing shortage of skilled labor, combined cycle plants can be installed in 2-3 years from contract signing to commissioning.

Pre-2006, construction times of 16-18 months were not uncommon. Now it is more like 24 months.

Bottom line

Turnkey equipment package price quotes are for no-frills combined cycle plants with minimal equipment and services.

Extended site work such as cogenerated process steam or utility plant tie-ins are not covered, nor are buildings, workshops, and substations.

Special tools and operational spares such as combustor baskets, blades and vanes, etc., are also not included.

Dry low NOx is generally included as standard on most plants. Water or steam injection systems for NOx abatement are extra.

So is selective catalytic reduction in the exhaust flow to meet single digit emission levels, which can add significantly to initial acquisition costs and operating expense.

Add-ons aside, there can be a wide range of $/kW prices for combined cycle plants depending on geographic location, OEM marketing strategies, currency valuations, order backlog and competitive situation.

Integrated Services		
	4%	Project Management/Subcontracting
	2%	Plant and Project Engineering/Software
	8%	Plant Erection/Commissions/Training
	1%	Transport, Insurance
	Σ15%	

Lots	Civil Works	Gas- And Steam Turbine Set	Balance of Plants	Electrical Systems	Instrumental And Control	Boiler Island
Σ85%	15%	32%	16%	7%	4%	11%

Basis : 350/700 MW CC Plant with a V94.3A Gas Turbine

Figure 3–63. *Cost breakdown for CC power plants. Basis: 350–700 MW plant with a V94.3A gas turbine Adapted from [3-6].*

2017 Combined Cycle Plant Prices

Estimated equipment-plus-construction budget price for standard OEM bare bones design

How much does a combined cycle plant cost? It depends on plant size and scope, and on engineering tradeoffs for the design and performance optimization for specific applications.

GTW's combined cycle plant prices are based on standard bare bones plants designed for single-fuel operation (gas-only) with conservative steam cycle design and without HRSG duct firing or other performance enhancing options.

The prices are quoted in US dollars FOB factory for EPC turnkey scope, including major equipment supply, plant engineering and construction. They do not cover transportation, project-specific options, owner's project costs or project contingencies.

Except for some individual cases, where new information from the marketplace has indicated otherwise, this year's estimated combined cycle plant prices reflect a slight downward trend compared to immediate prior years.

This follows the general movement of the power plant capital cost price index over the past two years (see https://www.ihs.com/info/cera/ihsindexes/). The impact of the stronger US dollar relative to other major international currencies this past year has also put downward pressure on price levels quoted in US dollars.

Equipment scope. Limited to minimum scope of supply for plants designed around one or more gas turbine gensets, one or more matching HRSGs (without SCR or CO catalyst), single steam turbine genset with water-cooled condenser and mechanical draft cooling tower, integrated plant controls. Includes:

- **Gas turbine.** Skid mounted single-fuel unit with acoustic enclosure for outdoor installation, with standard starting and control systems. Includes standard mechanical and electrical auxiliaries normally supplied with simple cycle gas turbine package (no inlet air chilling or de-icing).
- **Steam turbine.** Condensing subcritical design, with single or dual-pressure levels for small plants, triple-pressure levels with reheat for large plants. Axial or radial exhaust, steam bypass and controls, enclosure, and water-cooled condenser. Includes all valves and controls (typically hydraulic).
- **Unfired HRSG.** Heat recovery steam generator for outdoor installation, along with ductwork and short exhaust stack with silencing. Dual or triple-pressure reheat units as dictated by gas turbine and steam turbine size and technology.
- **Generator.** Air-cooled generators for small gas turbines; hydrogen cooled for larger units. Large air-cooled generators for combined cycle application typically use enclosed water-to-air cooling (TEWAC) design. Neutral grounding cubicle and bus to main breaker included with generator packages.
- **Control system.** Distributed control system (DCS) for integrating gas turbine, HRSG and steam turbine controls with overall combined cycle plant control and operation.

Balance of plant. Standard balance-of-plant equipment for installation and operation:

- **Mechanical auxiliaries.** Critical water handling systems with pumps and piping for boiler feed water, condenser cooling water and condensate.
- **Electrical auxiliaries.** Auxiliary power transformers and switchgear, voltage regulators, bus and breakers needed for plant operation. Main step-up transformers (one for each generator) for connecting plant output to the utility substation are excluded.
- **Engineering and construction.** Allowance is made in EPC costs for plant design and engineering, foundations and installation of all equipment assuming non-union labor.

Excluded options. Popular customer-specified options considered outside combined cycle budget prices for a bare bones combined cycle plant:

- **Bypass stack.** Allows independent operation of the gas turbine in simple cycle mode for quick start and flexible dispatch; option includes a mechanical damper in exhaust ducting to redirect flow.
- **Inlet cooling.** Evaporative and mechanical chilling systems that can boost plant output by up to 10% at 90°F hot day and 30% relative humidity operation.
- **Duct firing.** Supplementary duct firing to increase steam turbine output; also requires upgrades in steam and water handling systems.
- **Catalysts.** CO and SCR catalytic section for HRSG ammonia injection (to limit emissions) plus associated ammonia storage and feed systems.

• **Back-up fuel.** Storage and delivery of liquid fuel for back-up to natural gas supply. Usually includes fuel unloading station and alternative provisions for NOx control, such as water injection.

Boundary limits. The defined scope of supply narrowly sets boundary limits such that they do not include utility grid interconnections, any transmission lines, natural gas fuel pipelines, or service/access roads external to the plant site.

Within the plant site, such project specific balance-of-plant equipment such as fuel gas booster compressors, water treatment systems, waste water systems and cooling towers are also excluded.

Price estimates reflect overnight costs and exclude time-dependent costs such as escalation and interest during construction and highly variable project-specific owner expenses such as land, plant site preparation, project development, financing, permits, insurance, taxes, etc.

Nor do they cover the "first fill" of operating consumables such as lube oil, chemicals, catalysts, special tooling and replacement parts and spares, which, although not a significant percentage of total costs, is worth noting.

Pricing scope. GTW's budget cost estimates for combined cycles are based on OEM reference plant designs and EPC contractor costs. They include cost of equipment and construction, but exclude customized EPC services, project-specific options and owner's project costs.

In the real world, total plant costs for combined cycle plants powered by identical gas turbines can vary by as much as 25% depending on differences in engineering, design choices and add-on plant options and facilities.

Marketplace plant price quotes are invariably higher than GTW estimated budget prices. Result of extended scope of supply and project-specific costs related to site location and greater project complexity.

Given the uncertainty on scope of supply, even for a bare bones plant, we attach a plus or minus accuracy of 15% to the estimated price of combined cycle plants.

On the accompanying tables, combined cycle plant power and efficiency values are based on OEM ratings for optimized reference plant designs at ISO standard (59°F ambient and sea level) site conditions.

Size matters. As one might expect, prices for combined cycle power plants strongly exhibit the cost advantages of economies of scale.

The plot of combined cycle plant price versus power output shows how $ per kW prices sharply decrease with increasing plant size, although they level off at the upper end of the size spectrum.

Compared to simple cycle plants, this leveling off in the price vs. size curve is delayed somewhat with combined cycle plants due to the large percentage of total plant cost attributed to the steam bottoming cycle and balance-of-plant equipment.

There is also an associated rise in the cost of more advanced steam turbine cycle equipment to match advanced technology gas turbine designs for new generation combined cycle plants in the 500MW-plus size that operate at better than 60% net plant efficiencies.

On the gas turbine side, new materials and manufacturing processes (such as single crystal and directionally solidified castings) and thermal barrier coatings for nozzles and blades to withstand higher firing temperature, add substantially to costs.

The global growth in wind power and solar generation has also spurred the introduction of costly upgrades and more flexible gas and steam turbine designs for combined cycles capable of fast startup and ramping, operational flexibility and high part-load efficiencies and emissions control. ■

2017 Combined Cycle Plants

Pricing data for a wide range of combined cycle plant ratings. "Best Fit" curve for up to 600 MW plotted as $/kW = (3.07 x 10^4 x kW^-0.306) + 121. For plants over 600 MW the "Best Fit" curve is plotted as $/kW = (5 x 10^10 x kW^-1.55) + 610.

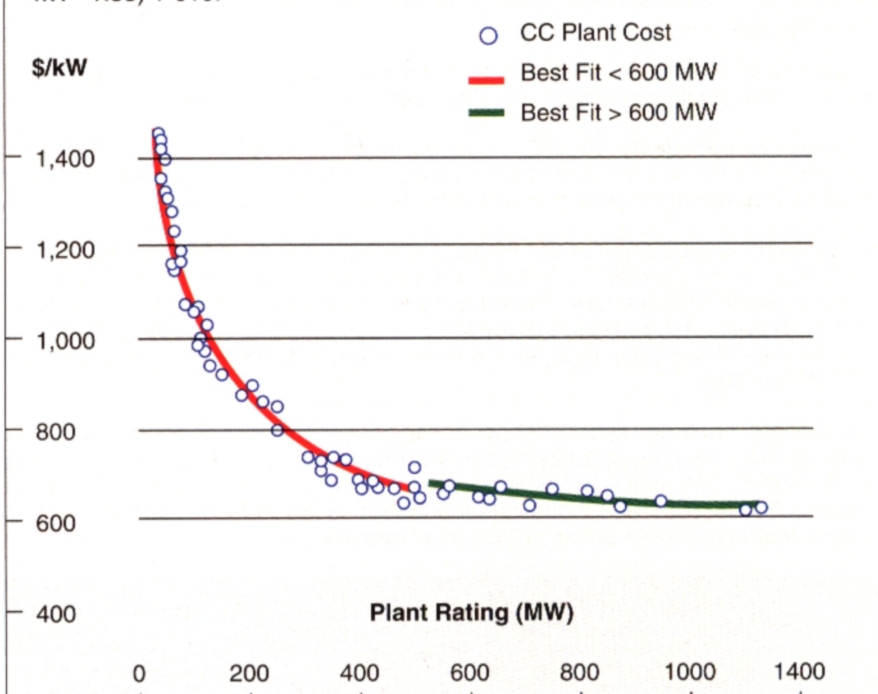

2017 Combined Cycle Plant Prices

Budget price in fixed 2017 US dollars for total plant including BOP equipment and construction

No. & Type Gas Turbine	Net Plant Rating	Heat Rate Btu/kWh	Efficiency	Steam Turbine	Budget Plant Price	$/kW
2 x THM 1304-12N	35.4 MW	7,160 Btu	47.7%	11.4 MW	$48,000,000	$1,356
1 x SGT-600	35.9 MW	6,843 Btu	49.9%	12.6 MW	$47,500,000	$1,323
1 x FT8-3	41.1 MW	6,950 Btu	49.1%	12.0 MW	$55,000,000	$1,338
1 x RB211-GT61 DLE	42.6 MW	6,464 Btu	52.8%	12.6 MW	$56,000,000	$1,315
1 x SGT-700	45.2 MW	6,517 Btu	52.4%	14.4 MW	$57,000,000	$1,261
1 x LM2500+ G4 DLE	47.7 MW	6,239 Btu	54.7%	14.2 MW	$62,000,000	$1,300
1 x SGT-750	51.6 MW	6,407 Btu	53.3%	13.5 MW	$63,800,000	$1,236
1 x LM6000PF	58.0 MW	6,179 Btu	55.2%	14.0 MW	$70,000,000	$1,207
1 x LM6000PF Sprint	64.0 MW	6,239 Btu	54.7%	15.1 MW	$73,500,000	$1,148
1 x Trent 60 DLE	66.4 MW	6,374 Btu	53.5%	16.0 MW	$79,500,000	$1,197
1 x 6B.03	67.0 MW	6,630 Btu	51.5%	25.3 MW	$73,500,000	$1,097
1 x SGT-800	71.4 MW	6,189 Btu	55.1%	23.1 MW	$77,000,000	$1,078
2 x SGT-600	73.3 MW	6,702 Btu	50.9%	26.5 MW	$80,000,000	$1,091
1 x Trent 60 DLE ISI	77.5 MW	6,376 Btu	53.5%	16.6 MW	$85,000,000	$1,097
2 x FT8-3	83.1 MW	6,878 Btu	49.6%	24.6 MW	$92,000,000	$1,107
2 x SGT-700	91.6 MW	6,474 Btu	52.7%	30.0 MW	$94,000,000	$1,026
1 x AE64.3A	115.8 MW	6,340 Btu	53.8%	40.5 MW	$115,000,000	$993
2 x LM6000PC	118.0 MW	6,555 Btu	52.1%	28.1 MW	$120,000,000	$1,017
1 x 6F.03	124.0 MW	6,155 Btu	55.4%	45.8 MW	$116,000,000	$935
1 x LMS100PA+	136.0 MW	6,591 Btu	51.8%	20.9 MW	$132,500,000	$974
2 x 6B.03	135.0 MW	6,600 Btu	51.7%	50.7 MW	$126,000,000	$933
1 x 7E.03	141.0 MW	6,560 Btu	52.0%	52.8 MW	$125,500,000	$890
2 x SGT-800	143.6 MW	6,155 Btu	55.4%	46.8 MW	$130,000,000	$905
1 x H-100	169.6 MW	6,115 Btu	55.8%	55.0 MW	$150,000,000	$884
1 x SGT6-2000E	174.0 MW	6,533 Btu	52.2%	60.0 MW	$155,000,000	$891
1 x M701DA	212.5 MW	6,635 Btu	51.4%	70.4 MW	$179,000,000	$842
2 x AE64.3A	233.0 MW	6,314 Btu	54.0%	82.6 MW	$200,000,000	$858
2 x 6F.03	250.0 MW	6,120 Btu	55.8%	93.4 MW	$207,000,000	$828
1 x SGT5-2000E	275.0 MW	6,403 Btu	53.3%	93.0 MW	$225,000,000	$818
2 x 7E.03	283.0 MW	6,530 Btu	52.3%	105.8 MW	$232,000,000	$820

No. & Type Gas Turbine	Net Plant Rating	Heat Rate Btu/kWh	Efficiency	Steam Turbine	Budget Plant Price	$/kW
1 x M501F	285.1 MW	5,976 Btu	57.1%	102.4 MW	$221,000,000	$775
1 x GT13E2	289.0 MW	6,206 Btu	55.0%	95.4 MW	$225,000,000	$779
2 x H-100	344.5 MW	6,018 Btu	56.7%	115.3 MW	$250,000,000	$726
1 x SGT6-5000F	370.0 MW	5,863 Btu	58.2%	126.0 MW	$260,000,000	$703
1 x 7F.05	376.0 MW	5,660 Btu	60.3%	144.7 MW	$270,000,000	$718
1 x 9F.03	405.0 MW	5,840 Btu	58.4%	148.6 MW	$275,000,000	$679
1 x 7HA.01	419.0 MW	5,520 Btu	61.8%	153.3 MW	$300,000,000	$716
1 x M501GAC	427.0 MW	5,640 Btu	60.7%	146.2 MW	$305,500,000	$715
1 x SGT6-8000H	460.0 MW	5,611 Btu	60.8%	N/A	$310,000,000	$674
1 x 9F.05	462.0 MW	5,640 Btu	60.5%	173.3 MW	$305,000,000	$660
1 x M501J	484.0 MW	5,504 Btu	62.0%	157.8 MW	$326,500,000	$675
1 x GT26-1	502.0 MW	5,678 Btu	60.1%	N/A	$335,000,000	$667
1 x M501JAC	540.0 MW	5,408 Btu	63.1%	174.9 MW	$355,000,000	$657
2 x SGT5-2000E	551.0 MW	6,403 Btu	53.3%	186.0 MW	$350,000,000	$635
1 x M701F	566.0 MW	5,504 Btu	62.0%	186.7 MW	$373,000,000	$659
2 x M501F	572.2 MW	5,955 Btu	57.3%	206.8 MW	$400,000,000	$699
2 x GT13E2-2	581.0 MW	6,178 Btu	55.2%	193.4 MW	$375,000,000	$645
1 x SGT5-8000H	630.0 MW	5,602 Btu	60.9%	225.0 MW	$410,000,000	$651
1 x 9HA.01	643.0 MW	5,450 Btu	62.6%	256.9 MW	$425,000,000	$661
1 x M701J	701.0 MW	5,477 Btu	62.3%	228.7 MW	$455,500,000	$650
1 x M701JAC	717.0 MW	5,408 Btu	63.1%	230.0 MW	$463,000,000	$646
2 x SGT6-5000F	746.0 MW	5,813 Btu	58.7%	257.0 MW	$490,000,000	$657
2 x 7F.05	756.0 MW	5,640 Btu	60.5%	293.0 MW	$500,000,000	$661
2 x 9F.03	815.0 MW	5,810 Btu	58.7%	302.5 MW	$512,000,000	$628
2 x 501GAC	856.0 MW	5,622 Btu	60.7%	294.4 MW	$560,000,000	$654
2 x SGT6-8000H	930.0 MW	5,602 Btu	60.9%	335.0 MW	$600,000,000	$645
2 x 9F.05	929.0 MW	5,610 Btu	60.8%	348.9 MW	$610,000,000	$657
2 x M501J	971.0 MW	5,486 Btu	62.2%	318.6 MW	$625,000,000	$644
2 x GT26-2	1,004.0 MW	5,678 Btu	60.1%	N/A	$625,000,000	$623
2 X 501JAC	1,083.0 MW	5,391 Btu	63.3%	352.8 MW	$685,000,000	$633
2 x SGT5-8000H	1,265.0 MW	5,602 Btu	60.9%	450.0 MW	$780,000,000	$617
2 x 9HA.01	1,289.0 MW	5,440 Btu	62.7%	515.2 MW	$800,000,000	$621

2016-17 GTW Combined Cycle Specs

Model	Intro Year	Gross Plant Output (kW)	Net Plant Output (kW)	Heat Rate (Btu/kWh)	Plant Efficiency	Heat Rate (kJ/kWh)	Condenser Pressure	Gas Turbine Power (kW)	Steam Turbine Power (kW)	No. & Type Gas Turbine	Comments
Ansaldo Energia (50/60 Hz)											
1AE643-CC1S	1996	*****	115 800 kW	6347 Btu	53.8%	6696 kJ	*****	78 000 kW	40 500 kW	1 x AE64.3A	
2AE643-CC1M	1996	*****	233 000 kW	6314 Btu	54.0%	6662 kJ	*****	176 000 kW	82 600 kW	2 x AE64.3A	
Ansaldo Energia (50 Hz)											
1AE942-CC1M	1981	*****	277 500 kW	6251 Btu	54.6%	6595 kJ	*****	185 000 kW	101 600 kW	1 x AE94.2	
2AE942-CC1M	1981	*****	561 500 kW	6178 Btu	55.2%	6518 kJ	*****	370 000 kW	206 300 kW	2 x AE94.2	
1AE943-CC1S	1995	*****	456 300 kW	5799 Btu	58.8%	6118 kJ	*****	310 000 kW	157 900 kW	1 x AE94.3A	
2AE943-CC1M	1995	*****	913 300 kW	5794 Btu	58.9%	6113 kJ	*****	620 000 kW	317 800 kW	2 x AE94.3A	
1GT26-CC1S	2011	*****	502 000 kW	5678 Btu	60.1%	5990 kJ	*****	345 000 kW	*****	1 x GT26	
2GT26-CC1M	2011	*****	1 004 000 kW	5678 Btu	60.1%	5990 kJ	*****	690 000 kW	*****	2 x GT26	
1GT36-S5-CC1M	2016	*****	720 000 kW	5548 Btu	61.5%	5854 kJ	*****	500 000 kW	*****	1 x GT36-S5	
2GT36-S5-CC1M	2016	*****	1 444 000 kW	5548 Btu	61.5%	5854 kJ	*****	1 000 000 kW	*****	2 x GT36-S5	
Note: ISO conditions with sea water condenser											
Ansaldo Energia (60 Hz)											
1GT36-S6-CC1M	2016	*****	500 000 kW	5566 Btu	61.3%	5873 kJ	*****	340 000 kW	*****	1 x GT36-S6	
2GT36-S6-CC1M	2016	*****	1 004 000 kW	5566 Btu	61.3%	5873 kJ	*****	680 000 kW	*****	2 x GT36-S6	
Note: ISO conditions with sea water condenser											
Bharat Heavy Electricals (50 Hz)											
CC105P	1988	39 216 kW	38 628 kW	8147 Btu	41.9%	8595 kJ	*****	25 800 kW	13 416 kW	1 x MS5001	2P
CC205P	1988	78 690 kW	77 510 kW	8120 Btu	42.0%	8567 kJ	*****	51 600 kW	27 090 kW	2 x MS5001	2P
CC305P	1988	118 422 kW	116 764 kW	8086 Btu	42.2%	8530 kJ	*****	77 400 kW	41 022 kW	3 x MS5001	2P
CC106B	1997	64 600 kW	63 631 kW	6963 Btu	49.0%	7346 kJ	*****	42 500 kW	22 100 kW	1 x MS6001B	2P
CC206B	1997	129 455 kW	127 513 kW	6950 Btu	49.1%	7332 kJ	*****	85 000 kW	44 455 kW	2 x MS6001B	2P
CC106FA	2003	118 499 kW	116 722 kW	6343 Btu	53.8%	6692 kJ	*****	76 500 kW	41 999 kW	1 x MS6001FA	3P non reheat
CC206FA	2003	243 117 kW	239 470 kW	6182 Btu	55.2%	6522 kJ	*****	153 000 kW	90 117 kW	2 x MS6001FA	3P reheat
CC109E	2003	195 900 kW	192 900 kW	6640 Btu	51.4%	7005 kJ	*****	127 700 kW	68 200 kW	1 x MS9001E	2P non reheat
CC209E	2003	394 100 kW	388 188 kW	6600 Btu	51.7%	6963 kJ	*****	255 400 kW	138 700 kW	2 x MS9001E	2P non reheat
CC309E	2003	594 100 kW	585 500 kW	6560 Btu	52.0%	6921 kJ	*****	383 100 kW	211 000 kW	3 x MS9001E	2P non reheat

Model	Intro Year	Gross Plant Output (kW)	Net Plant Output (kW)	Heat Rate (Btu/kWh)	Plant Efficiency	Heat Rate (kJ/kWh)	Condenser Pressure	Gas Turbine Power (kW)	Steam Turbine Power (kW)	No. & Type Gas Turbine	Comments
Bharat Heavy Electricals (50 Hz) (cont'd)											
CC109E (AGP)	2016	198 508 kW	195 468 kW	6601 Btu	51.7%	6964 kJ	*****	129 400 kW	69 108 kW	1 x MS9001E	2P non reheat
CC209E (AGP)	2016	399 346 kW	393 355 kW	6561 Btu	52.0%	6921 kJ	*****	258 800 kW	140 546 kW	2 x MS9001E	2P non reheat
CC309E (AGP)	2016	602 009 kW	593 295 kW	6525 Btu	52.3%	6883 kJ	*****	388 200 kW	213 809 kW	3 x MS9001E	2P non reheat
CC1.942	1998	237 500 kW	232 500 kW	6630 Btu	51.5%	6990 kJ	*****	152 000 kW	85 500 kW	1 x V94.2	2P
CC2.942	1998	477 000 kW	467 500 kW	6600 Btu	51.7%	6960 kJ	*****	304 000 kW	173 000 kW	2 x V94.2	2P
CC3.942	1998	715 000 kW	701 000 kW	6600 Btu	51.7%	6960 kJ	*****	456 000 kW	259 000 kW	3 x V94.2	2P
CC109FA	2003	400 200 kW	394 900 kW	5995 Btu	56.9%	6325 kJ	*****	258 700 kW	141 500 kW	1 x MS9001FA	3P
CC209FA	2003	804 400 kW	794 100 kW	5965 Btu	57.2%	6290 kJ	*****	517 400 kW	287 000 kW	2 x MS9001FA	3P
CC109FB	2012	459 300 kW	452 600 kW	5765 Btu	59.2%	6080 kJ	*****	295 300 kW	164 000 kW	1 x MS9001FB	3P
CC209FB	2012	923 100 kW	910 100 kW	5765 Btu	59.5%	6050 kJ	*****	590 600 kW	332 500 kW	2 x MS9001FB	3P
EthosEnergy (50/60 Hz)											
TG20B7/8UG	2014	69 881 kW	68 395 kW	6632 Btu	51.5%	6996 kJ	1.2 inch Hg	44 001 kW	25 880 kW	1 x TG20B7/8UG	
TG20B7/8UG	2014	140 524 kW	137 491 kW	6598 Btu	51.7%	6961 kJ	1.2 inch Hg	88 002 kW	52 522 kW	2 x TG20B7/8UG	
EthosEnergy (50 Hz)											
TG50D5U	2007	214 370 kW	209 969 kW	6255 Btu	54.6%	6599 kJ	1.2 inch Hg	140 767 kW	73 603 kW	1 x TG50D5U	3P HRSG
TG50D5U	2007	431 074 kW	422 171 kW	6222 Btu	54.8%	6564 kJ	1.2 inch Hg	281 534 kW	149 540 kW	2 x TG50D5U	3P HRSG
GE Power & Water Aeroderivative (50 Hz)											
LM2500	1981	70 031 kW	68 600 kW	6916 Btu	49.3%	7297 kJ	1.2 inch Hg	23 786 kW	22 459 kW	2 x LM2000	2P non reheat
LM2500	1981	34 913 kW	34 200 kW	6943 Btu	49.1%	7325 kJ	1.2 inch Hg	23 786 kW	11 127 kW	1 x LM2500	2P non reheat
LM2500 DLE	1981	67 173 kW	65 800 kW	6507 Btu	52.4%	6865 kJ	1.2 inch Hg	22 417 kW	22 339 kW	2 x LM2000	2P non reheat
LM2500 DLE	1981	35 730 kW	35 000 kW	6844 Btu	49.9%	7221 kJ	1.2 inch Hg	22 417 kW	13 313 kW	1 x LM2500	2P non reheat
LM2500+	1995	42 366 kW	41 500 kW	6931 Btu	49.2%	7312 kJ	1.2 inch Hg	30 031 kW	12 335 kW	1 x LM2500+	2P non reheat
LM2500+	1995	84 936 kW	83 200 kW	6907 Btu	49.4%	7287 kJ	1.2 inch Hg	30 031 kW	24 874 kW	2 x LM2500+	2P non reheat
LM2500+ DLE	1995	44 918 kW	44 000 kW	6384 Btu	53.4%	6736 kJ	1.2 inch Hg	31 059 kW	13 859 kW	1 x LM2500+	2P non reheat
LM2500+ DLE	1995	90 040 kW	88 200 kW	6361 Btu	53.6%	6711 kJ	1.2 inch Hg	31 059 kW	27 922 kW	2 x LM2500+	2P non reheat
LM2500+ G4	2005	49 205 kW	48 200 kW	6884 Btu	49.6%	7263 kJ	1.2 inch Hg	34 500 kW	14 705 kW	1 x LM2500+ G4	2P non reheat, gearbox
LM2500+ G4	2005	98 819 kW	96 800 kW	6860 Btu	49.7%	7238 kJ	1.2 inch Hg	34 500 kW	29 819 kW	2 x LM2500+ G4	2P non reheat, gearbox
LM2500+ G4 DLE	2005	48 695 kW	47 700 kW	6343 Btu	53.8%	6693 kJ	1.2 inch Hg	33 400 kW	15 295 kW	1 x LM2500+ G4	2P non reheat, gearbox
LM2500+ G4 DLE	2005	97 696 kW	95 700 kW	6320 Btu	54.0%	6668 kJ	1.2 inch Hg	33 400 kW	30 896 kW	2 x LM2500+ G4	2P non reheat, gearbox
TM2500	****	44 918 kW	44 000 kW	6909 Btu	49.4%	7289 kJ	1.2 inch Hg	34 300 kW	10 618 kW	1 x TM2500	2P non reheat
TM2500	****	99 023 kW	97 000 kW	6885 Btu	49.6%	7264 kJ	1.2 inch Hg	34 300 kW	30 423 kW	2 x TM2500	2P non reheat

Model	Intro Year	Gross Plant Output (kW)	Net Plant Output (kW)	Heat Rate (Btu/kWh)	Plant Efficiency	Heat Rate (kJ/kWh)	Condenser Pressure	Gas Turbine Power (kW)	Steam Turbine Power (kW)	No. & Type Gas Turbine	Comments
GE Power & Water Aeroderivative (50 Hz) (cont'd)											
LM6000PC	1997	58 918 kW	57 900 kW	6621 Btu	51.5%	6986 kJ	1.2 inch Hg	45 424 kW	13 494 kW	1 x LM6000PC	2P non reheat, gearbox
LM6000PC	1997	118 039 kW	116 000 kW	6603 Btu	51.7%	6966 kJ	1.2 inch Hg	45 424 kW	27 191 kW	2 x LM6000PC	2P non reheat, gearbox
LM6000PC Sprint	1998	67 669 kW	66 500 kW	6577 Btu	51.9%	6939 kJ	1.2 inch Hg	51 057 kW	16 612 kW	1 x LM6000PC Sprint	2P non reheat, gearbox
LM6000PC Sprint	1998	135 338 kW	133 000 kW	6559 Btu	52.0%	6920 kJ	1.2 inch Hg	51 057 kW	33 224 kW	2 x LM6000PC Sprint	2P non reheat, gearbox
LM6000PF	1997	59 020 kW	58 000 kW	6214 Btu	54.9%	6556 kJ	1.2 inch Hg	45 000 kW	14 020 kW	1 x LM6000 PF	2P non reheat, gearbox
LM6000PF	1997	119 057 kW	117 000 kW	6196 Btu	55.1%	6537 kJ	1.2 inch Hg	45 000 kW	29 057 kW	2 x LM6000 PF	2P non reheat, gearbox
LM6000PF Sprint 25	2006	65 125 kW	64 000 kW	6273 Btu	54.4%	6619 kJ	1.2 inch Hg	50 000 kW	15 125 kW	1 x LM6000PF Sprint	2P non reheat, gearbox
LM6000PF Sprint 25	2006	130 250 kW	128 000 kW	6255 Btu	54.6%	6599 kJ	1.2 inch Hg	50 000 kW	30 250 kW	2 x LM6000PF Sprint	2P non reheat, gearbox
LM6000PG	2010	74 283 kW	73 000 kW	6535 Btu	52.2%	6894 kJ	1.2 inch Hg	56 000 kW	18 283 kW	1 x LM6000PG	2P non reheat, gearbox
LM6000PG	2010	148 567 kW	146 000 kW	6515 Btu	52.4%	6873 kJ	1.2 inch Hg	56 000 kW	36 567 kW	2 x LM6000PG	2P non reheat, gearbox
LM6000PG Sprint	2010	77 336 kW	76 000 kW	6550 Btu	52.1%	6911 kJ	1.2 inch Hg	59 000 kW	18 336 kW	1 x LM6000PG Sprint	2P non reheat, gearbox
LM6000PG Sprint	2010	155 690 kW	153 000 kW	6530 Btu	52.3%	6890 kJ	1.2 inch Hg	59 000 kW	37 690 kW	2 x LM6000PG Sprint	2P non reheat, gearbox
LM6000PF+	2016	71 231 kW	70 000 kW	6101 Btu	55.9%	6437 kJ	1.2 inch Hg	53 000 kW	18 231 kW	1 x LM6000PF+	2P non reheat, gearbox
LM6000PF+	2016	142 461 kW	140 000 kW	6081 Btu	56.1%	6416 kJ	1.2 inch Hg	53 000 kW	36 461 kW	2 x LM6000PF+	2P non reheat, gearbox
LM6000PF+ Sprint	2016	75 301 kW	74 000 kW	6230 Btu	54.8%	6573 kJ	1.2 inch Hg	57 000 kW	18 301 kW	1 x LM6000PF+ Sprint	2P non reheat, gearbox
LM6000PF+ Sprint	2016	151 619 kW	149 000 kW	6211 Btu	54.9%	6553 kJ	1.2 inch Hg	57 000 kW	37 619 kW	2 x LM6000PF+ Sprint	2P non reheat, gearbox
LMS100 PA+	2015	136 909 kW	135 000 kW	6626 Btu	51.5%	6991 kJ	1.2 inch Hg	114 000 kW	22 909 kW	1 x LMS100PA+	2P non reheat
LMS100 PA+	2015	273 819 kW	270 000 kW	6608 Btu	51.6%	6971 kJ	1.2 inch Hg	114 000 kW	45 819 kW	2 x LMS100PA+	2P non reheat
LMS100PB+	2016	128 796 kW	127 000 kW	6517 Btu	52.4%	6876 kJ	1.2 inch Hg	108 000 kW	20 796 kW	1 x LMS100PB+	2P non reheat
LMS100PB+	2016	259 621 kW	256 000 kW	6498 Btu	52.5%	6934 kJ	1.2 inch Hg	108 000 kW	43 621 kW	2 x LMS100PB+	2P non reheat
GE Power & Water Aeroderivative (60 Hz)											
LM2500	1981	35 730 kW	35 000 kW	6844 Btu	49.9%	7221 kJ	1.2 inch Hg	24 800 kW	10 930 kW	1 x LM2500	2P non reheat
LM2500	1981	71 664 kW	70 200 kW	6819 Btu	50.0%	7195 kJ	1.2 inch Hg	24 800 kW	22 064 kW	2 x LM2500	2P non reheat
LM2500 DLE	1981	33 893 kW	33 200 kW	6456 Btu	52.9%	6811 kJ	1.2 inch Hg	23 200 kW	10 693 kW	1 x LM2500	2P non reheat
LM2500 DLE	1981	67 989 kW	66 600 kW	6431 Btu	53.1%	6785 kJ	1.2 inch Hg	23 200 kW	21 589 kW	2 x LM2500	2P non reheat
LM2500+	1995	43 897 kW	43 000 kW	6809 Btu	50.1%	7184 kJ	1.2 inch Hg	31 800 kW	12 097 kW	1 x LM2500+	2P non reheat
LM2500+	1995	88 100 kW	86 300 kW	6787 Btu	50.3%	7161 kJ	1.2 inch Hg	31 800 kW	24 500 kW	2 x LM2500+	2P non reheat
LM2500+ DLE	1995	44 816 kW	43 900 kW	6299 Btu	54.2%	6645 kJ	1.2 inch Hg	31 900 kW	12 916 kW	1 x LM2500+	2P non reheat
LM2500+ DLE	1995	90 040 kW	88 200 kW	6277 Btu	54.4%	6622 kJ	1.2 inch Hg	31 900 kW	26 240 kW	2 x LM2500+	2P non reheat
LM2500+ G4	2005	51 349 kW	50 300 kW	6729 Btu	50.7%	7099 kJ	1.2 inch Hg	37 100 kW	14 249 kW	1 x LM2500+ G4	2P non reheat, gearbox
LM2500+ G4	2005	103 005 kW	100 900 kW	6707 Btu	50.9%	7076 kJ	1.2 inch Hg	37 100 kW	28 805 kW	2 x LM2500+ G4	2P non reheat, gearbox
LM2500+ G4 DLE	2005	48 695 kW	47 700 kW	6239 Btu	54.7%	6583 kJ	1.2 inch Hg	34 500 kW	14 195 kW	1 x LM2500+ G4	2P non reheat, gearbox
LM2500+ G4 DLE	2005	97 696 kW	95 700 kW	6218 Btu	54.9%	6560 kJ	1.2 inch Hg	34 500 kW	28 696 kW	2 x LM2500+ G4	2P non reheat, gearbox

Model	Intro Year	Gross Plant Output (kW)	Net Plant Output (kW)	Heat Rate (Btu/kWh)	Plant Efficiency	Heat Rate (kJ/kWh)	Condenser Pressure	Gas Turbine Power (kW)	Steam Turbine Power (kW)	No. & Type Gas Turbine	Comments
GE Power & Water Aeroderivative (60 Hz) (cont'd)											
TM2500	****	50 022 kW	49 000 kW	6730 Btu	50.7%	7100 kJ	1.2 inch Hg	37 100 kW	12 922 kW	1 x TM2500	2P non reheat
TM2500	****	100 044 kW	98 000 kW	6708 Btu	50.9%	7077 kJ	1.2 inch Hg	37 100 kW	25 844 kW	2 x TM2500	2P non reheat
LM6000PC	1997	59 630 kW	58 600 kW	6573 Btu	51.9%	6935 kJ	1.2 inch Hg	46 000 kW	13 630 kW	1 x LM6000PC	2P non reheat, gearbox
LM6000PC	1997	120 074 kW	118 000 kW	6555 Btu	52.1%	6916 kJ	1.2 inch Hg	46 000 kW	28 074 kW	2 x LM6000PC	2P non reheat, gearbox
LM6000PC Sprint	1998	67 160 kW	66 000 kW	6551 Btu	52.1%	6911 kJ	1.2 inch Hg	52 000 kW	15 160 kW	1 x LM6000PC Sprint	2P non reheat, gearbox
LM6000PC Sprint	1998	135 338 kW	133 000 kW	6532 Btu	52.2%	6891 kJ	1.2 inch Hg	52 000 kW	31 338 kW	2 x LM6000PC Sprint	2P non reheat, gearbox
LM6000PF	1997	59 020 kW	58 000 kW	6179 Btu	55.2%	6520 kJ	1.2 inch Hg	45 000 kW	14 020 kW	1 x LM6000PF	2P non reheat, gearbox
LM6000PF	1997	119 057 kW	117 000 kW	6161 Btu	55.4%	6500 kJ	1.2 inch Hg	45 000 kW	29 057 kW	2 x LM6000PF	2P non reheat, gearbox
LM6000PF Sprint 25	2006	65 125 kW	64 000 kW	6239 Btu	54.7%	6583 kJ	1.2 inch Hg	50 000 kW	15 125 kW	1 x LM6000PF Sprint	2P non reheat, gearbox
LM6000PF Sprint 25	2006	131 268 kW	129 000 kW	6221 Btu	54.8%	6563 kJ	1.2 inch Hg	50 000 kW	31 268 kW	2 x LM6000PF Sprint	2P non reheat, gearbox
LM6000PG	2010	74 283 kW	73 000 kW	6535 Btu	52.2%	6895 kJ	1.2 inch Hg	56 000 kW	18 283 kW	1 x LM6000PG	2P non reheat, gearbox
LM6000PG	2010	148 567 kW	146 000 kW	6516 Btu	52.4%	6874 kJ	1.2 inch Hg	56 000 kW	36 567 kW	2 x LM6000PG	2P non reheat, gearbox
LM6000PG Sprint	2010	77 336 kW	76 000 kW	6551 Btu	52.1%	6912 kJ	1.2 inch Hg	59 000 kW	18 336 kW	1 x LM6000PG Sprint	2P non reheat, gearbox
LM6000PG Sprint	2010	155 690 kW	153 000 kW	6532 Btu	52.2%	6891 kJ	1.2 inch Hg	59 000 kW	37 690 kW	2 x LM6000PG Sprint	2P non reheat, gearbox
LM6000PF+	2016	71 231 kW	70 000 kW	6105 Btu	55.9%	6441 kJ	1.2 inch Hg	53 000 kW	18 231 kW	1 x LM6000PF+	2P non reheat, gearbox
LM6000PF+	2016	142 461 kW	140 000 kW	6085 Btu	56.1%	6420 kJ	1.2 inch Hg	53 000 kW	36 461 kW	2 x LM6000PF+	2P non reheat, gearbox
LM6000PF+ Sprint	2016	75 301 kW	74 000 kW	6232 Btu	54.7%	6575 kJ	1.2 inch Hg	57 000 kW	18 301 kW	1 x LM6000PF+ Sprint	2P non reheat, gearbox
LM6000PF+ Sprint	2016	151 619 kW	149 000 kW	6213 Btu	54.9%	6555 kJ	1.2 inch Hg	57 000 kW	37 619 kW	2 x LM6000PF+ Sprint	2P non reheat, gearbox
LMS100PA+	2015	137 924 kW	136 000 kW	6591 Btu	51.8%	6953 kJ	1.2 inch Hg	117 000 kW	20 924 kW	1 x LMS100PA+	2P non reheat
LMS100PA+	2015	276 861 kW	273 000 kW	6573 Btu	51.9%	6934 kJ	1.2 inch Hg	117 000 kW	42 861 kW	2 x LMS100PA+	2P non reheat
LMS100PB+	2016	129 810 kW	128 000 kW	6521 Btu	52.3%	6880 kJ	1.2 inch Hg	109 000 kW	20 810 kW	1 x LMS100PB+	2P non reheat
LMS100PB+	2016	259 621 kW	256 000 kW	6503 Btu	52.5%	6861 kJ	1.2 inch Hg	109 000 kW	41 621 kW	2 x LMS100PB+	2P non reheat
GE Power & Water Heavy Duty (50/60 Hz)											
6B.03	1987	68 900 kW	67 000 kW	6630 Btu	51.5%	6995 kJ	1.2 inch Hg	43 655 kW	25 245 kW	1 x 6B.03	2P non reheat
6B.03	1979	138 000 kW	135 000 kW	6600 Btu	51.7%	6963 kJ	1.2 inch Hg	87 311 kW	50 689 kW	2 x 6B.03	2P non reheat
6F.01	2003	77 400 kW	76 000 kW	6030 Btu	56.6%	6362 kJ	1.2 inch Hg	50 753 kW	26 647 kW	1 x 6F.01	2P non reheat
6F.01	2003	157 100 kW	154 000 kW	6000 Btu	56.9%	6330 kJ	1.2 inch Hg	101 506 kW	55 594 kW	2 x 6F.01	2P non reheat
6F.03	1991	126 000 kW	124 000 kW	6155 Btu	55.4%	6499 kJ	1.2 inch Hg	80 178 kW	45 822 kW	1 x 6F.03	2P non reheat
6F.03	1991	253 800 kW	250 000 kW	6120 Btu	55.9%	6436 kJ	1.2 inch Hg	160 355 kW	93 445 kW	2 x 6F.03	2P non reheat

Model	Intro Year	Gross Plant Output (kW)	Net Plant Output (kW)	Heat Rate (Btu/kWh)	Plant Efficiency	Heat Rate (kJ/kWh)	Condenser Pressure	Gas Turbine Power (kW)	Steam Turbine Power (kW)	No. & Type Gas Turbine	Comments
GE Power & Water Heavy Duty (50 Hz)											
9E.03	1979	203 800 kW	201 000 kW	6460 Btu	52.8%	6816 kJ	1.2 inch Hg	130 636 kW	73 164 kW	1 x 9E.03	2P non reheat
9E.03	1979	411 500 kW	405 000 kW	6410 Btu	53.2%	6763 kJ	1.2 inch Hg	261 272 kW	150 228 kW	2 x 9E.03	2P non reheat
9E.04	2014	215 100 kW	212 000 kW	6270 Btu	54.4%	6615 kJ	1.2 inch Hg	141 407 kW	73 693 kW	1 x 9E.04	2P non reheat
9E.04	2014	433 800 kW	428 000 kW	6220 Btu	54.9%	6562 kJ	1.2 inch Hg	282 814 kW	150 986 kW	2 x 9E.04	2P non reheat
GT13E2 2005	2005	267 900 kW	264 000 kW	6209 Btu	55.0%	6551 kJ	1.2 inch Hg	179 504 kW	88 396 kW	1 x GT13E2 (2005)	2P non reheat
GT13E2 2005	2005	537 700 kW	530 000 kW	6186 Btu	55.2%	6527 kJ	1.2 inch Hg	359 008 kW	178 692 kW	2 x GT13E2 (2005)	2P non reheat
GT13E2 2012	2012	293 100 kW	289 000 kW	6206 Btu	55.0%	6548 kJ	1.2 inch Hg	197 750 kW	95 350 kW	1 x GT13E2 (2012)	2P non reheat
GT13E2 2012	2012	588 900 kW	581 000 kW	6178 Btu	55.2%	6518 kJ	1.2 inch Hg	395 500 kW	193 400 kW	2 x GT13E2 (2012)	2P non reheat
9F.03	1994	410 100 kW	405 000 kW	5840 Btu	58.4%	6162 kJ	1.2 inch Hg	261 461 kW	148 639 kW	1 x 9F.03	3P reheat
9F.03	1994	825 600 kW	815 000 kW	5810 Btu	58.7%	6130 kJ	1.2 inch Hg	523 125 kW	302 475 kW	2 x 9F.03	3P reheat
9F.04	2015	434 300 kW	429 000 kW	5740 Btu	59.4%	6056 kJ	1.2 inch Hg	278 166 kW	156 134 kW	1 x 9F.04	3P reheat
9F.04	2015	872 300 kW	861 000 kW	5710 Btu	59.8%	6024 kJ	1.2 inch Hg	556 467 kW	315 833 kW	2 x 9F.04	3P reheat
9F.05	2002	468 600 kW	462 000 kW	5640 Btu	60.5%	5951 kJ	1.2 inch Hg	295 374 kW	173 226 kW	1 x 9F.05	3P reheat
9F.05	2002	940 900 kW	929 000 kW	5610 Btu	60.8%	5919 kJ	1.2 inch Hg	592 006 kW	348 894 kW	2 x 9F.05	3P reheat
9F.06	2016	515 600 kW	508 000 kW	5580 Btu	61.1%	5887 kJ	1.2 inch Hg	337 853 kW	177 747 kW	1 x 9F.06	3P reheat
9F.06	2016	1 033 200 kW	1 020 000 kW	5560 Btu	61.4%	5866 kJ	1.2 inch Hg	675 706 kW	357 494 kW	2 x 9F.06	3P reheat
9HA.01	2011	****	659 000 kW	5383 Btu	63.4%	5679 kJ	1.2 inch Hg	446 000 kW	213 000 kW	1 x 9HA.01	3P reheat
9HA.01	2011	****	1 320 000 kW	5373 Btu	63.5%	5669 kJ	1.2 inch Hg	892 000 kW	428 000 kW	2 x 9HA.01	3P reheat
9HA.02	2014	****	804 000 kW	5373 Btu	63.5%	5669 kJ	1.2 inch Hg	544 000 kW	260 000 kW	1 x 9HA.02	reheat
9HA.02	2014	****	1 613 000 kW	5314 Btu	63.7%	5729 kJ	1.2 inch Hg	1 088 000 kW	525 000 kW	2 x 9HA.02	reheat
GE Power & Water Heavy Duty (60 Hz)											
7E.03	1977	143 400 kW	141 000 kW	6560 Btu	52.0%	6921 kJ	1.2 inch Hg	90 601 kW	52 799 kW	1 x 7E.03	2P non reheat
7E.03	1979	287 000 kW	283 000 kW	6530 Btu	52.3%	6890 kJ	1.2 inch Hg	181 202 kW	105 798 kW	2 x 7E.03	2P non reheat
7F.04	2009	305 700 kW	302 000 kW	5760 Btu	59.2%	6077 kJ	1.2 inch Hg	191 309 kW	114 391 kW	1 x 7F.04	3P reheat
7F.04	2009	616 800 kW	609 000 kW	5710 Btu	59.8%	6024 kJ	1.2 inch Hg	382 619 kW	234 181 kW	2 x 7F.04	3P reheat
7F.05	2009	381 100 kW	376 000 kW	5660 Btu	60.3%	5972 kJ	1.2 inch Hg	236 390 kW	144 710 kW	1 x 7F.05	3P reheat
7F.05	2009	765 800 kW	756 000 kW	5640 Btu	60.3%	5972 kJ	1.2 inch Hg	472 780 kW	293 020 kW	2 x 7F.05	3P reheat
7F.06	2016	399 500 kW	394 000 kW	5650 Btu	60.4%	5961 kJ	1.2 inch Hg	269 077 kW	130 423 kW	1 x 7F.06	3P reheat
7F.06	2016	801 500 kW	792 000 kW	5620 Btu	60.7%	5929 kJ	1.2 inch Hg	538 154 kW	263 346 kW	2 x 7F.06	3P reheat

Model	Intro Year	Gross Plant Output (kW)	Net Plant Output (kW)	Heat Rate (Btu/kWh)	Plant Efficiency	Heat Rate (kJ/kWh)	Condenser Pressure	Gas Turbine Power (kW)	Steam Turbine Power (kW)	No. & Type Gas Turbine	Comments
GE Power & Water Heavy Duty (60 Hz) (cont'd)											
7HA.01	2012	****	436 000 kW	5497 Btu	62.1%	5799 kJ	1.2 inch Hg	289 000 kW	147 000 kW	1 x 7HA.01	3P reheat
7HA.01	2012	****	877 000 kW	5466 Btu	62.4%	5767 kJ	1.2 inch Hg	578 000 kW	299 000 kW	2 x 7HA.01	3P reheat
7HA.02	2014	****	560 000 kW	5408 Btu	63.1%	5706 kJ	1.2 inch Hg	372 000 kW	188 000 kW	1 x 7HA.02	3P reheat
7HA.02	2014	****	1 122 000 kW	5398 Btu	63.2%	5695 kJ	1.2 inch Hg	744 000 kW	378 000 kW	2 x 7HA.02	3P reheat
IHI Power Systems (50/60 Hz)											
LM2500PE	1986	32 500 kW	31 790 kW	7093 Btu	48.1%	7484 kJ	****	22 230 kW	10 270 kW	1 x LM2500PE	
LM2500PK	1998	41 390 kW	40 540 kW	6944 Btu	49.1%	7326 kJ	****	29 660 kW	11 730 kW	1 x LM2500PK	
LM2500RB	2006	43 980 kW	43 120 kW	6497 Btu	52.5%	6855 kJ	****	31 430 kW	12 550 kW	1 x LM2500RB	
LM2500RC	2005	48 760 kW	47 780 kW	6818 Btu	50.0%	7193 kJ	****	34 660 kW	14 100 kW	1 x LM2500RB	
LM2500RD	2005	44 790 kW	43 900 kW	6533 Btu	52.2%	6893 kJ	****	31 350 kW	13 440 kW	1 x LM2500RB	
Note: All IHI ratings with inlet and exhaust losses											
IHI Power Systems (50 Hz)											
LM6000PC	1997	56 320 kW	55 250 kW	6687 Btu	51.0%	7055 kJ	****	42 900 kW	13 420 kW	1 x LM6000PC	
LM6000PC	1997	113 330 kW	111 130 kW	6649 Btu	51.3%	7015 kJ	****	85 800 kW	27 530 kW	2 x LM6000PC	
LM6000PC Sprint	1997	63 290 kW	62 120 kW	6655 Btu	51.3%	7021 kJ	****	48 430 kW	14 860 kW	1 x LM6000PC Sprint	
LM6000PC Sprint	1997	127 240 kW	124 820 kW	6623 Btu	51.5%	6988 kJ	****	96 860 kW	30 380 kW	2 x LM6000PC Sprint	
LM6000PD	1997	56 220 kW	55 180 kW	6402 Btu	53.3%	6754 kJ	****	42 260 kW	13 960 kW	1 x LM6000PD	
LM6000PD	1997	113 110 kW	110 970 kW	6366 Btu	53.6%	6717 kJ	****	84 520 kW	28 590 kW	2 x LM6000PD	
LM6000PD Sprint	1997	60 930 kW	59 830 kW	6475 Btu	52.7%	6831 kJ	****	46 460 kW	14 470 kW	1 x LM6000PD Sprint	
LM6000PD Sprint	1997	122 530 kW	120 220 kW	6443 Btu	53.0%	6798 kJ	****	92 920 kW	29 610 kW	2 x LM6000PD Sprint	
LM6000PF	1997	56 220 kW	55 180 kW	6402 Btu	53.3%	6754 kJ	****	42 260 kW	13 960 kW	1 x LM6000PF	
LM6000PF	1997	113 110 kW	110 970 kW	6366 Btu	53.6%	6717 kJ	****	84 520 kW	28 590 kW	2 x LM6000PF	
LM6000PF Sprint	1997	60 930 kW	59 830 kW	6474 Btu	52.7%	6830 kJ	****	46 460 kW	14 470 kW	1 x LM6000PF Sprint	
LM6000PF Sprint	1997	122 530 kW	120 220 kW	6443 Btu	53.0%	6798 kJ	****	92 920 kW	29 610 kW	2 x LM6000PF Sprint	
LM6000PG	2009	71 310 kW	70 000 kW	6524 Btu	52.3%	6883 kJ	****	53 980 kW	17 330 kW	1 x LM6000PG	
LM6000PG	2009	143 290 kW	140 600 kW	6495 Btu	52.5%	6853 kJ	****	107 960 kW	35 330 kW	2 x LM6000PG	
LM6000PG Sprint	2009	73 670 kW	72 320 kW	6559 Btu	52.0%	6920 kJ	****	55 850 kW	17 820 kW	1 x LM6000PG Sprint	
LM6000PG Sprint	2009	148 000 kW	145 230 kW	6532 Btu	52.2%	6892 kJ	****	111 700 kW	36 300 kW	2 x LM6000PG Sprint	
LM6000PH	2011	64 850 kW	63 660 kW	6335 Btu	53.9%	6684 kJ	****	48 240 kW	16 610 kW	1 x LM6000PH	
LM6000PH	2011	130 360 kW	127 890 kW	6307 Btu	54.1%	6654 kJ	****	96 480 kW	33 880 kW	2 x LM6000PH	
LM6000PH Sprint	2011	67 300 kW	66 080 kW	6389 Btu	53.4%	6741 kJ	****	50 660 kW	16 640 kW	1 x LM6000PH Sprint	
LM6000PH Sprint	2011	135 280 kW	132 760 kW	6360 Btu	53.7%	6710 kJ	****	101 320 kW	33 960 kW	2 x LM6000PH Sprint	

Model	Intro Year	Gross Plant Output (kW)	Net Plant Output (kW)	Heat Rate (Btu/kWh)	Plant Efficiency	Heat Rate (kJ/kWh)	Condenser Pressure	Gas Turbine Power (kW)	Steam Turbine Power (kW)	No. & Type Gas Turbine	Comments
IHI Power Systems (50 Hz) (cont'd)											
LM6000PF+	2016	68 470 kW	67 200 kW	6203 Btu	55.0%	6545 kJ	****	50 240 kW	18 230 kW	1 x LM6000PF+	
LM6000PF+	2016	137 680 kW	135 020 kW	6175 Btu	55.3%	6515 kJ	****	100 480 kW	37 200 kW	2 x LM6000PF+	
LM6000PF+ Sprint	2016	72 570 kW	71 230 kW	6337 Btu	53.8%	6686 kJ	****	54 110 kW	18 460 kW	1 x LM6000PF+ Sprint	
LM6000PF+ Sprint	2016	145 820 kW	143 020 kW	6313 Btu	54.0%	6661 kJ	****	108 220 kW	37 600 kW	2 x LM6000PF+ Sprint	
Note: All IHI ratings with inlet and exhaust losses											
MAN Diesel & Turbo (50/60 Hz)											
THM 1304-12N	2004	35 400 kW	****	7160 Btu	47.7%	7550 kJ	1.0 inch Hg	24 000 kW	11 400 kW	2 x THM 1304-12N	2P HRSG
Note: Heat rate and efficiency gross plant performance for MAN Diesel & Turbo											
Mapna Group (50Hz)											
MCC-35	2016	35 120 kW	34 980 kW	7071 Btu	48.2%	7467 kJ	1.8 inch Hg	24 600 kW	10 950 kW	1 x MGT-30	2P non reheat
MCC-500	2016	515 830 kW	508 100 kW	6776 Btu	50.4%	7149 kJ	2.6 inch Hg	177 600 kW	160 630 kW	2 x MGT-70(3)	2P non reheat
MCC-540	2016	544 300 kW	536 100 kW	6422 Btu	53.1%	6776 kJ	1.8 inch Hg	177 600 kW	189 100 kW	2 x MGT-70(3)	3P reheat
Mitsubishi Hitachi Power Systems (50/60 Hz)											
MPCP1(H-25)	2008	60 100 kW	****	6319 Btu	54.0%	6667 kJ	1.2 inch Hg	39 600 kW	20 500 kW	1 x H-25	
MPCP2(H-25)	2008	121 400 kW	****	6261 Btu	54.5%	6606 kJ	1.2 inch Hg	79 200 kW	42 200 kW	2 x H-25	
MPCP1(H-50)	2015	82 000 kW	****	6262 Btu	54.4%	6607 kJ	1.2 inch Hg	55 900 kW	26 100 kW	1 x H-50	
MPCP2(H-50)	2015	166 300 kW	****	6175 Btu	55.2%	6515 kJ	1.2 inch Hg	111 800 kW	54 500 kW	2 x H-50	
Mitsubishi Hitachi Power Systems (50 Hz)											
MPCP1(H-100)	2013	169 600 kW	****	6115 Btu	55.8%	6452 kJ	1.2 inch Hg	114 600 kW	55 000 kW	1 x H-100	
MPCP2(H-100)	2013	344 500 kW	****	6018 Btu	56.7%	6350 kJ	1.2 inch Hg	229 200 kW	115 300 kW	2 x H-100	
MPCP1(M701DA)	1981	213 200 kW	212 500 kW	6635 Btu	51.4%	7000 kJ	1.5 inch Hg	142 100 kW	70 400 kW	1 x M701DA	
MPCP2(M701DA)	1981	427 900 kW	426 600 kW	6610 Btu	51.6%	6974 kJ	1.5 inch Hg	284 200 kW	142 400 kW	2 x M701DA	
MPCP3(M701DA)	1981	647 000 kW	645 000 kW	6585 Btu	51.8%	6947 kJ	1.5 inch Hg	426 300 kW	218 700 kW	3 x M701DA	
MPCP1(M701F)	1992	567 700 kW	566 000 kW	5504 Btu	62.0%	5807 kJ	1.5 inch Hg	379 300 kW	186 700 kW	1 x M701F	
MPCP2(M701F)	1992	1 138 500 kW	1 135 000 kW	5486 Btu	62.2%	5788 kJ	1.5 inch Hg	758 600 kW	376 400 kW	2 x M701F	
MPCP1(M701G)	1997	499 500 kW	498 000 kW	5755 Btu	59.3%	6071 kJ	1.5 inch Hg	325 700 kW	172 300 kW	1 x M701G	
MPCP2(M701G)	1997	1 002 400 kW	999 400 kW	5735 Btu	59.5%	6051 kJ	1.5 inch Hg	651 400 kW	348 000 kW	2 x M701G	
MPCP1(M701J)	2014	703 200 kW	701 000 kW	5477 Btu	62.3%	5779 kJ	1.5 inch Hg	472 300 kW	228 700 kW	1 x M701J	
MPCP1(M701JAC)	2015	719 200 kW	717 000 kW	5408 Btu	63.1%	5706 kJ	1.5 inch Hg	487 000 kW	230 000 kW	1 x M701JAC	

Model	Intro Year	Gross Plant Output (kW)	Net Plant Output (kW)	Heat Rate (Btu/kWh)	Plant Efficiency	Heat Rate (kJ/kWh)	Condenser Pressure	Gas Turbine Power (kW)	Steam Turbine Power (kW)	No. & Type Gas Turbine	Comments
Mitsubishi Hitachi Power Systems (60 Hz)											
MPCP1(H-100)	2010	150 000 kW	****	6193 Btu	55.1%	6534 kJ	1.2 inch Hg	102 500 kW	47 500 kW	1 x H-100	
MPCP2(H-100)	2010	305 700 kW	****	6083 Btu	56.1%	6418 kJ	1.2 inch Hg	205 000 kW	100 700 kW	2 x H-100	
MPCP1(M501)	1981	168 000 kW	167 400 kW	6635 Btu	51.4%	7000 kJ	1.5 inch Hg	112 100 kW	55 300 kW	1 x M501DA	
MPCP2(M501)	1981	337 300 kW	336 200 kW	6610 Btu	51.6%	6974 kJ	1.5 inch Hg	224 200 kW	112 000 kW	2 x M501DA	
MPCP3(M501)	1981	507 800 kW	506 200 kW	6585 Btu	51.8%	6947 kJ	1.5 inch Hg	336 300 kW	169 900 kW	3 x M501DA	
MPCP1(M501F)	1994	286 000 kW	285 100 kW	5976 Btu	57.1%	6305 kJ	1.5 inch Hg	182 700 kW	102 400 kW	1 x M501F	
MPCP2(M501F)	1994	574 000 kW	572 200 kW	5955 Btu	57.3%	6283 kJ	1.5 inch Hg	365 400 kW	206 800 kW	2 x M501F	
MPCP1(M501G)	1995	400 100 kW	398 900 kW	5843 Btu	58.4%	6165 kJ	1.5 inch Hg	264 400 kW	134 500 kW	1 x M501G	
MPCP2(M501G)	1995	803 000 kW	800 500 kW	5823 Btu	58.6%	6144 kJ	1.5 inch Hg	528 800 kW	271 700 kW	2 x M501G	
MPCP1(M501GAC)	2011	428 300 kW	427 000 kW	5640 Btu	60.5%	5951 kJ	1.5 inch Hg	280 800 kW	146 200 kW	1 x M501GAC	
MPCP2(M501GAC)	2011	858 600 kW	856 000 kW	5622 Btu	60.7%	5931 kJ	1.5 inch Hg	561 600 kW	294 400 kW	2 x M501GAC	
MPCP1(M501J)	2011	485 500 kW	484 000 kW	5504 Btu	62.0%	5807 kJ	1.5 inch Hg	326 200 kW	157 800 kW	1 x M501J	
MPCP2(M501J)	2011	974 000 kW	971 000 kW	5486 Btu	62.2%	5788 kJ	1.5 inch Hg	652 400 kW	318 600 kW	2 x M501J	
MPCP1(M501JAC)	2015	541 700 kW	540 000 kW	5408 Btu	63.1%	5706 kJ	1.5 inch Hg	365 100 kW	174 900 kW	1 x M501JAC	
Note: All MHPS ratings on natural gas fuel, LHV at generator terminals, with inlet and exhaust losses											
PW Power Systems (50/60 Hz)											
FT8 SWIFTPAC 30	1990	42 100 kW	41 050 kW	6950 Btu	49.1%	7333 kJ	1.4 inch Hg	30 100 kW	12 000 kW	1 x FT8-3	
FT8 SWIFTPAC 60	1990	85 100 kW	83 100 kW	6878 Btu	49.6%	7257 kJ	1.4 inch Hg	60 500 kW	24 600 kW	2 x FT8-3	
FT4000 SWIFTPAC 60	2012	84 053 kW	82 599 kW	6846 Btu	49.8%	7224 kJ	1.5 inch Hg	67 184 kW	16 869 kW	1 x FT4000	
FT4000 SWIFTPAC 120	2012	169 167 kW	166 240 kW	6803 Btu	50.2%	7179 kJ	1.5 inch Hg	134 662 kW	34 505 kW	2 x FT4000	
Siemens Energy (50/60 Hz)											
Industrial RB211-G62 DLE	1993	****	37 700 kW	6801 Btu	50.2%	7175 kJ	1.5 inch Hg	26 716 kW	12 045 kW	1 x RB211	2P no reheat
Industrial RB211-GT62 DLE	1999	****	39 800 kW	6639 Btu	51.4%	7005 kJ	1.5 inch Hg	28 626 kW	12 205 kW	1 x RB211	2P no reheat
Industrial RB211-GT61 DLE	2000	****	42 600 kW	6464 Btu	52.8%	6820 kJ	1.5 inch Hg	31 171 kW	12 593 kW	1 x RB211	2P no reheat
SCC-600 1x1	1981	****	35 900 kW	6843 Btu	49.9%	7220 kJ	1.3 inch Hg	23 880 kW	12 600 kW	1 x SGT-600	2P no reheat
SCC-600 2x1	1981	****	73 280 kW	6702 Btu	50.9%	7071 kJ	1.3 inch Hg	47 780 kW	26 450 kW	2 x SGT-600	2P no reheat
SCC-700 1x1	1999	****	45 160 kW	6517 Btu	52.3%	6876 kJ	1.3 inch Hg	32 300 kW	14 410 kW	1 x SGT-700	2P no reheat
SCC-700 2x1	1999	****	91 620 kW	6424 Btu	53.1%	6778 kJ	1.3 inch Hg	62 600 kW	30 040 kW	2 x SGT-700	2P no reheat
SCC-750 1X1	2012	****	51 550 kW	6407 Btu	53.3%	6760 kJ	1.3 inch Hg	38 650 kW	13 480 kW	1 x SGT-750	2P no reheat
SCC-750 2X1	2012	****	103 740 kW	6367 Btu	53.6%	6718 kJ	1.3 inch Hg	77 300 kW	27 480 kW	2 x SGT-750	2P no reheat

Model	Intro Year	Gross Plant Output (kW)	Net Plant Output (kW)	Heat Rate (Btu/kWh)	Plant Efficiency	Heat Rate (kJ/kWh)	Condenser Pressure	Gas Turbine Power (kW)	Steam Turbine Power (kW)	No. & Type Gas Turbine	Comments
Siemens Energy (50/60 Hz) (cont'd)											
SCC-800 1x1	1998	****	66 600 kW	6344 Btu	53.8%	6693 kJ	1.3 inch Hg	46 300 kW	21 000 kW	1 x SGT-800	2P no reheat
SCC-800 2x1	1998	****	135 400 kW	6239 Btu	54.7%	6583 kJ	1.3 inch Hg	92 600 kW	44 200 kW	2 x SGT-800	2P no reheat
SCC-800 3x1	1998	****	203 500 kW	6227 Btu	54.8%	6569 kJ	1.3 inch Hg	138 900 kW	66 700 kW	3 x SGT-800	2P no reheat
SCC-800 1x1	2010	****	71 400 kW	6189 Btu	55.1%	6530 kJ	1.3 inch Hg	49 100 kW	23 100 kW	1 x SGT-800	2P no reheat
SCC-800 2x1	2010	****	143 600 kW	6155 Btu	55.4%	6494 kJ	1.3 inch Hg	98 300 kW	46 800 kW	2 x SGT-800	2P no reheat
SCC-800 3x1	2010	****	215 700 kW	6147 Btu	55.5%	6485 kJ	1.3 inch Hg	147 500 kW	70 500 kW	3 x SGT-800	2P no reheat
SCC-800 1x1	2010	****	75 900 kW	6092 Btu	56.0%	6427 kJ	1.3 inch Hg	51 700 kW	23 200 kW	1 x SGT-800	2P no reheat
SCC-800 2x1	2010	****	153 700 kW	6018 Btu	56.7%	6349 kJ	1.3 inch Hg	105 500 kW	49 800 kW	2 x SGT-800	2P no reheat
SCC-800 3x1	2010	****	229 900 kW	6033 Btu	56.6%	6365 kJ	1.3 inch Hg	158 300 kW	74 000 kW	3 x SGT-800	2P no reheat
Siemens Energy (50 Hz)											
Industrial Trent 60 DLE	1998	****	65 300 kW	6367 Btu	53.6%	6718 kJ	1.5 inch Hg	50 767 kW	15 820 kW	1 x Trent 60 DLE	2P no reheat
Industrial Trent 60 DLE ISI	2010	****	77 700 kW	6384 Btu	53.4%	6736 kJ	1.5 inch Hg	61 978 kW	17 100 kW	1 x Trent DLE ISI	2P no reheat
Industrial Trent 60 WLE	1998	****	81 247 kW	6633 Btu	51.4%	6998 kJ	1.5 inch Hg	64 479 kW	18 291 kW	1 x Trent WLE	2P unfired
Industrial Trent 60 WLE ISI	2011	****	82 900 kW	6656 Btu	51.2%	7022 kJ	1.5 inch Hg	66 000 kW	18 433 kW	1 x Trent WLE ISI	2P no reheat
SCC5-2000E 1x1	1981	****	275 000 kW	6403 Btu	53.3%	6755 kJ	****	187 000 kW	93 000 kW	1 x SGT5-2000E	2P no reheat
SCC5-2000E 2x1	1981	****	551 000 kW	6403 Btu	53.3%	6755 kJ	****	374 000 kW	186 000 kW	2 x SGT5-2000E	2P no reheat
SCC5-4000F 1S*	1995	****	475 000 kW	5716 Btu	59.7%	6030 kJ	****	****	****	1 x SGT5-4000F	3P reheat
SCC5-4000F 2x1	1995	****	950 000 kW	5716 Btu	59.7%	6030 kJ	****	658 000 kW	320 000 kW	2 x SGT5-4000F	3P reheat
SCC5-8000H 1S*	2009	****	630 000 kW	5602 Btu	61.0%	5910 kJ	****	****	****	1 x SGT5-8000H	3P reheat
SCC5-8000H 2x1	2010	****	1 265 000 kW	5602 Btu	61.0%	5910 kJ	****	850 000 kW	435 000 kW	2 x SGT5-8000H	3P reheat

*Siemens model 1S designates single shaft

Model	Intro Year	Gross Plant Output (kW)	Net Plant Output (kW)	Heat Rate (Btu/kWh)	Plant Efficiency	Heat Rate (kJ/kWh)	Condenser Pressure	Gas Turbine Power (kW)	Steam Turbine Power (kW)	No. & Type Gas Turbine	Comments
Siemens Energy (60 Hz)											
Industrial Trent 60 DLE	1998	****	66 400 kW	6374 Btu	53.5%	6725 kJ	1.5 inch Hg	51 674 kW	16 010 kW	1 x Trent 60 DLE	2P no reheat
Industrial Trent 60 DLE ISI	2010	****	77 500 kW	6376 Btu	53.5%	6727 kJ	1.5 inch Hg	60 200 kW	16 641 kW	1 x Trent DLE ISI	2P no reheat
Industrial Trent 60 WLE	2001	****	77 952 kW	6633 Btu	51.4%	6998 kJ	1.5 inch Hg	64 479 kW	18 290 kW	1 x Trent WLE	2P unfired
Industrial Trent 60 WLE ISI	2011	****	80 300 kW	6723 Btu	50.7%	7093 kJ	1.5 inch Hg	64 036 kW	17 798 kW	1 x Trent WLE ISI	2P no reheat
SCC6-2000E 1X1	1989	****	174 000 kW	6533 Btu	52.2%	6893 kJ	****	117 000 kW	60 000 kW	1 x SGT6-2000E	
SCC6-2000E 2X1	1989	****	347 000 kW	6541 Btu	52.2%	6901 kJ	****	234 000 kW	119 000 kW	2 x SGT6-2000E	
SCC6-5000F 1X1	1989	****	370 000 kW	5863 Btu	58.2%	6186 kJ	****	250 000 kW	126 000 kW	1 x SGT6-5000F	3P reheat, 9 ppm Nox
SCC6-5000F 2X1	1989	****	746 000 kW	5813 Btu	58.7%	6133 kJ	****	500 000 kW	257 000 kW	2 x SGT6-5000F	3P reheat, 9 ppm Nox
SCC6-8000H 1S*	2010	****	460 000 kW	5611 Btu	61.0%	5920 kJ	****	****	****	1 x SGT6-8000H	3P reheat
SCC6-8000H 2X1	2010	****	930 000 kW	5602 Btu	61.0%	5910 kJ	****	620 000 kW	325 000 kW	2 x SGT6-8000H	3P reheat

*Siemens model 1S designates single shaft

Chapter 7: Economic Optimisation

1. Investitionsentscheidung mit Hilfe von Entscheidungsbäumen (1996)
2. Primärenergieeinsparung dezentraler Blockheizkraftwerke (2012)

A knowledge-based decision support system for combined heat and power investment appraisal and plant selection

R A Hughes, BEng, MSc and **B Ramsay**, BSc, PhD, CEng, MIEE, MIEEE
Department of Applied Physics and Electronic and Mechanical Engineering, The University of Dundee, Scotland

C Rossini, BSc, MBA, CEng, MIEE
Scottish Hydro Electric plc, Perth, Scotland

Combined heat and power (CHP) can, in the most suitable cases, reduce a consumer's total energy costs by up to 40 per cent. It is important to stress that CHP is not viable at all sites and further that poor choice of CHP plant often results in inefficient and uneconomic operation. It is therefore vitally important to build a clear picture of what specific factors determine the profitability of a CHP scheme. The development of an accurate, reliable economic model is necessary for any sector where a potential market for CHP exists. Conventional economic models have a number of limitations, particularly where situations involve a high degree of risk and uncertainty. This paper shows how decision analysis techniques can be combined with a conventional spreadsheet to overcome these weaknesses and demonstrates the power and flexibility of the resulting model with a case study.

Key words: combined heat and power, energy costs, economic model, knowledge-based decision support system, decision analysis

1 COMBINED HEAT AND POWER

Conventionally, the thermal demands of industrial plants, commercial, residential and many other building types have been met by on-site boilers. A site's electrical demand would normally be met by power imported from the grid network.

Combined heat and power (CHP) is the generation of electrical and 'useful' thermal energy in a single process. A CHP plant generates electricity in the conventional manner, an alternator being driven by a prime mover. The equipment employed for the recovery of heat would depend on the type of prime mover selected and the quality or 'grade' of heat required. The recovery of waste heat makes CHP a highly efficient process and over recent years CHP has increasingly been considered as a feasible alternative to traditional means of meeting site energy demands.

The high efficiency of CHP plants (typically 75–90 per cent) and their utilization of relatively inexpensive fuels (most commonly natural gas) means that CHP installation can greatly reduce a consumer's total energy costs. Such systems often have a further benefit; many are capable of operating without connection to the grid network, thus increasing security of supply. CHP is very site specific, however, and many factors must be taken into account when the suitability of CHP is being assessed at a site (**1**).

1.1 Small-scale CHP and factors affecting its viability

CHP systems capable of generating up to 500 kW of electricity are termed small-scale CHP. Small-scale CHP units are based around reciprocating engines and are normally gas fired. They tend to be packaged units in which all components are factory assembled on a skid-mounted plate.

The MS was received on 20 July 1994 and was accepted for publication on 20 March 1995.

Demand profiles determine, to a large extent, the most suitable CHP plant for a site and the period over which such plant will operate daily. Small-scale CHP plants are predominantly 'heat-led', their output being controlled to maintain the site heating system temperature within an acceptable range. The cost of thermally over-sizing such a CHP system is the underutilization of the plant and poor efficiency of operation due to prolonged periods of partial operation or even non-operation, although such over-sizing may be economically justifiable in order to provide a plant that meets electricity requirements. Over-sizing electrically does not affect system efficiency but is generally undesirable as the return on electricity export is poor at the present time.

The electricity and gas tariffs or contracts offered by suppliers have a great bearing on the potential for CHP at a site. The principal effect of CHP operation, from an economic point of view, is the displacement of imported electricity by on-site generation and the resulting increase in overall gas consumption. The low cost of gas relative to imported electricity is therefore likely to be crucial to the long-term success of a CHP project.

The capital cost and operating cost of CHP plant also have significant effects on the profitability of a CHP project. It is essential that these, along with site energy demand and fuel tariff details, are accurately modelled for CHP viability to be correctly appraised and for the correct choice of plant to be made. These and various other data relating to CHP projects are conventionally modelled within spreadsheet programs.

2 SPREADSHEET MODELLING OF CHP PROJECTS

The spreadsheet model developed for CHP investment appraisal is of conventional form, consisting of:

1. *An input section*, in which site energy demand data, fuel tariffs, details of existing boiler-room plant and

details of the CHP system to be considered for installation are entered.
2. *A calculation section*, built to give the model two important features:
   (a) The model reflects the deterioration in overall system performance caused by over-sizing.
   (b) The model takes the additional security of supply associated with the installation of multiple units into consideration.
3. *A results summary*. A breakdown of costs associated with the proposed CHP scheme is listed along with the expected annual savings and payback period. Savings and running costs are projected over a 5 year period and are expressed as net present value equivalents, that is the discounted cash flow (DCS) technique is used.

A basic spreadsheet model such as this gives a good indication of the potential profitability of a CHP project. It does, however, have some serious weaknesses. Spreadsheets are unable to deal effectively with uncertainties and risk associated with projects; they do not effectively communicate the implications of their results and rely on the user to identify the factors that have the greatest influence on the outcome.

3 DECISION ANALYSIS

In broad terms a decision is a judgement or conclusion reached from examination of a choice of alternatives; more narrowly, in the context of this paper, this judgement should form part of a strategy leading to a specific set of objectives. It may mean an irrevocable commitment of resources, and hence the factors defining the alternatives must be clearly understood and applied. The outcomes of each alternative must be foreseen and assessed, usually in financial terms, and the probabilities of successful outcomes must be evaluated. The criteria on which a decision is to be based should be well defined so that alternatives can be correctly compared.

Decision analysis is a formal methodology for decision making largely based on quantitative algorithms using mathematical methods (**2**). In business terms, decision analysis is largely based on risk assessment and management. In relation to the building of a power plant, many factors are strongly affected by unpredictable actions, such as changes in regulatory practices, technological developments, etc. These risks must, as far as possible, be quantified so that the options can be properly compared, and, in the final case, the risk can be limited by anticipatory action, for example by expenditure on appropriate insurance, or designing and constructing a power plant for choice of fuel source (**3**), or hedging through the use of financial instruments such as long-term electricity and fuel contracts.

Decision analysis has become an integral part of management information systems, and the techniques of decision making have been implemented in computer-based decision support systems (**4**).

4 SOFTWARE (DPL)

DPL, a sophisticated decision analysis package from Applied Decision Analysis Inc., California, was used to increase the power and robustness of the CHP investment appraisal model. DPL compliments the spreadsheet, manipulating its calculations and increasing the depth in which the risks and uncertainties associated with a CHP project are analysed. A spreadsheet model can be integrated into a decision support system without modification. The spreadsheet, when run within a decision support system, is responsible for modelling site demands, fuel tariffs (or contracts) and CHP plant operation, and for calculating the various costs associated with CHP projects; that is it performs exactly the same function as it would when running in the standalone mode. DPL provides the spreadsheet with CHP system specifications and feeds it data relating to the uncertainties surrounding the project. The basic weaknesses of spreadsheet modelling are overcome when decision analysis techniques are employed:

1. DPL offers an efficient and effective means of representing the uncertainties and risks inherent in a problem.
2. DPL manipulates calculations to clearly show the implications of the model's results. Risk analysis may be carried out, allowing an organization's attitude to risk to be full considered when the optimal decision policy is determined.
3. DPL, through its sensitivity comparison facility, shows the relative effects of the influencing factors on the outcome, allowing greater insight to be gained into a problem. Sensitivity analysis indicates ways in which an economic model should be refined. Alterations resulting from such analysis add to the robustness of a model and the reliability of its results.

Data transfer between DPL and the spreadsheet is by means of dynamic data exchange (DDE). The spreadsheet calculates its cell values and exports the contents of cells labelled as site energy costs to DPL. As DPL runs through its analysis it continually updates spreadsheet parameters, the spreadsheet returning newly calculated results. The decision analysis package processes the data received from the spreadsheet, using a built-in algorithm to evaluate each of the options available and then to make its policy decision.

Two modelling tools are utilized by DPL in its representation of problems: influence diagrams and decision trees. The synthesis of these two modelling tools allows problems to be modelled with far more sophistication and to be analysed in far greater depth than would otherwise be possible. The superior power and flexibility of the synthesis model representation was the primary reason for employing DPL.

4.1 The synthesis of decision trees and influence diagrams in DPL

A synthesis model is built in a way that takes advantage of the strengths of decisions trees and influence diagrams. The influence diagram is used to define the elements of the problem (the decisions to be made and the factors that are thought to influence these decisions) and the relationships among them. It is also within the influence diagram that the model data (both deterministic and probabilistic) is input. The decision tree is used to define the sequence in which chance events are handled and to define the order in which decisions are

© IMechE 1996

to be taken. Any asymmetries in the problems are modelled within the decision tree.

5 MODELLING THE CHP INVESTMENT APPRAISAL PROBLEM

The investment appraisal problem was first represented as an influence diagram. The first step in the building of the influence diagram was the definition of each of the decisions to be made. Three decision cells are seen in Fig. 1, the influence diagram representation of the problem, shown as rectangular boxes:

1. *Install CHP*. This decision node addresses the question: 'Is CHP economically preferable to the existing means of meeting the site's energy demands?' Other options, such as alternative energy sources could be included here, but are not addressed in this paper.

The two further decision nodes are related, together determining the best matching CHP system for a site:

2. *Chosen unit*. The decision support system is given a choice of a number of alternative CHP plants to choose from. Five units are considered in the case study below with electric outputs ranging from 38 to 110 kW.
3. *Number of units*. This node is used to determine whether it would be advantageous to install multiple units at a site. This decision has been reduced to have just two possible output states, 'one' or 'two'. The installation of more than two units at a site is very uncommon and the inclusion of additional output states was therefore not justified, considering the additional analysis run-time that would be required.

5.1 Value and chance nodes

All influencing factors have to be represented either deterministically as value nodes or probabilistically as chance nodes. The former is based on definite known data and in this particular application will, in several cases, correspond to specific spreadsheet cells.

Ten value nodes, shown as rectangles with rounded edges, are entered in the model to influence the outcome of DPL's analysis. These form four groups of data:

1. *Details of each of the CHP systems under consideration*. Four nodes are used to provide data for the input section of the spreadsheet model, effectively acting as a database for CHP system specifications. Five CHP set-ups are considered in this model, with electrical outputs ranging from 38 to 100 kW_e. The specifications for each are based on figures given for commercially available CHP units.
2. *Present gas per unit price*. The inclusion of this node was found convenient for purposes of calculation.
3. *Annual site energy requirements without CHP*. Site electricity demand and fuel consumed by a site's conventional boilers are entered in value nodes.
4. *Breakdown of costs for CHP schemes*. Calculations of CHP fuel cost, electricity import (to make up for any shortfall in electrical generation) and fuel cost for conventional boilers (in case of insufficient thermal energy recovery from the CHP system) are each entered in value nodes.

The data listed in groups 1 and 2 are exported directly to the equivalent cells in the input section of the spreadsheet model. These cell values are automatically updated for every CHP set-up considered. Groups 3 and 4 are imported by DPL from the results section of the spreadsheet model.

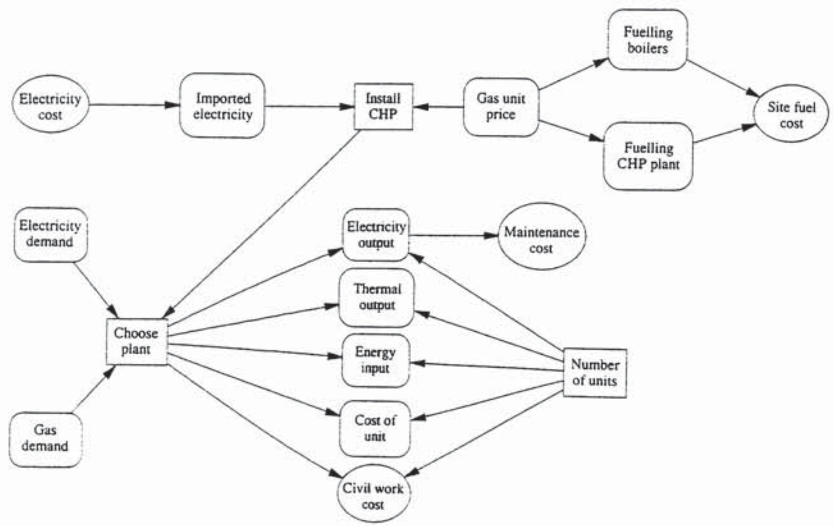

Fig. 1 Influence diagram of the Leisure Centre CHP model

© IMechE 1996

Four chance nodes are included in the influence diagram, seen as oval blocks. These nodes represent influencing factors involving uncertainty, that is where the actual value of a variable is unknown and is outside the control of the decision maker:

1. *Civil work cost*. The Energy Efficiency Office quotes typical ranges of civil work cost in terms of total CHP installation cost (6). The probabilistic data entered into the 'civil work cost' node were based on this information.
2. *Maintenance cost*. The data held in this node represent typical maintenance cost data for the unit types considered in this model. If a fixed cost contract was offered for a given unit then the actual value could be used in DPL's analysis, the 'maintenance cost' node effectively becoming a deterministic node in the model.
3. *Electricity cost* and 4. *Site fuel cost*. The profitability of CHP projects is affected by the tariffs offered by electricity and gas suppliers. Chance nodes are used to represent the uncertainty surrounding future energy costs.

5.2 Influences and node data

The lines and arcs between the nodes of the influence diagram indicate conditioning relationships, that is influences. Each influence arc will have an arrow indicating which of the two linked nodes is being conditioned by the other. An influence arc may be specified so that the value and/or probability distribution of the conditioned node is determined by the state of the conditioning node. Alternatively, an influence arc can be included simply to indicate a mathematical relationship between nodes; links are optional in such cases. Figure 2 is a typical example of the data held within the nodes of the influence diagram.

6 DECISION TREE MODEL

The decision tree built for the investment appraisal problem is shown in Fig. 3. The decision tree model is largely self-explanatory with each node and branch being clearly labelled.

6.1 Representation of decisions and chance events

All decisions (shown as square boxes) and chance nodes (circles) are previously defined within the influence diagram. A label is displayed immediately above each branch leaving a node, with a value expression displayed below where appropriate. Each value expression comprises only constants, standard functions or influence-diagram-defined variables or a combination of these.

The model's decision is made, by default, on a purely financial basis. A DPL model can, however, be converted very easily to consider multi-attribute problems. If, for example, security of supply was critical at a site, a suitable function could be built into the model, ensuring that the decision policy reflected the level of priority given to both this and the financial return on the

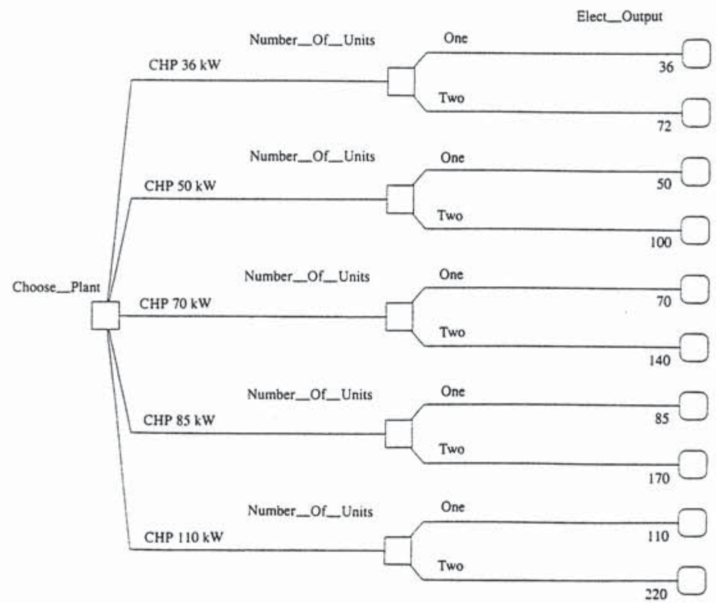

Fig. 2 Data held within the node 'electrical output'

© IMechE 1996

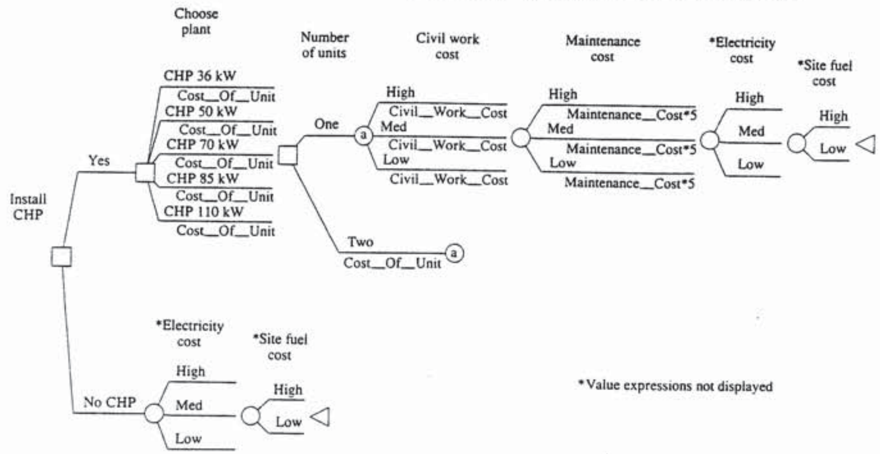

Fig. 3 Decision tree representation of the Leisure Centre CHP model

project. Utility functions can be specified or standard functions can be used within DPL for a model's analysis to fully consider an organization's attitude to risk.

By following the branches along the decision tree it is immediately seen what factors are considered in the assessment of the potential profitability of each scheme. The total cost for any single option is obtained by summing together the results of each of the value expressions along a branch and, for the CHP decision tree model, is summarized as follows:

The no CHP option:
Total cost* = 5 × annual site conventional energy costs

Installation of CHP:
Initial cost = N × cost of 1 unit + civil work
(N = number of CHP units installed)
Annual running costs = CHP fuel cost + electricity import + conventional boiler fuelling + maintenance cost
Total cost* = initial cost + 5 × annual running costs

7 DEMONSTRATION OF THE SUITABILITY OF DECISION ANALYSIS TECHNIQUES FOR CHP INVESTMENT APPRAISAL

A single 75 kW$_e$ CHP unit was installed at Llantrisant Leisure Centre in South Wales in February 1990. This case study was used to demonstrate the suitability of decision analysis techniques for the assessment of CHP project viability. In the Llantrisant case the gas tariff is fairly typical (32p per therm) though the electricity tariff is relatively low (4.3p per kW h). This indicates that a CHP project is unlikely to have an exceptionally low payback period at this site.

The opening hours of a Leisure Centre determine the period of the day over which there will be a sizeable demand for heat and thermal energy at the site and effectively fixes the hours over which a CHP unit would operate. The Leisure Centre at Llantrisant is open for 15 hours a day. Site demands rise rapidly around 1 hour before the centre is opened to the public, coinciding with the arrival of staff; this effectively restricts CHP operation to 16 hours a day. Following this and the fact that the Centre is open 250 days a year, the potential annual CHP operating hours are calculated to be 5760 hours. This is well above the widely recognized figure of 4500 hours below which CHP installation is generally thought to be unviable at present.

The electrical and thermal baseloads at the site are 80 kW$_e$ and 130 kW$_t$ respectively. Suitable CHP systems would be those with rated outputs below these figures.

7.1 Generation of an output

When the decision analysis is run on the model, DPL runs through the paths of the decision tree, sequentially evaluating each of the cost expressions. These individual costs are determined by the data and interrelations between nodes in the influence diagram and the calculations made within the spreadsheet model.

DPL generates its output in decision tree form. Figure 4, the output generated for the CHP investment appraisal model, shows two sets of figures displayed along each branch of the tree:

1. The un-bracketed figures correspond to the cost expressions (maintenance cost, etc.) entered in the model. These figures, when followed along a single branch, give a full breakdown of the costs resulting from that particular course of action. The diagram, for simplicity, shows just one branch leaving each chance node. The chance node values displayed are the mean of the individual branch calculations weighted by the probability assigned to each, that is the expected value.
2. A bracketed value is displayed immediately above each of the branches in the tree. These are policy

* A factor of 5 is used as cashflows are projected over five years.

© IMechE 1996

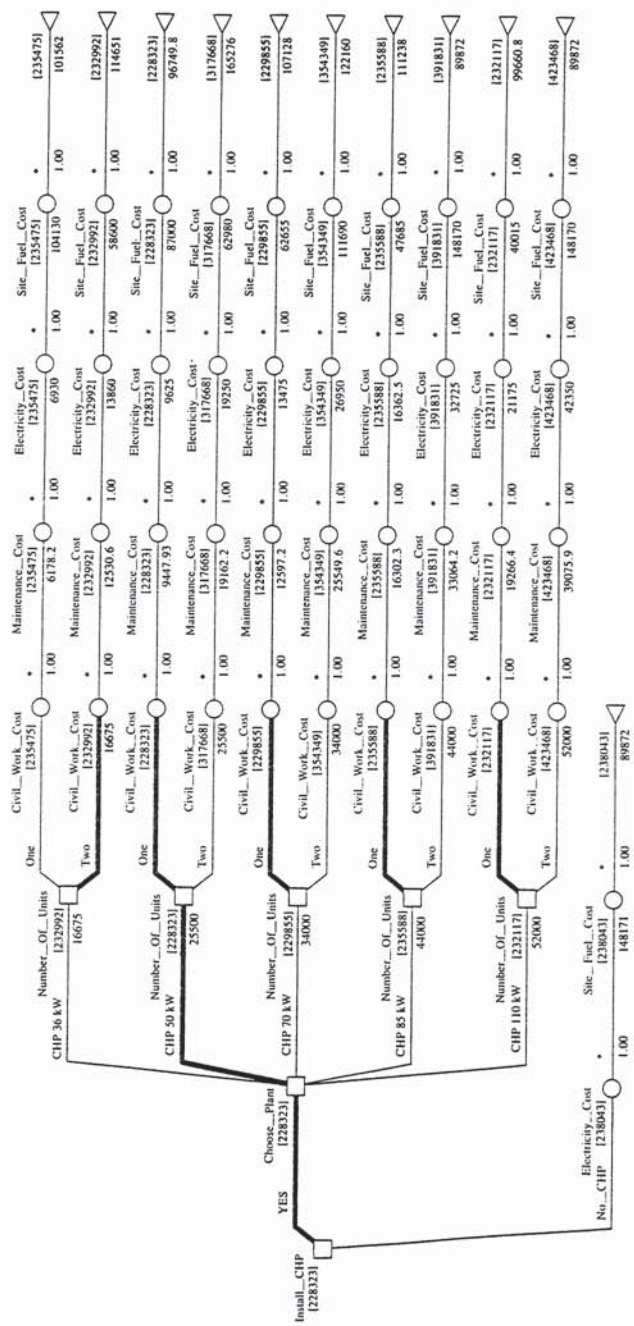

Note: bracketed values represent the total expenditure associated with a project. The un-bracketed values give a breakdown of costs and correspond to the cost expressions in Fig. 3.

Fig. 4 Decision policy tree showing breakdown of project costs

 © IMechE 1996

expected values, the overall cost of each option as predicted by DPL. DPL obtains figures by rolling back through each branch of the tree in turn, summing the individual costs on each. Expected branch values are the basis on which DPL will normally makes its decisions. The expected value of each alternative is compared at a decision node, the lowest of these figures becoming the expected value carried back down the tree.

DPL highlights its chosen decision path along with the outcomes of all downstream decisions on the non-optimal paths. The chosen option in this model is that with the smallest figure calculated for it, that is the option involving the least cost over the 5 year period considered. If this is the 'no CHP' option then it would follow that none of the CHP systems considered would have a payback period within 5 years and CHP will be regarded as economically unviable at the site.

8 DISCUSSION OF RESULTS

8.1 Decision policy tree

The most significant result of the decision analysis is the confirmation that CHP is economically viable at the site. The total projected 5 year expenditure resulting from the chosen CHP project is lower than that calculated for the 'no CHP' option. The bracketed figures above the branches exiting the first decision node show that the chosen option would involve an expected total expenditure of £228 320 compared to the £238 043 required to meet the site energy requirements by existing means.

The outcomes of the downstream decisions, that is those used to determine the best CHP system, were very marginal. The decision support system selected a relatively small CHP system comprising a single 50 kW unit: the model predicted that several of the alternatives would result in similar expenditure over the initial 5 years of operation.

The recommendation made by the decision support system is greatly affected by the capital investment policy of an organization. The decision made by the DSS would clearly change if a long-term view was taken. Table 1 shows that the installation of a 50 kW CHP unit would reduce the combined annual maintenance and energy costs at the site by approximately £9000. Operation of the 70 kW CHP option would reduce this total by a further £2000 p.a., due to the further reduction in the requirement of imported electricity. Long-term reduction of energy costs and maximization of energy efficiency will both be high priorities to a Local Authority.

Table 1 Comparison of cost breakdowns

Chosen system	Present system	A single 50 kW unit	A single 70 kW unit
Plant capital cost (£)	—	25500	34000
Civil work cost (£)	—	9448	12597
Maintenance cost (£)	—	9625	13475
Electricity import (£)	148171	87000	62655
Fuelling CHP plant and conventional boilers (£)	89872	96748	107124
Total (£)	238043	228320	229851

The model can easily be modified to allow its decisions to be based on and its decision policy displayed in terms of the payback period. A cost breakdown would no longer be appropriate, but this representation gives a clearer, more immediate, appreciation of the marginality of a decision.

Up to this point DPL has been little more than an effective means of handling uncertainties and an attractive means of presenting the results of the spreadsheet economic model. The full value of decision analysis is realized at this stage of investment appraisal when policy decisions need to be justified.

8.2 Risk profiles

An 'expected value' and breakdown of costs is, by itself, insufficient to convince a potential customer to invest in a CHP scheme. To justify a sizeable capital investment it would be necessary to have a clear picture of how the uncertainties and risks inherent in a project could potentially alter its profitability and to be convinced that these risks are acceptable.

DPL generates an outcome value distribution profile (risk profile) following its analysis of a model. A cumulative outcome distribution profile generated for the policy decision at the Llantrisant site is shown in Fig. 5. This figure displays the expected value as a vertical line, but also predicts the degree to which this value could potentially be affected by the uncertainties surrounding the project. Although displayed in terms of projected costs, a risk profile could just as easily be displayed with the payback period, or any other measure of profitability, along the x axis.

The most significant information obtained from Fig. 5 is the level of certainty with which it can be predicted that the chosen CHP project will be profitable. Decision analysis predicted that the 'do nothing' option would result in expenditure of £238 043 over 5 years. The risk profile predicts an 89 per cent chance of the chosen CHP system reducing overall costs over this period. Figure 4 also predicts that even with all uncertainties under worst-case conditions the project would lead to very modest losses. The final decision will be determined by the organizations attitude to risk, but in this case, with an expected saving of almost £10 000 and an 89 per cent probability of savings of some sort, the CHP installation would almost definitely go ahead.

DPL allows alternative decision policies to be fully compared, allowing the user to display the risk profile of up to four competing options in a single diagram. This is a particularly important feature of the model. Decision analysis has already shown DPL's choice of plant to be very marginal when based on expected values. A comparison of risk profiles affords an alternative and more robust basis on which to make policy decisions.

Figure 6 shows the risk profiles of the 50 kW project with the best non-optimal alternatives graphed together. If one plot was wholly to the left of the other then this would clearly be the best option as it would lead to lower expenditure under all circumstances. This is not the case in Fig. 6 and even more significantly the two plots overlap. This suggests that under certain circumstances the 70 kW$_e$ alternative could result in lower expenditure.

© IMechE 1996

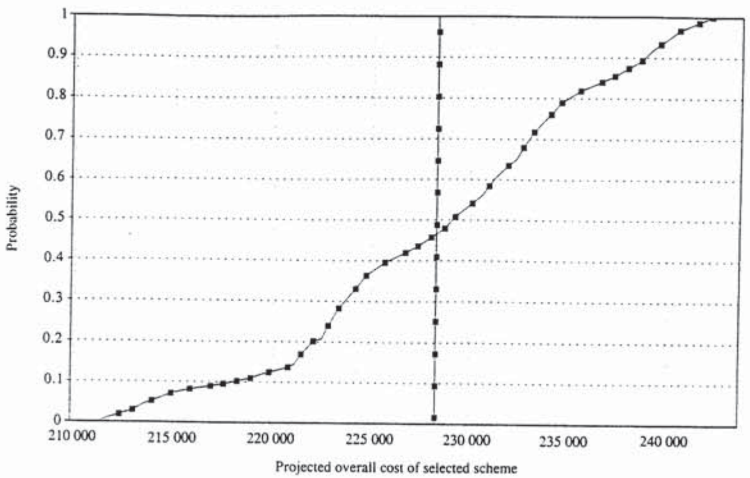

Fig. 5 Cumulative outcome distribution risk profile

8.3 Sensitivity analysis

The robustness of any model and the credibility of its results is limited by the availability of accurate data. This is a particular weakness of spreadsheet modelling techniques. Decision analysis is superior in this respect as it includes a sensitivity analysis facility.

Sensitivity analysis is a particularly important part of investment appraisal as it will often provide further insight into a problem and lead to refinements in a model, even where specific data items are not known, for example the extent to which the efficiency of a unit may deteriorate over time. Sensitivity analysis gives the user a clear indication of how sensitive a model's results are to a factor and, therefore, how critical the availability of this information is to the reliability of the model. The results of sensitivity analysis will often prompt a prospective investor to consider further options, to ensure that contingencies exist or, where possible, to take measures that would limit the chance element associated with certain critical factors.

Two distinct forms of sensitivity analysis are offered by DPL, either of which may be carried out on deterministic or probabilistic model data.

8.3.1 Value sensitivity comparison

Value sensitivity comparison tracks the changes in the decision policy and the expected value calculated by the

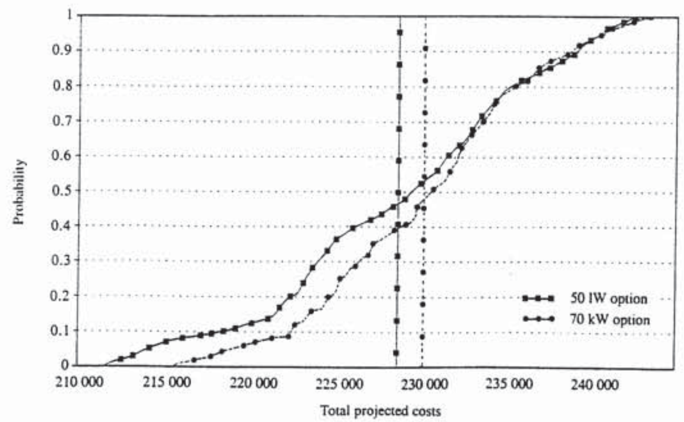

Fig. 6 Comparison of risk profiles for CHP investment appraisal

© IMechE 1996

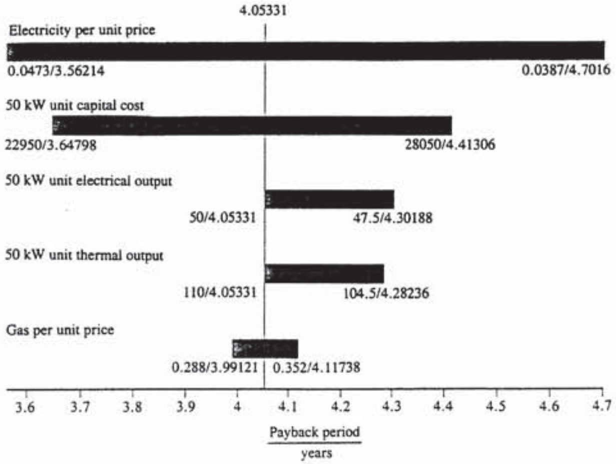

Note: the two figures at the end of each bar, *X/Y*, represent:
X = extreme value of influencing factor at which analysis was run
Y = expected payback period with factor set to extreme value

Fig. 7 Tornado diagram: a value sensitivity comparison

model as one particular value in the model is varied. Displaying the results of several sensitivity runs on a single diagram shows the relative impacts of various factors on the model's results. Figure 7 shows the result of value sensitivity analysis in the form of a tornado diagram.

Figure 7 clearly demonstrates the way in which sensitivity analysis generates insights into problems. The relative sensitivity of CHP profitability to variations in gas and electricity tariffs, for example, would not be easily obtainable by conventional modelling techniques. The extreme points used in the analysis represent electricity and gas unit prices of 10 per cent above and 10 per cent below the present values. It is clear from the results of this analysis that the outcome is far more sensitive to changes in electricity tariffs. This implies that the accurate forecasting of electricity tariffs would be of relatively high priority and should be modelled probabilistically.

The sensitivity run carried out on capital outlay is of significance in Fig. 7. The change in shading represents a change in the model's decision policy. Further investigation of the decision tree would quickly establish that the revised policy would involve the installation of a single 70 kW CHP unit.

Electrical and thermal efficiency can deteriorate over a period of time. The tornado diagram shows how the economics of CHP may be affected by below-specification performance. Sensitivity runs were carried out with the electrical and thermal outputs of the 50 kW unit 5 per cent below specified levels. The figure shows that the additional cost incurred would be quite sizeable if the average output was at these levels.

8.3.2 Value sensitivity analysis

Value sensitivity analysis offers a more in-depth look at the effect of variations in a single variable on the optimal decision policy and the expected value returned by the model.

Figure 8 is an example of value sensitivity analysis run on the model and shows how variations in the electricity price offered by the local REC affect the optimum decision and the payback period that would be expected. In this case a change of policy occurs at an electricity price of between 3.7 and 3.75 pence per unit. This is the point at which CHP becomes viable at the site. The chart also shows how the CHP option becomes increasingly more attractive as the electricity unit price is increased beyond 3.75 pence.

9 CONCLUSIONS

Decision analysis techniques can be successfully applied to the assessment of the financial viability of CHP projects. The economic model resulting from the synthesis of the decision analysis package, DPL, and Lotus 1-2-3 has been developed into a very powerful and flexible decision support system for CHP investment appraisal and plant selection. The model enables uncertainties and an organization's attitude to risk to be fully considered when investment appraisal is being carried out, and includes several forms of sensitivity analysis to be carried out, allowing models to be modified as further insights are gained.

© IMechE 1996

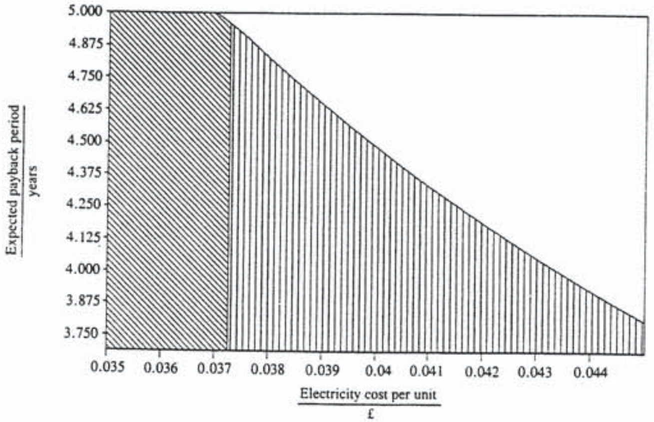

Fig. 8 The model's sensitivity to electricity cost per unit: a value sensitivity analysis

10 FUTURE WORK

DPL's ability to be linked to multiple spreadsheets of great complexity will enable the decision support system to develop into a generic model for small-scale CHP investment appraisal. The model is also to be expanded to cover the wider field of site energy management.

ACKNOWLEDGEMENT

The authors wish to thank Scottish Hydro Electric plc for their assistance in promoting this work.

REFERENCES

1 **Hu, S. D.** *Cogeneration*, 1985 (Reston Publishing).
2 **Gregory, G.** *Decision analysis*, 1988 (Plenum Press, New York).
3 **Cooper, D. F.** and **Chapman, C. B.** *Management for engineers*, 1987 (John Wiley, Chichester).
4 **Klein, M.** and **Methlie, L. B.** *Expert systems—a decision support approach*, 1990 (Addison-Wesley, Reading, Massachusetts).
5 ADA Decision Systems *DPL advanced version user guide*, 1992.
6 Energy Efficiency Office *Good practice guide 3*, 1993 (Energy Efficiency Office, London).

© IMechE 1996

PRIMÄRENERGIEEINSPARUNG DEZENTRALER BLOCKHEIZ-KRAFTWERKE IM VERGLEICH ZU GUD-KRAFTWERKEN UNTER BERÜCKSICHTIGUNG ÜBERREGIONALER VERSORGUNGSAUFGABEN

Dipl. Ing. Dr. techn. Jürgen Neubarth[1]

[1] e3 consult, Andreas-Hofer-Straße 28a, 6020 Innsbruck
Tel: +43 512 908892, j.neubarth@e3-consult.at; www.e3-consult.at

Kurzfassung: Der dezentralen Stromerzeugung wird zur Erreichung der Effizienz- und Klimaschutzziele i. Allg. ein hoher Stellenwert zugeschrieben. Vielfach wird die dezentrale Stromerzeugung aus fossilen Energieträgern in kleinen KWK-Anlagen in diesem zusammenhang als mögliche Alternative zu einer Stromerzeugung in großen GuD-Kraftwerken gesehen. Diese wird energiewirtschaftlich allerdings nur dann sinnvoll sein, wenn die eingesetzten fossilen Energieträger effizienter und damit klimaschonender genutzt und darüber Kostenvorteile erzielt werden können. Zusätzlich muss sie die Stromnachfrage in selber Art und Weise bedienen können wie die zentrale Erzeugung (d. h. gleiche Erzeugungscharakteristik), um das Niveau der Versorgungszuverlässigkeit nicht negativ zu beeinflussen.

Die vorliegende Analyse zeigt dabei, dass dezentrale KWK-Anlagen im wärmegeführten Betrieb Strom und Wärme gegenüber GuD-Kraftwerken in Kombination mit einer dezentralen Wärmeerzeugung zwar deutlich effizienter bereitstellen können. Allerdings ist hier das Potenzial zur Verdrängung von Erzeugungsleistung im konventionellen Kraftwerkspark vergleichsweise gering. Umgekehrt sinkt mit zunehmender Ausrichtung des BHKW-Betriebs auf die Anforderungen des Strommarktes die Energieeffizienz, da die Abwärme dann nicht immer vollständig genutzt werden kann. Diese grundsätzliche Problematik, dass eine parallele Optimierung von zwei nur eingeschränkt korrelierenden Systemen (öffentliche Stromversorgung bzw. Wärmeversorgung eines Objektes) nur bedingt darstellbar ist, lässt sich durch größere Wärmespeicher zwar zum Teil verringern, eine vollständige Substitution von GuD-Kraftwerken durch Klein- und Kleinst-BHKWs ist energiewirtschaftlich jedoch nicht zielführend.

Keywords: Blockheizkraftwerk, GuD-Kraftwerk, dezentrale Erzeugung, Energieeffizienz, Versorgungssicherheit

1 Einleitung und Fragestellung

Der dezentralen Stromerzeugung wird zur Erreichung der Effizienz- und Klimaschutzziele i. Allg. ein hoher Stellenwert zugeschrieben. Dies trifft insbesondere auf eine dezentrale Stromerzeugung aus erneuerbaren zunehmend aber auch aus fossilen Energieträgern zu. Es sind jedoch nicht nur Effizienz- und Klimaschutzgründe, die eine dezentrale Stromerzeugung heute sehr häufig als vorteilhaft gegenüber einer zentralen Stromerzeugung in Großkraftwerken erscheinen lassen. Auch aus emotionalen Gründen wird eine vom gefühlten „Diktat" der Großkonzerne unabhängige Erzeugung positiv bewertet. Beispielsweise wünschen sich nach einer von der Unternehmensberatung Accenture [1] in Deutschland durchgeführten Umfrage 84 % der Teilnehmer eine stärker dezentrale Energieerzeugung; 12 % der Befragten überlegen dabei sogar, selbst ein Mini-Blockheizkraftwerk zu installieren. Für Österreich kann davon ausgegangen werden, dass dezentrale Erzeugungstechnologien einen ähnlich hohen Zuspruch innerhalb der Bevölkerung finden.

Diese zunehmend pauschale Bewertung im Sinne „dezentral ist besser als zentral" erfordert aus energiewirtschaftlicher Sicht jedoch eine differenziertere Betrachtung, um die dezentrale Stromerzeugung innerhalb des Zielsystems der österreichischen Energiepolitik (Abb. 1) entsprechend ihres Beitrags zu den Dimensionen Umwelt-/Klimaschutz, Versorgungssicherheit, Wettbewerbsfähigkeit und Kosteneffizienz (Wirtschaftlichkeit) sowie soziale Verträglichkeit einordnen zu können.

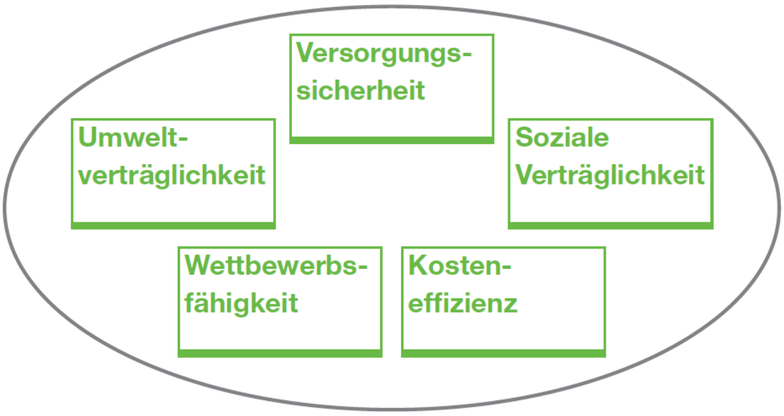

Abb. 1: Ziele der österreichischen Energiepolitik [2]

Während heute weitgehend gesellschaftlicher Konsens darüber besteht, dass dezentrale erneuerbare Technologien in Zukunft eine größere Rolle im österreichischen Stromversorgungssystem spielen sollen, ist die mögliche Rolle der dezentralen Stromerzeugung aus fossilen Energieträgern noch nicht klar definiert. Grundsätzlich geht die Energiestrategie Österreich davon aus, dass fossile Kohlenwasserstoffe weiterhin einen wichtigen Beitrag zur österreichischen Energieversorgung leisten werden. Die dezentrale Stromerzeugung aus fossilen Energieträgern in Klein- und Kleinst-Anlagen mit Kraft-Wärme-Kopplung (KWK) wird dabei vielfach als mögliche Alternative zu einer Stromerzeugung in großen GuD(Gas- und Dampfturbinen)-Kraftwerken gesehen. So sieht etwa die Energiestrategie Österreich nicht nur allgemeine Vorteile in der gekoppelten Strom- und Wärmeerzeugung, sondern im Speziellen in der dezentralen Stromerzeugung - *„Keine Kraftwerke ohne KWK – Kraftwerksbau immer wärmebedarfsgesteuert, mittels dezentraler KWK-Anlagen"* ([2], vgl. Maßnahmenliste Punkt 86). Diese wird energiewirtschaftlich allerdings nur dann sinnvoll sein, wenn die eingesetzten fossilen Energieträger effizienter genutzt und darüber Kostenvorteile generiert werden können. Andererseits sollte über eine dezentrale Stromerzeugung auf Basis fossiler Brennstoffe auch eine Minderung der Klimagasemissionen erreicht bzw. ein Beitrag zu den österreichischen Klimaschutzzielen geleistet werden. Zusätzlich muss sie die Stromnachfrage in selber Art und Weise bedienen können wie die zentrale Erzeugung (d. h. gleiche Erzeugungscharakteristik), um das Niveau der Versorgungszuverlässigkeit nicht negativ zu beeinflussen.

Dabei ist zu berücksichtigen, dass eine „positive“ energiewirtschaftliche Gesamtbewertung der dezentralen Stromerzeugung nicht zwangsläufig in allen Dimensionen des Zielsystems der österreichischen Energiepolitik einen Vorteil gegenüber der zentralen Stromerzeugung erfordert. Durch die dezentrale Stromerzeugung muss vielmehr insgesamt, über alle Wertschöpfungsstufen des Stromversorgungssystems betrachtet, ein positiver Effekt erzielt werden. Für die energiewirtschaftliche Bewertung der dezentralen Erzeugung bedeutet dies, dass die Systemgrenze bspw. nicht am Verknüpfungspunkt mit dem öffentlichen Stromnetz gezogen werden darf, sondern auch die Wechselwirkungen mit dem zentralen Stromversorgungssystem zu berücksichtigen sind.

Vor diesem Hintergrund wurden im Rahmen einer von der Energie-Control Austria beauftragten Studie „Dezentrale Erzeugung in Österreich“ insbesondere auch die energiewirtschaftlichen Aspekte Effizienz, Klimaschutz, Stromgestehungskosten sowie Beitrag zur Versorgungssicherheit dezentraler KWK-Anlagen analysiert [3]. Der vorliegende Beitrag stellt dabei die Ergebnisse eines dort beschriebenen Fallbeispiels dar, in dem die Aspekte Energieeffizienz und Versorgungssicherheit der dezentralen im Vergleich zu einer zentralen Stromerzeugung anhand eines Vergleichs der Stromerzeugung aus Erdgas in einem GuD-Kraftwerk und einem Mikro-/Kleinst-BHKW diskutiert werden.

2 Methodik und Ergebnisse

Ausgangspunkt des in [3] analysierten Fallbeispiels ist die Fragestellung, ob eine zentrale Stromerzeugung in einem Erdgas-GuD-Kraftwerk durch ein Kollektiv aus dezentralen Erdgas-Mikro- und/oder Kleinst-BHKWs ersetzt werden kann, so dass einerseits dieselbe Versorgungsaufgabe wahrgenommen und andererseits eine Primärenergieeinsparung erzielt werden kann. An dieser Stelle nicht betrachtet werden demgegenüber die unterschiedlichen wirtschaftlichen Aspekte der beiden Erzeugungsoptionen. Folgende Vorgehensweise wird zur Beantwortung der o. a. Fragestellung gewählt:

1. Modellierung des Einsatzes eines erdgasbefeuerten GuD-Kraftwerks für die Jahre 2008 bis 2009 anhand der EXAA-Spotmarktnotierungen sowie der entsprechenden Erdgas- und CO_2-Zertifikatspreise.
2. Ermittlung der Einsatzcharakteristik wärmegeführter BHKWs für zwei exemplarische Versorgungsaufgaben.
3. Überlagerung der Einsatzcharakteristik des wärmegeführten Betriebs aus Punkt 2 mit dem GuD-Einsatzprofil aus Punkt 1 zu einer strom-/wärmegeführten Betriebsweise der BHKWs.

2.1 Einsatzcharakteristik eines GuD-Kraftwerks am Strommarkt

Die Entscheidung über den Einsatz eines GuD-Kraftwerks am Strommarkt hängt im Wesentlichen von zwei Randbedingungen ab - dem Strompreis (Erlös) sowie den variablen Einsatzkosten. Sind dabei die variablen Kosten der Erzeugung geringer als der zu erzielende Erlös kann ein positiver Deckungsbeitrag erzielt werden und der Einsatz der Erzeugungsanlage ist wirtschaftlich sinnvoll. Die Investitions- und sonstigen Fixkosten sind für die Einsatzentscheidung nicht relevant, da diese unabhängig vom tatsächlichen Einsatz anfallen. Allerdings müssen Investitions- und sonstigen Fixkosten über die Lebensdauer des Kraftwerks aus den Deckungsbeiträgen erwirtschaftet werden können.

Für die Ermittlung der Erzeugungscharakteristik und damit der Einsatzdauer eines österreichischen Erdgas-GuD-Kraftwerks wird von einem vereinfachten Ansatz ausgegangen. Der Einsatz wird ausschließlich gegen die Spotmarktpreise an der österreichischen Strombörse EXAA optimiert. Eine alternative Vermarktung an der deutschen Strombörse EEX (European Energy Exchange) sowie an den österreichischen und deutschen Regelenergiemärkten wird hier nicht betrachtet. Als variable Kosten des Kraftwerkseinsatzes werden die in Tabelle 1 angeführten Kostenelemente sowie zusätzliche An- und Abfahrkosten in Höhe von 27 €/MW*Start berücksichtigt.

Tabelle 1: Eingangsparameter zur Ermittlung der variablen Einsatzkosten eines Erdgas-GuD-Kraftwerks in Oberösterreich (u. a.[5], [6], [7] und [8])

		2008	2009
Wirkungsgrad	%	56	56
CO_2-Emissionsfaktor	t_{CO2}/MWh_{Hu}	0,2	0,2
CO_2-Zertifikatspreis	€/t_{CO2}	EEX CARBIX	
Gaspreis	€/MWh_{Ho}	EEX Spotpreis	
Netznutzung Gas	€/MWh_{Ho}	0,429	0,425
Netzverlustentgelt Strom (Netzebene 3)	€/MWh_{el}	0	0,7
Systemdienstleistungsentgelt Strom	€/MWh_{el}	1,1	1,55
Sonstige variable Betriebskosten	€/MWh_{el}	4,0	4,0
An- und Abfahrkosten	€/MW_{el}*Start	27	27

Da die langfristigen Erdgasbezugspreise der Kraftwerksbetreiber nicht bekannt sind, werden für die Modellierung die tagesscharfen Spotgaspreise der EEX herangezogen, da an der österreichischen Erdgasbörse (Central European Gas Hub, CEGH) die Spotpreise erst seit Dezember 2009 notiert werden. Der Fehler aus der Projektion deutscher Spotgaspreise auf Österreich ist allerdings vergleichsweise gering. Beispielsweise lagen im ersten Halbjahr 2010 die Spotgaspreise an der CEGH im Mittel nur etwa 7 % über der EEX [5], [7]. Die Preise der CO_2-Zertifikate werden tagesscharf aus den Veröffentlichungen der EEX entnommen und für das Gasnetznutzungsentgelt sowie Netzverlustentgelt ein Standort in Oberösterreich unterstellt. In die „Sonstigen variablen Betriebskosten" geht neben den Kosten für u. a. Rauchgasreinigung auch eine Mindestmarge für den Betrieb der Anlage ein. Die Erdgasabgabe fließt hingegen nicht in die variablen Kosten ein, da diese bei der Erzeugung von Elektrizität rückerstattet wird.

Aus der Summe der variablen Kosten kann nun für jede Stunde der Einsatz des modellierten GuD-Kraftwerks an der EXAA abgeleitet werden. In Abb. 2 ist dies beispielhaft für den Zeitraum 1.- bis 7. Jänner 2008 dargestellt. Auf Grund der zu berücksichtigenden An- und Abfahrkosten wird dabei die Anlage bspw. am Samstag nicht in der schwach ausgeprägten Mittagspitze sondern nur in der Abendspitze eingesetzt.

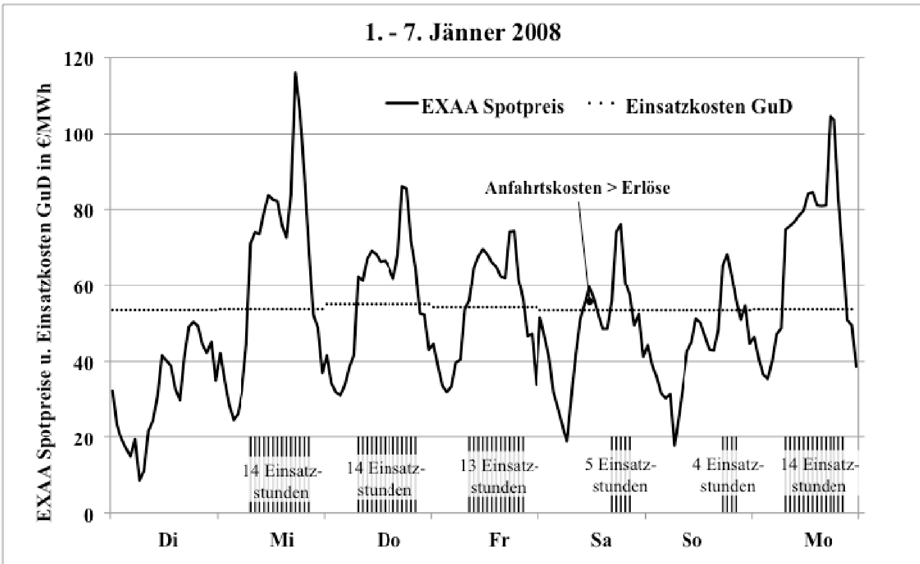

Abb. 2: Prinzip der Einsatzplanung eines GuD-Kraftwerks am Strommarkt

In Summe ergeben sich für das Jahr 2008 rd. 4.300 und für das Jahr 2009 ca. 4.800 Einsatzstunden mit jeweils knapp 330 An- und Abfahrvorgängen. Nicht berücksichtigt wurden dabei allerdings geplante und nicht geplante Nichtverfügbarkeiten auf Grund von Revisionen und Kraftwerksausfällen, sodass die tatsächlichen Einsatzstunden etwa 5 - 8 % unter den ermittelten theoretischen Einsatzstunden liegen. Dies wird bei den weiteren Betrachtungen vernachlässigt, sodass sich für 2008 und 2009 die in Abb. 3 dargestellte Verteilung der täglichen Einsatzstunden für das modellierte GuD-Kraftwerk ergibt.

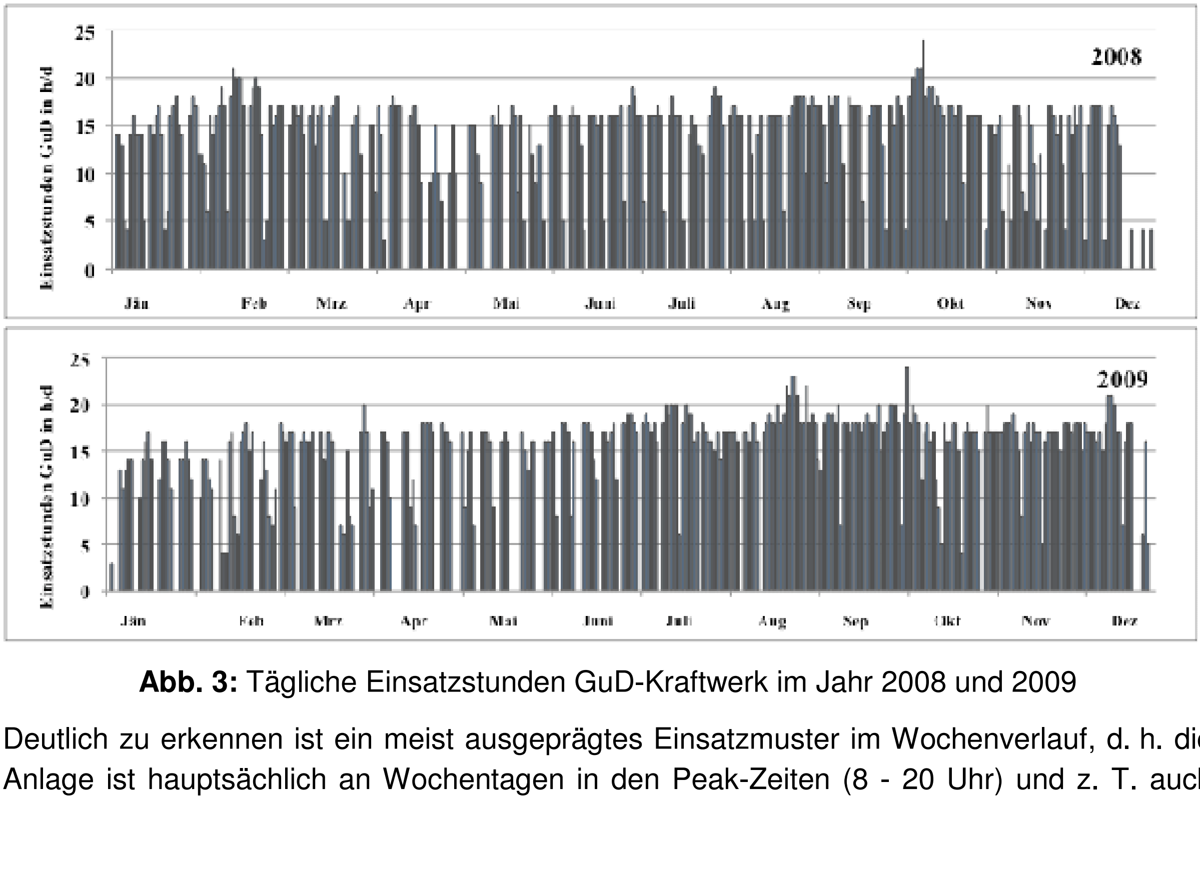

Abb. 3: Tägliche Einsatzstunden GuD-Kraftwerk im Jahr 2008 und 2009

Deutlich zu erkennen ist ein meist ausgeprägtes Einsatzmuster im Wochenverlauf, d. h. die Anlage ist hauptsächlich an Wochentagen in den Peak-Zeiten (8 - 20 Uhr) und z. T. auch unmittelbar angrenzenden Stunden in Betrieb. Zusätzlich läuft die GuD-Anlage häufig an Samstagen in einzelnen Stunden (meist weniger als 6 Stunden) und teilweise auch an Sonntagen (z. B. August bis Mitte Dezember 2009). Demgegenüber können ausgeprägte Phasen mit niedrigen Strompreisen (z. B. Mitte bis Ende Dezember 2008, April und Mai 2009) dazu führen, dass GuD-Kraftwerke nur in sehr wenig Stunden einen positiven Deckungsbeitrag erzielen können und damit kaum eingesetzt werden.

2.2 Wärmegeführter Betrieb Erdgas-BHKW

Entsprechend der Modellierung des Einsatzes eines GuD-Kraftwerks wird im Folgenden die Einsatzcharakteristik für zwei exemplarische Referenzsysteme mit erdgasbefeuerten BHKWs ermittelt. Die Versorgungsaufgabe der BHKWs lehnt sich an den Wärmebedarf eines „typischen“ Ein- (EFH) und Mehrfamilienhauses (MFH) mit mittlerem Wärmedämmstandard an, wobei das Einfamilienhaus ohne und das Mehrfamilienhaus mit Spitzenlastkessel ausgestattet ist (Tabelle 2). Die dargestellte Vorgehensweise lässt sich grundsätzlich auch auf andere Versorgungsaufgaben übertragen (z. B. Industrie- und Gewerbe).

Tabelle 2: Referenzsystem Ein- und Mehrfamilienhaus mit BHKW-Kenndaten

		EFH	MFH
Wärmebedarf			
Heizung	kWh/a	15.000	250.000
Warmwasser	kWh/a	4.000	50.000
Gesamt	kWh/a	19.000	300.000
BHKW			
Elektrische Leistung	kW_{el}	3	20
Thermische Leistung	kW_{th}	8	35
Wirkungsgrad elektrisch	%	25	32
Wirkungsgrad thermisch	%	67	56
Wirkungsgrad gesamt	%	92	88
Spitzenlastkessel			
Thermische Leistung	kW_{th}	-	150
Wirkungsgrad thermisch	%	-	90

Für die Herleitung des täglichen Heizwärmebedarfs wird vereinfachend unterstellt, dass dieser entsprechend der täglichen Gradtagzahlen in ein kalendertägliches Raster übergeführt werden kann[1]. Da die Summen der Gradtagzahlen der Jahre 2008 und 2009 nur sehr geringfügig voneinander abweichen (1,5 %), muss der in Tabelle 2 angeführte Heizwärmebedarf nicht temperaturbereinigt sondern kann im Rahmen dieser Analyse für beide Jahre unverändert herangezogen werden. Auf eine Differenzierung unterschiedlicher Gebäudetypen bzw. Wärmedämmstandards kann dabei ebenfalls verzichtet werden, da Ergebnisse aus anderen Studien zeigen, dass der jahreszeitliche Verlauf des normierten Raumwärmebedarfes (mittlerer Tageswärmebedarf bezogen auf den Jahreswärmebedarf) für die unterschiedlichen Gebäudegrößen und Energiekennzahlen sehr ähnlich ist (Abb. 4). D. h. der Wärmebedarf der

[1] Es wird hierzu auf das arithmetische Mittel der Gradtagzahlen der Messstationen Wien-Hohe Warte, Wien-Innere Stadt, Linz, Salzburg-Freisaal, Innsbruck-Universität und Graz-Universität gebildet [9].

Gebäude unterscheidet sich nur durch die Höhe und nicht im Zeitverlauf. Der Zeitverlauf des Wärmebedarfs wird dabei im Wesentlichen durch das saisonabhängige Benutzerverhalten bestimmt, das in diesem Fallbeispiel über die Gradtagzahlen abgebildet wird.

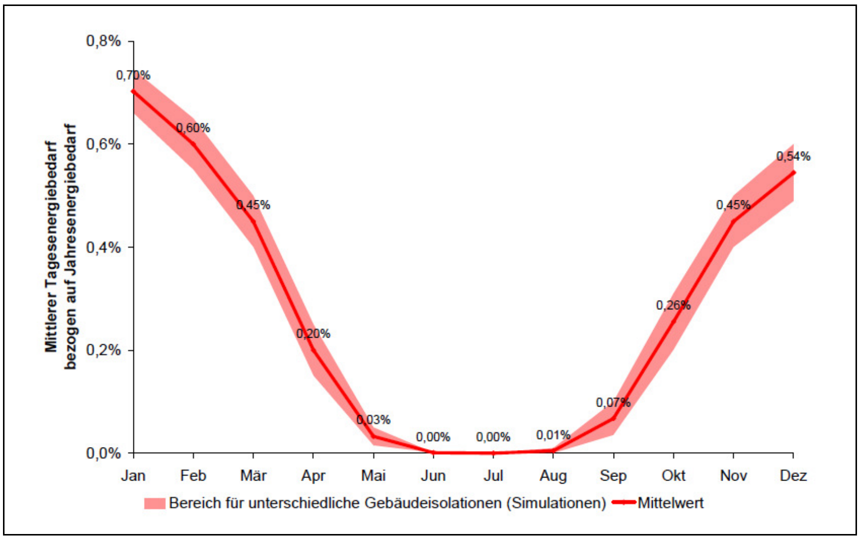

Abb. 4: Normierter Raumwärmebedarf (Tagesenergiebedarf) für Wohngebäude mit unterschiedlichen thermischen Isolationszuständen [4]

Zusätzlich zum Heizwärmebedarf wird der Wärmebedarf zur Warmwasserbereitung dadurch berücksichtigt, dass der jährliche Warmwasserverbrauch gleichmäßig über alle Tage eines Jahres verteilt wird. Auf eine stundenscharfe Betrachtung kann unter der Annahme eines ausreichend dimensionierten Wärmespeichers verzichtet werden, wobei hier unterstellt wird, dass die für die Wärmebereitstellung erforderlichen täglichen Einsatzstunden der BHKWs im wärmegeführten Betrieb flexibel innerhlab eines Kalendertags erbracht werden können. Mit diesen Randbedingungen kann nun die Einsatzcharakteristik der BHKWs im wärmegeführten Betrieb ermittelt werden, die in Abb. 5 für die beiden Referenzsysteme EFH und MFH dargestellt ist.

Der Einsatz des BHKW im Einfamilienhaus folgt dabei dem Verlauf der Gradtagzahlen mit einer dem täglichen Warmwasserbedarf überlagerten Grundlast. Mit durchschnittlich 2.380 Jahresvolllaststunden läuft die Anlage nur etwa halb so lange wie das in Abb. 3 dargestellte GuD-Kraftwerk, wobei das BHKW in rd. 2.800 Stunden nicht in Betrieb ist, in denen die GuD-Anlage Strom erzeugt. Umgekehrt erzeugt das BHKW in rd. 600 Stunden Strom, in denen das GuD-Kraftwerk nicht am Netz ist.

Anders stellt sich die Situation bei dem betrachteten Referenzsystem MFH dar, wo das BHKW die Wärmegrundlast und nicht den gesamten Wärmebedarf abdeckt. Dadurch erreicht das BHKW 5.500 (2008) bzw. 5.000 (2009) Volllaststunden und deckt damit 65 bzw. 58 % des Gesamtwärmebedarfs ab. Das BHKW läuft dabei während dem Winterhalbjahr praktisch ohne Unterbrechung mit Volllast. Umgekehrt muss im Sommerhalbjahr durch das BHKW im Wesentlichen nur der Warmwasserbedarf abgedeckt werden, wodurch die Betriebsstunden vergleichsweise gering sind. Dadurch ergeben sich gegenüber der Einsatzcharakteristik einer GuD-Anlage rd. 1.700 Stunden, in denen das BHKW nicht in Betrieb ist bzw. 2.300 Stunden in denen die dezentrale Anlage Strom erzeugt, nicht aber das GuD-Kraftwerk.

Aus Sicht der Energieeffizienz liefert dieser wärmegeführte Betrieb der BHKWs die höchsten Energieeinsparungen gegenüber einer getrennten Strom- und Wärmeerzeugung. Für den Vergleich mit einer ungekoppelten Strom- und Wärmeerzeugung wird im folgenden unterstellt, dass die alternative Wärmebereitstellung in einem Gasbrennwertkessel mit 90 % Wirkungsgrad erfolgt und durch die GuD-Anlage dieselbe Strommenge bereitgestellt wird, wie die dezentralen Anlagen erzeugen. Zusätzlich werden die, im Vergleich zur Stromerzeugung in einem Großkraftwerk vermiedenen Netzverluste der dezentralen Erzeugung mit 5 % berücksichtigt. Für das Referenzsystem EFH liegt der gesamtenergetische Wirkungsgrad der dezentralen Variante bei 91,5 %, wohingegen die Stromerzeugung in einer GuD-Anlage mit getrennter Wärmeerzeugung eine Gesamteffizienz von ca. 76 % zeigt. Demgegenüber erreicht im Referenzsystem MFH die Variante BHKW + Spitzenlastkessel eine Gesamteffizienz von ca. 89 % und die Variante GuD + Gas-Brennwertkessel von rd. 76 %.

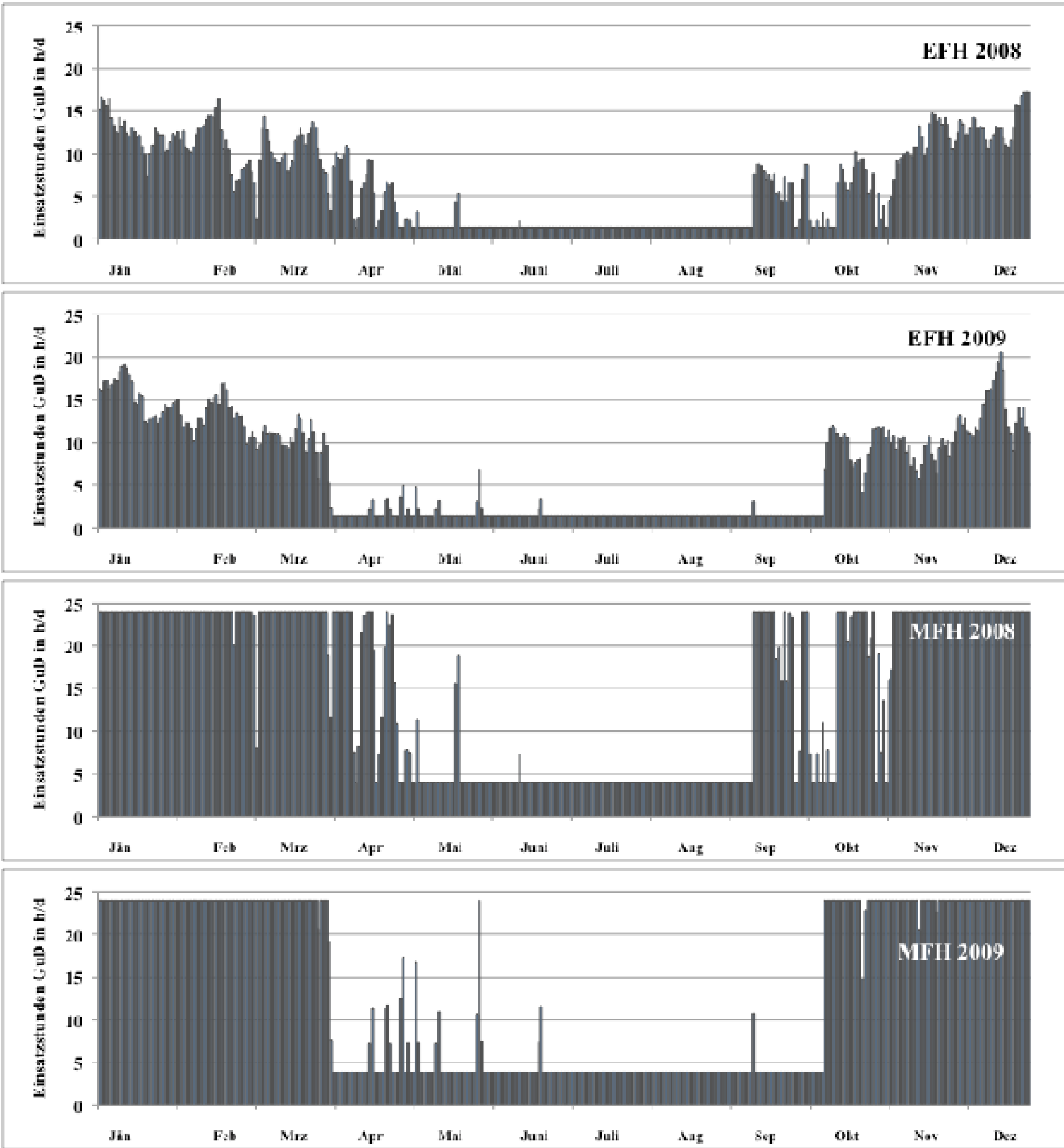

Abb. 5: Einsatzcharakteristik BHKW im wärmegeführten Betrieb für die Referenzsysteme EFH und MFH in den Jahren 2008 und 2009

Aus Sicht der Versorgungssicherheit können die Varianten dezentral und zentral allerdings nicht unmittelbar miteinander verglichen werden. Während das GuD-Kraftwerk bedarfsorientiert Strom erzeugt, wird die Stromerzeugung der dezentralen Anlagen vom Wärmebedarf der zu versorgenden Gebäude bestimmt. Werden beispielsweise die Spotpreise als Indikator für die vom konventionellen Kraftwerkspark zu deckende Nachfrage herangezogen, zeigt sich in den Jahren 2008 und 2009 keine einheitliche Beziehung zwischen Strom- und Wärmebedarf (Abb. 6). Während 2008 die EXAA Spotpreise (Tagesmittelwert) mit zunehmendem Wärmebedarf tendenziell abnahmen, kann für 2009 eine umgekehrte Tendenz festgestellt werden. Dies bestätigt damit die in Abb. 3 dargestellten täglichen Einsatzstunden eines GuD-Kraftwerks, wo auch während der Sommermonate ein häufiger Einsatz festzustellen ist.

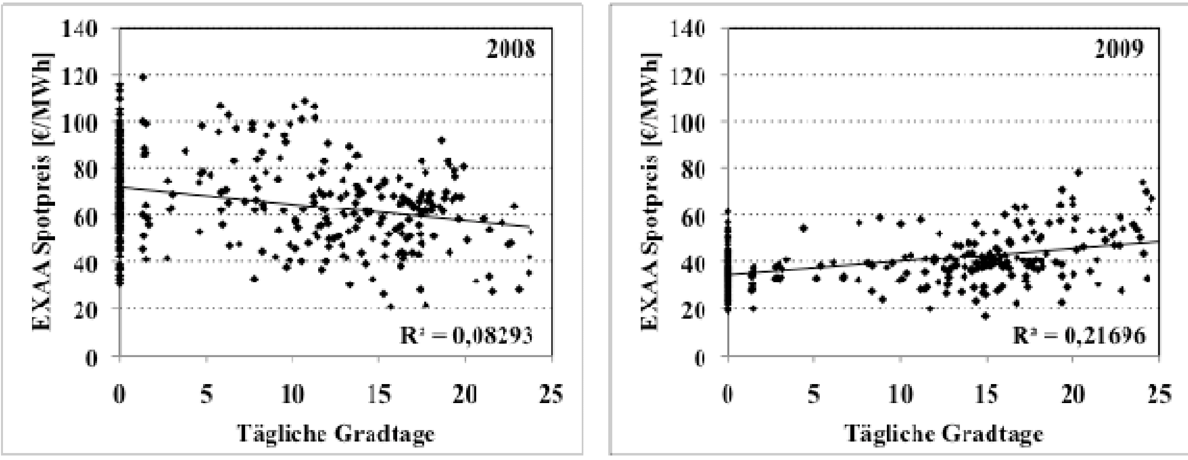

Abb. 6: Korrelation EXAA Spotpreise (Tagesmittelwert) und tägliche Gradtagzahlen ausgewählter österreichischer Messstationen im Jahr 2008 und 2009 (Daten: [6], [9])

Durch diese unterschiedlichen jahreszeitlichen Anforderungen an die Strom- und Wärmebereitstellung müssen die Erzeugungsschwankungen dezentraler KWK-Anlagen vom Kraftwerkspark der öffentlichen Versorgung ausgeglichen werden. Während es im Winter vor allem in den Nachtstunden zu Rückspeisungen in das Netz kommen kann, muss im Sommer ein Großteil des benötigten Stroms von außen bezogen werden. Die wärmegeführte Betriebsweise von dezentralen KWK-Anlagen führt damit insbesondere bei Anlagen mit ausgeprägter saisonaler Einspeisecharakteristik, wie sie typischerweise bei der Heizwärmebereitstellung zu finden ist, zu einer geringeren Auslastung des konventionellen Kraftwerksparks.

2.3 Strom-/Wärmegeführter Betrieb Erdgas-BHKW

Die in 2.2 diskutierte wärmegeführte Betriebsweise der BHKWs liefert zwar die höchsten Primärenergieeinsparungen gegenüber einer ungekoppelten Strom- und Wärmerzeugung, kann die Versorgungsaufgabe eines GuD-Kraftwerks allerdings nicht ersetzten. Im folgenden Abschnitt wird daher analysiert, wie sich eine zusätzliche übergeordnete stromgeführte Betriebsweise der BHKW auf die Gesamteffizienz auswirkt. Hierzu wird das ex post modellierte Einsatzprofil der GuD-Anlage auf die dezentralen Anlagen übertragen, d. h. die dezentralen Anlagen sollen zusätzlich zu dem vom Wärmebedarf abhängigen Betrieb auch in den selben Stunden wie das Großkraftwerk Strom erzeugen, um dadurch dessen Versorgungsaufgabe übernehmen zu können. Abb. 7 zeigt die entsprechende Einsatzcharakteristik der BHKWs für die Referenzsysteme EFH und MFH.

Deutlich zu erkennen ist dabei die Überlagerung der Einsatzprofile aus dem strom- (Abb. 3) und wärmegeführten Betrieb (Abb. 5). Durch diese geänderte Betriebsweise kann die Abwärme der BHKWs jedoch nicht mehr vollständig genutzt und muss daher teilweise über den Notkühler abgeführt werden. Entsprechend sinkt damit auch die Gesamteffizienz der dezentralen Varianten auf etwa rd. 56 % (EFH) bzw. rd. 78 % (MFH). Gegenüber einer ungekoppelten Strom- und Wärmeerzeugung zeigt das Referenzsystem MFH im Mittel der Jahre 2008 und 2009 eine um knapp 3 %-Punkte höhere, das Referenzsystem EFH hingegen eine um rd. 15 %-Punkte geringere Gesamteffizienz.

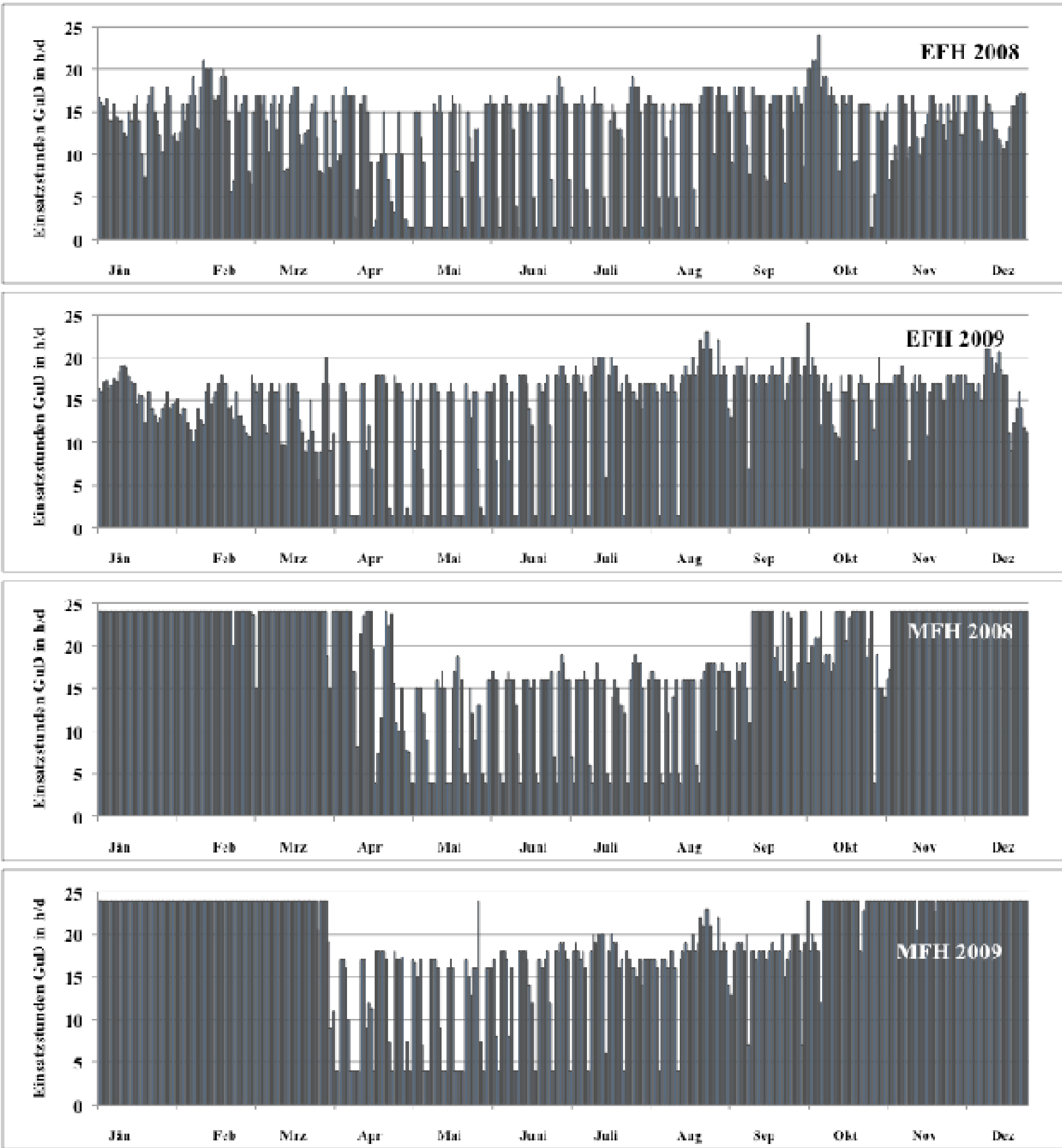

Abb. 7: Einsatzcharakteristik BHKW im strom-/wärmegeführten Betrieb für die Referenzsysteme EFH und MFH in den Jahren 2008 und 2009

3 Bewertung der Ergebnisse

Im wärmegeführten Betrieb können dezentrale KWK-Anlagen Strom und Wärme deutlich effizienter bereitstellen. Allerdings ist das Potenzial zur Verdrängung von Erzeugungsleistung im konventionellen Kraftwerkspark im wärmegeführten BHKW-Betrieb vergleichsweise gering. Mit zunehmender Ausrichtung des BHKW-Betriebs auf die Anforderungen des Strommarktes sinkt jedoch die Energieeffizienz, da die Abwärme dann nicht immer vollständig genutzt werden kann. Diese grundsätzliche Problematik, dass eine parallele Optimierung von zwei nur eingeschränkt korrelierenden Systemen (öffentliche Stromversorgung bzw. Wärmeversorgung eines Objektes) nur bedingt darstellbar ist, lässt sich durch größere Wärmespeicher zwar zum Teil verringern, eine vollständige Substitution von GuD-Kraftwerken durch Klein- und Kleinst-BHKWs ist energiewirtschaftlich jedoch nicht zielführend.

BHKW-Systeme mit Spitzenlastkessel sind dabei deutlich flexibler als Systeme ohne zusätzlichen Wärmeerzeuger, d. h. die Wärmeerzeugung kann unabhängig vom Stromverbrauch des zu versorgenden Objektes bzw. von den Randbedingungen am Strommarkt erfolgen. Durch die zu erwartende weitere Zunahme der Stromerzeugung aus fluktuierenden erneuerbaren Energien kann es unter dem Aspekt CO_2-Minimierung zukünftig daher durchaus sinnvoll sein, ein BHKW nur dann zu betreiben, wenn der Strom aus dem öffentlichen Netz nicht aus erneuerbaren Energien kommt. Anderenfalls würde das BHKW indirekt Strom aus erneuerbaren Energien verdrängen und damit eine Abschaltung von Wind- oder PV-Anlagen erzwingen. Neben der höheren Flexibilität haben BHKW-Systeme mit Spitzenlastkessel einen weiteren energiewirtschaftlichen Vorteil: Die Erzeugung ist konstanter und damit langfristiger planbar, da aus dem BHKW in solchen Systemen i. Allg. nur die Wärmegrundlast abgedeckt wird und dadurch hohe Jahresvolllaststunden erreicht.

Grundsätzlich kann die dezentrale Stromerzeugung damit zu einer Verringerung der Abhängigkeit von fossilen Energieimporten sowie einer Reduzierung der CO_2-Emissionen einen Beitrag leisten. Ein Ausbau der dezentralen Stromerzeugung in Österreich führt auf Grund der engen Einbindung des österreichischen in das europäische Elektrizitätsversorgungssystem jedoch kaum zu einer Verdrängung fossiler Stromerzeugung in Österreich selbst. Vielmehr werden die Erzeugung und damit die CO_2-Emissionen fossiler Kraftwerke an einer anderen Stelle in Europa substituiert. Auch ist in der Diskussion über den Ausbau der dezentralen KWK zu berücksichtigen, dass die dezentrale Stromerzeugung aus fossilen Energieträgern einen negativen Effekt auf die von der EU vorgegebenen nationalen Klimaschutzziele haben kann, da die CO_2-Emissionen dezentraler Anlagen nicht vom EU-weiten Emissionshandelssystem erfasst werden und damit die österreichische Treibhausgasbilanz belasten.

4 Literatur

[1] ACCENTURE: *Ausbau von dezentraler Energieerzeugung*, Pressemitteilung vom 20.1.2010.

[2] BUNDESMINISTERIUM FÜR LAND- UND FORSTWIRTSCHAFT, UMWELT UND WASSERWIRTSCHAFT, BUNDESMINISTERIUM FÜR WIRTSCHAFT, FAMILIE UND JUGEND: *Energiestrategie Österreich – Maßnahmenvorschläge*, Wien, 2010.

[3] NEUBARTH, J.; WOLTER, M.: Dezentrale Erzeugung in Österreich, Studie im Auftrag der Energie-Control Austria (Veröffentlichung für Q1/2012 vorgesehen), Wien (2012)

[4] BRAUNER, G. ET AL: *Verbraucher als virtuelles Kraftwerk*, Projektbericht im Rahmen der Programmlinie Energiesysteme der Zukunft, Berichte aus Energie- und Umweltforschung 44/2006, BMVIT, 2006.

[5] CENTRAL EUROPEAN GAS HUB: *Natural Gas Spot Market Data*, www.cegh.at/index.php?id=116, 2010.

[6] ENERGY EXCHANGE AUSTRIA: *Marktinformationen*, www.exaa.at/market/, 2010.

[7] EUROPEAN ENERGY EXCHANGE: *Marktdaten*, www.eex.com/de/Downloads, 2010.

[8] SNT-VO 2010: *Verordnung der Energie-Control Kommission, mit der die Tarife für die Systemnutzung bestimmt werden (Systemnutzungstarife-Verordnung 2010).*

[9] ZENTRALANSTALT FÜR METEOROLOGIE UND GEODYNAMIK: *Heizgradtage für verschiedene Messstationen in Österreich (kostenpflichtige Daten)*, Wien, 2010.